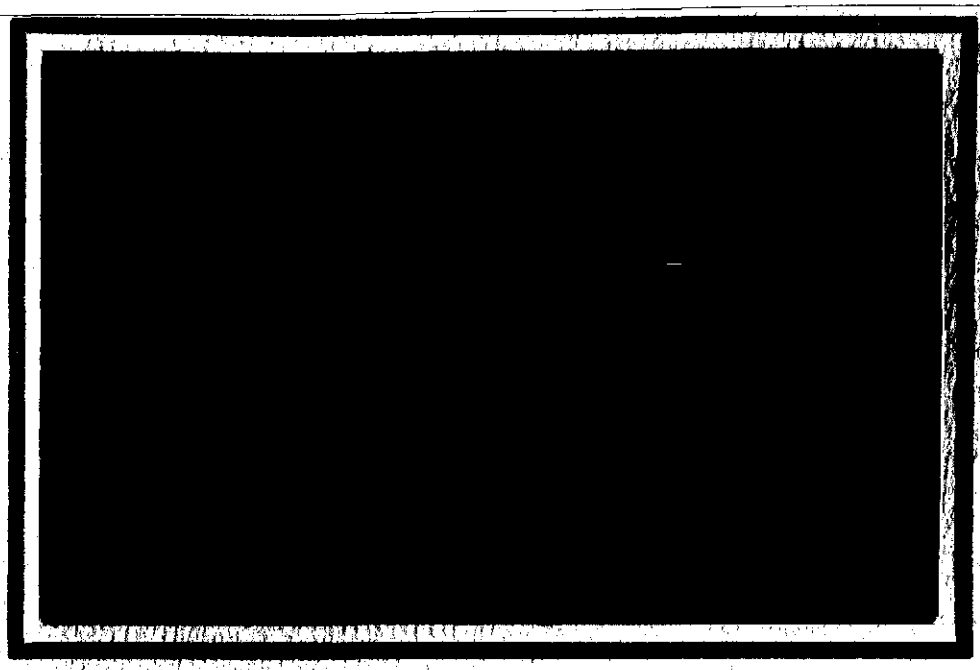

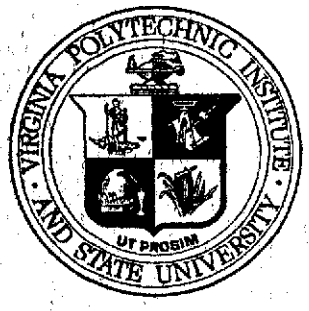

Virginia Polytechnic Institute
and State University

Department of Aerospace Engineering
Blacksburg, Virginia 24061

VPI-AERO-006 NASA CR-132312

VORTEX AGE AS A WAKE TURBULENCE SCALING PARAMETER

J. R. Marshall and

J. F. Marchman, III

August 1973

Prepared Under Contract No. NAS1-10646-15
Aerospace Engineering Department
Virginia Polytechnic Institute and State University
Blacksburg, Virginia 24061

for

NATIONAL AERONAUTICS AND SPACE ADMINISTRATION
LANGLEY RESEARCH CENTER

Abstract

A program of research was conducted in the Virginia Tech Stability Wind Tunnel to determine the significance of vortex age as a scaling parameter in wake turbulence development and dissipation. Tests were conducted at three angles of attack, three free stream speeds, and seven downstream positions from 2 to 30 chordlengths using an NACA 0012 wing and a five hole yawhead pitot probe. The end surface of the wing tip was flat. Speeds were selected to give a predetermined range of vortex ages. The complete velocity structure of the vortex was measured at each station and speed. The resulting plots of maximum tangential velocity and vortex core diameter versus downstream distance and vortex age indicate that vortex age is not a self sufficient scaling parameter. In addition to the expected effect of lift coefficient there is also a definite free stream speed influence at high wing angles of attack. The exact cause and nature of this effect is not fully understood, but it does not appear to be explainable in terms of Mach number or Reynolds number; however, the influence of tip edge shape on spanwise flow separation appears to be an important factor.

Table of Contents

Nomenclature

C	- wing chord .666 ft.
D	- vortex core diameter
Q	- dynamic pressure - inches of water
t	- vortex age - z/V_∞
V_{axial}	- axial velocity
V_{tan}	- tangential velocity
$V_{t_{max}}$	- maximum tangential velocity
V_∞	- freestream velocity
z	- downstream distance
α	- angle of attack of wing

List of Figures

INTRODUCTION

Wake turbulence or aircraft trailing vortices have been a topic of research and concern in the aviation field for approximately a half century. Yet, despite this large and long term effort to deal with the problems of wake turbulence, they still persist and research is continuing in an effort to eliminate or diffuse the trailing vortex and its resulting hazard to encountering aircraft (Fig. 1). One of the most perplexing problems of wake turbulence research has been the inability to compare one researcher's test data with that of another on a meaningful basis. Data exists ranging from full scale flight test results to very small scale wind tunnel model test data. Measurements have been made with hot wire probes, pitot static tubes, yaw head probes and even taken from analyses of tuft grids, smoke, and bubble photographs. This wide range of test and data reduction procedures has, unfortunately, led to a very wide range of results with order of magnitude differences resulting in different reports. Attempts to apply standard similarity parameters such as Reynolds number or Mach number to the results in order to facilitate data comparison has met with failure, partly because of the inability to define meaningful characteristic dimensions, velocities, and viscosities in a vortex. Mason and Marchman[1], for example, showed that standard methods for computing viscosity in a vortex did not produce meaningful results, and were not consistent with wind tunnel test data.

Without some similarity or scaling parameter it will remain difficult, if not impossible, to compare data taken under widely divergent test conditions. Researchers will continue to seek refuge by blaming lack

of compatability of their results with those of others on different instrumentation, different test speeds and model sizes, different wind tunnel turbulence levels, etc.

It appeared that this problem might have been solved recently when Rorke and Moffitt reported the results of their wind tunnel vortex tests.[2] In this study, tests were run with different size, geometrically similar wings at different speeds and over a range of angles of attack. The results of the study indicated that vortex age or time of flight from the wing tip to the point under examination was the single parameter which governed vortex core diameter, vortex rollup, peak swirl velocity, and mean axial velocity for a given lift coefficient. The report concluded that the usual processes observed in vortex growth and dissipation were independent of Mach number and Reynolds number, but were strongly dependent on vortex age for a specified C_L. If this, indeed, was an accurate conclusion it would represent a real breakthrough in the field of wake turbulence research.

In an effort to verify and extend the work of Rorke and Moffitt[2], the present study was conducted by examining the flow downstream of a single NACA 0012 wing at various angles of attack over a range of downstream distances and free stream speeds designed to produce several predetermined values of vortex age. The end surface of the wing tip was flat. Downstream test stations were at distances from two to thirty chordlengths from the wing. It was hoped that this systematic approach would give less data scatter than that encountered by Rorke and Moffitt, and that the larger downstream distances of this study would provide a more general view of the vortex development than was possible in very short downstream distances (2 or 5 chordlengths) studied in that report.

EXPERIMENTAL PROCEDURE

Tests were conducted in the six by six foot test section of the Virginia Tech Stability Wind Tunnel shown in Figure 2. All tests were run using an NACA 0012 wing of eight inch chord and four foot span, the airfoil was hung from the wind tunnel test section ceiling as shown in Figure 3. The trailing vortex was examined using a 1/8 inch diameter, five hole yaw head pitot probe (Fig. 4) mounted on a vertical traverse mechanism as shown in Figure 3. This traverse system was also capable of horizontal motion. This probe could be positioned at downstream distances up to thirty chordlengths from the wing. Each pressure tap was connected to a sensitive inclined manometer for data accumulation. A detailed description of the apparatus involved is given in Reference 1. The probe was fully calibrated using the Winternitz method as described in Reference 3.

The test procedure was a straightforward one. A complete test schedule is given in Table 1. Before each test series the probe was aligned with the undisturbed uniform tunnel flow at the test speed and at the desired downstream position. The airfoil was then mounted at the desired angle of attack and the tunnel set at the test speed. The test procedure began by finding the vortex center where flow angularity was zero. After finding the vortex center, the probe was moved slowly spanwise to preset intervals and data recorded after the flow and resulting pressure had stabilized. Using this procedure, both the inboard and outboard sides of the vortex were investigated. In the reduction of the data, axes were fixed at the center of the vortex core with inboard distances along the wing span considered positive.

TABLE I

TEST SCHEDULE

α	z/c	Q	Run No.
4	2	1.5	34
4	5	1.5	33
4	10	0.97	19
4	10	2.2	18
4	15	0.54	22
4	15	0.97	23
4	15	2.2	24
4	20	0.97	13
4	20	2.2	14
4	25	0.97	3
4	25	1.5	2
4	25	2.2	1
4	30	0.97	9
4	30	2.2	8
6	15	0.54	25
6	20	0.97	15
6	25	1.5	7
6	30	2.2	10
8	2	0.97	31
8	2	2.2	29
8	5	0.97	32
8	5	2.2	30
8	10	0.97	20
8	10	2.2	21
8	15	0.54	26
8	15	0.97	27
8	15	2.2	28
8	20	0.97	16
8	20	2.2	17
8	25	0.97	4
8	25	1.5	5
8	25	2.2	6
8	30	0.97	12
8	30	2.2	11

RESULTS AND DISCUSSION

The results of the tests are given as plots of nondimensional tangential velocity, dimensional tangential velocity and axial velocity across the vortex in Figures 5-106. In all figures distances inboard of the vortex center are shown as positive. These data are similar to those obtained by many previous researchers and at first glance show nothing surprising. It should be noted that at stations near the wing (z/c = 2,5) the vortex does not appear as symmetrical as at stations further downstream. This is due to the highly three dimensional nature of the flow in the immediate wing wake and the ensuing difficulty in measuring the resulting flow components. At most test stations this problem was not encountered and the results indicate the classical vortex flow pattern. The consistency of the results suggests confidence in the data and data reduction procedures, however, the goal of this study was to examine the development of the vortex downstream of the wing rather than the detailed vortex structure. Since the peak swirl or tangential velocity and the core size are considered to be the significant growth and/or dissipation aspects of the vortex structure, these were examined in more detail.

Figure 107 plots the change in the normalized maximum tangential velocity with downstream distance. This is a fairly conventional method of plotting vortex growth or dissipation and, as in most previous studies, a slow decrease in peak swirl speed is noted as the flow proceeds downstream of the wing. The significant result noted in this figure is that while all the data taken at an angle of attack of four degrees seem to fall on a single curve, those at eight degrees form two distinct curves although data in both cases were taken over the same speed increments. The nature of the data is

consistent with previous studies such as Reference 4, however these results are the first known to the authors which show a definite speed effect at a given angle of attack. It is evident that the effect is not one of speed alone but is also dependent on angle of attack. It appears that freestream speed has an increasing influence on peak swirl velocity in the vortex as angle of attack approaches stall conditions. It was at first thought that this effect might be due to stall; however, the NACA 0012 wing does not stall until an angle of attack of approximately twelve degrees is reached.

Since the object of this research was to investigate the dependence of the vortex on age, a second plot of the peak tangential velocity was made as Figure 108. It was felt that, if age was the significant governing parameter in vortex growth, plotting the data versus age would possibly collapse the $\alpha = 8^{o}$ data into a single curve, thus indicating that the effect seen in Figure 107 was due to the different ages resulting from the different speeds used. However, Figure 108 again shows consistency in the data and two separate curves for the different speeds used at eight degrees angle of attack. It is evident from this graph that vortex age is not a self-sufficent parameter for the description of vortex growth or dissipation. There is a very real speed effect at the eight degree angle of attack which is not explained by considering vortex age.

Another significant parameter usually considered in vortex dissipation or growth is the core diameter. Figures 109 and 110 show vortex diameter (nondimensionalized by wing chord) plotted versus downstream distance and vortex age, respectively. There is more scatter in this data than in the tangential velocity data due largely to the difficulty of accurately determining the exact core limits (points of maximum tangential velocity) from the velocity profiles. These plots indicate that core size might be more

directly dependent than the tangential velocity on age, however the scatter in the data precludes a definitive conclusion to that effect.

These conclusions, particularly those based on the eight degree data of Figures 107 and 108, contradict those of Rorke and Moffitt[2] who ruled out any Reynolds number or Mach number effects for their particular six degree and nine degree data. The principal data of Rorke and Moffitt are presented as Figures 111 and 112. When their data is broken down according to both speed and angle of attack as it is in these figures one notes that there is really insufficient data to note any speed effect at high (9^{o}) angles of attack. Since the data in Figure 111 does not overlap agewise sufficiently to conclude whether the nine degree data forms a single curve or three separate curves and the data in Figure 112 shows considerable scatter, it is impossible to conclude that speed effects are negligible at high angles of attack. A comparison of the data in Figure 111 with that of Figure 108 is given in Figure 113. It is seen that the data of Reference 2 is in the same range as that of the present study, however, it is not possible to draw further conclusions from this graph. A plot of the same data versus downstream distance is also presented as Figure 114.

Part of the problem in the consistency of the Rorke and Moffitt[2] data stems from their close proximity to the wing. The highly three dimensional flows at two and five chordlengths distance from the wing gives results which make it quite difficult to obtain meaningful values of maximum tangential velocity and core diameter. When the peak swirl speed on one side of a vortex is twice that on the other side, it is difficult to define an average velocity which would be representative. Similar problems occurred

in the present study at test stations close to the wing; however, by comparing the data at these stations with those taken further downstream, where there was no problem of this type, a more meaningful result could be concluded.

In examining the data for the eight degree angle of attack tests in an attempt to isolate the cause for the noted speed-effect it was found that the axial velocity plots (Figs. 73 - 106) show a velocity excess for all the higher speed tests whereas almost all the low speed runs (except those close to the wing) fail to exhibit such an velocity pattern. At lower angles of attack a small axial velocity deficit is always present. It appears that axial velocity is dependent on angle of attack and speed and this dependency exhibits an effect similar to that of the tengential velocity. Figures 115 and 116 show the peak axial velocities versus downstream distance and time.

CONCLUSIONS

This study has shown conclusively that vortex age is not a self sufficient wake turbulence scaling parameter. The results indicate that free stream speed has a definite influence on vortex growth and decay, especially at higher angles of attack. This effect does not seem to be one due to Mach number or Reynolds number in a classical sense. Attempts were made to further define this apparent speed effect at higher angles of attack; however,they were unsuccessful. A possible explanation may come from the nature of the flow at the wing tip itself. At high angles of attack these is a spanwise flow separation on the upper surface at the wing tip as the flow moves around the tip. This separation is, of course, highly dependent on wing tip shape.

Since the wing tip in these tests was not rounded (a straight sawed off tip was used), there is more of a tendency for spanwise tip separation at high angles of attack. This separation would be affected by free stream speed and may account for some of the speed effect noted at high angles. The net effect of such separation may be to cause early formation of the vortex over the upper surface of the wing, leading to the development of a much stronger vortex with higher swirl velocities and large axial velocity excesses. Tuft and oil flow visualization studies were used to try to observe such an effect but the results failed to shed further light on the subject. The study of Rorke and Moffitt[2] employed a rounded wing tip which may have reduced this effect. It is known that wing tip planform has a great effect on trailing vortices and it may well be that the tip edge shape also has some effect.

Further study of this phenomenon is recommended to determine the exact nature of the speed effect noted in this investigation. It appears that vortex age is a significant parameter in the description of wake turbulence; however, it cannot be used alone.

REFERENCES

1. Mason, H. W. and Marchman, J. F., "Farfield Structure of an Aircraft Trailing Vortex, Including Effects of Mass Injection", NASA CR-62078, April, 1972.

2. Rorke, J. B. and Moffitt, R. C., "Wind Tunnel Simulation of Full Scale Vortices", NASA CR-2180, March 1973.

3. Winternitz, F. A. A., "Probe Measurements in Three Dimensional Flow", Aircraft Engineering, August 1956, p. 273

4. Chigier, N. A. and Corsiglia, V. R., "Wind Tunnel Studies of Wing Wake Turbulence", AIAA Paper No. 72-41. January 1972.

FIGURES

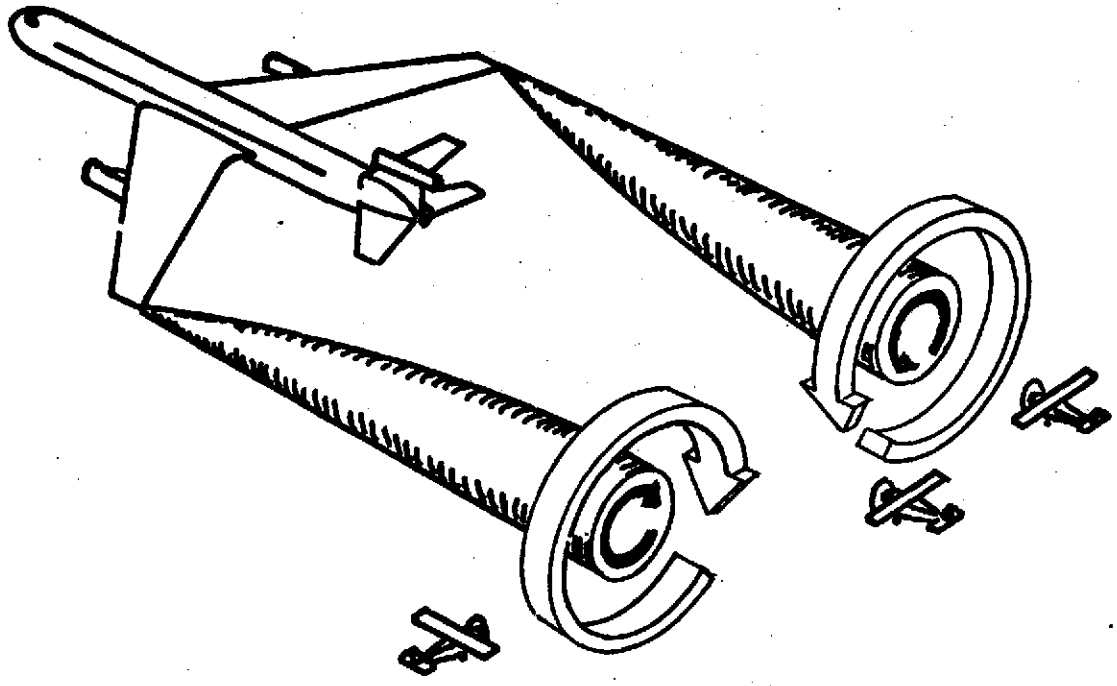

Figure 4 Illustration of typical trailing vortices and types of encounter.

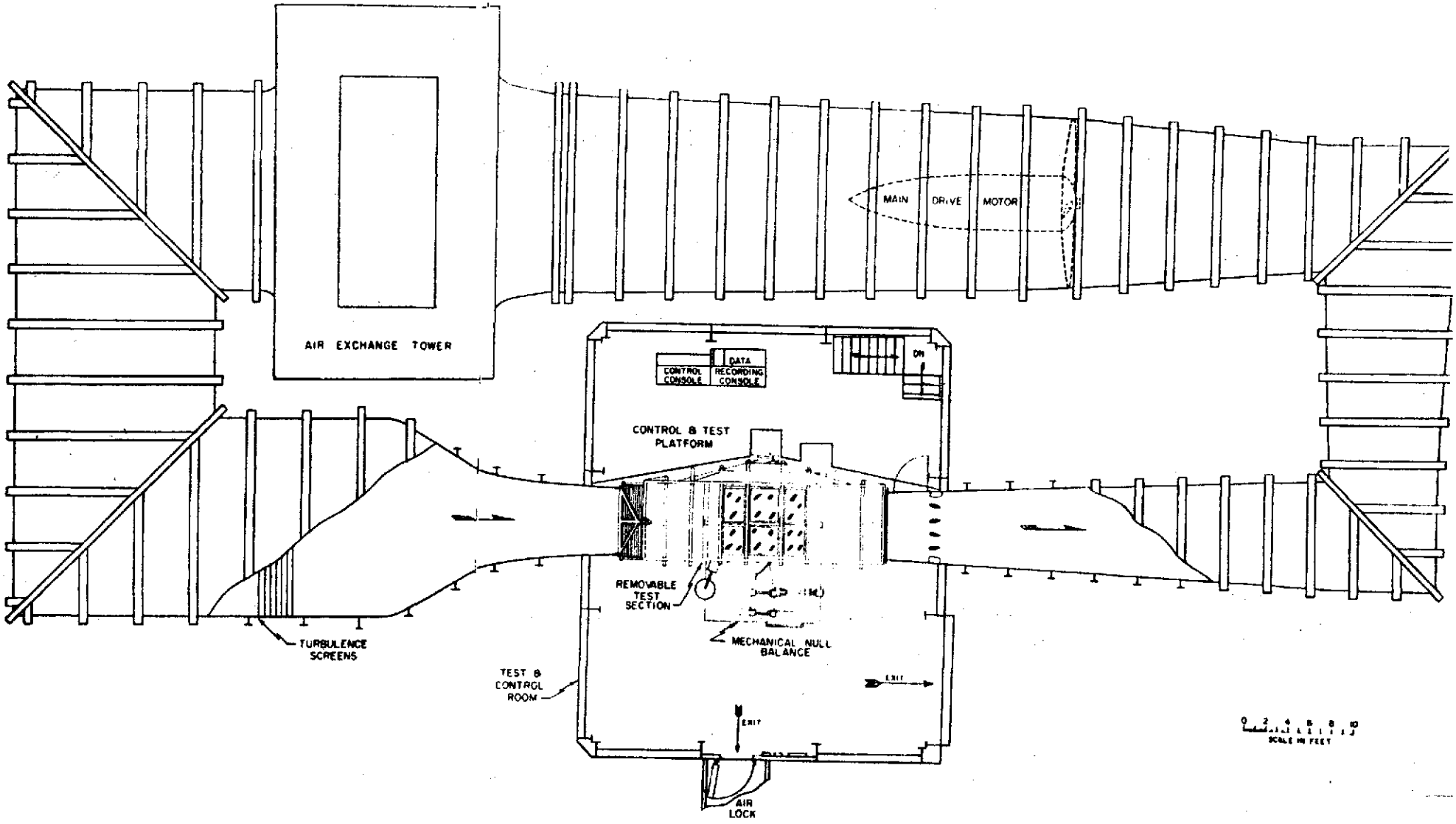

Fig. 2. Virginia Tech Stability Wind Tunnel

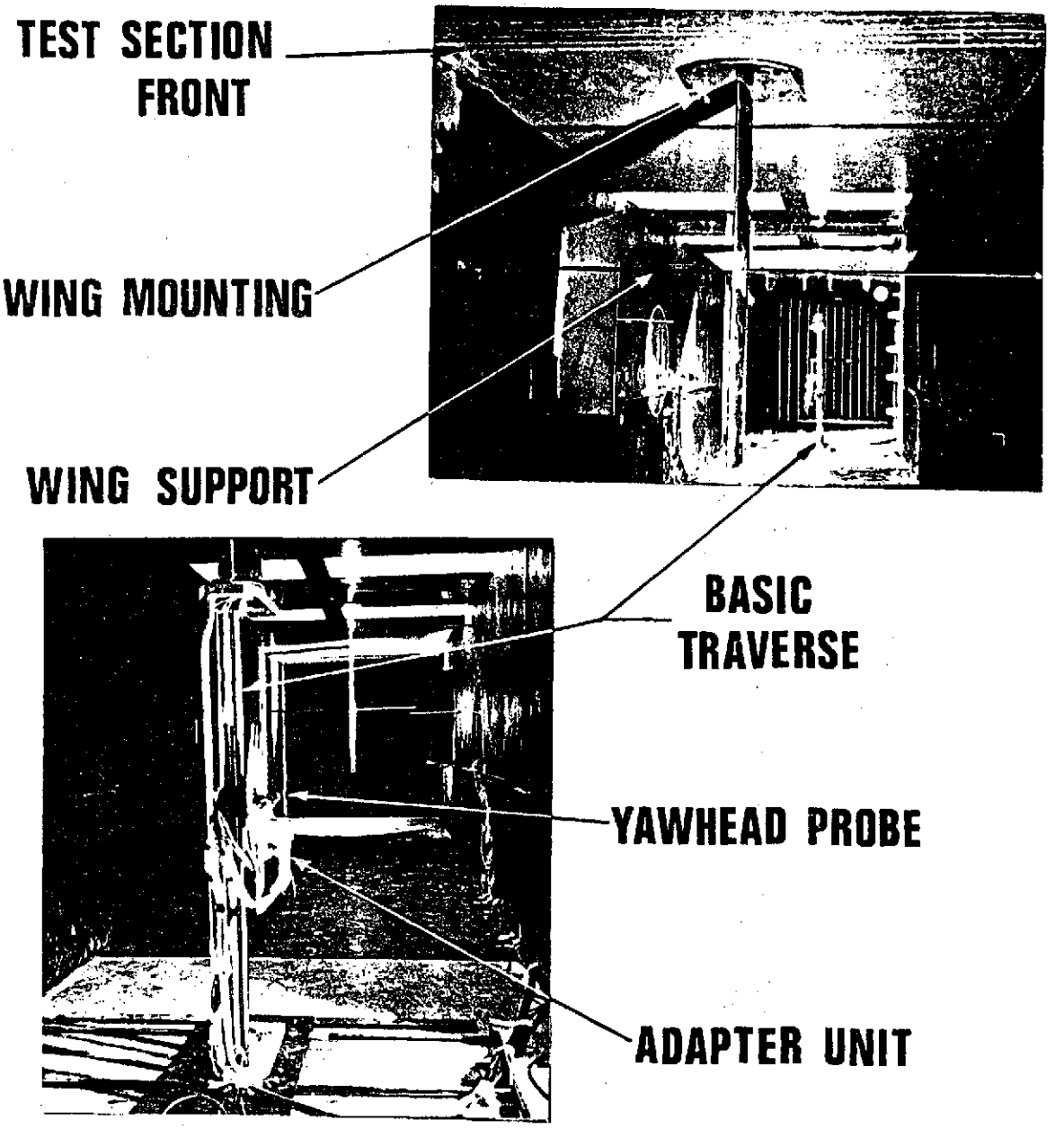

FIG.3 WIND TUNNEL TEST SET UP

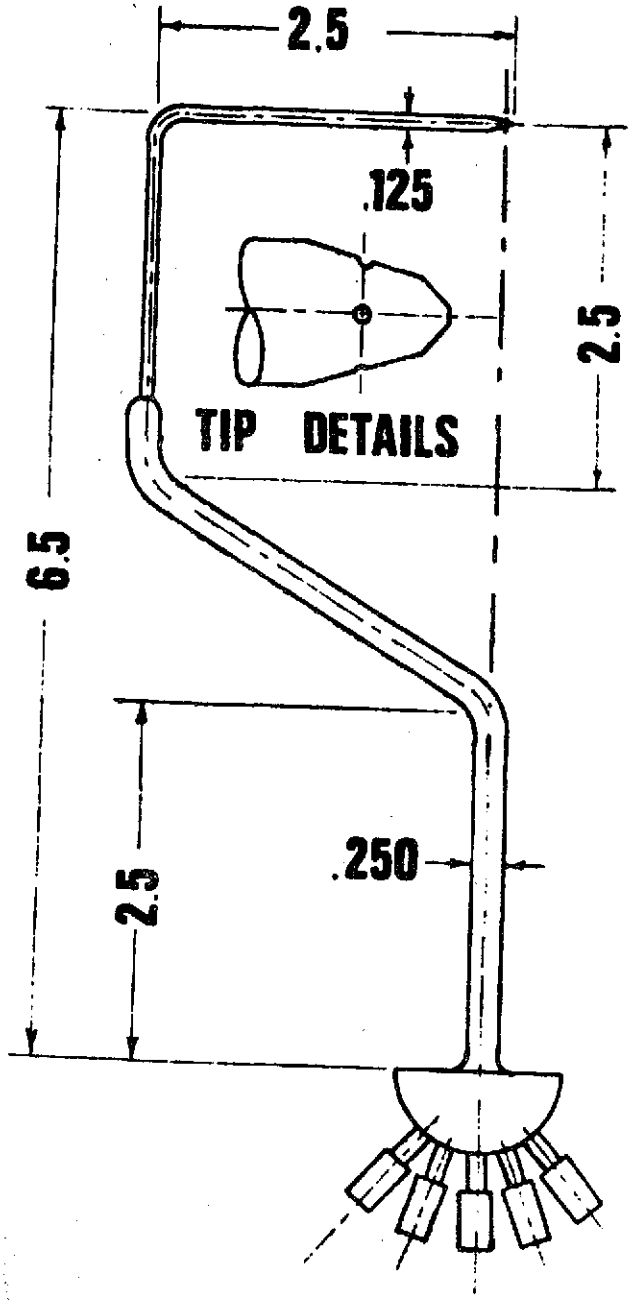

FIG 4. YAWHEAD PROBE

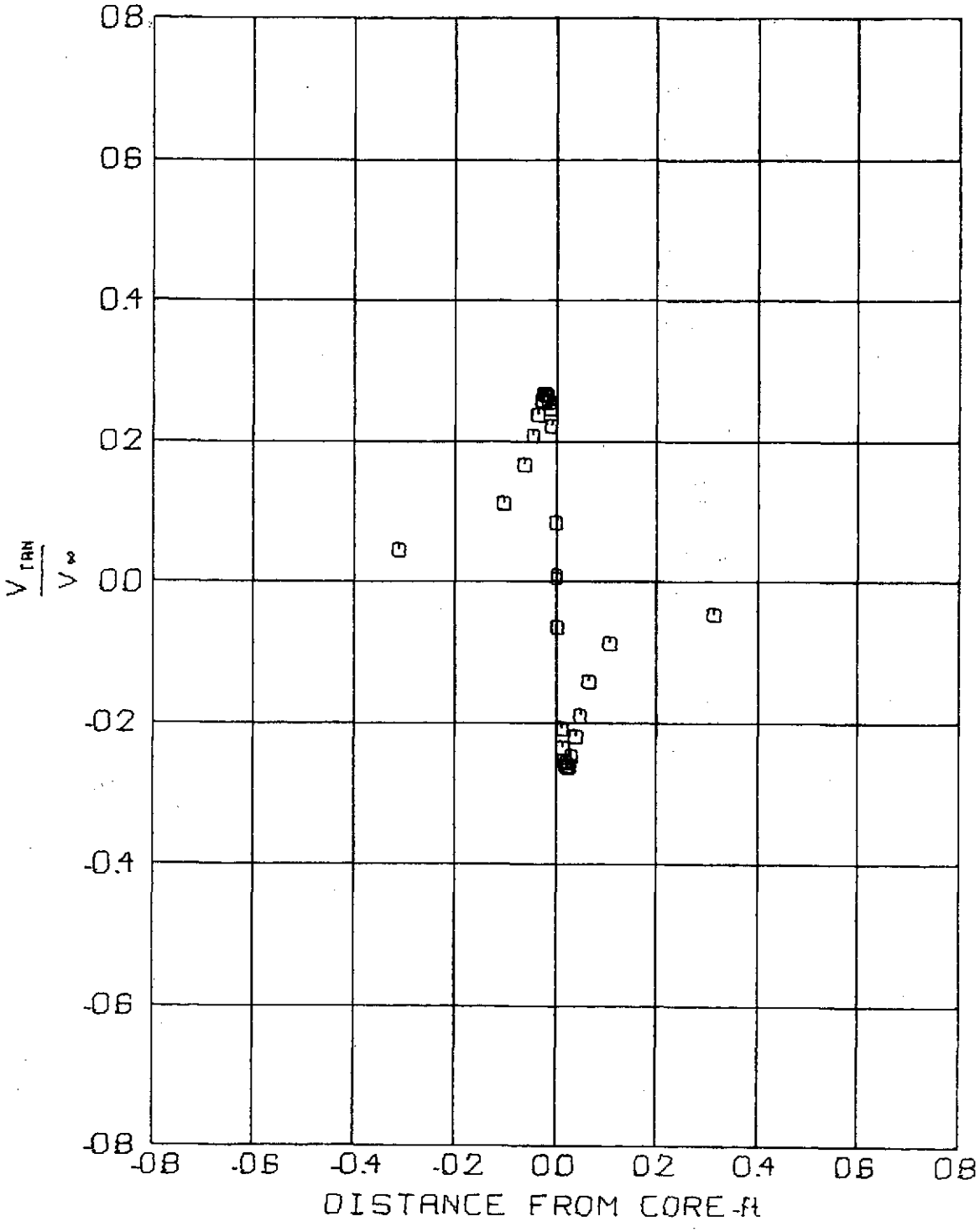

FIG 5 TANGENTIAL VELOCITY PROFILE

V_∞ = 86.8 f/s Z/C = 2
α = 4° t = .01535 sec

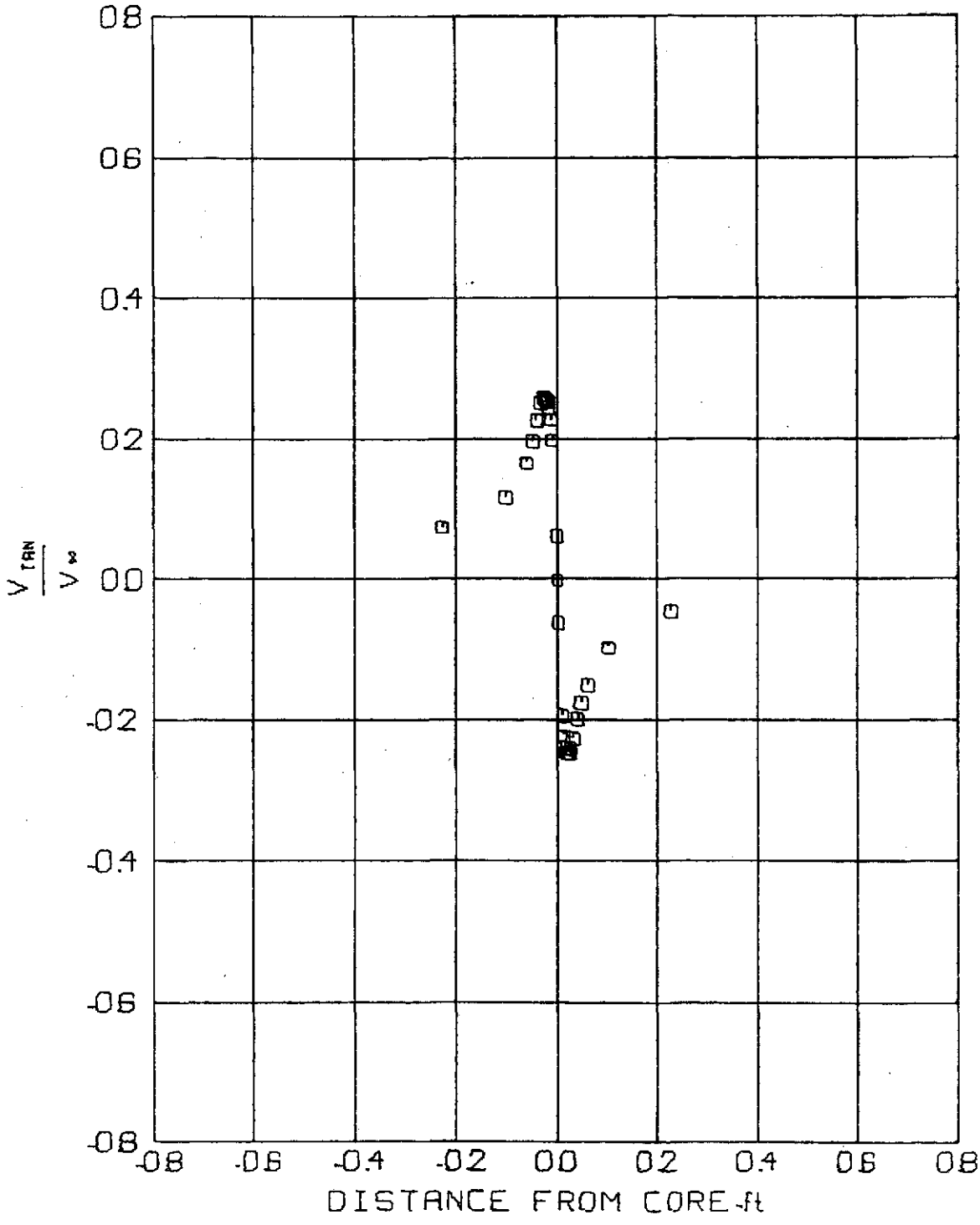

FIG 6 TANGENTIAL VELOCITY PROFILE

V_∞ = 86.7 f/s Z/C = 5
α = 4° t = .03840 sec

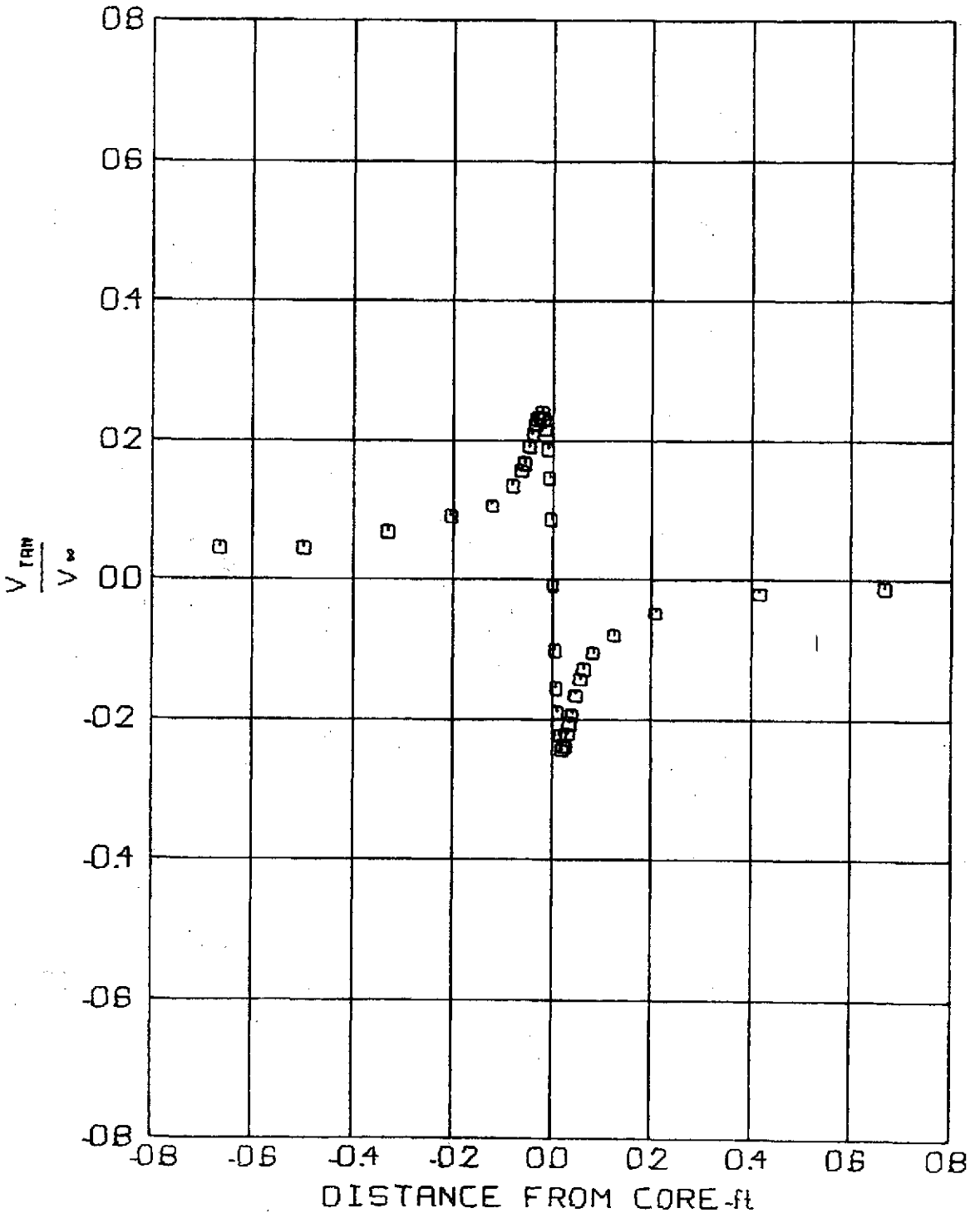

FIG 7 TANGENTIAL VELOCITY PROFILE

V_∞ = 68.6 f/s Z/C = 1.0
α = 4° t = .09713 sec

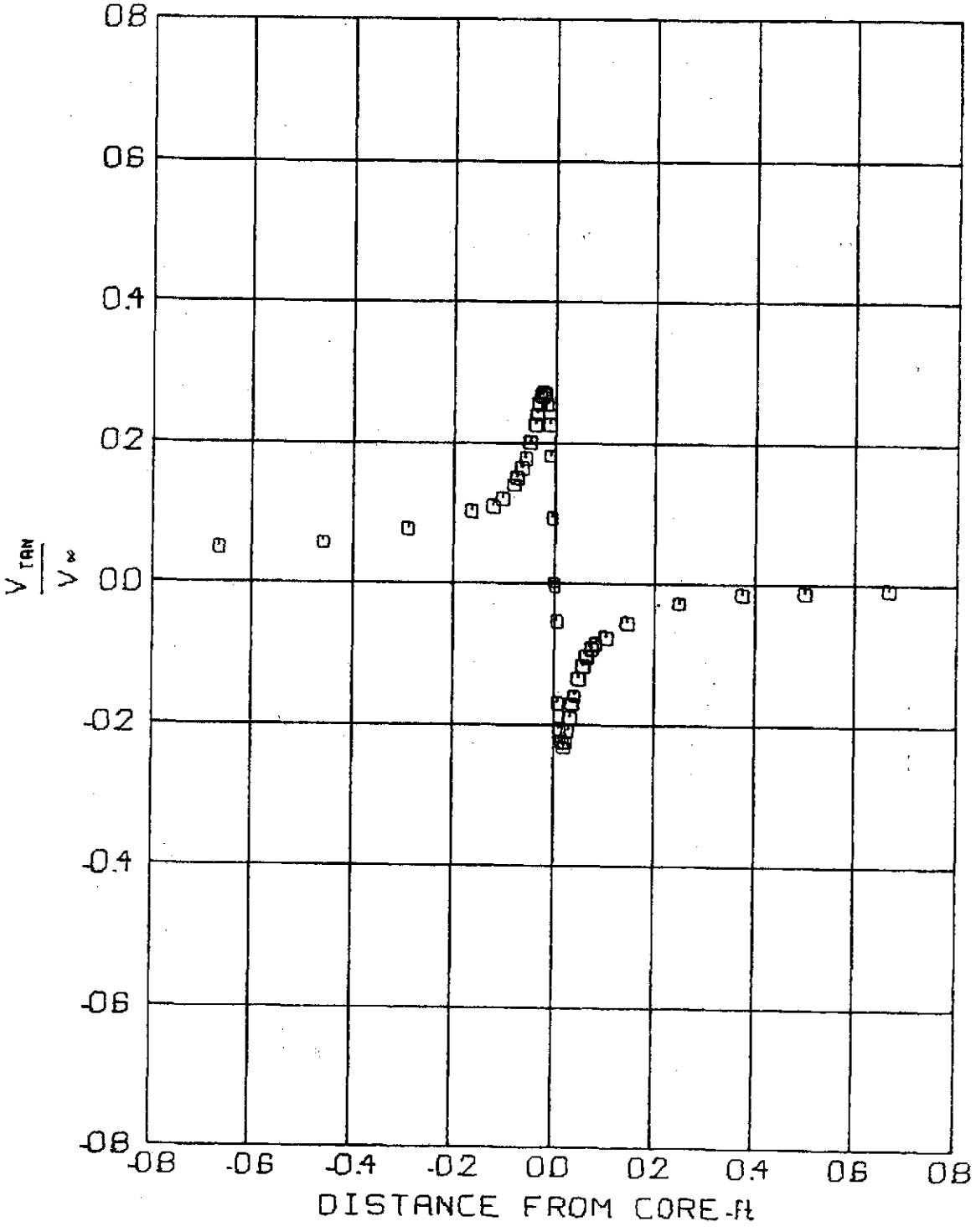

FIG 8 TANGENTIAL VELOCITY PROFILE

V_∞ = 98.3 f/s Z/C = .10
α = 4° t = .06780 sec

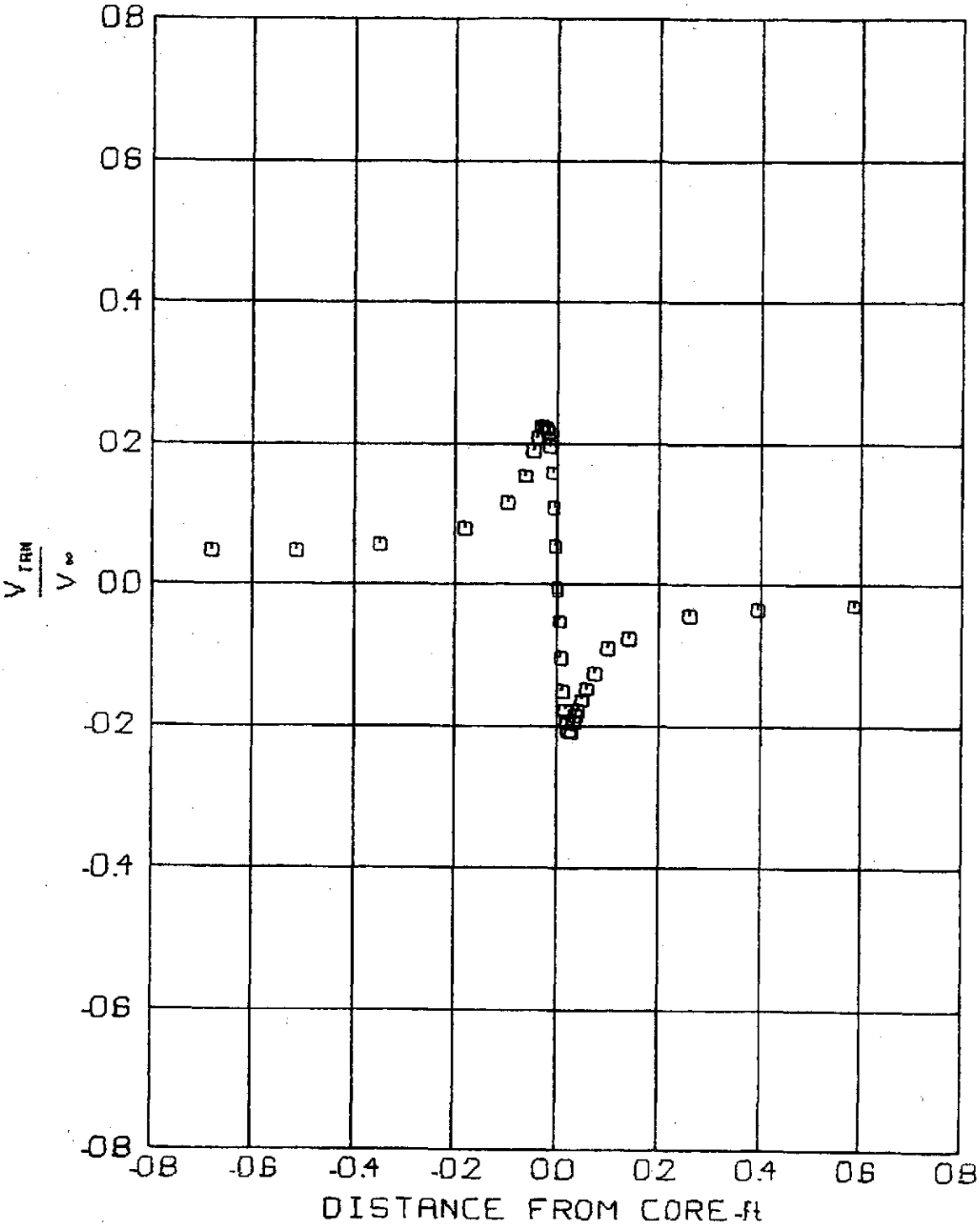

FIG 9 TANGENTIAL VELOCITY PROFILE

V_∞ = 49.3 f/s Z/C = 1.5
α = 4° t = .20246 sec

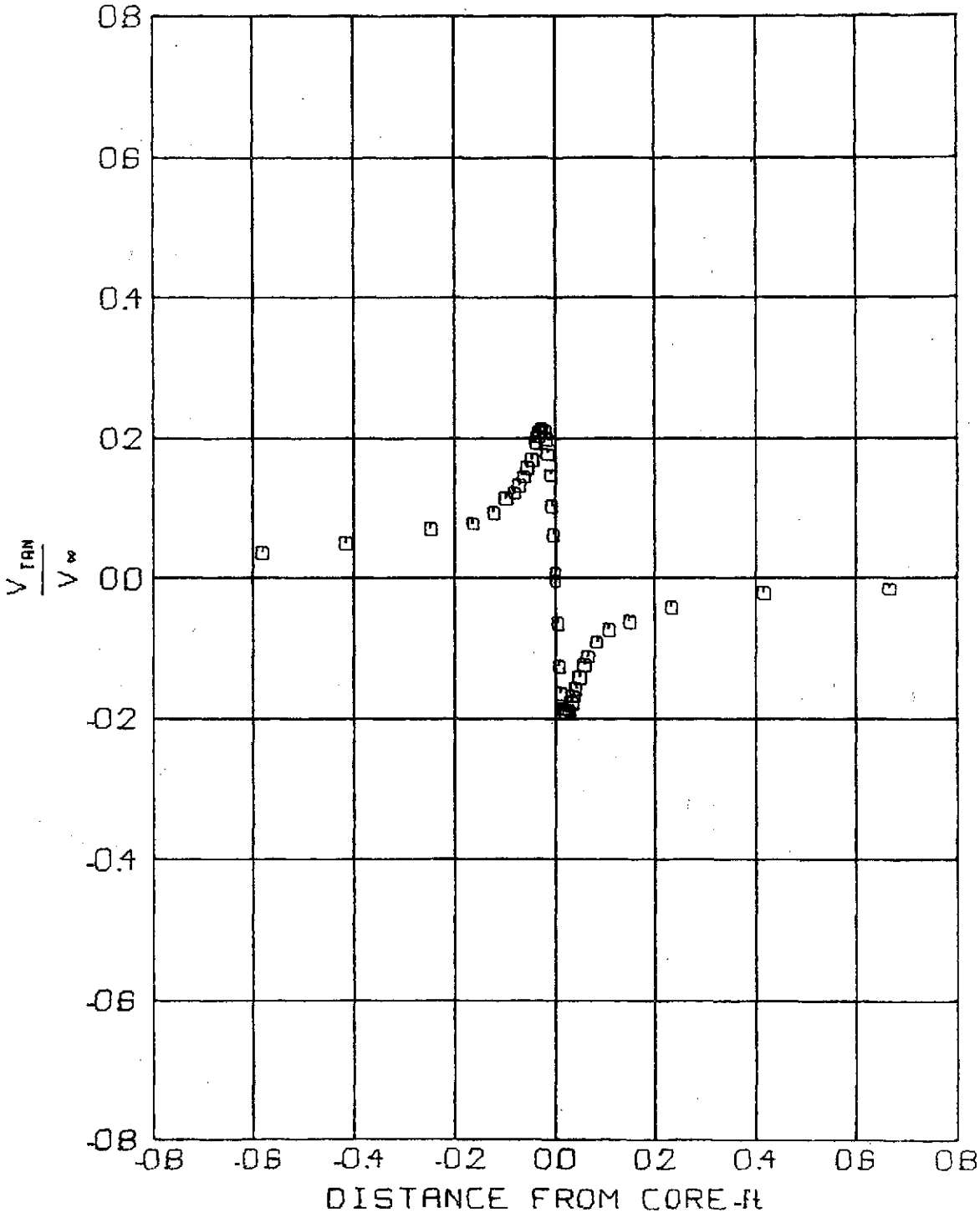

FIG 10 TANGENTIAL VELOCITY PROFILE

V_∞ = 67.2 f/s Z/C = 15
α = 4° t = .14879 sec

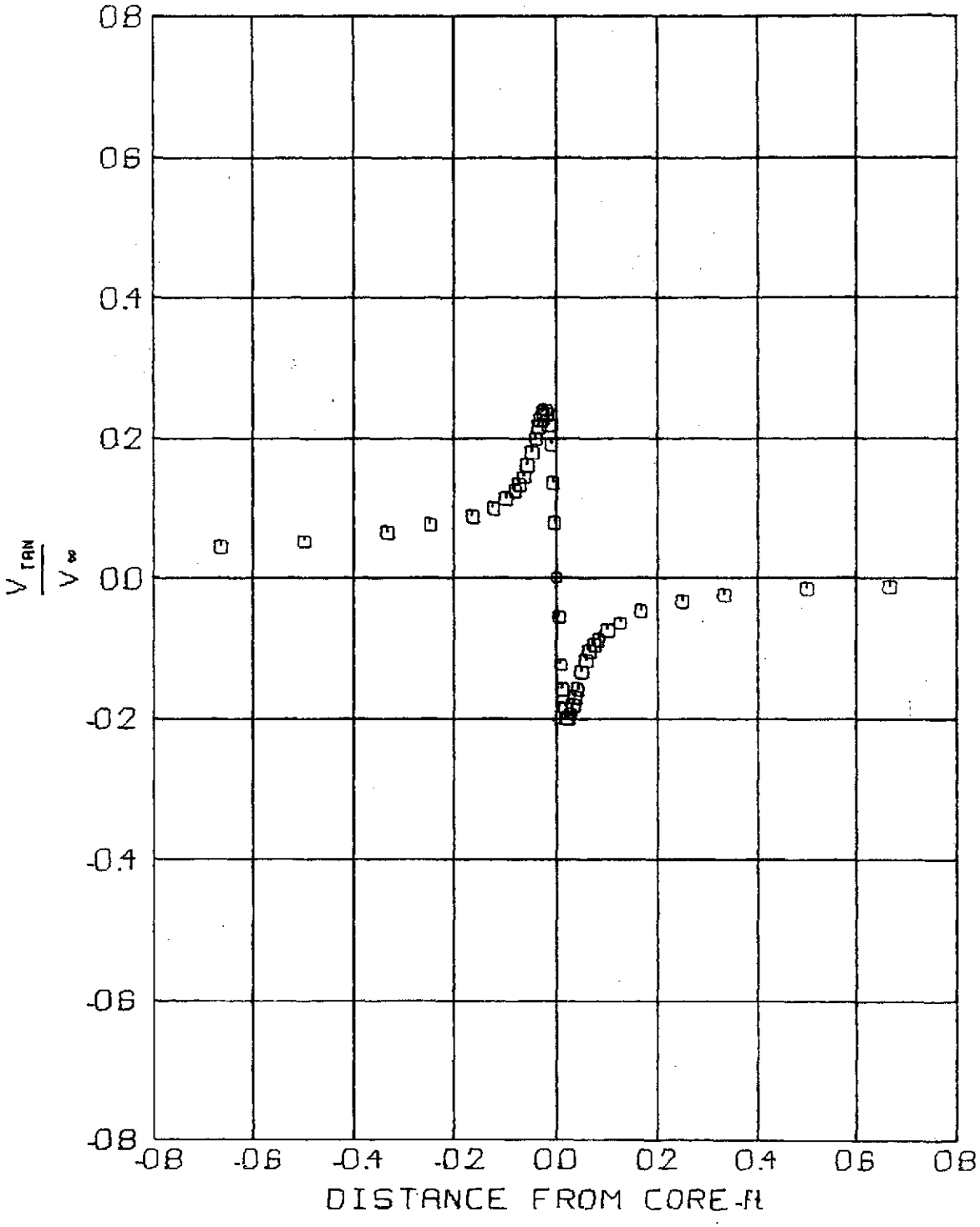

FIG 11 TANGENTIAL VELOCITY PROFILE

V_∞ = 100.8 f/s Z/C = 15
α = 4° t = .09920 sec

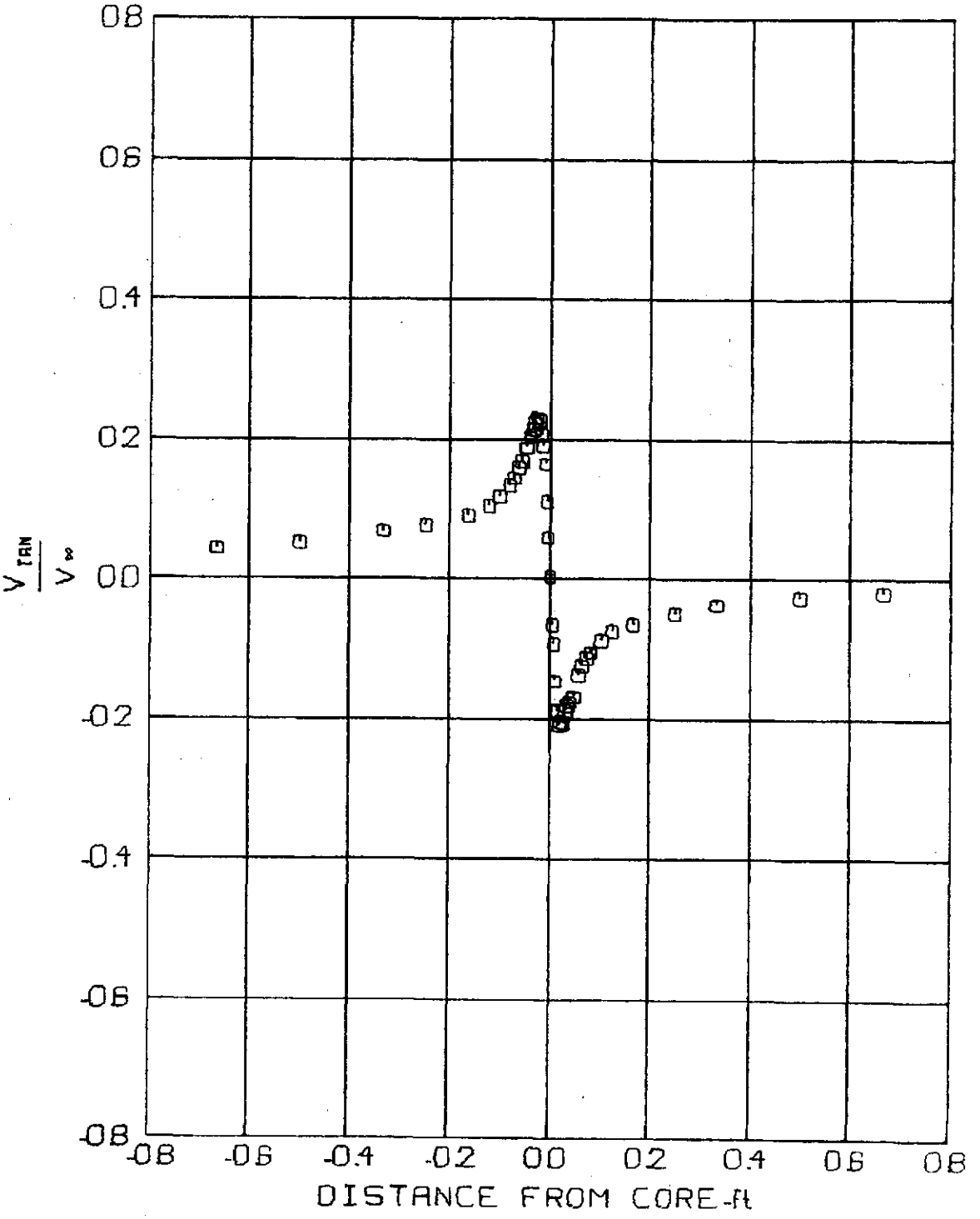

FIG 12 TANGENTIAL VELOCITY PROFILE

V_∞ = 68.4 f/s Z/C = 20
α = 4° t = .19469 sec

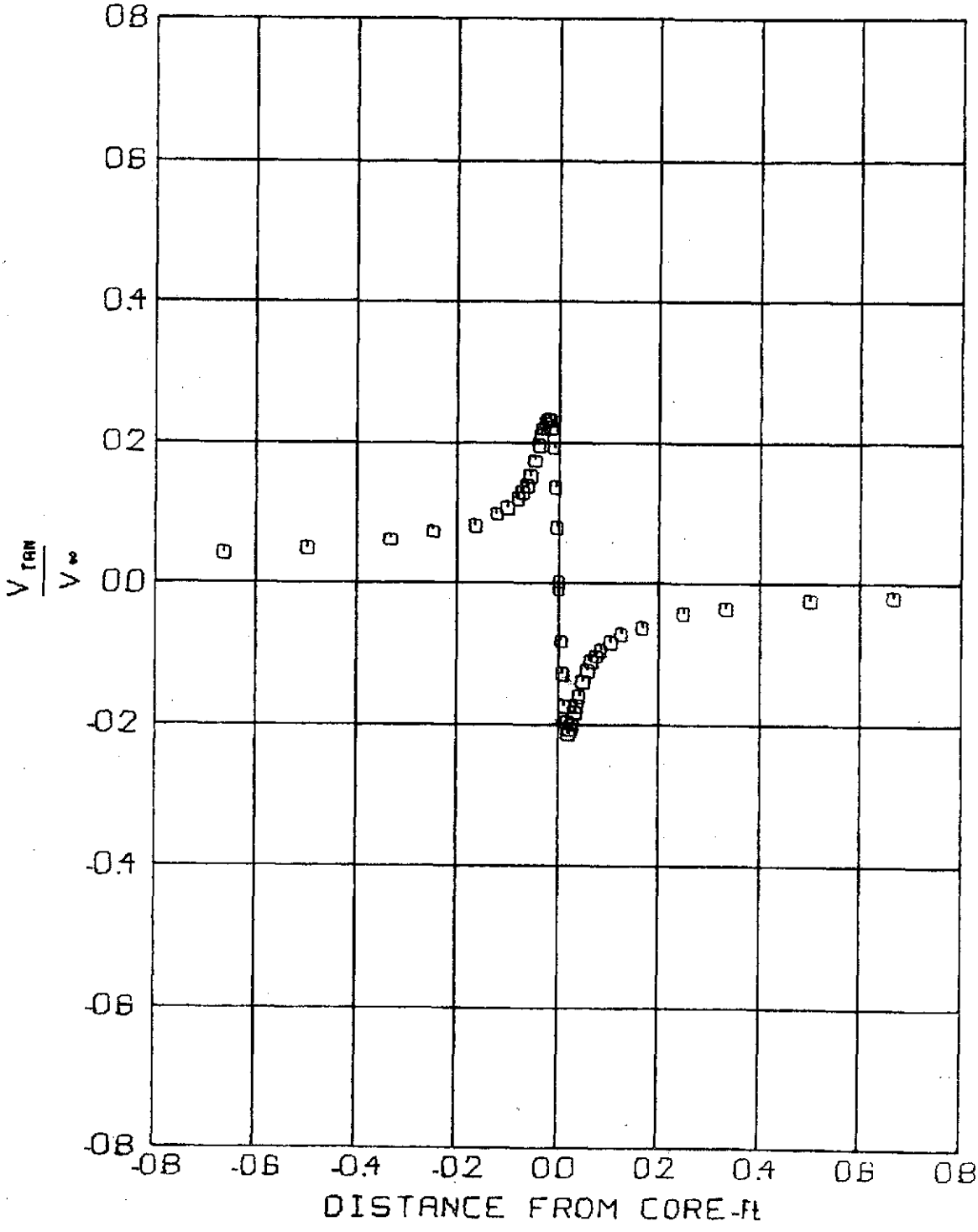

FIG 13 TANGENTIAL VELOCITY PROFILE

V_∞ = 103.3 f/s Z/C = 20
α = 4° t = .12897 sec

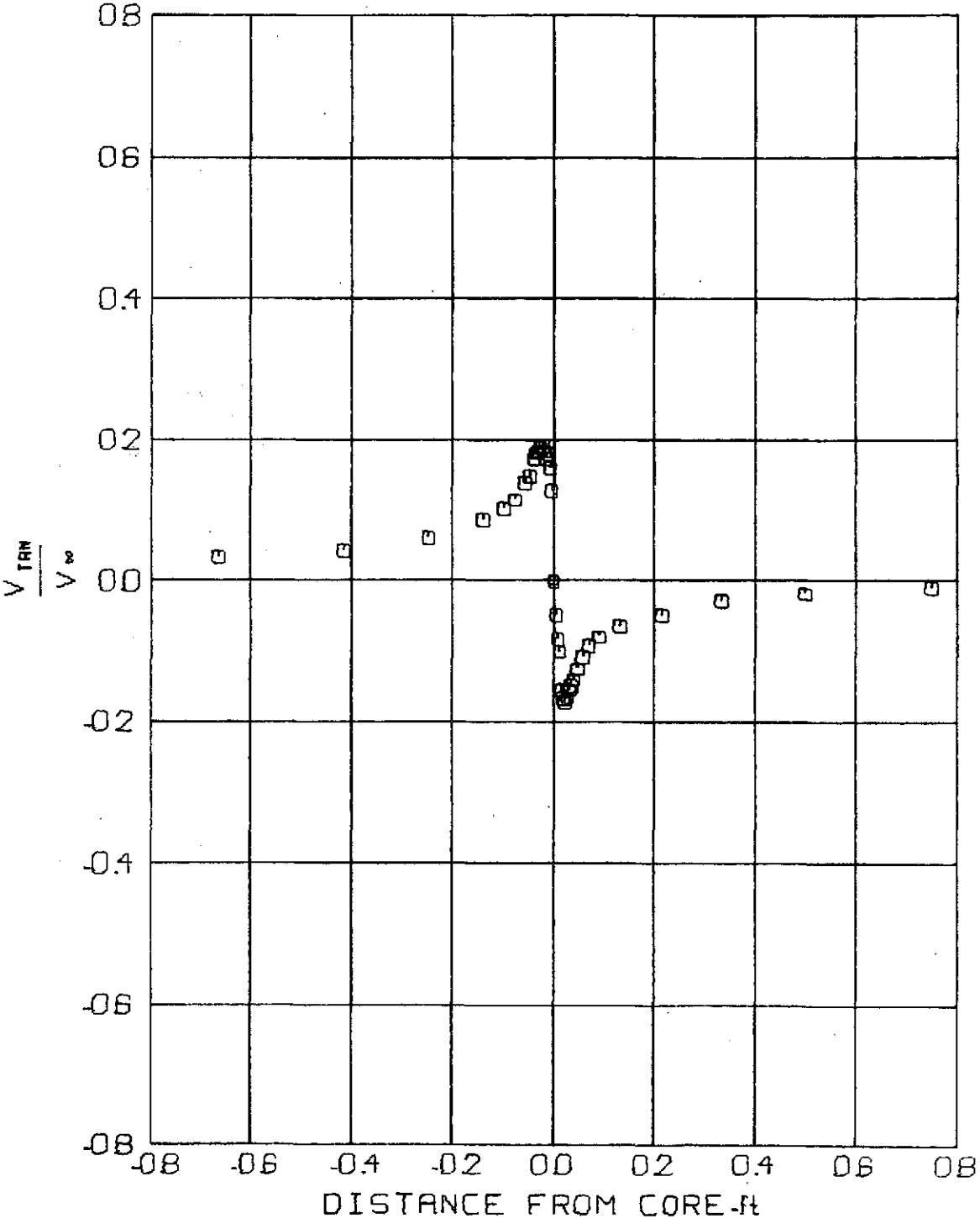

FIG 14 TANGENTIAL VELOCITY PROFILE

V_∞ = 68.4 f/s Z/C = 25
α = 4° t = .24337 sec

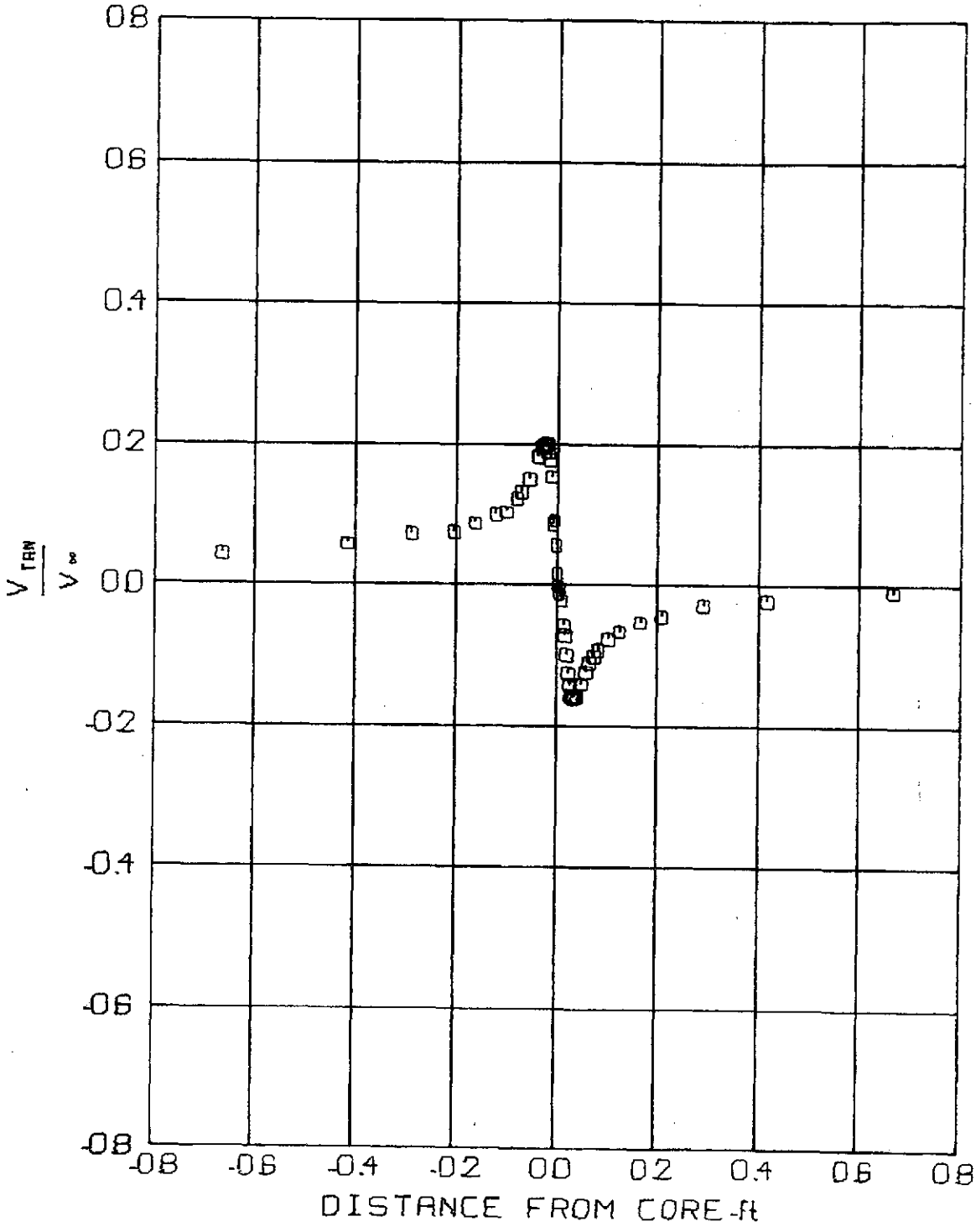

FIG 15 TANGENTIAL VELOCITY PROFILE

V_∞ = 86.5 f/s Z/C = 25
α = 4° t = .19256 sec

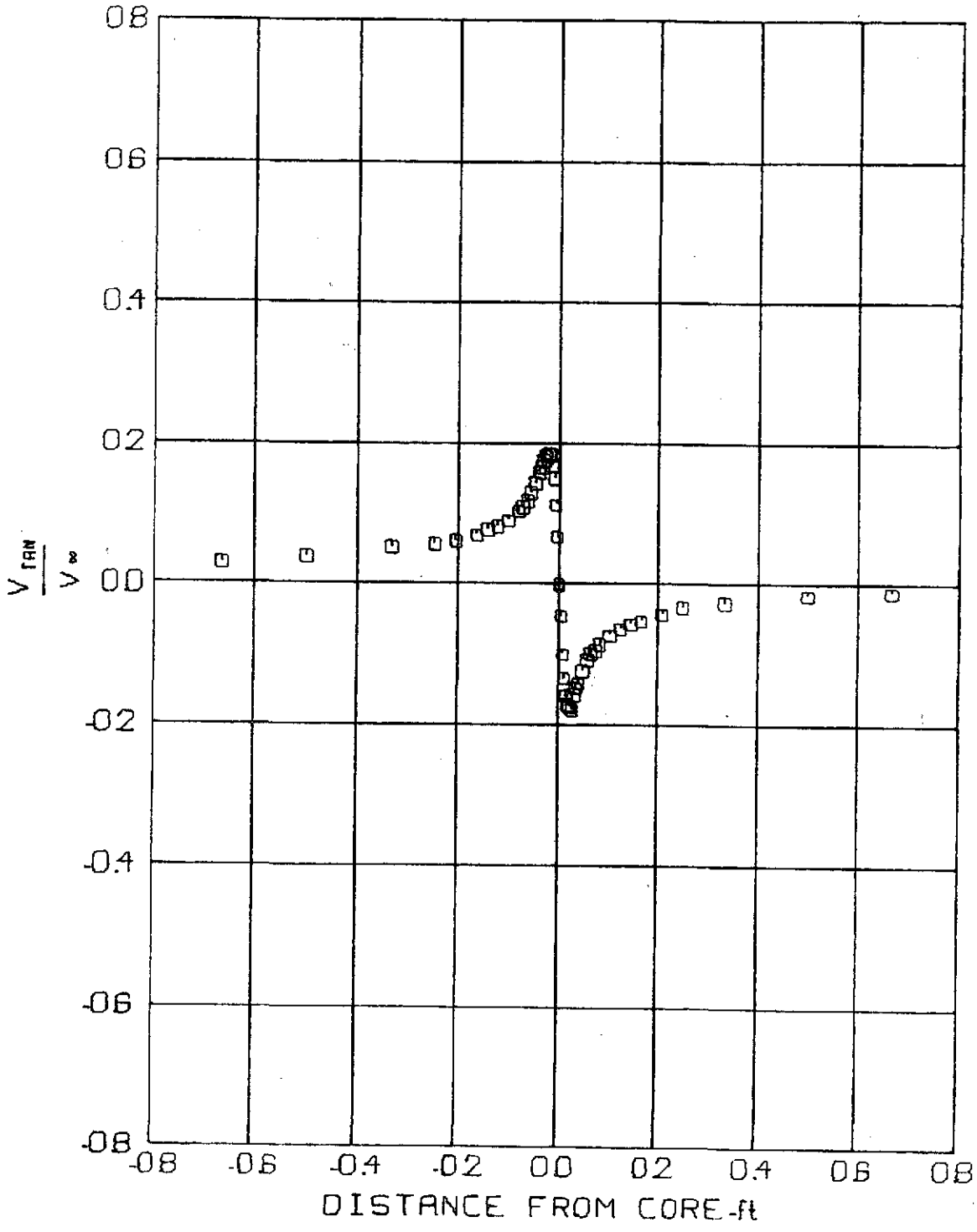

FIG 16 TANGENTIAL VELOCITY PROFILE

V_∞ = 102.8 f/s Z/C = 25
α = 4° t = .16199 sec

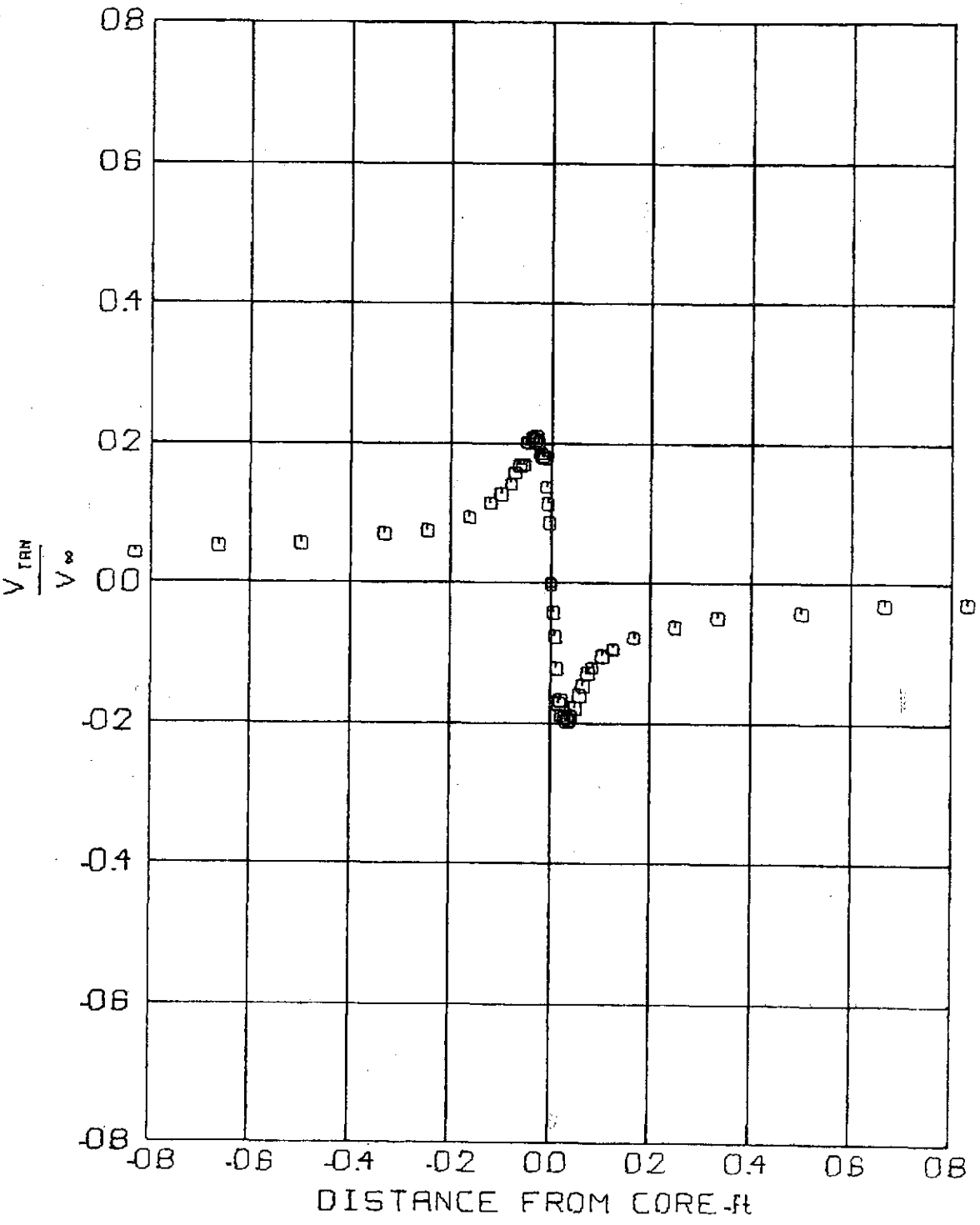

FIG 17 TANGENTIAL VELOCITY PROFILE

V_∞ = 69.4 f/s Z/C = 30
α = 4° t = .28790 sec

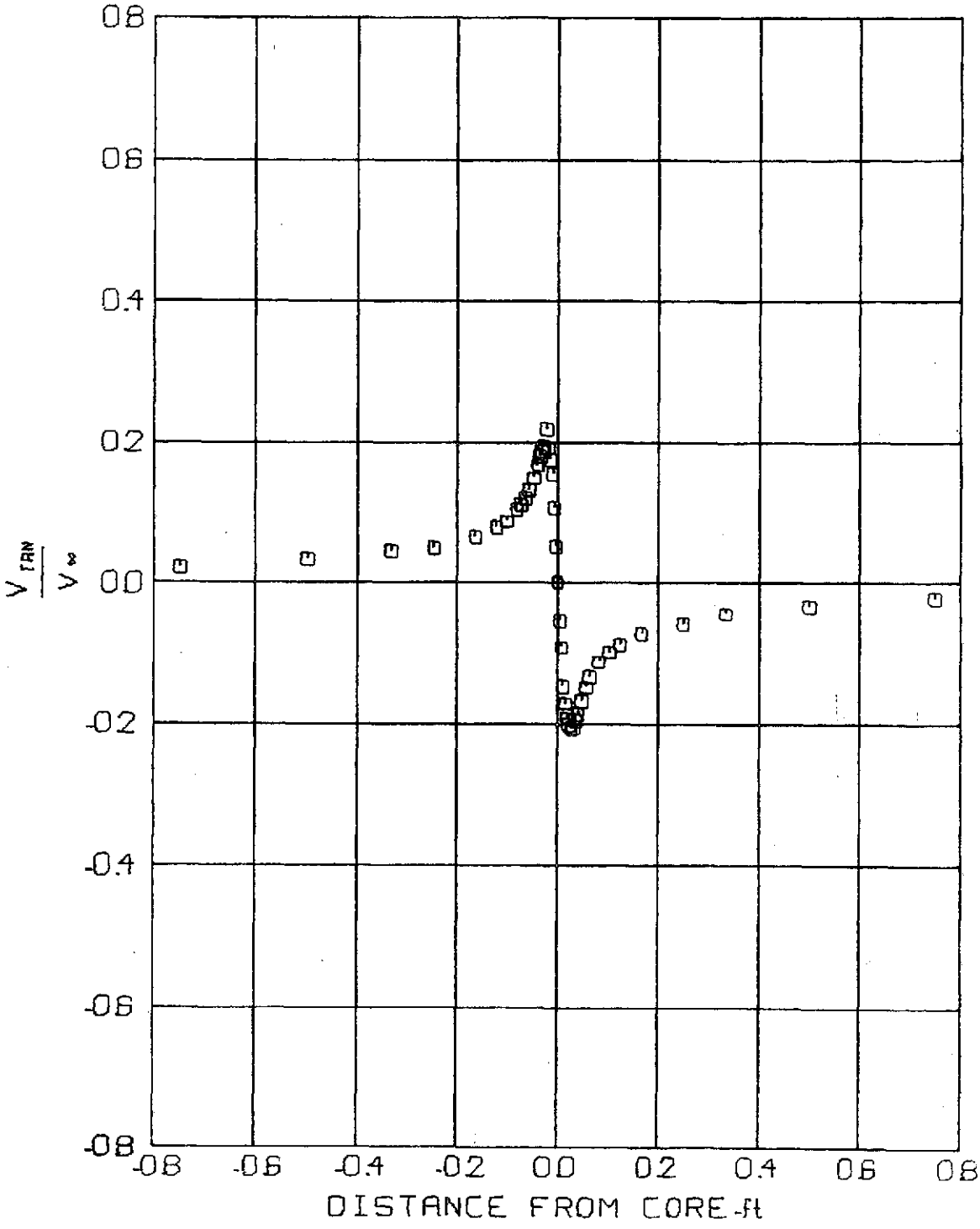

FIG 18 TANGENTIAL VELOCITY PROFILE

V_∞ = 105.6 f/s Z/C = 30
α = 4° t = .18928 sec

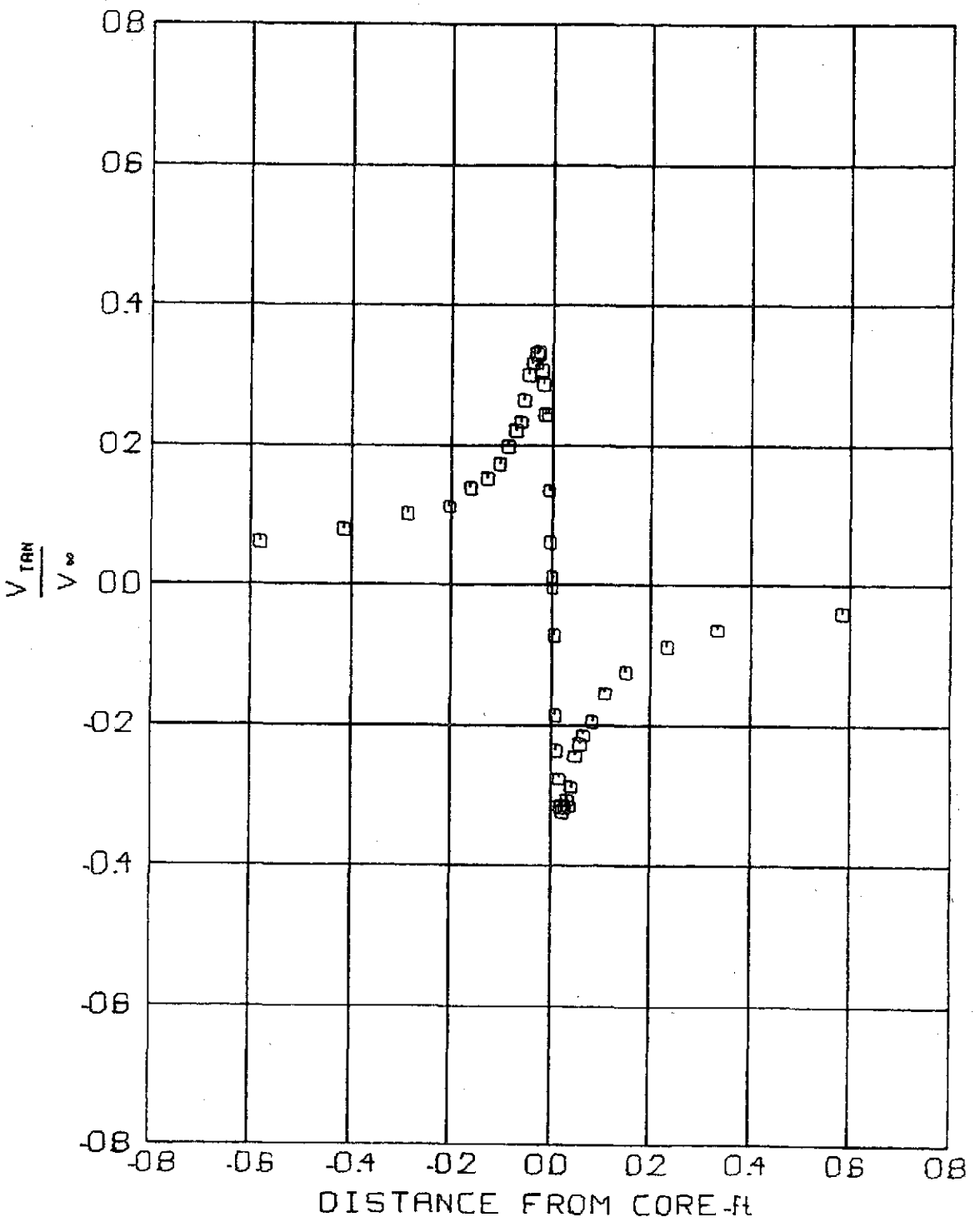

FIG 19 TANGENTIAL VELOCITY PROFILE

V_∞ = 49.1 f/s Z/C = 15
α = 6° t = .20348 sec

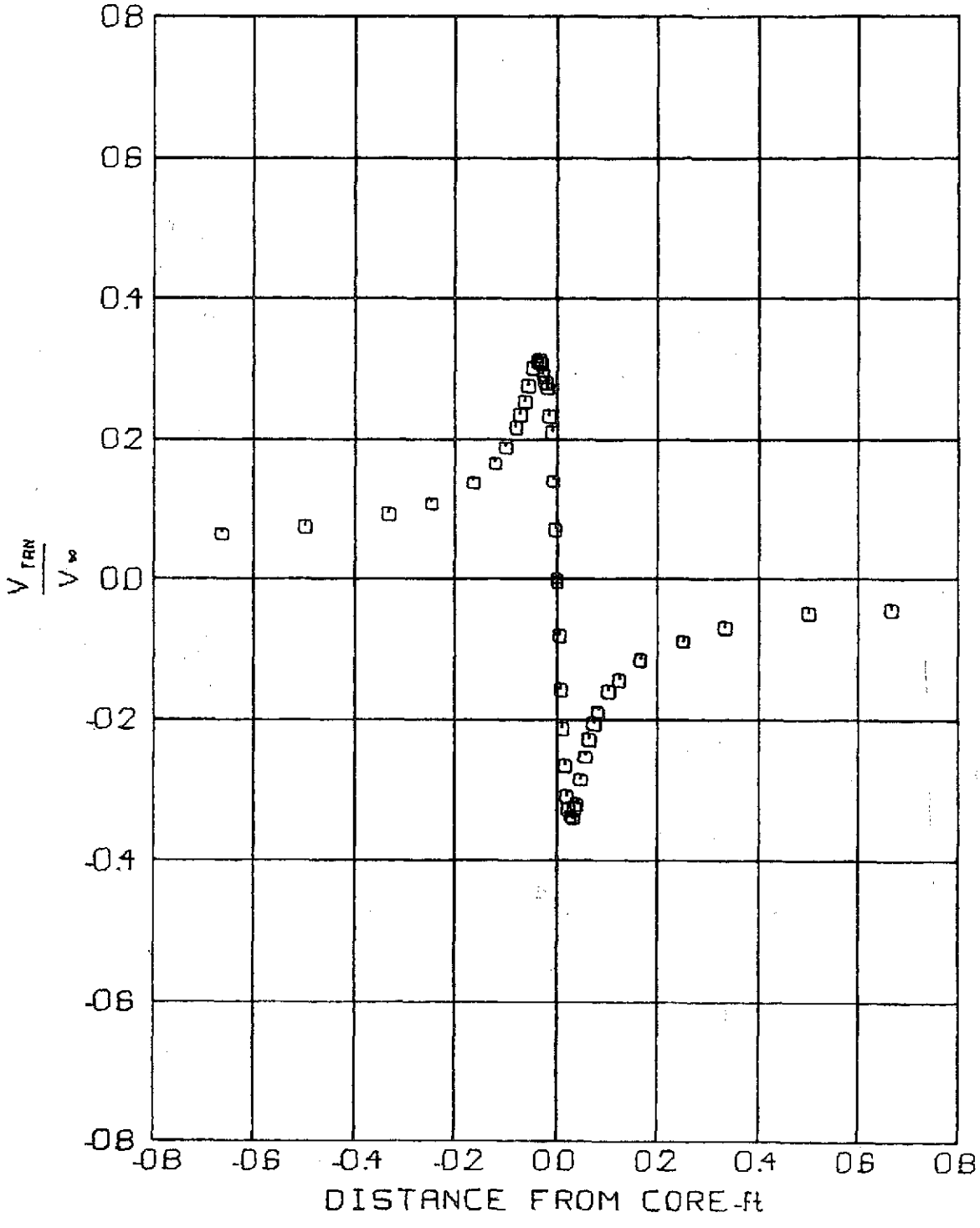

FIG 20 TANGENTIAL VELOCITY PROFILE

V_∞ = 69.5 f/s Z/C = 20
α = 6° t = .19162 sec

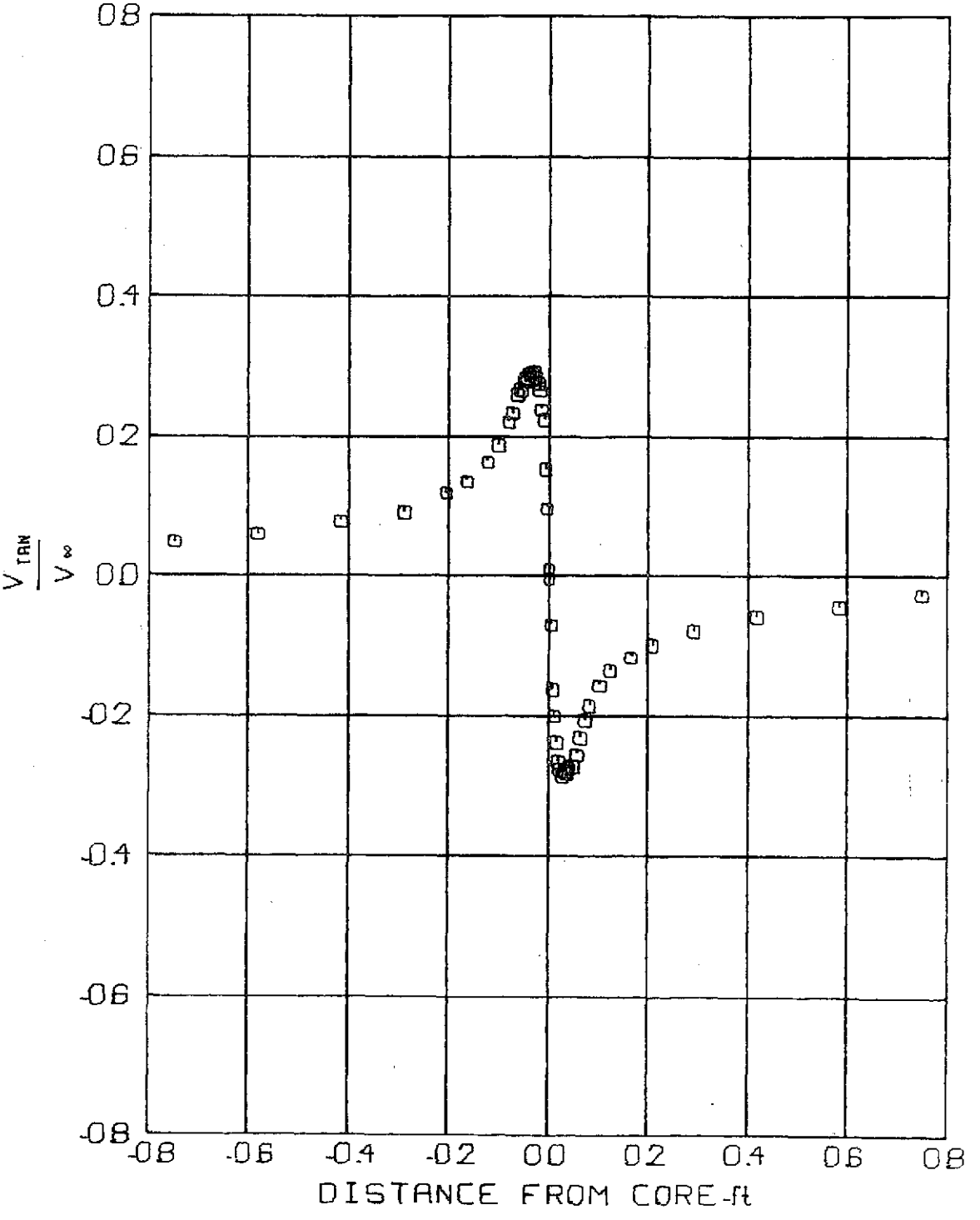

FIG 21 TANGENTIAL VELOCITY PROFILE

V_∞ = 86.9 f/s Z/C = 25
α = 6° t = .19174 sec

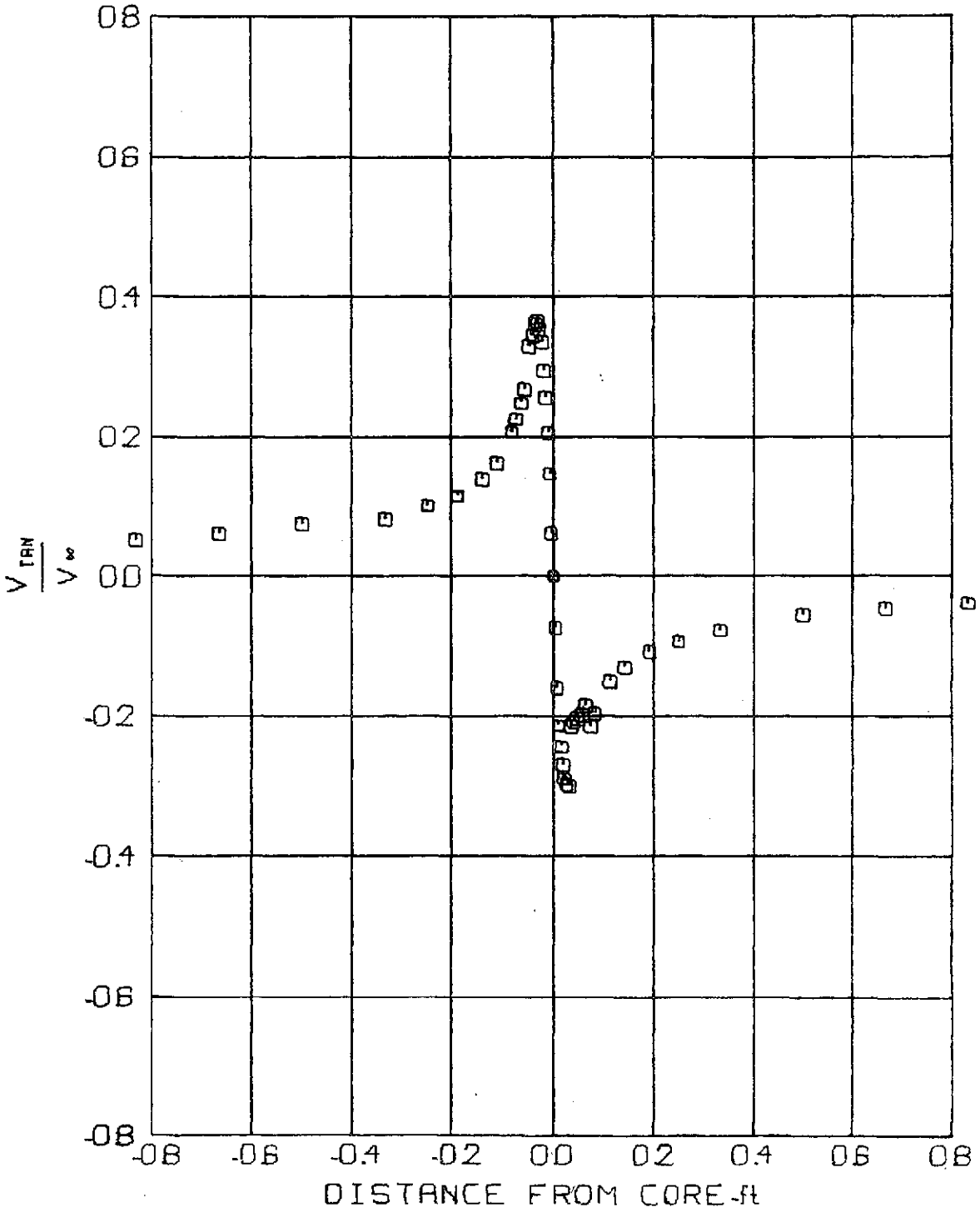

FIG 22 TANGENTIAL VELOCITY PROFILE

V_∞ = 103.6 f/s Z/C = 30
α = 6° t = .19288 sec

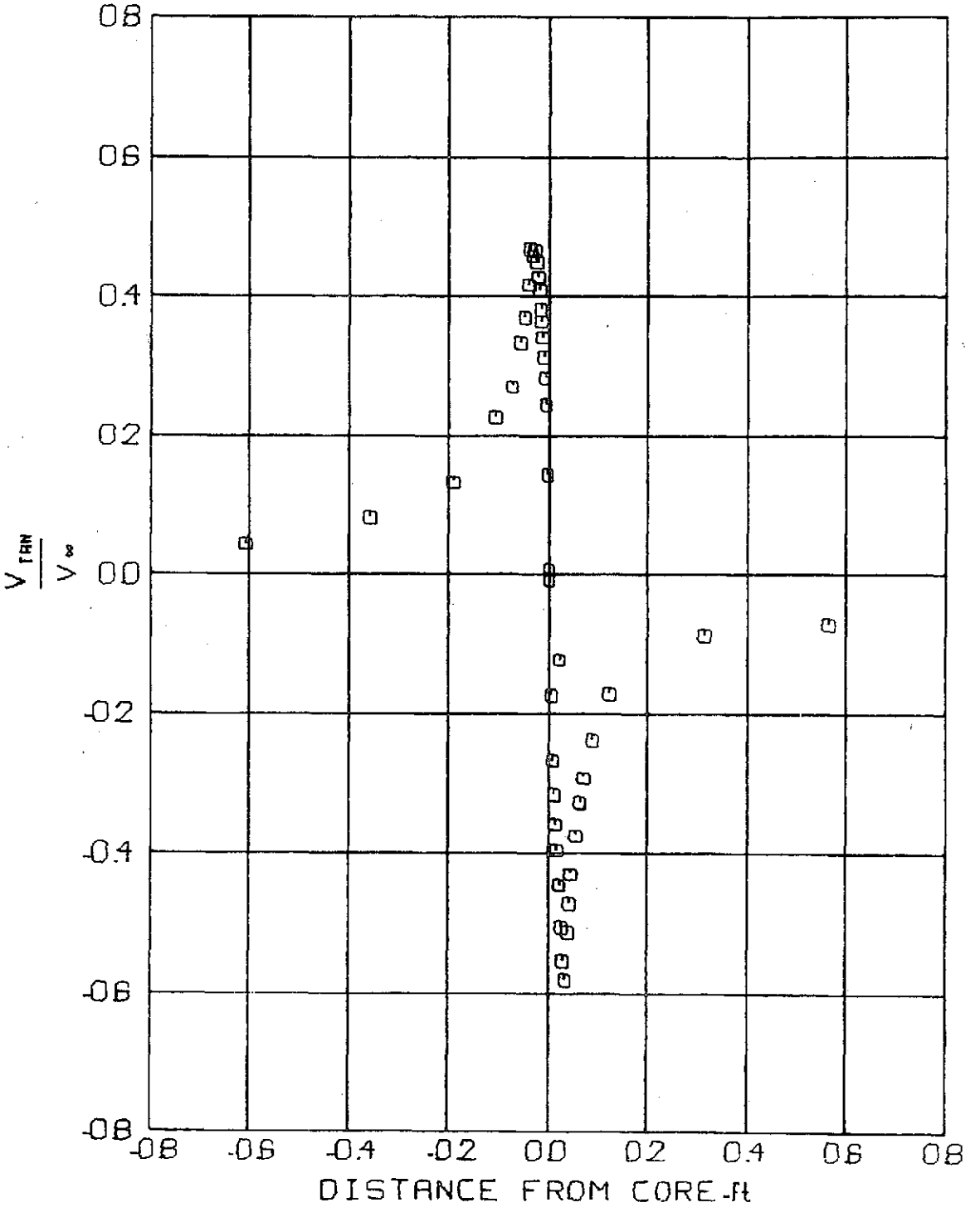

FIG 23 TANGENTIAL VELOCITY PROFILE

V_∞ = 68.7 f/s Z/C = 2
α = 8° t = .01939 sec

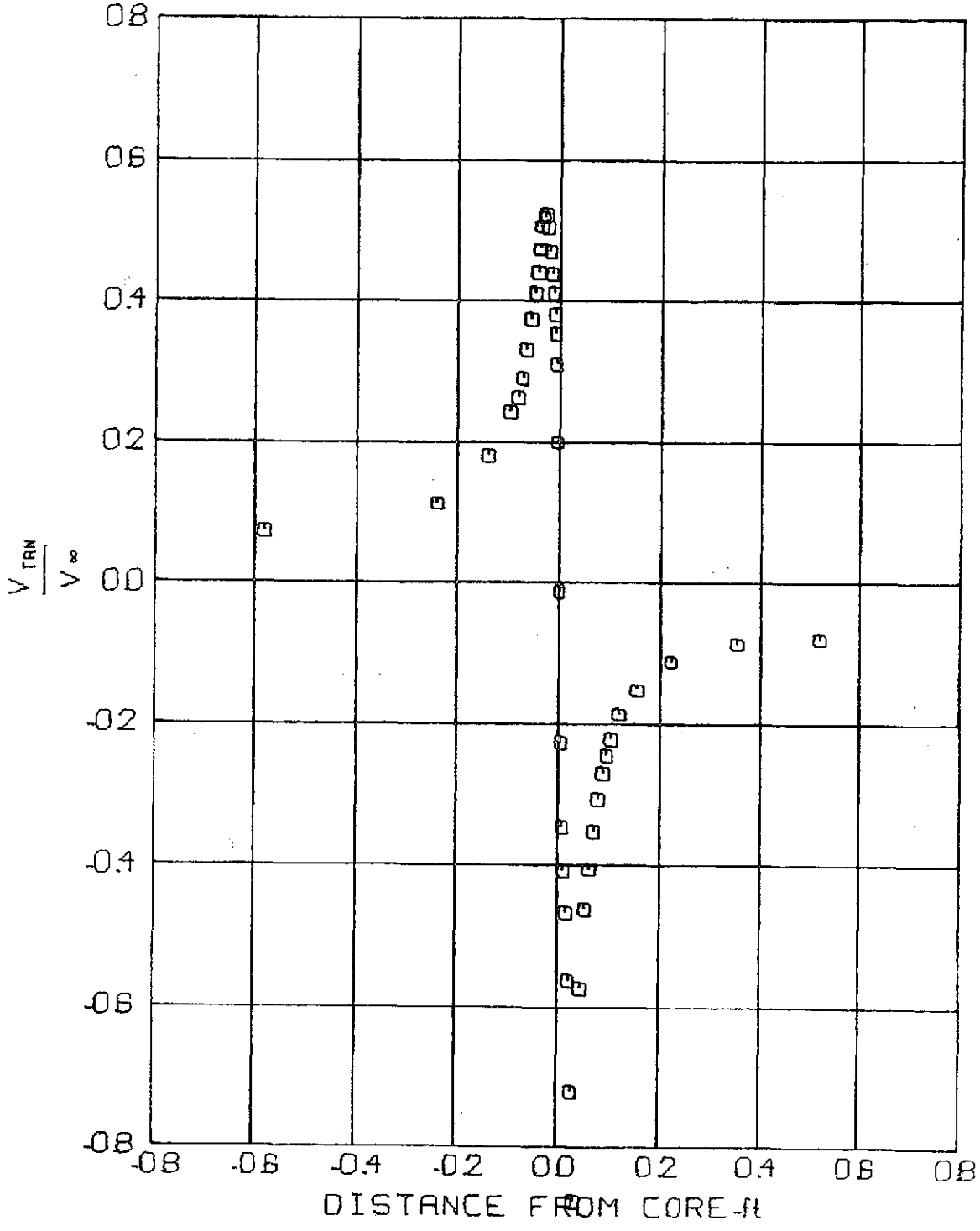

FIG 24 TANGENTIAL VELOCITY PROFILE

V_∞ = 105.8 f/s Z/C = 2
α = 8° t = .01259 sec

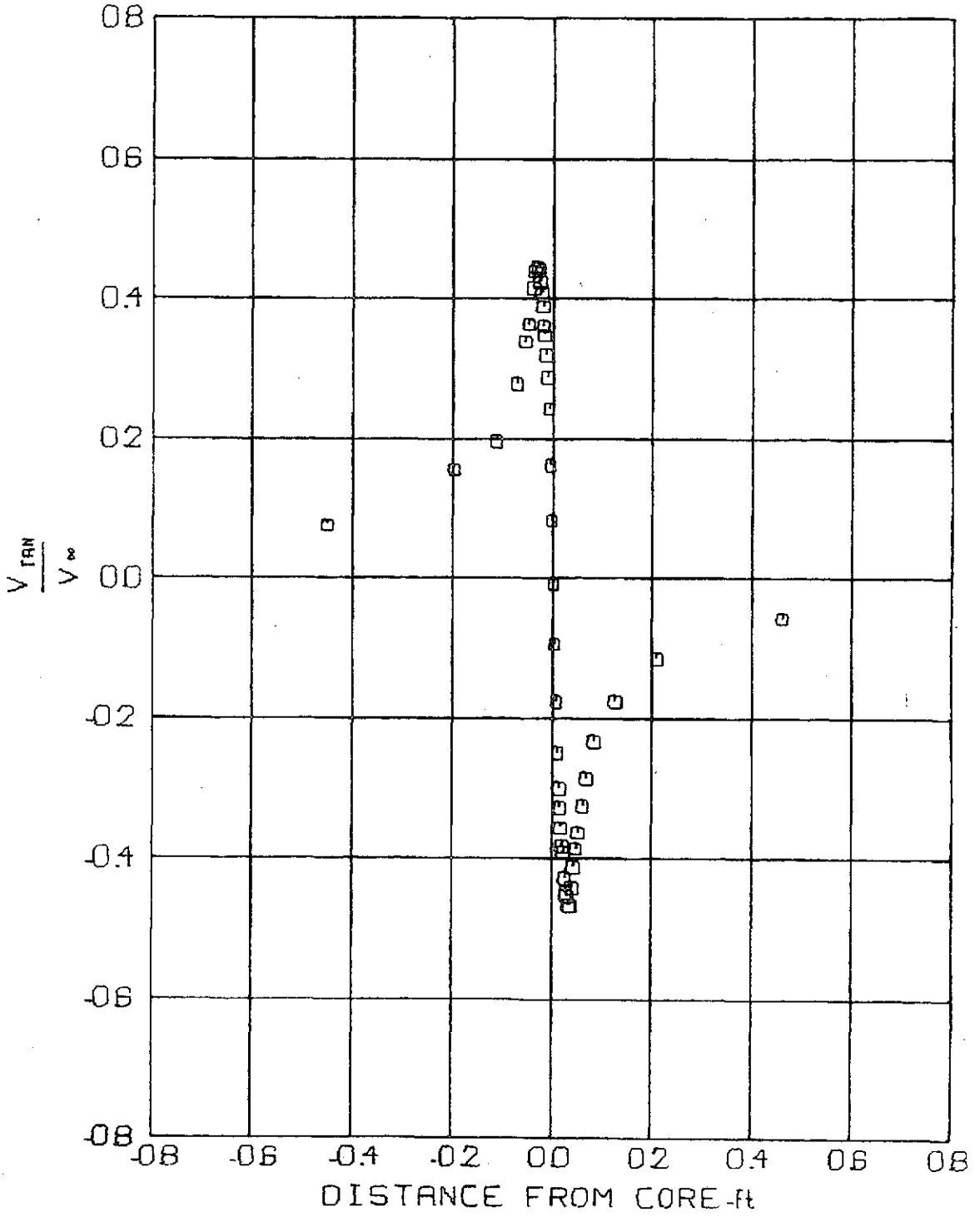

FIG 25 TANGENTIAL VELOCITY PROFILE

V_∞ = 69.7 f/s Z/C = .5
α = 8° t = .04780 sec

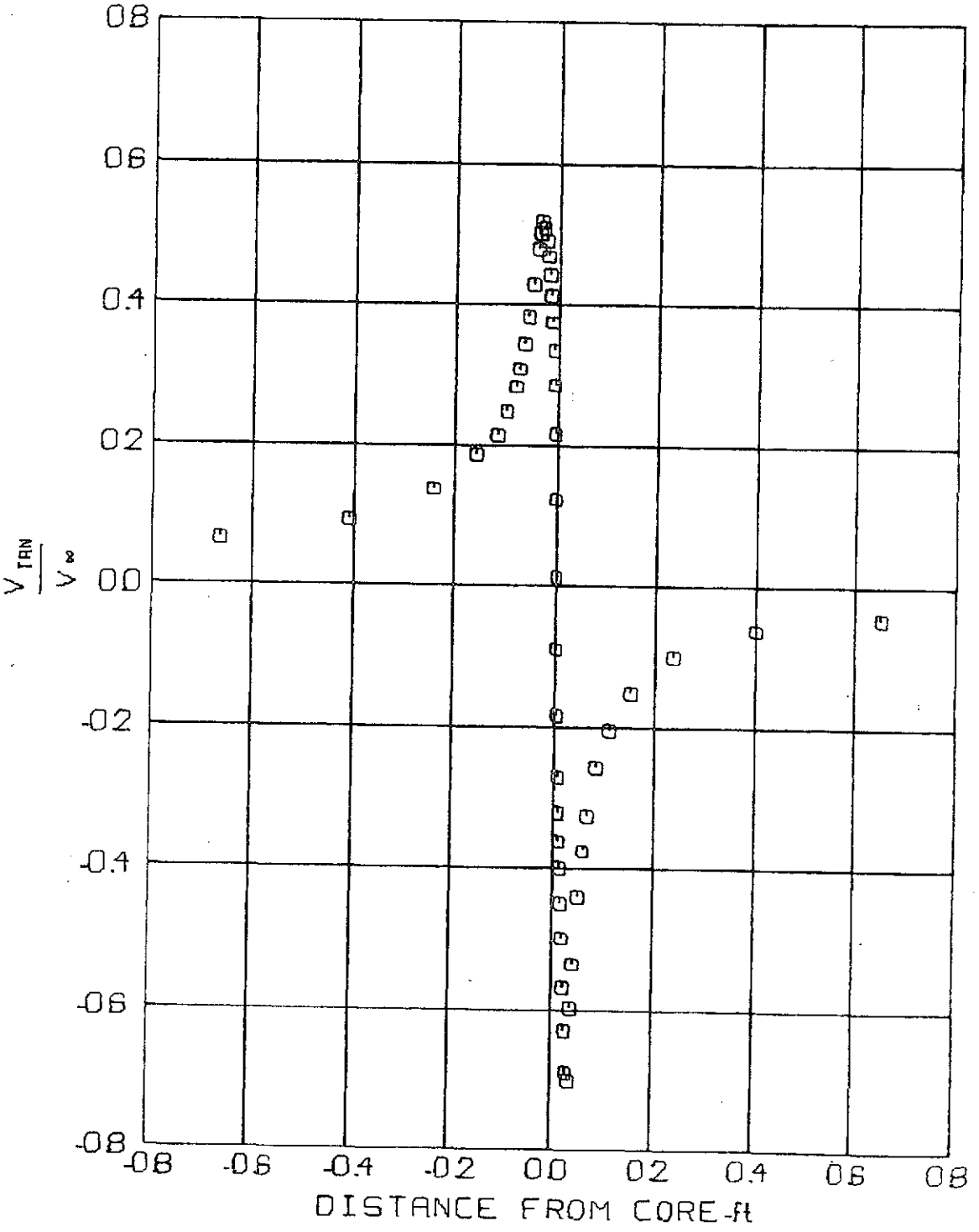

FIG 26 TANGENTIAL VELOCITY PROFILE

V_∞ = 103.9 f/s Z/C = .5
α = 8° t = .03207 sec

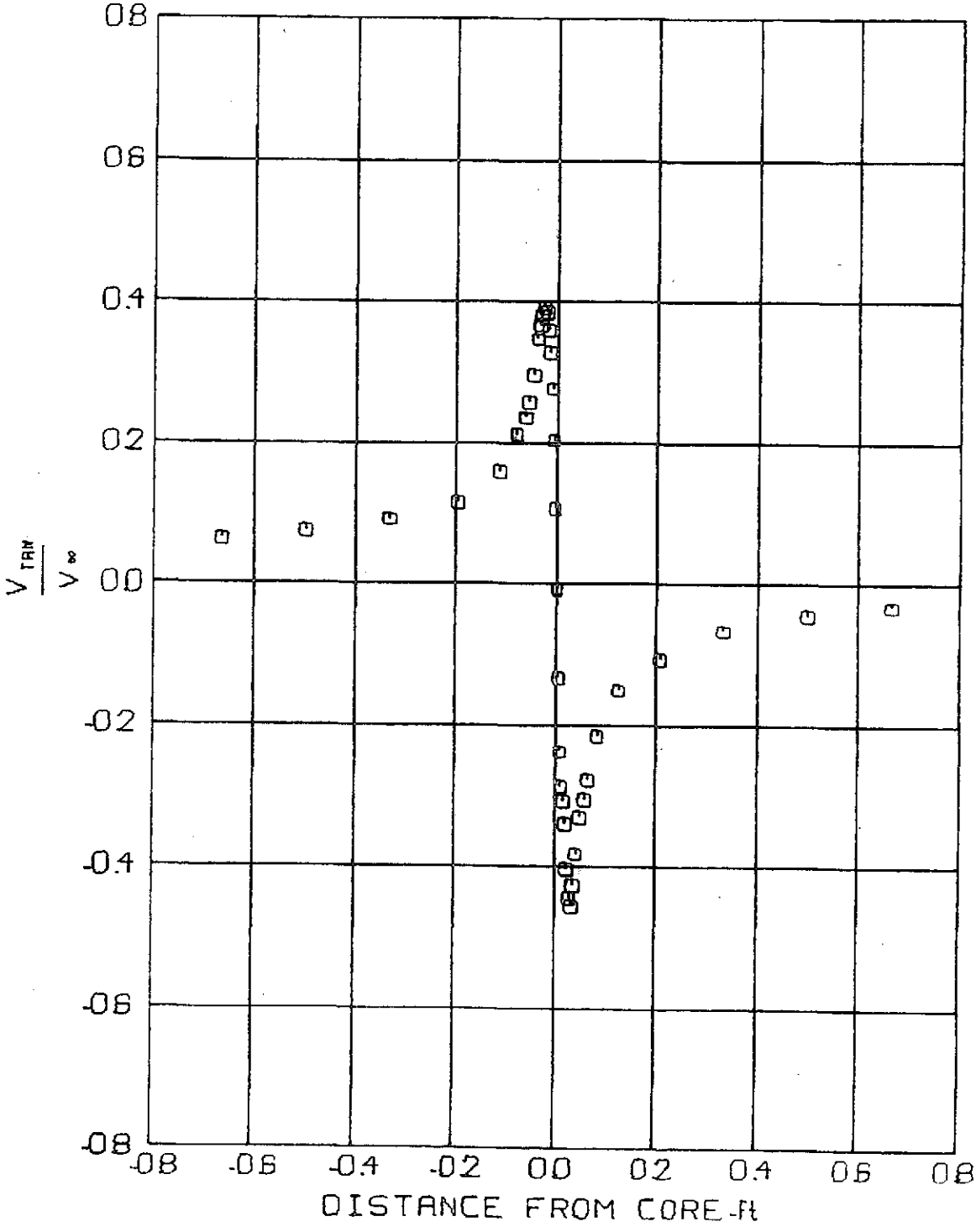

FIG 27 TANGENTIAL VELOCITY PROFILE

V_∞ = 66.1 f/s Z/C = 10
α = 8° t = .10076 sec

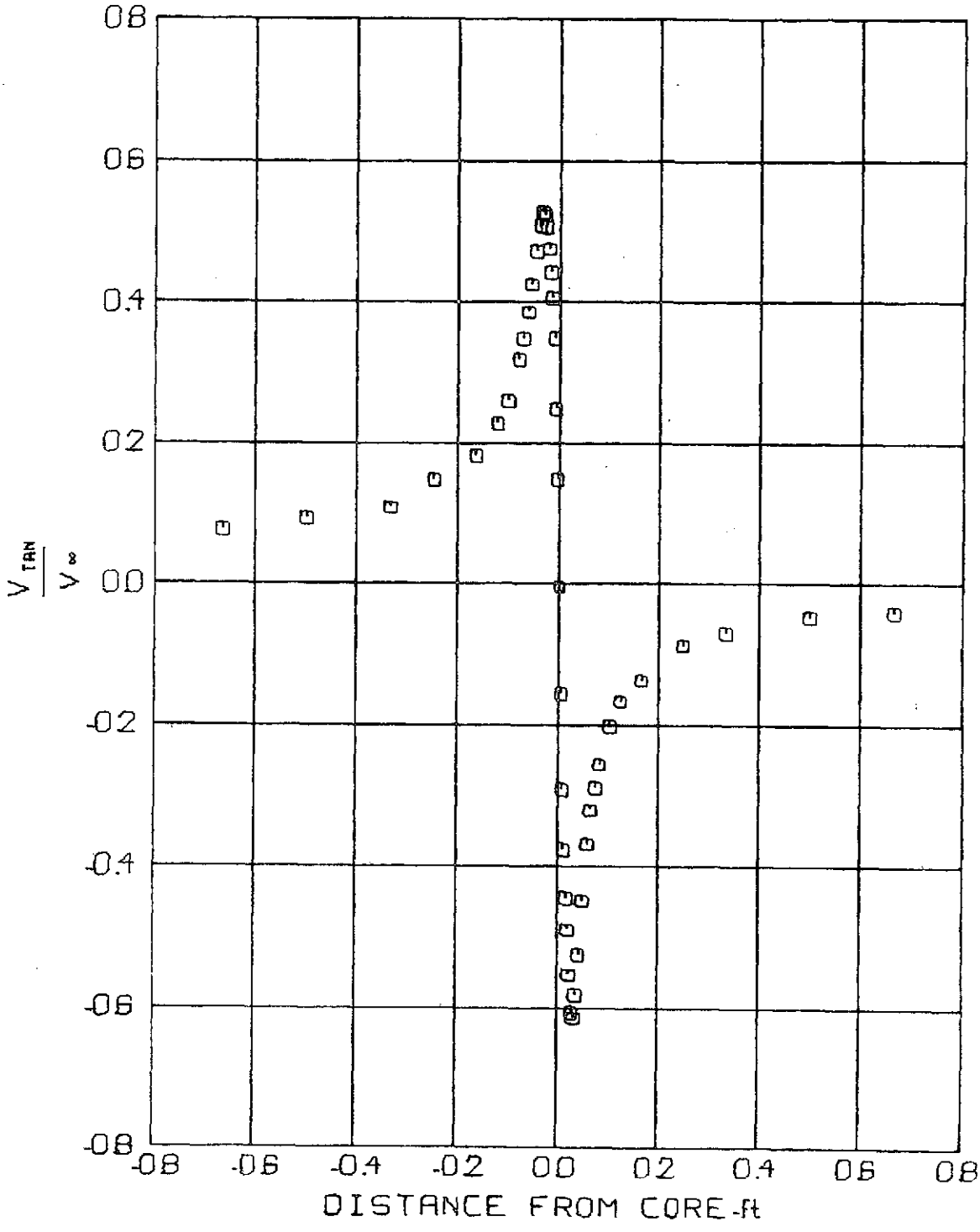

FIG 28 TANGENTIAL VELOCITY PROFILE

V_∞ = 98.8 f/s Z/C = 10
α = 8° t = .06742 sec

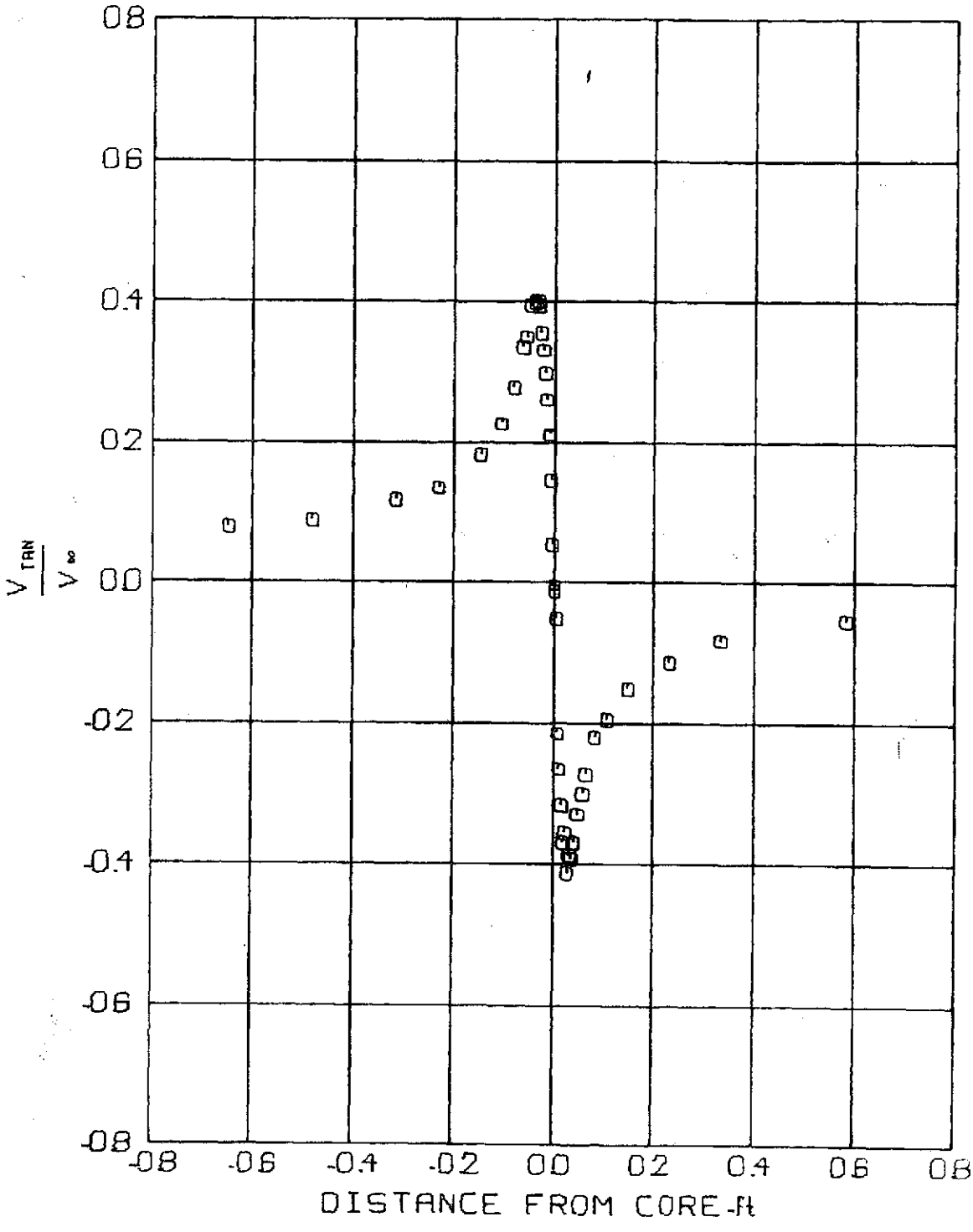

FIG 29 TANGENTIAL VELOCITY PROFILE

V_∞ = 48.7 f/s Z/C = 1.5
α = 8° t = .20529 sec

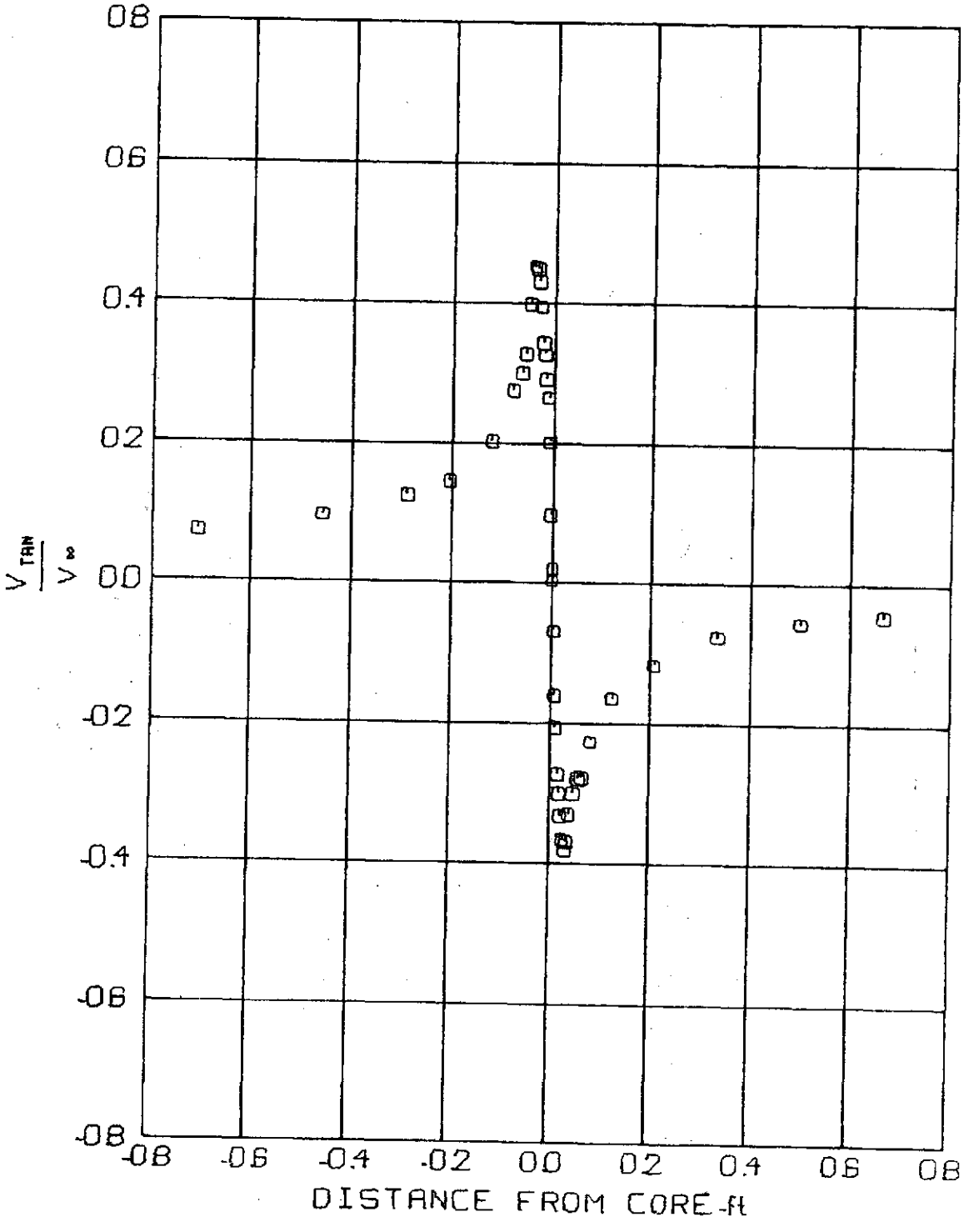

FIG 30 TANGENTIAL VELOCITY PROFILE

V_∞ = 65.8 f/s Z/C = 1.5
α = 8° t = .15195 sec

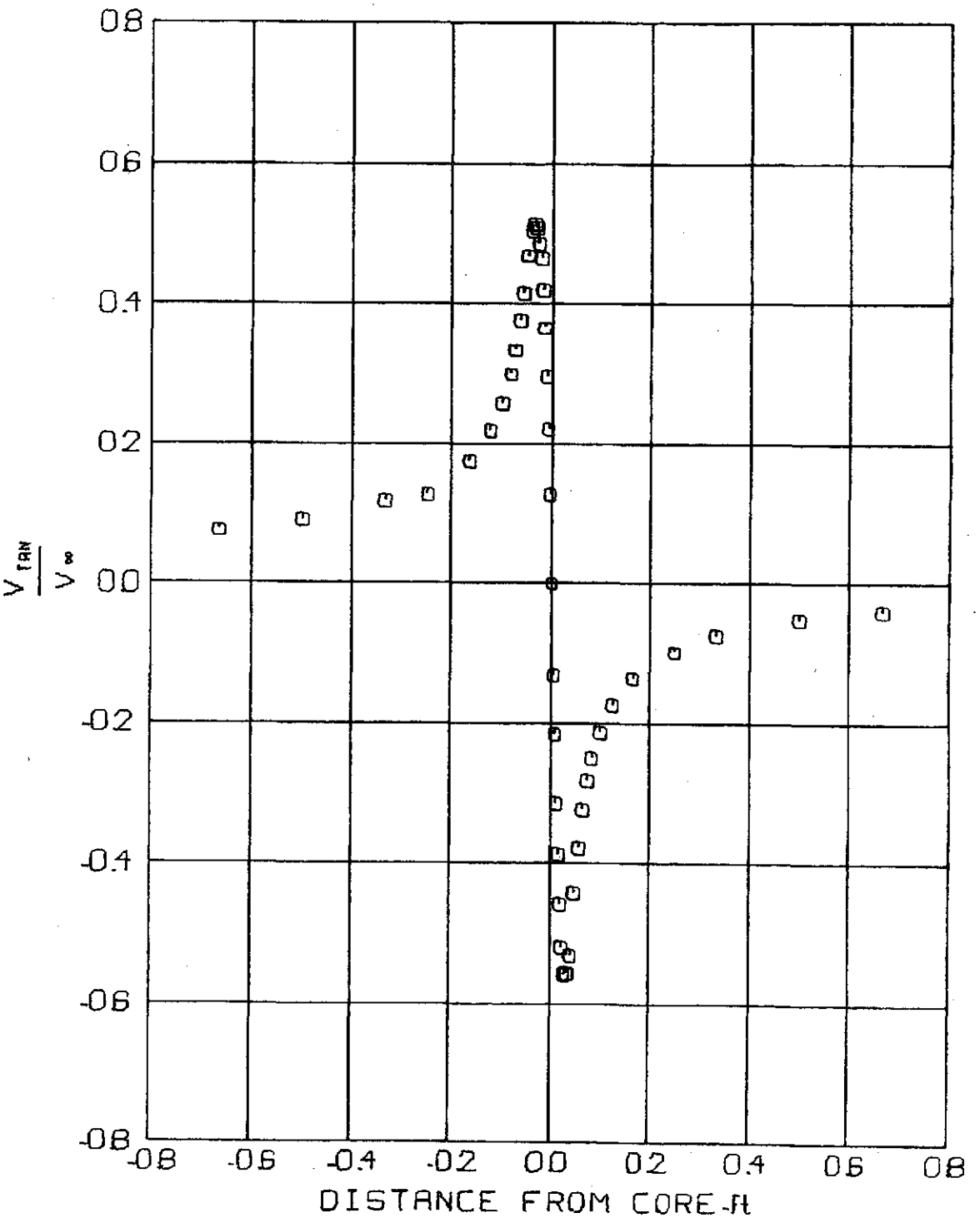

FIG 31 TANGENTIAL VELOCITY PROFILE

V_∞ = 100.4 f/s Z/C = 15
α = 8° t = .09957 sec

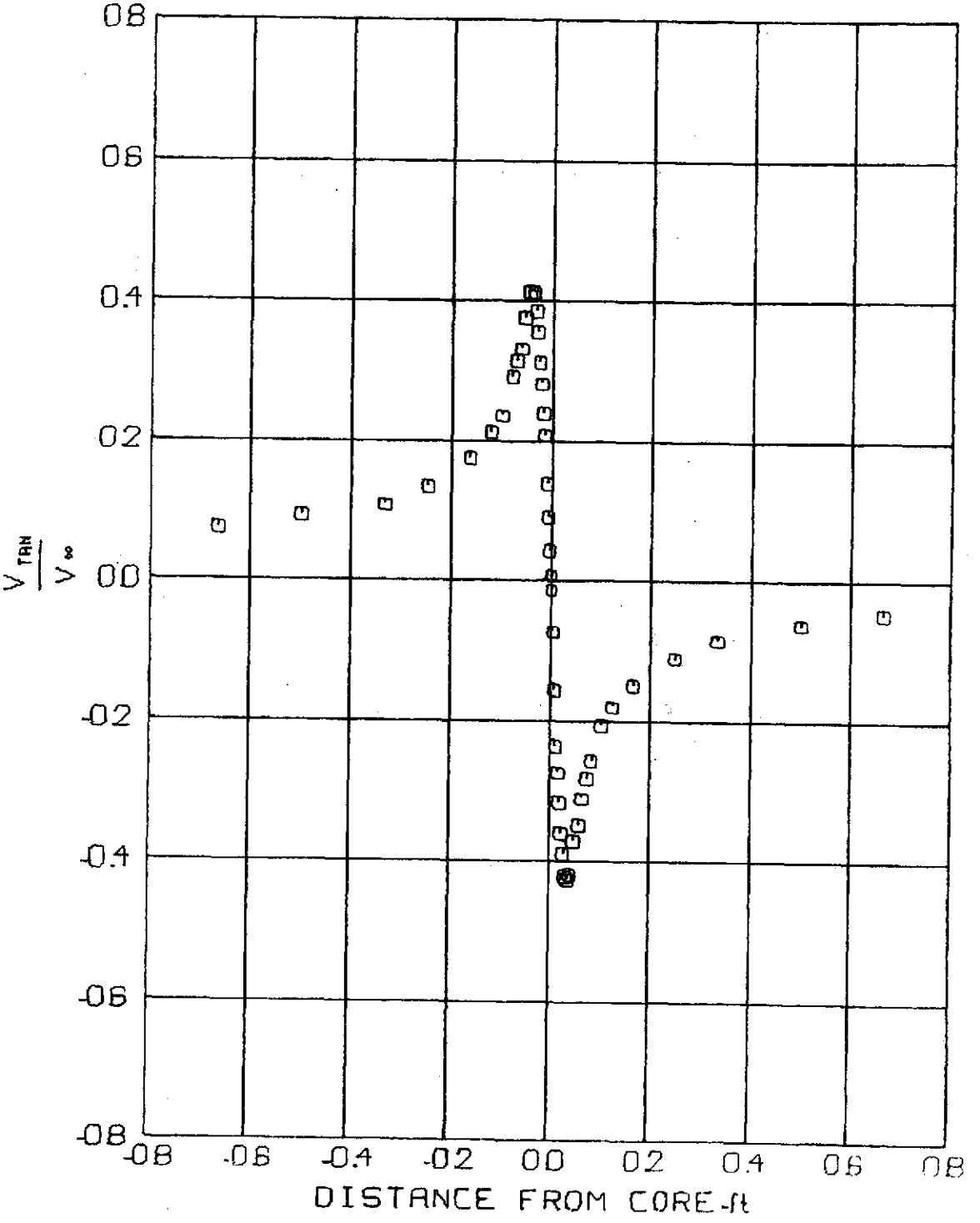

FIG 32 TANGENTIAL VELOCITY PROFILE

V_∞ = 69.0 f/s Z/C = 20
α = 8° t = .19303 sec

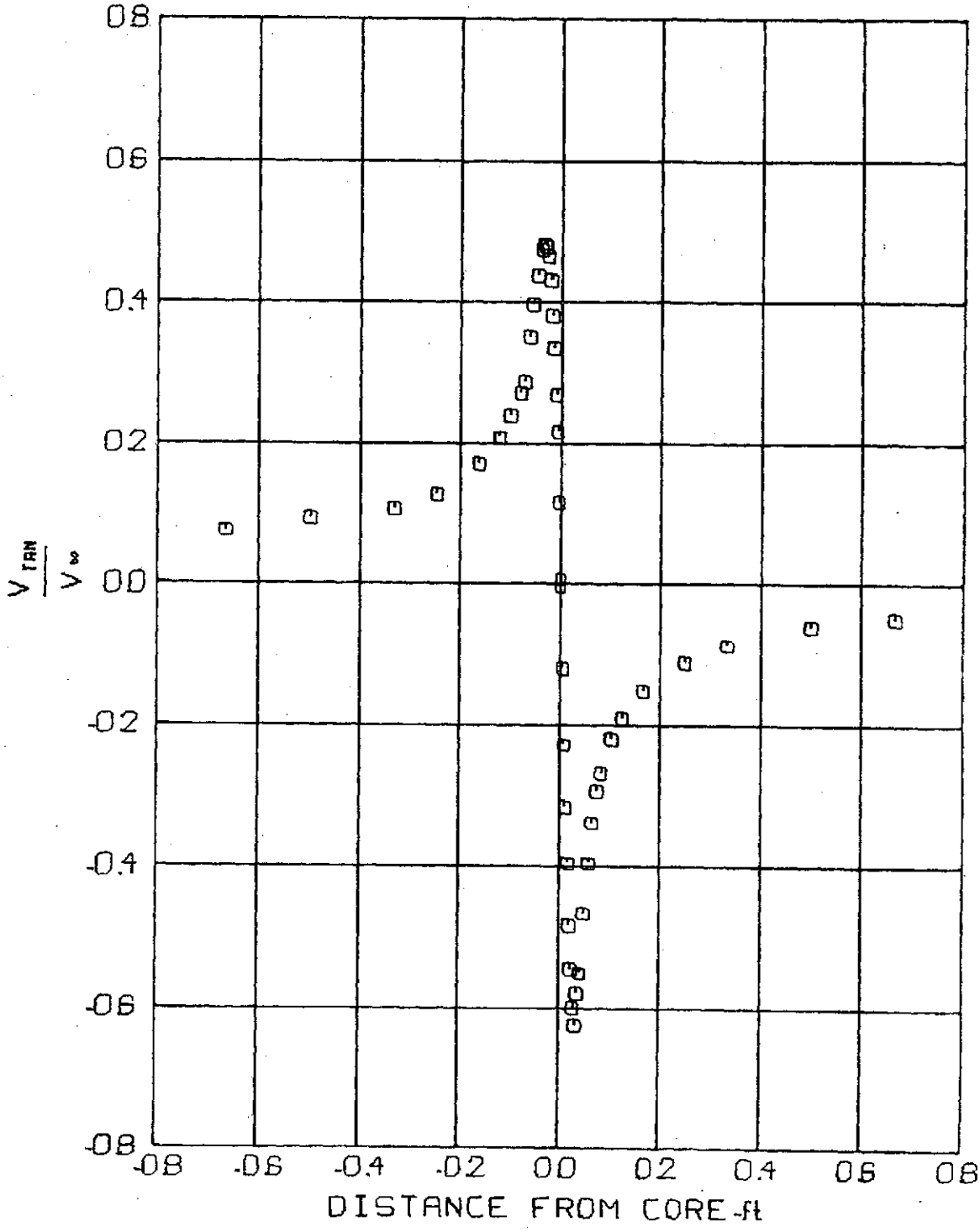

FIG 33 TANGENTIAL VELOCITY PROFILE

V_∞ = 104.7 f/s Z/C = 20
α = 8° t = .12729 sec

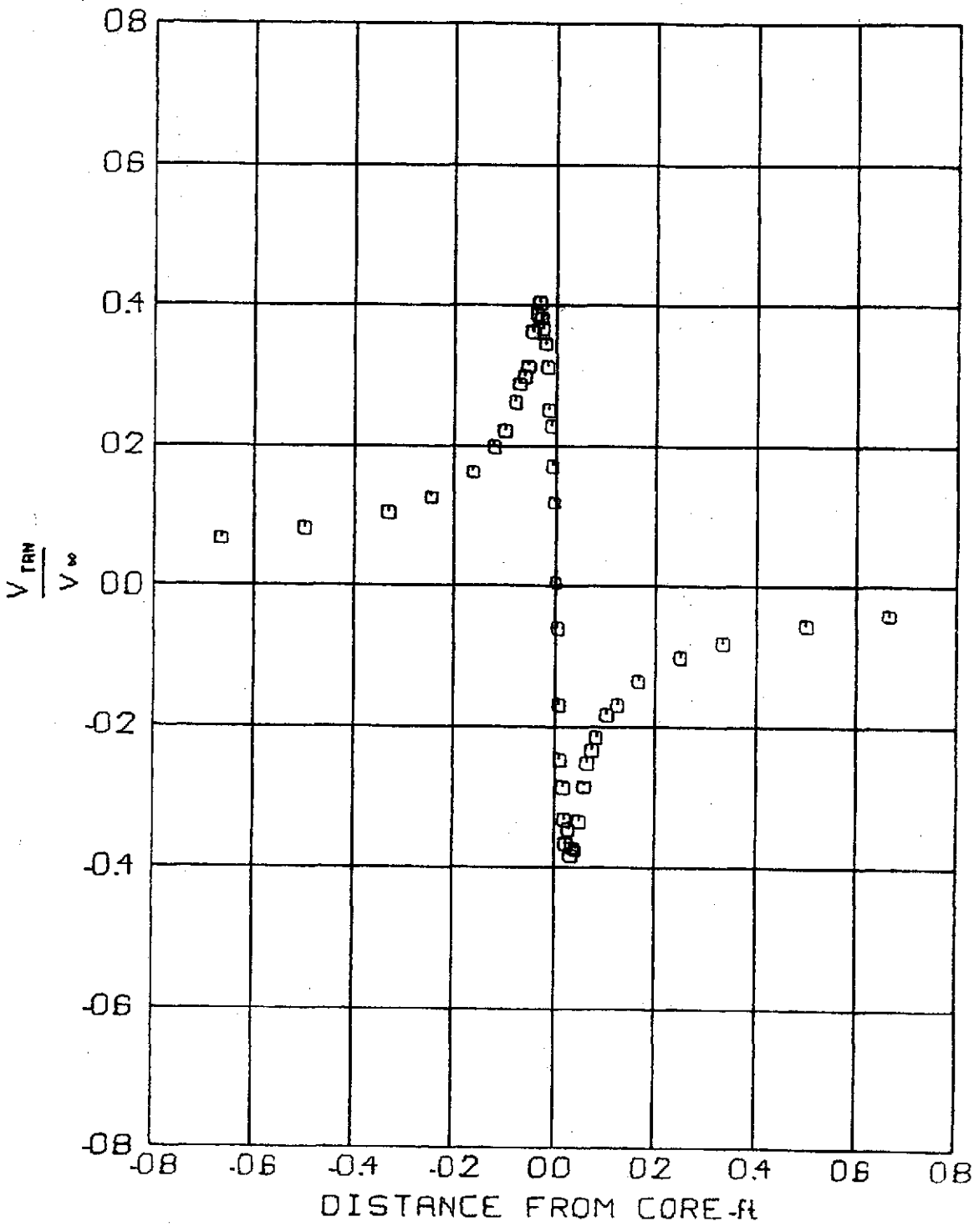

FIG 34 TANGENTIAL VELOCITY PROFILE

V_∞ = 68.2 f/s Z/C = .25
α = 8° t = .24413 sec

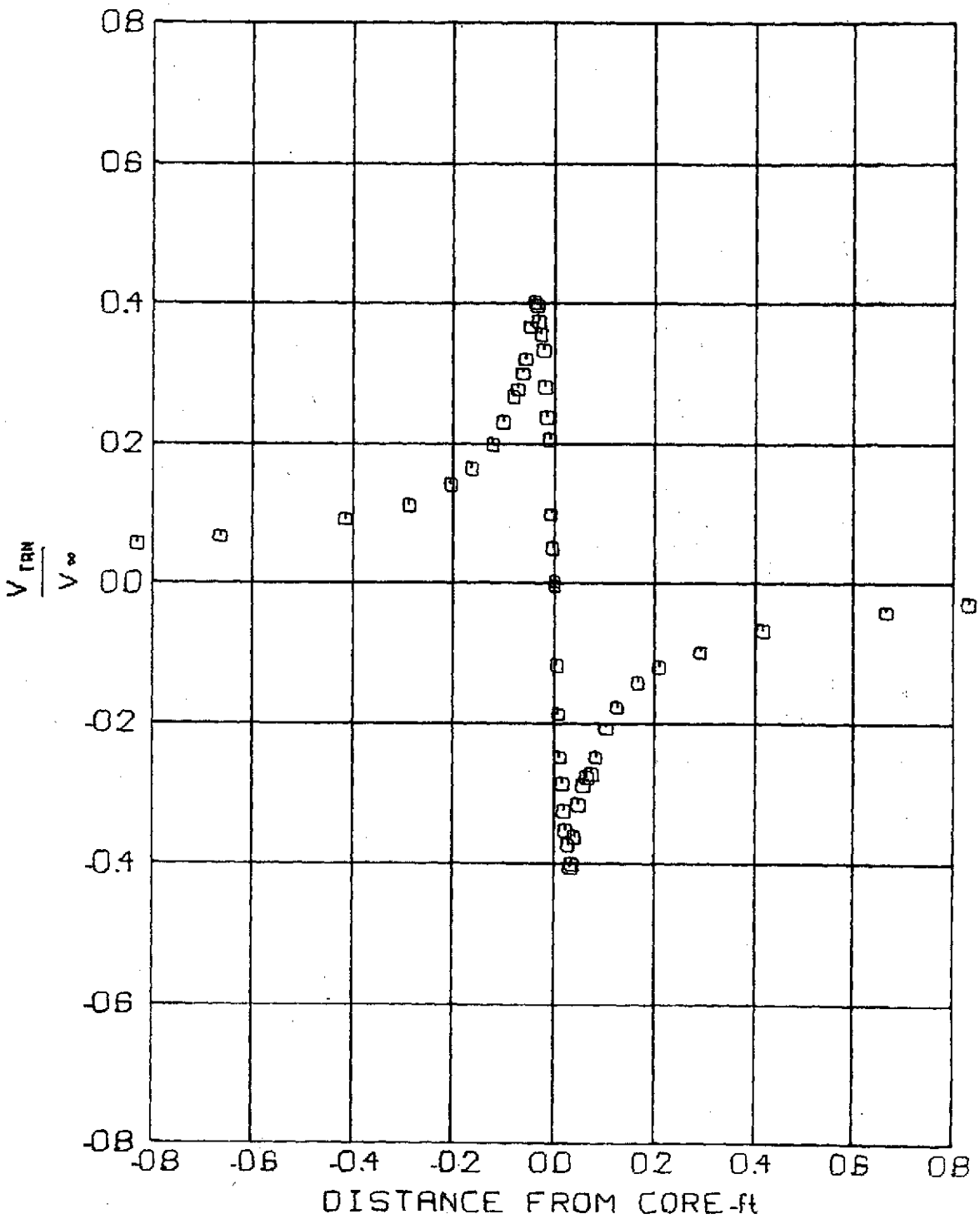

FIG 35 TANGENTIAL VELOCITY PROFILE

V_∞ = 86.5 f/s Z/C = 25
α = 8° t = .19256 sec

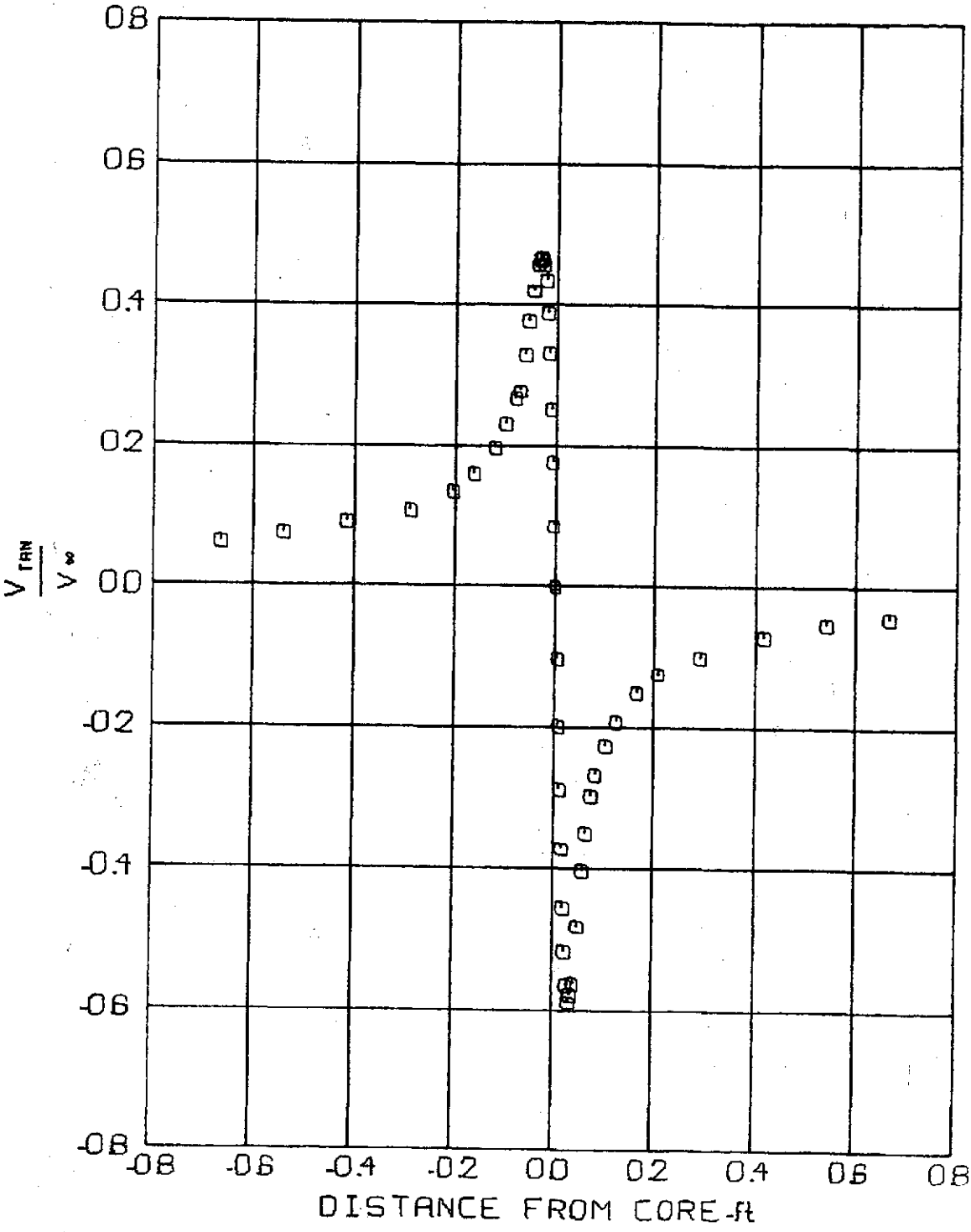

FIG 36 TANGENTIAL VELOCITY PROFILE

V_∞ = 105.3 f/s Z/C = 25
α = 8° t = .15818 sec

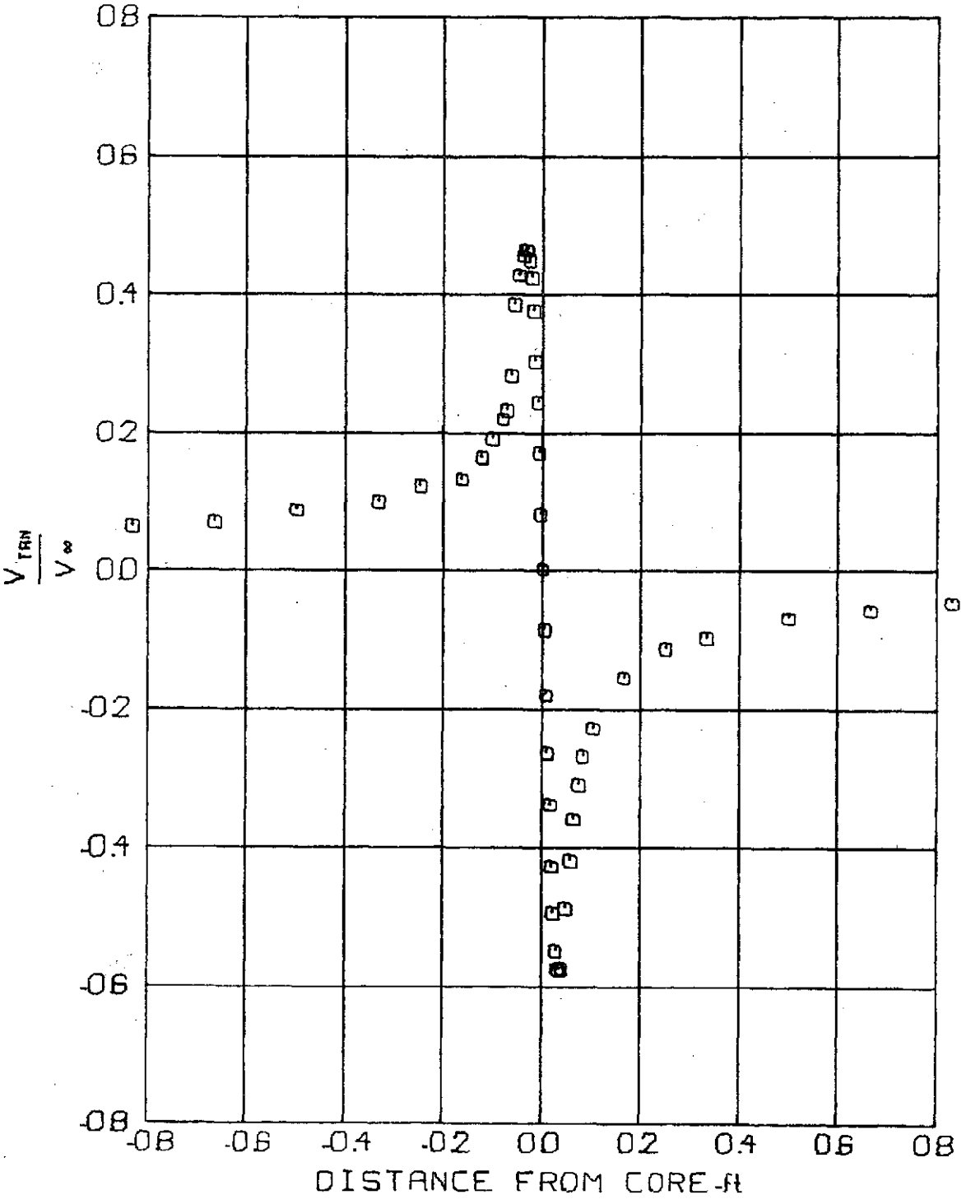

FIG 37 TANGENTIAL VELOCITY PROFILE

V_∞ = 104.0 f/s Z/C = 30
α = 8° t = .19221 sec

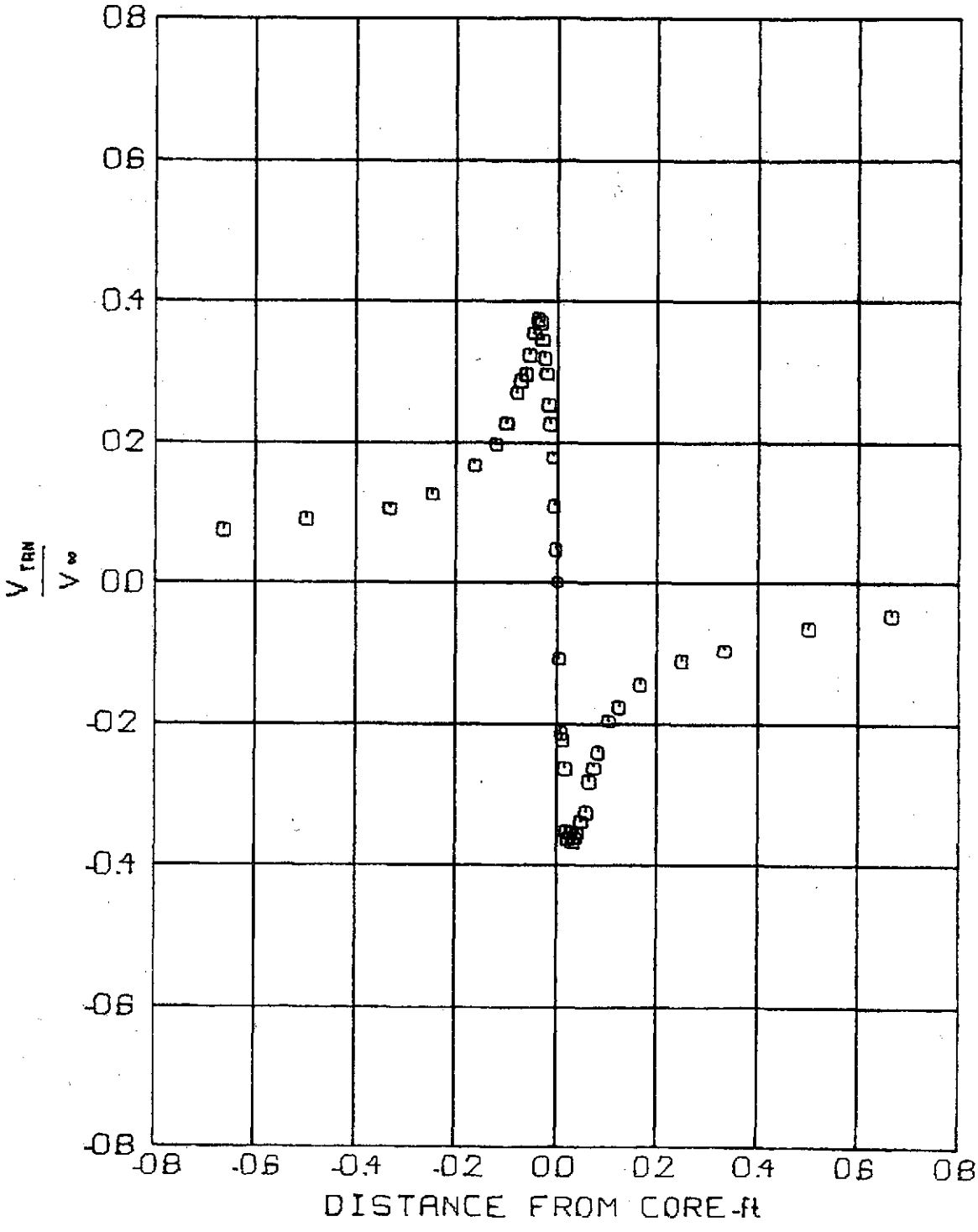

FIG 38 TANGENTIAL VELOCITY PROFILE

V_∞ = 68.0 f/s Z/C = 30
α = 8° t = .29398 sec

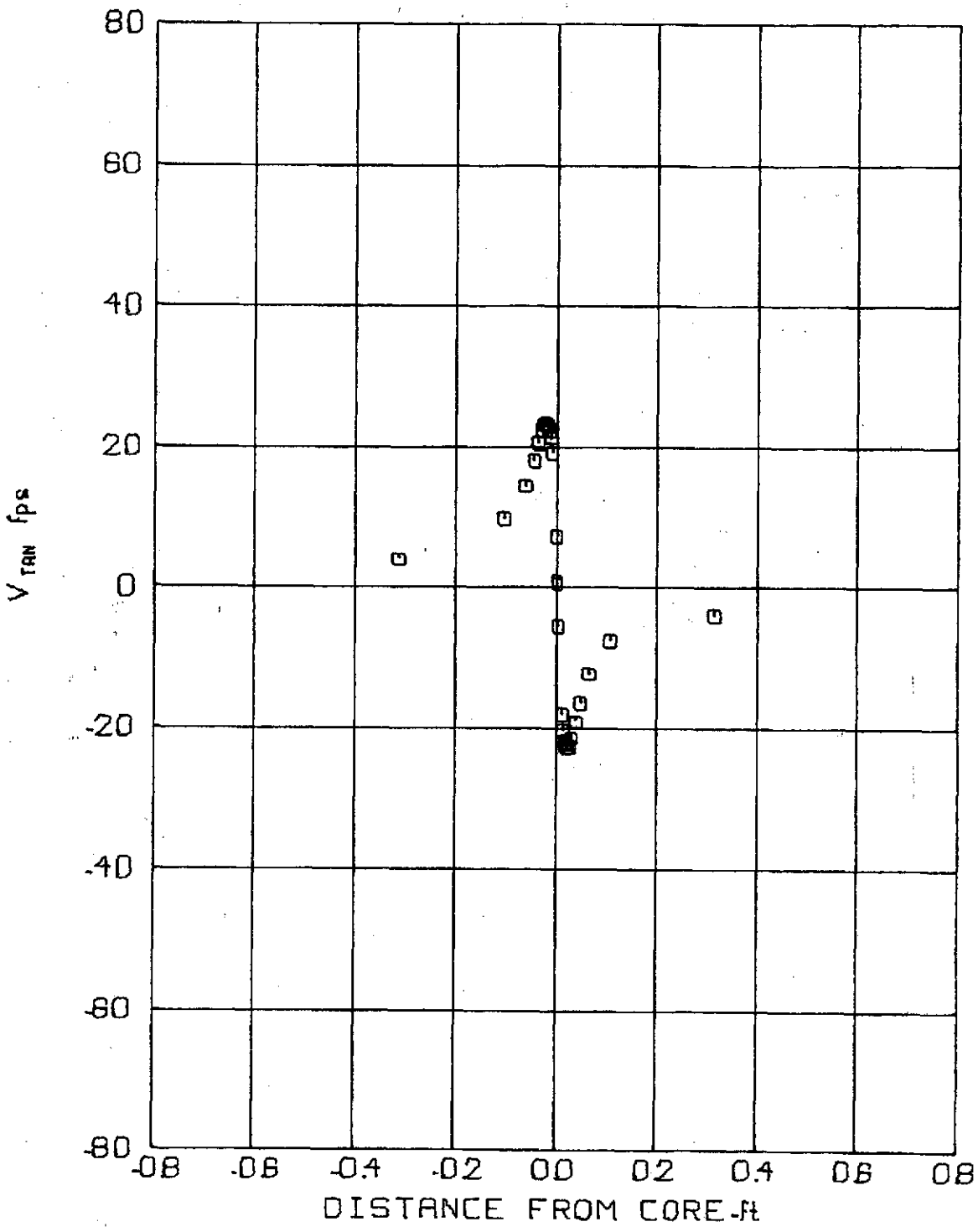

FIG 39 TANGENTIAL VELOCITY PROFILE

V_∞ = 86.8 f/s Z/C = 2
α = 4° t = .01535 sec

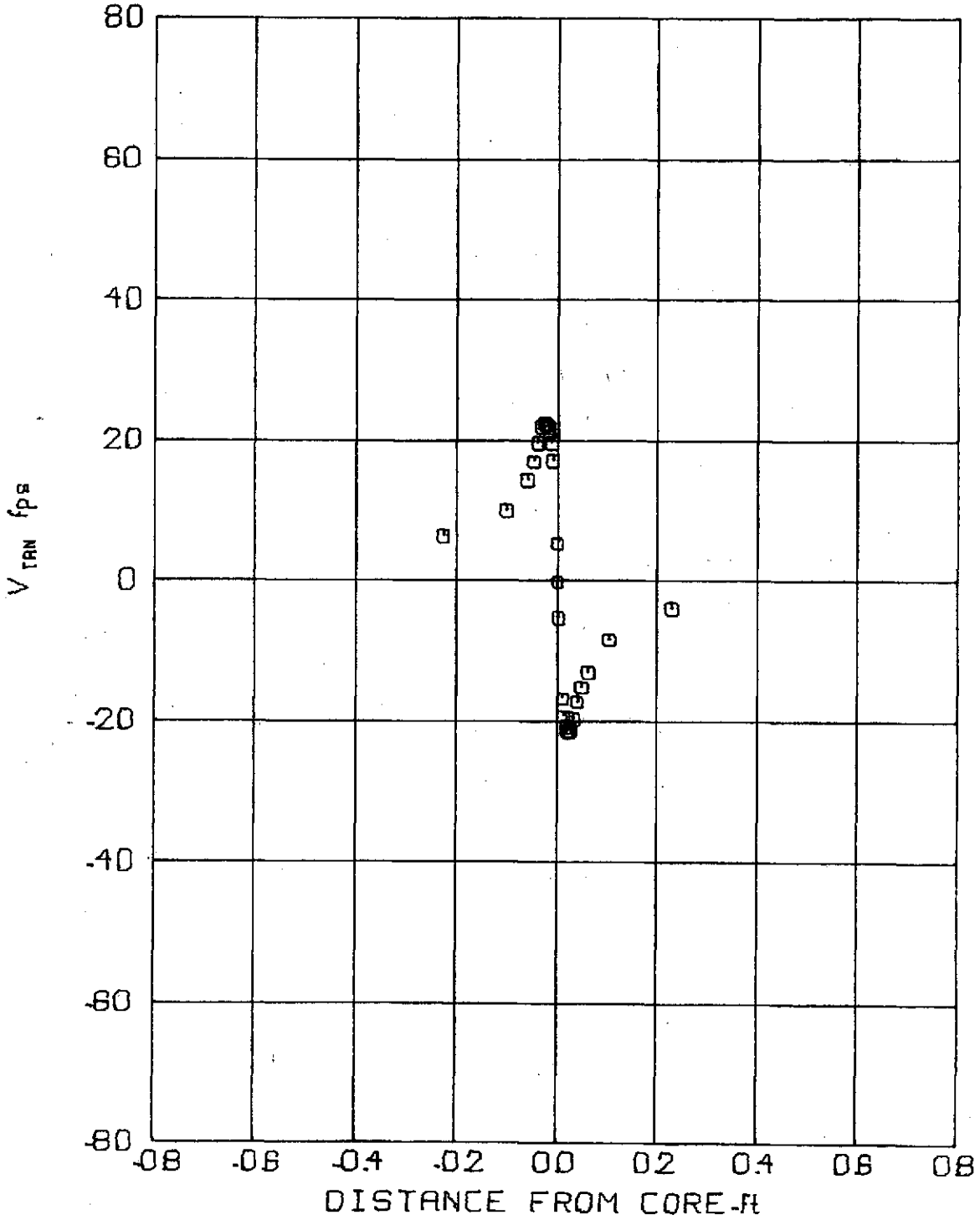

FIG 40 TANGENTIAL VELOCITY PROFILE

V_∞ = 86.7 f/s Z/C = 5
α = 4° t = .03840 sec

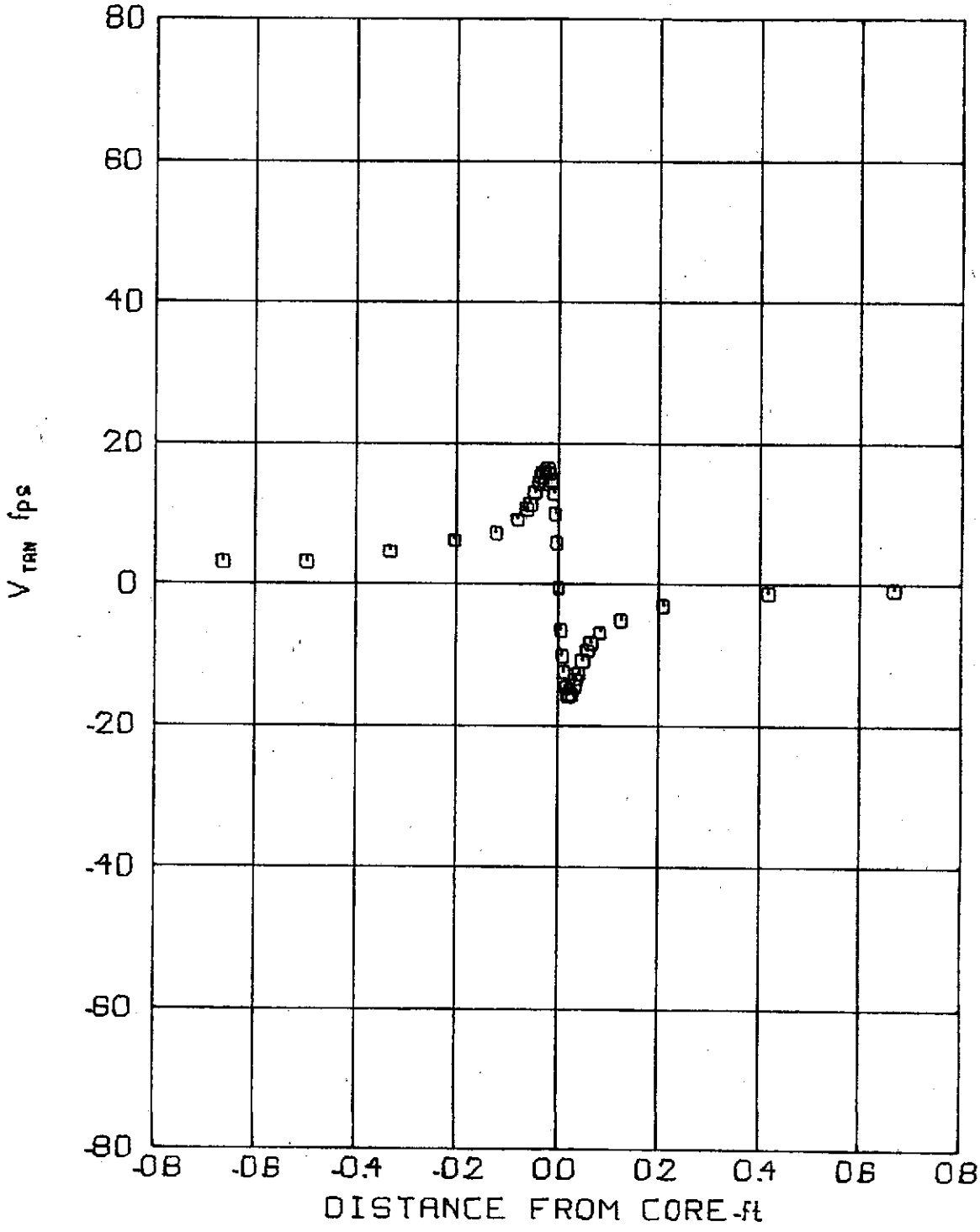

FIG 41 TANGENTIAL VELOCITY PROFILE

V_∞ = 68.6 f/s Z/C = 10
α = 4° t = .09713 sec

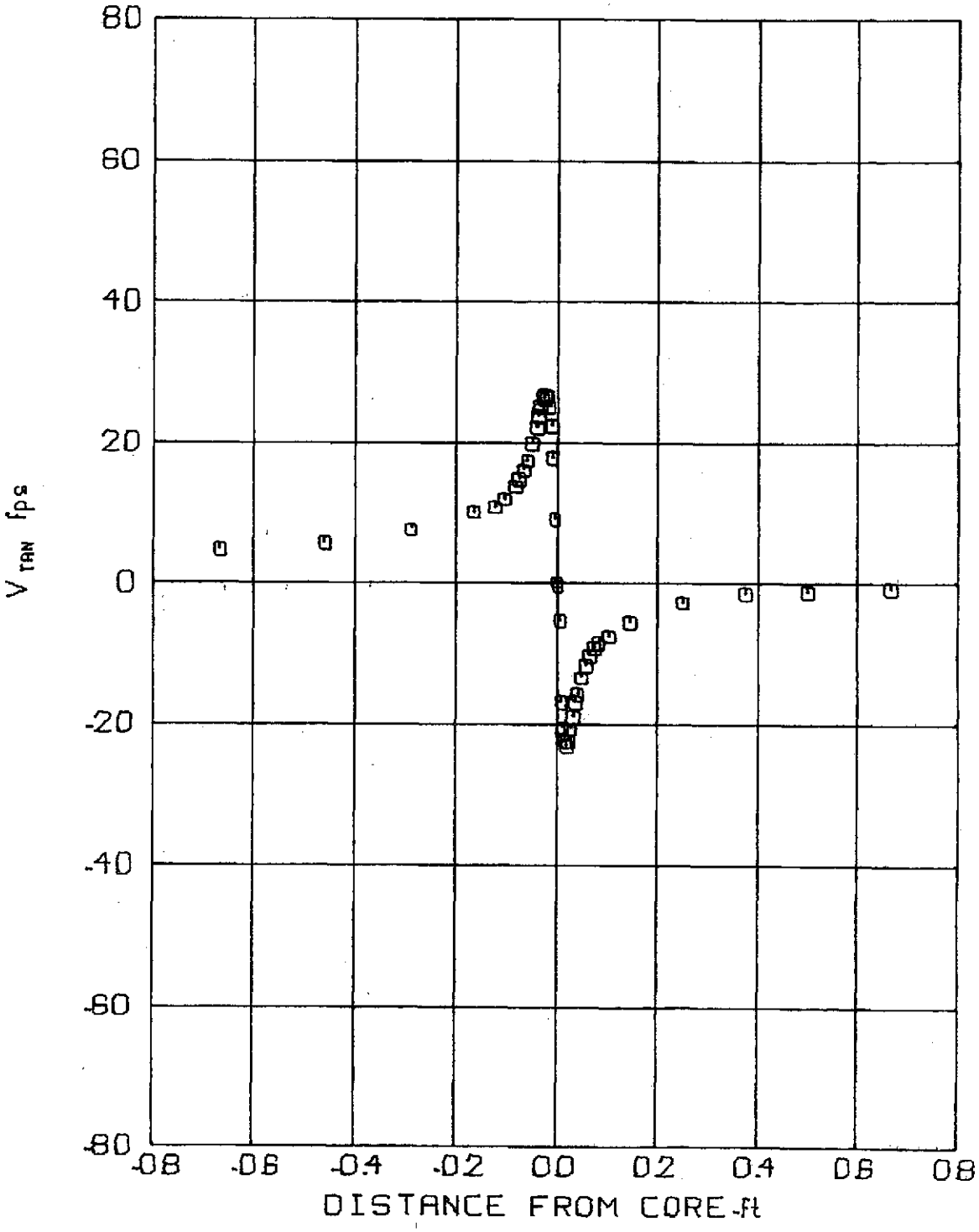

FIG 42 TANGENTIAL VELOCITY PROFILE

V_∞ = 98.3 f/s Z/C = 10
α = 4° t = .06780 sec

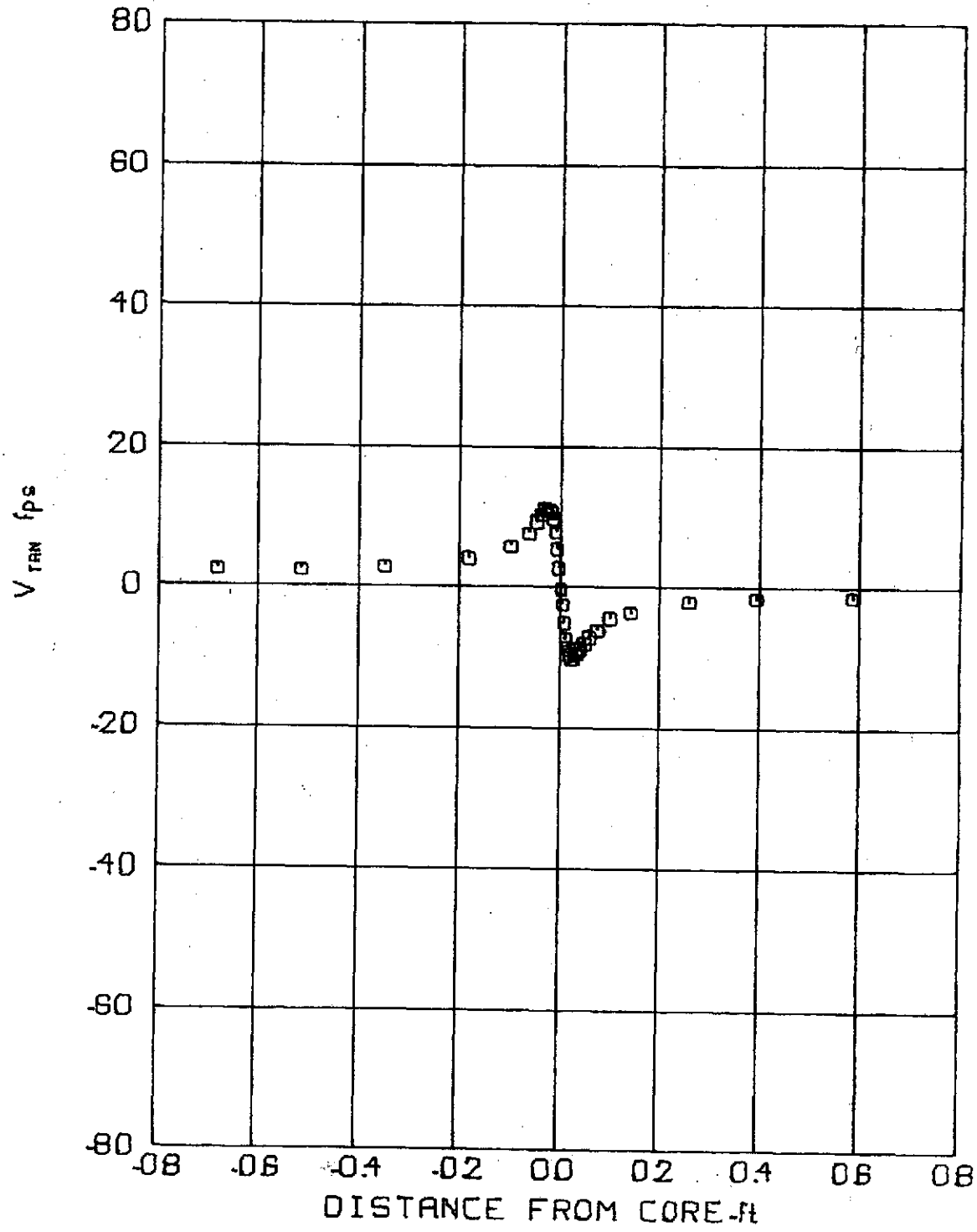

FIG 43 TANGENTIAL VELOCITY PROFILE

V_∞ = 49.3 f/s Z/C = 15
α = 4° t = .20246 sec

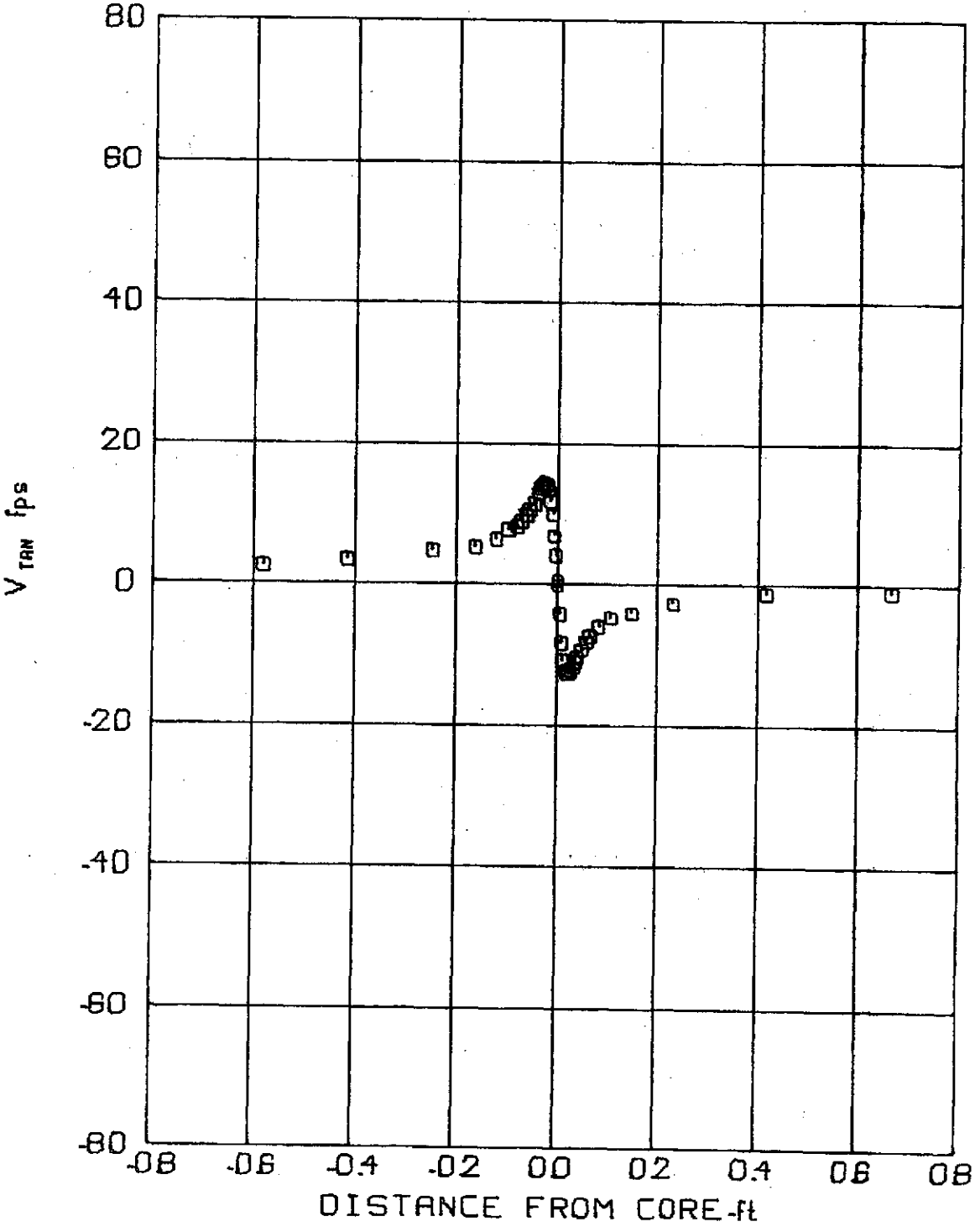

FIG 44 TANGENTIAL VELOCITY PROFILE

V_∞ = 87.2 f/s Z/C = 15
α = 4° t = .14879 sec

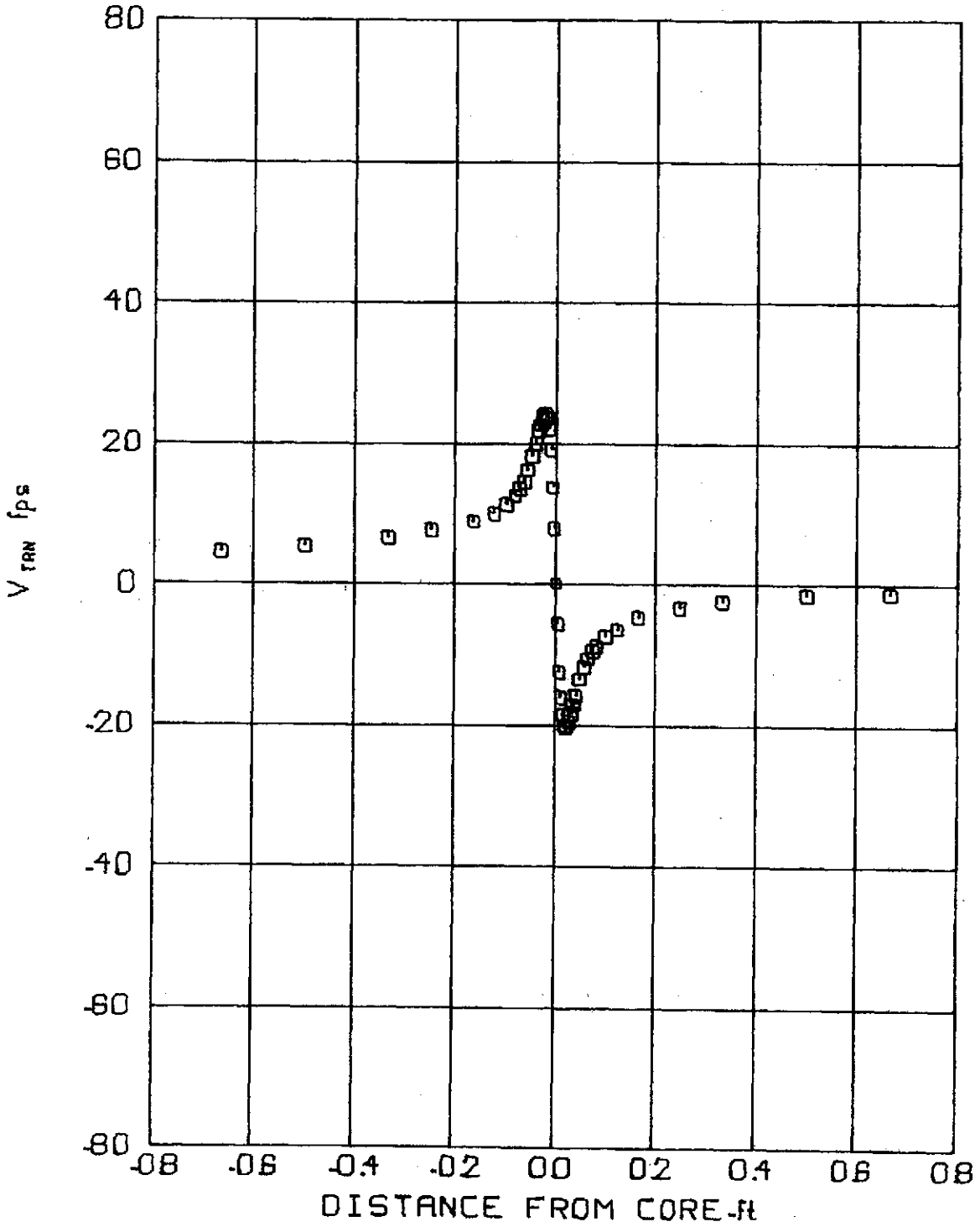

FIG 45 TANGENTIAL VELOCITY PROFILE

V_∞ = 100.8 f/s Z/C = 15
α = 4° t = .09920 sec

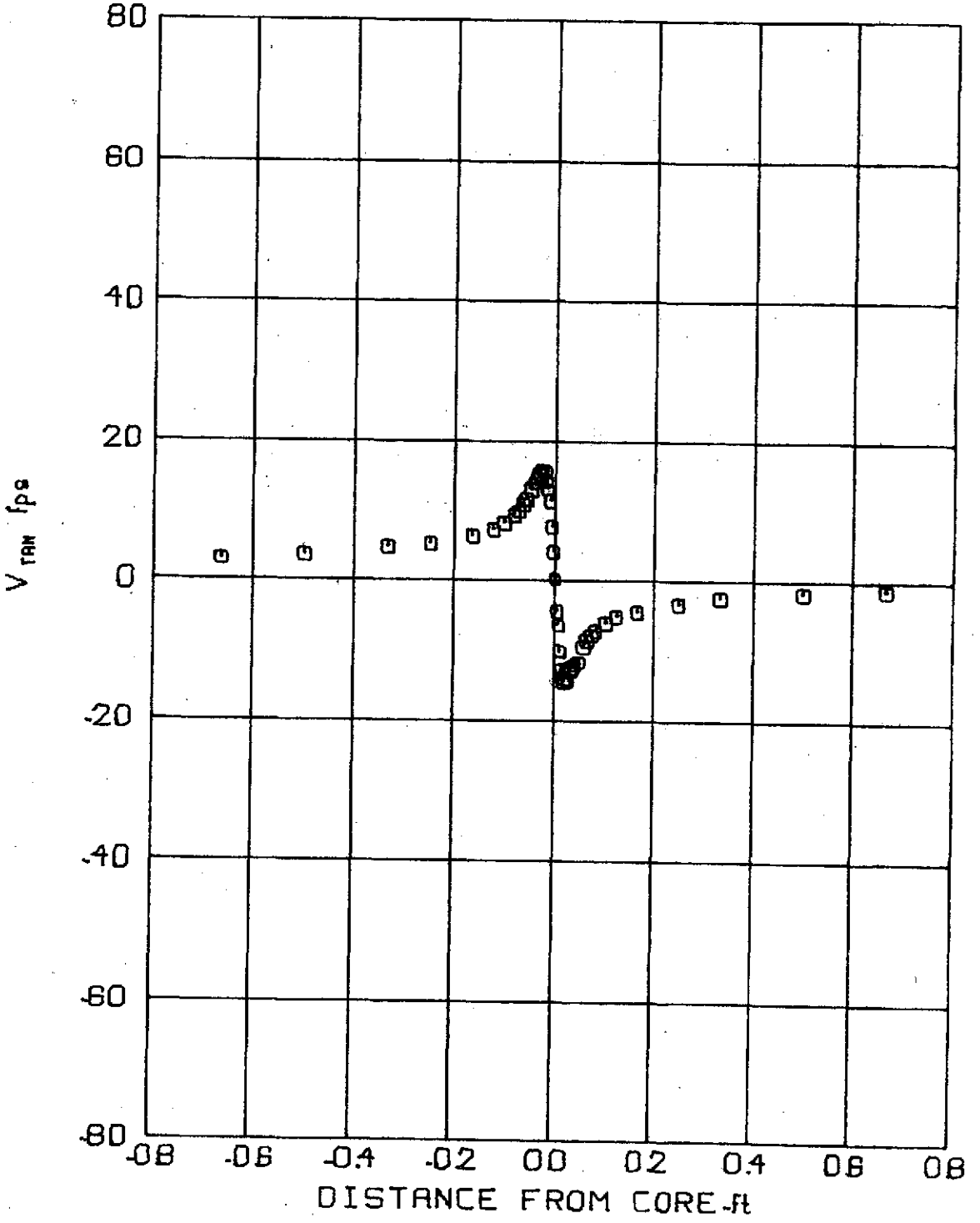

FIG 46 TANGENTIAL VELOCITY PROFILE

V_∞ = 68.4 f/s Z/C = 20
α = 4° t = .19469 sec

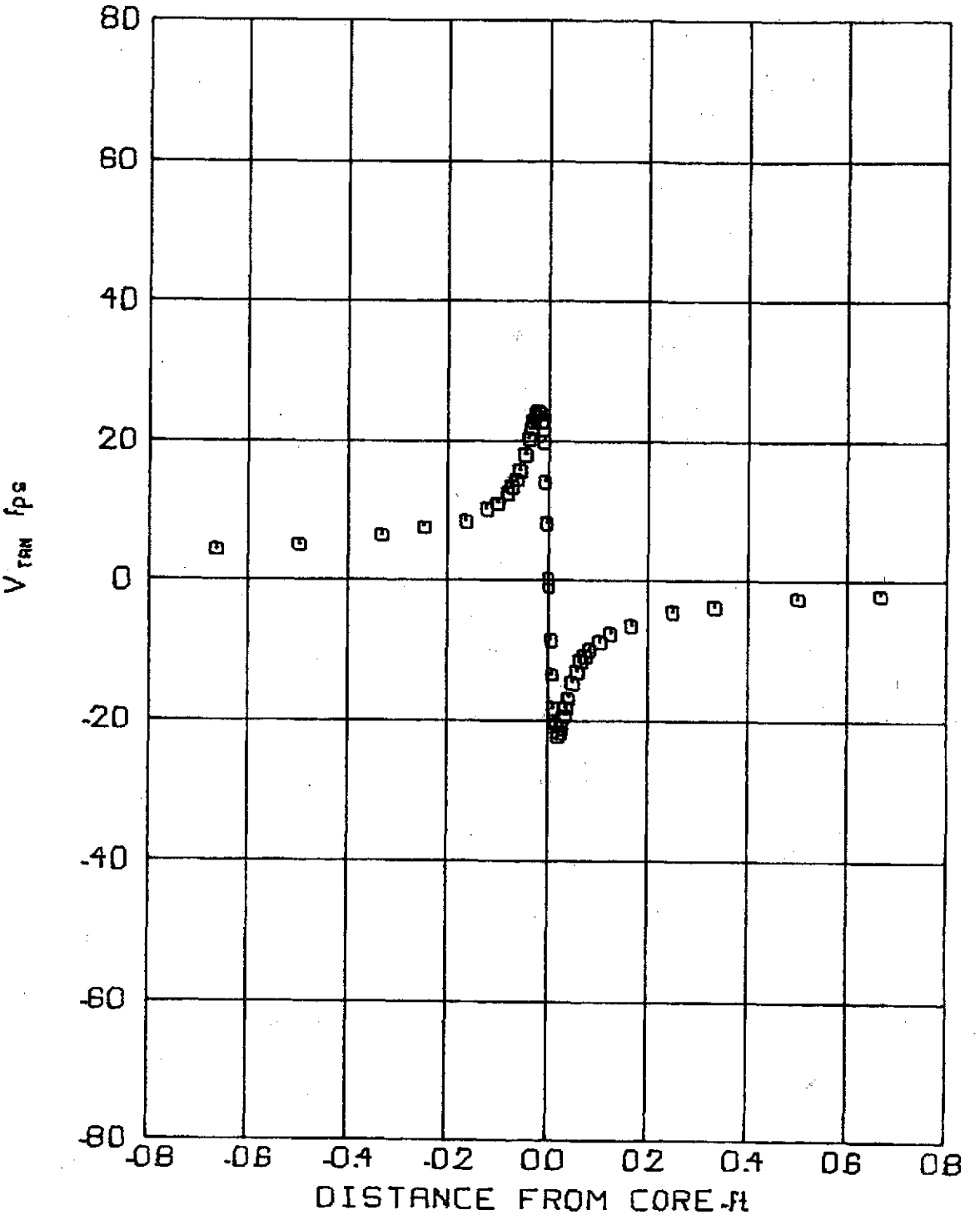

FIG 47 TANGENTIAL VELOCITY PROFILE

V_∞ = 103.3 f/s Z/C = 20
α = 4° t = .12897 sec

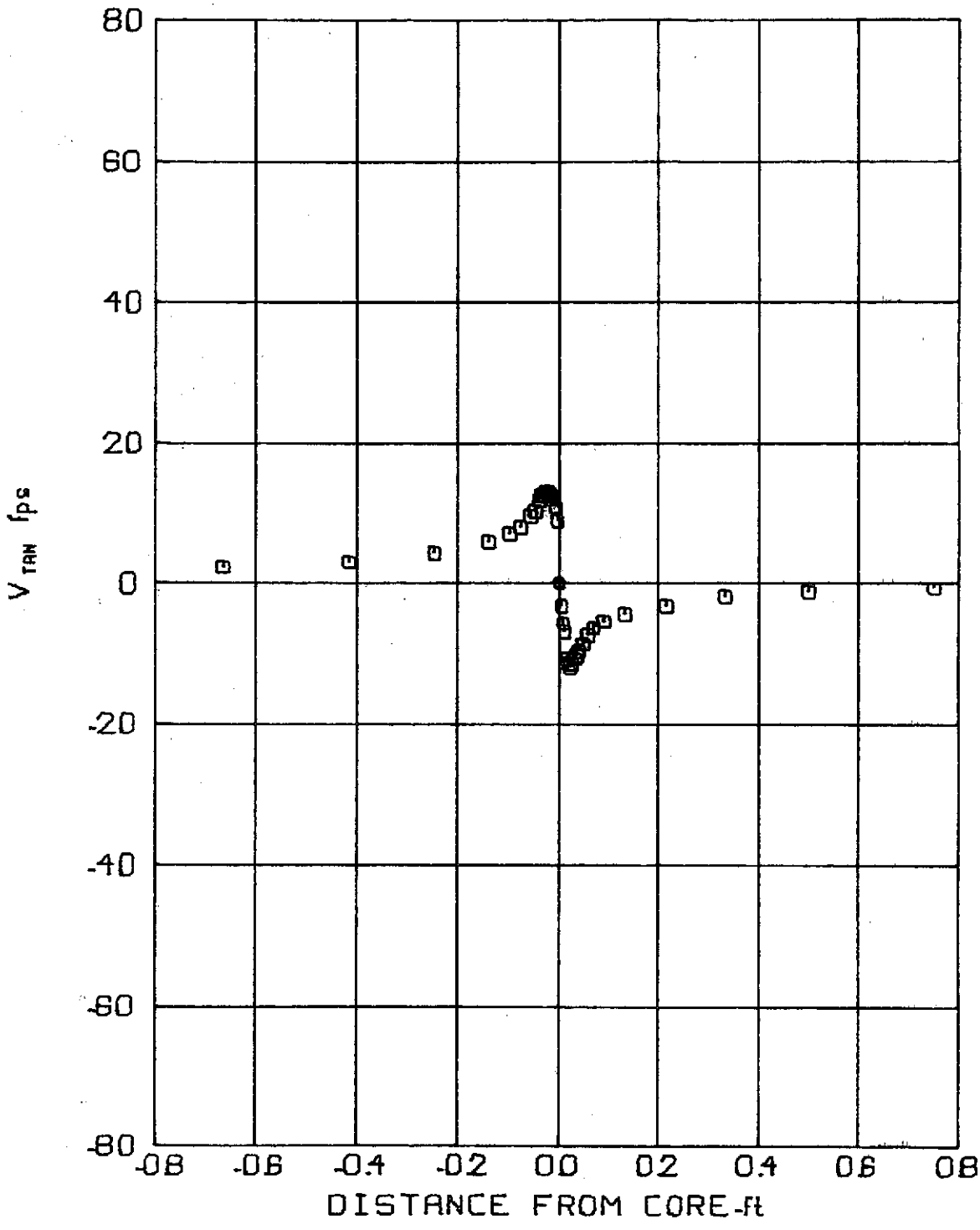

FIG 48 TANGENTIAL VELOCITY PROFILE

V_∞ = 88.4 f/s Z/C = 25
α = 4° t = .24337 sec

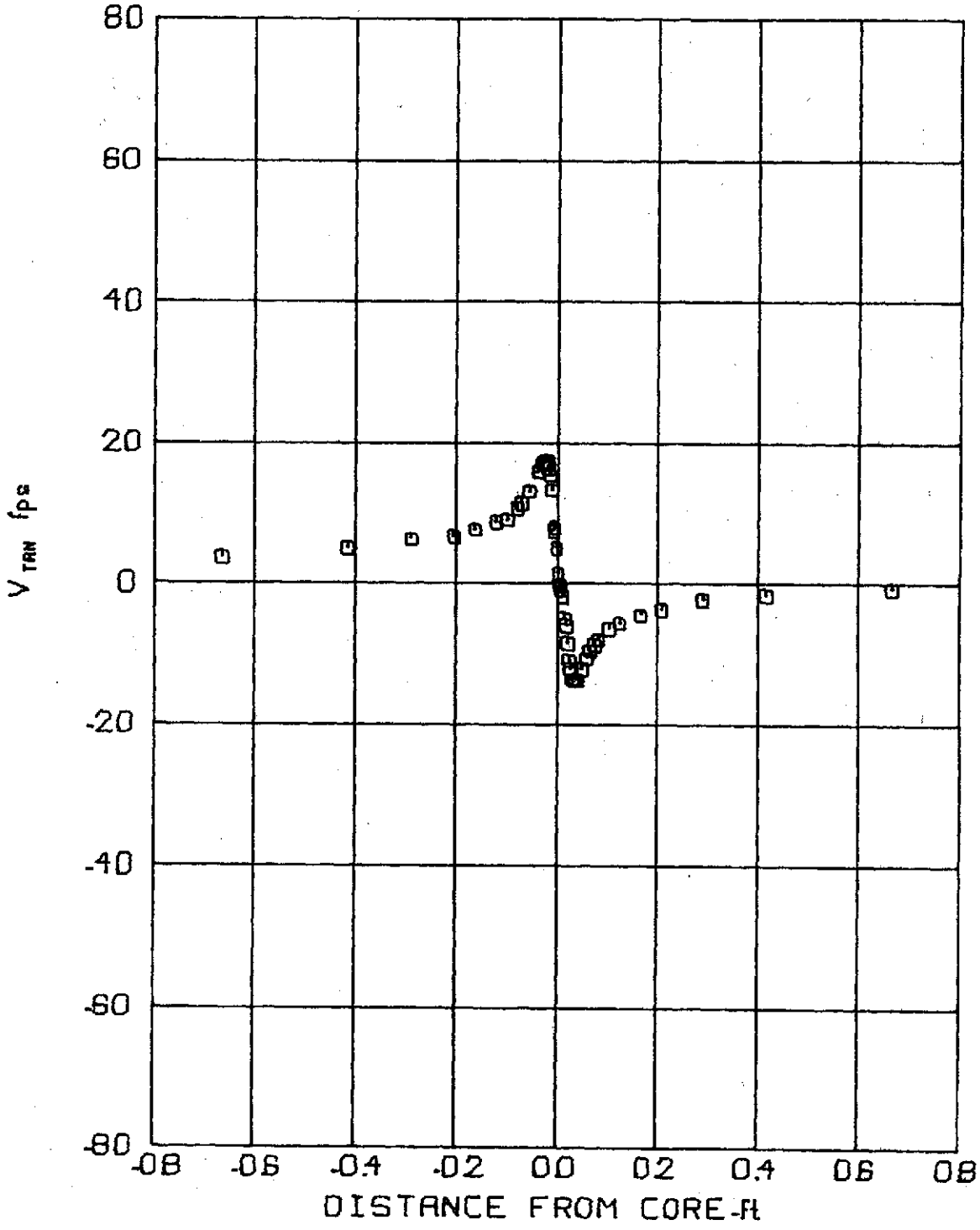

FIG 49 TANGENTIAL VELOCITY PROFILE

V_∞ = 86.5 f/s Z/C = 25
α = 4° t = .19256 sec

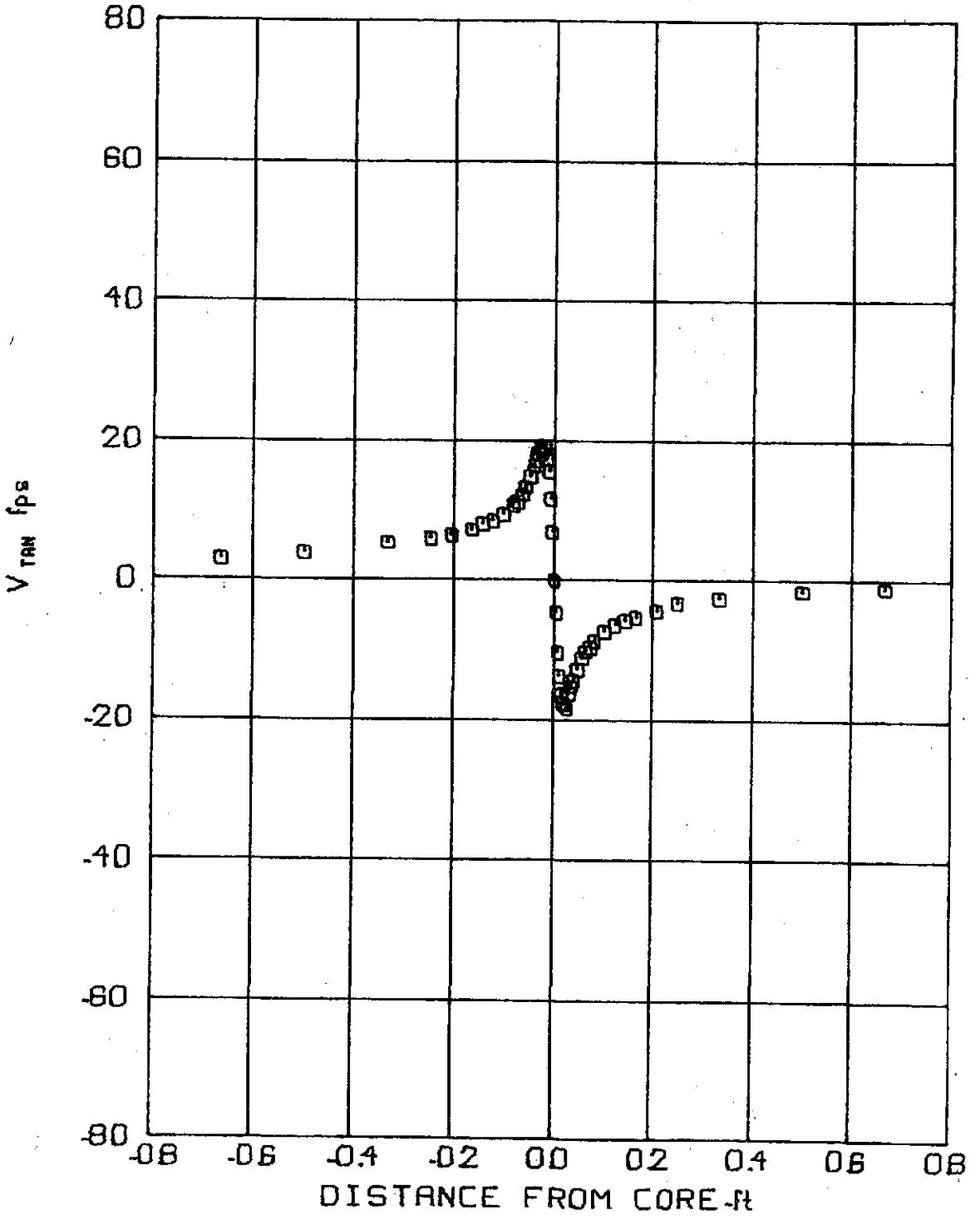

FIG 50 TANGENTIAL VELOCITY PROFILE

V_∞ = 102.8 f/s Z/C = .25
α = 4° t = .16199 sec

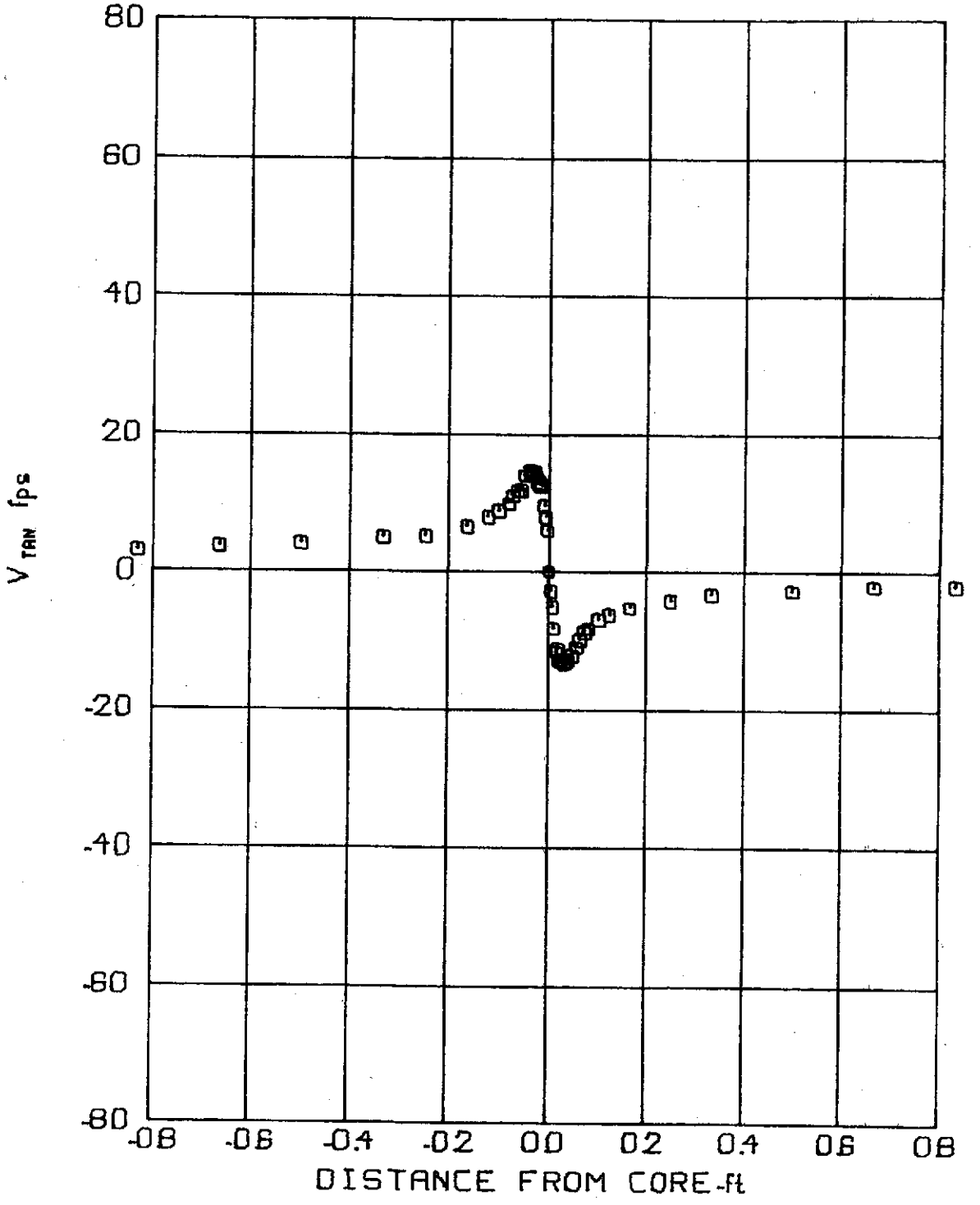

FIG 51 TANGENTIAL VELOCITY PROFILE

V_∞ = 69.4 f/s Z/C = 30
α = 4° t = .28790 sec

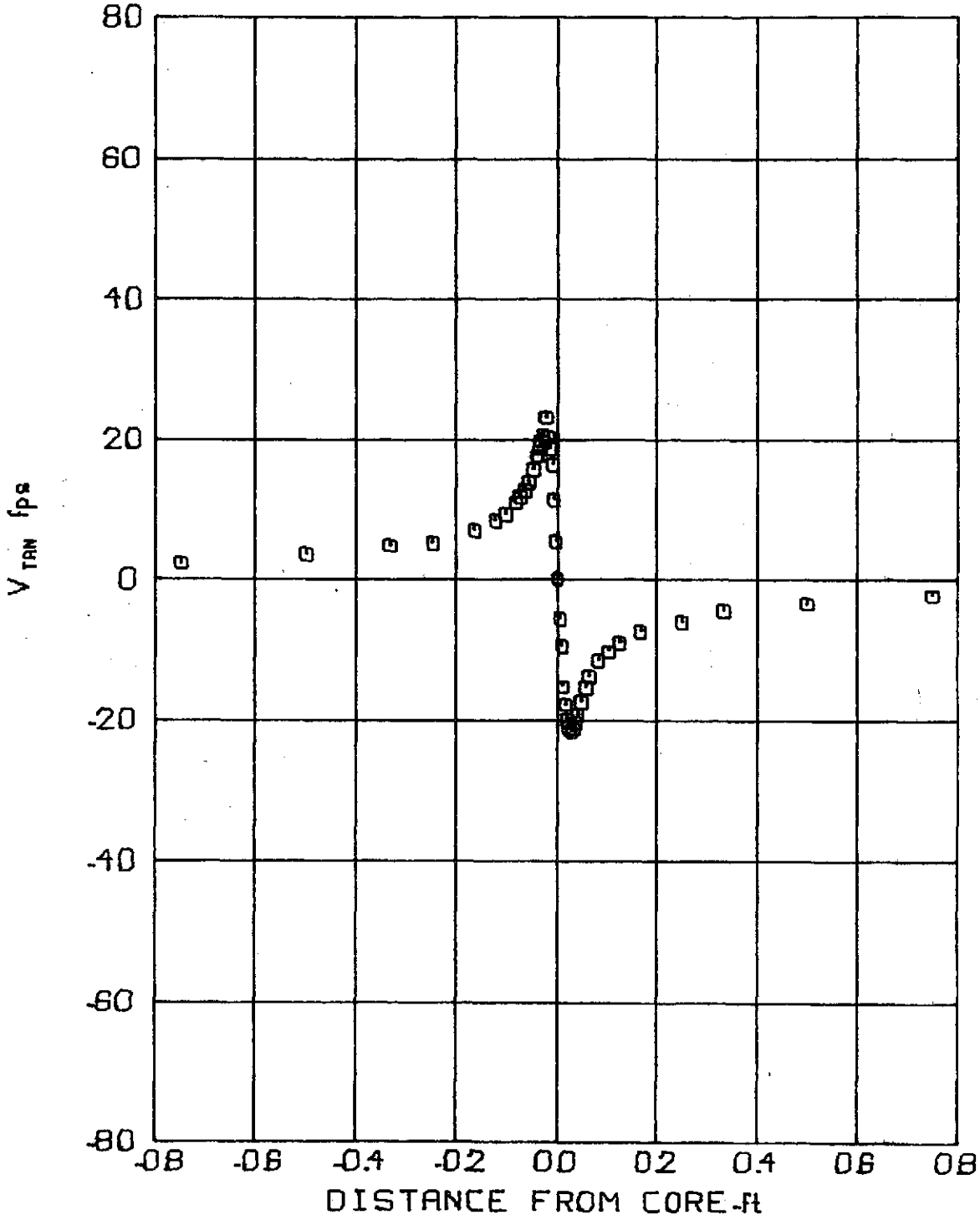

FIG 52 TANGENTIAL VELOCITY PROFILE

V_∞ = 105.6 f/s Z/C = 30
α = 4° t = .18928 sec

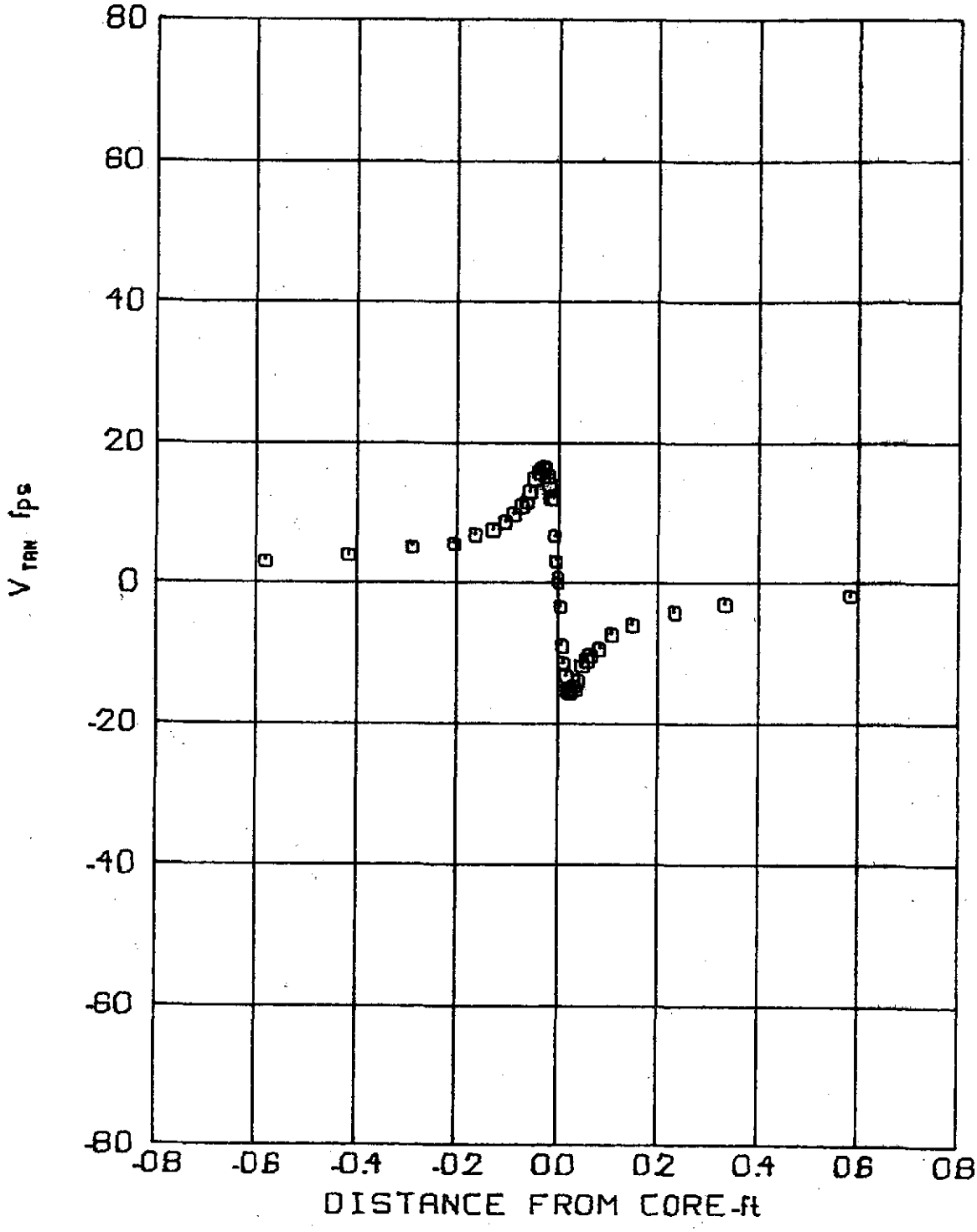

FIG 53 TANGENTIAL VELOCITY PROFILE

V_∞ = 49.1 f/s Z/C = 15
α = 8° t = .20348 sec

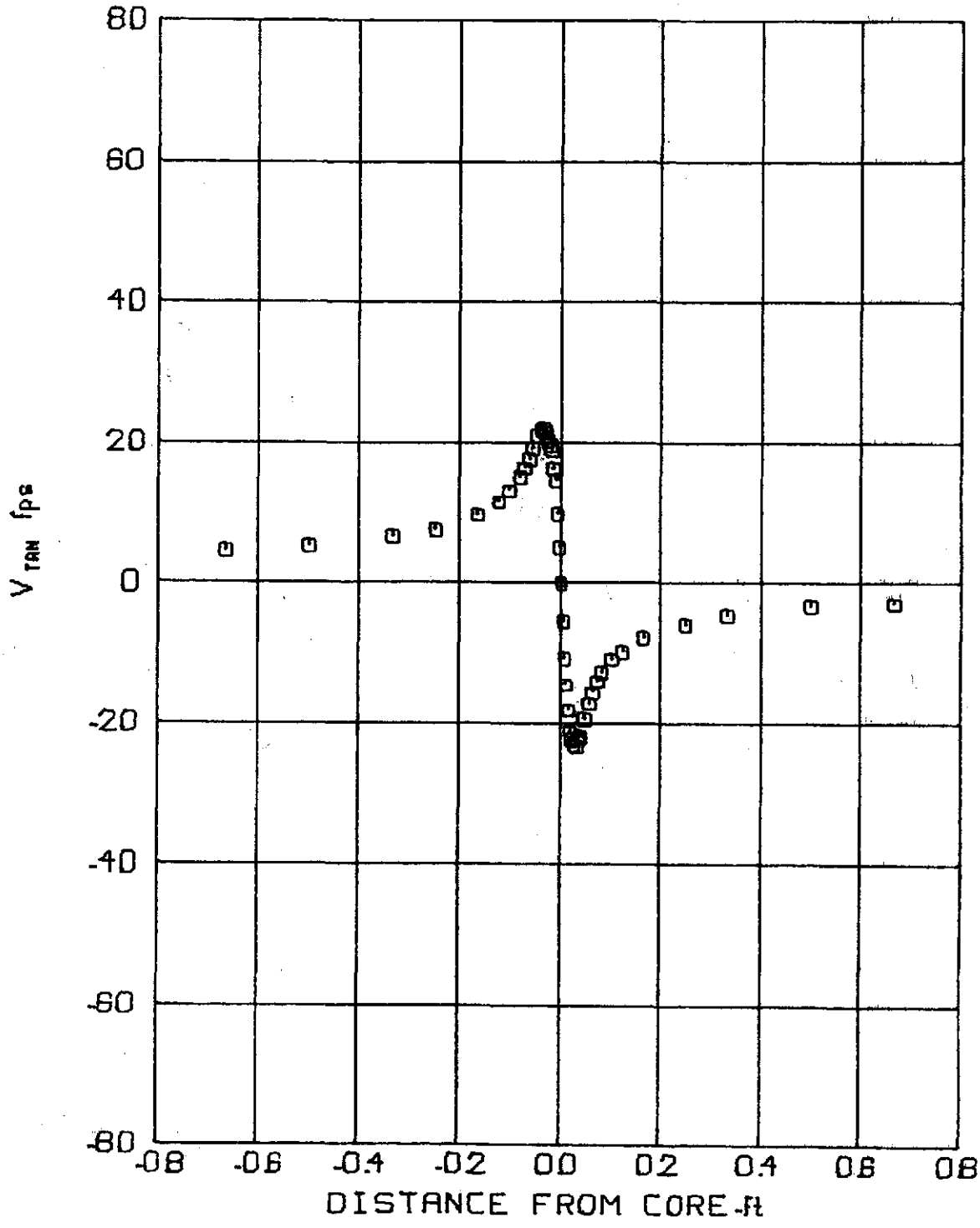

FIG 54 TANGENTIAL VELOCITY PROFILE

V_∞ = 69.5 f/s Z/C = 20
α = 6° t = .19162 sec

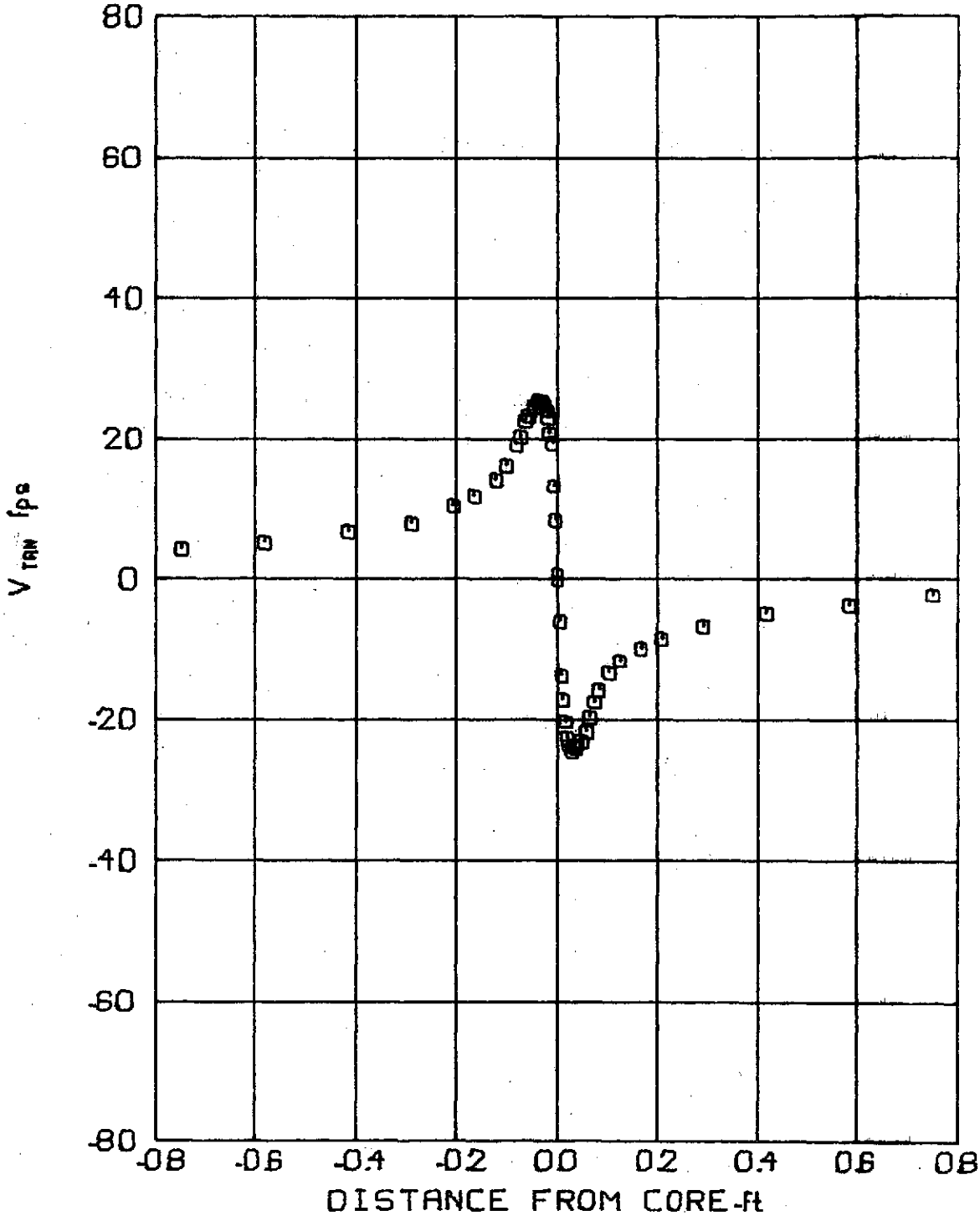

FIG 55 TANGENTIAL VELOCITY PROFILE

V_∞ = 86.9 f/s Z/C = 25
α = 6° t = .19174 sec

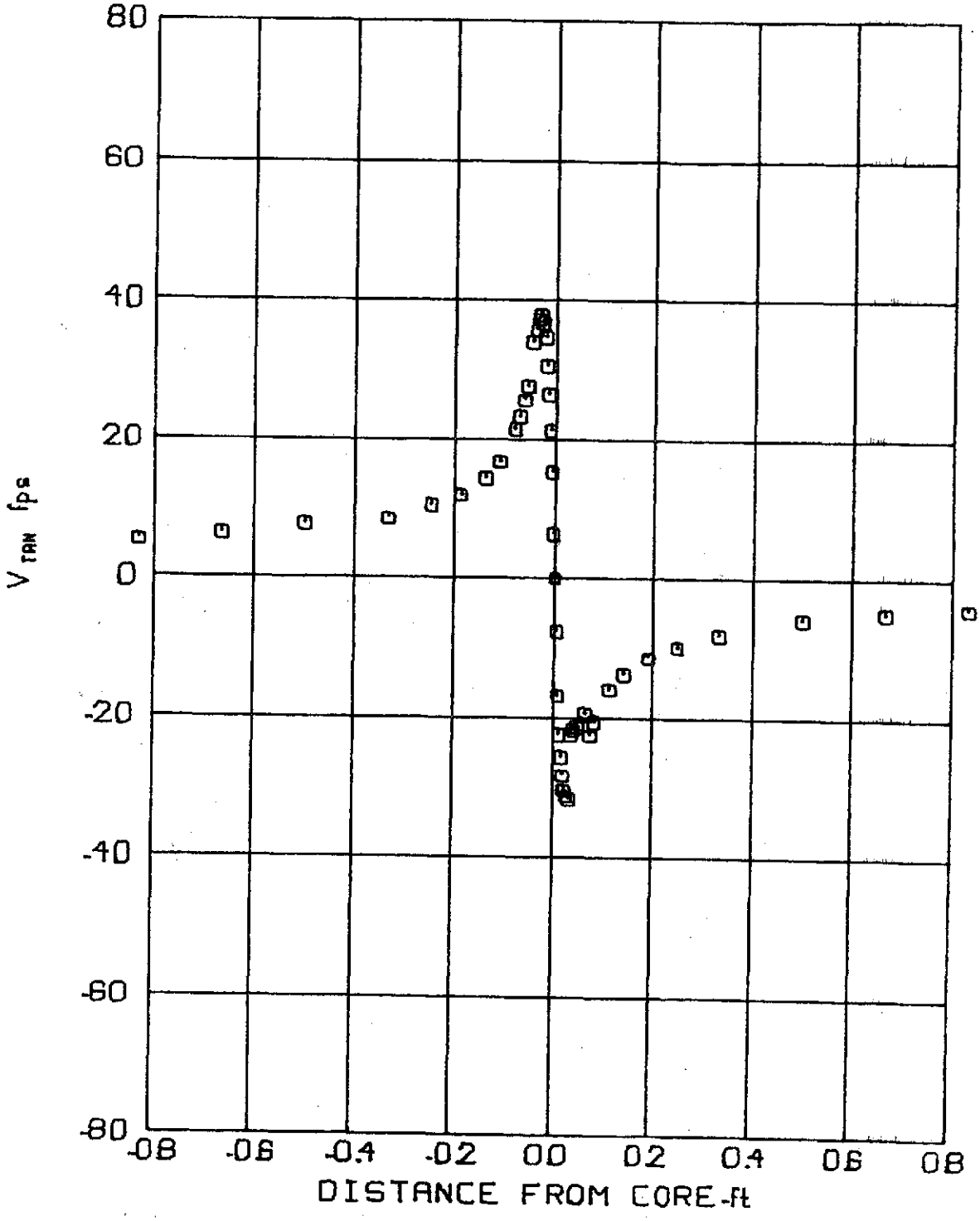

FIG 56 TANGENTIAL VELOCITY PROFILE

V_∞ = 103.6 f/s Z/C = 30
α = 6° t = .19288 sec

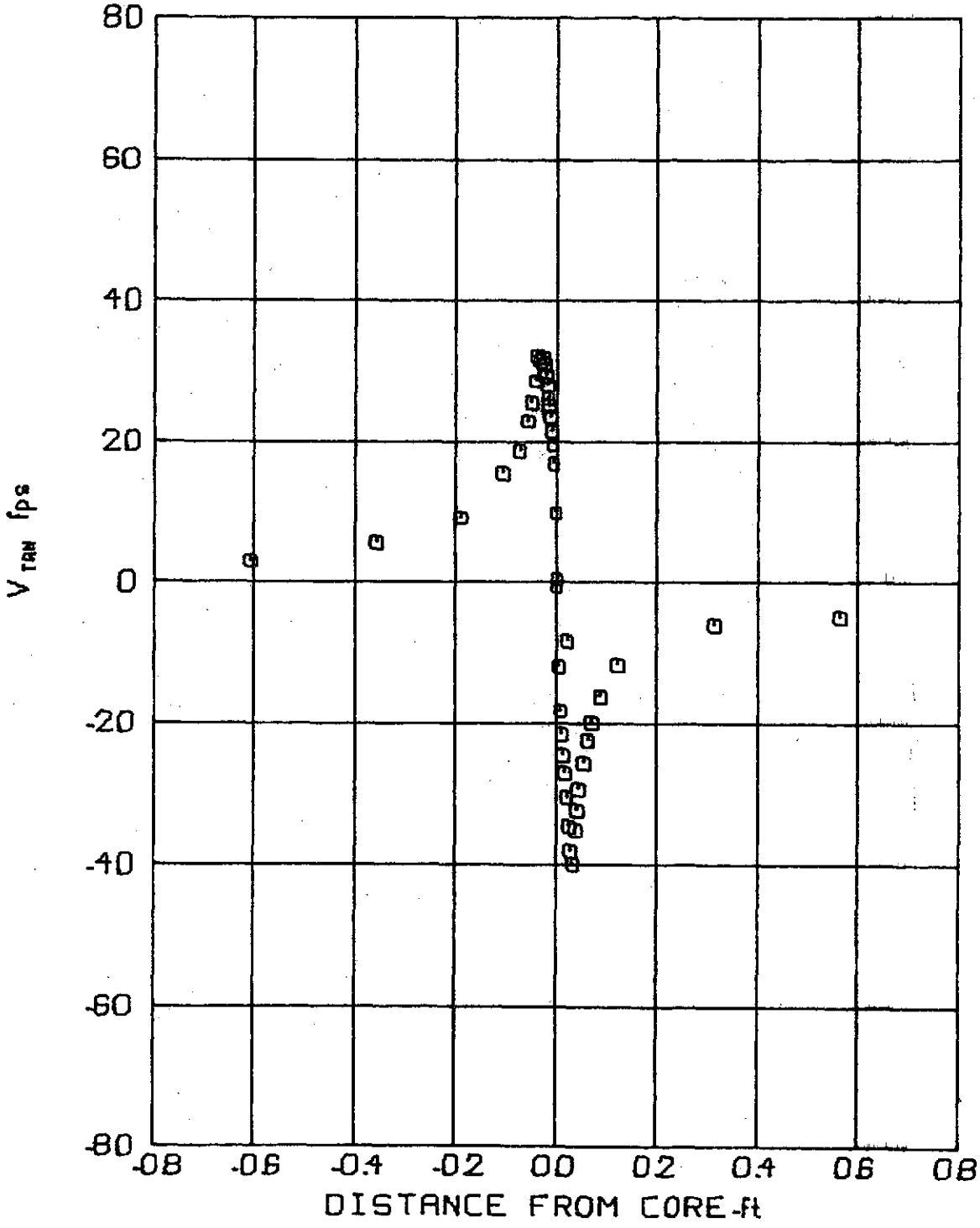

FIG 57 TANGENTIAL VELOCITY PROFILE

V_∞ = 68.7 f/s Z/C = 2
α = 8° t = .01939 sec

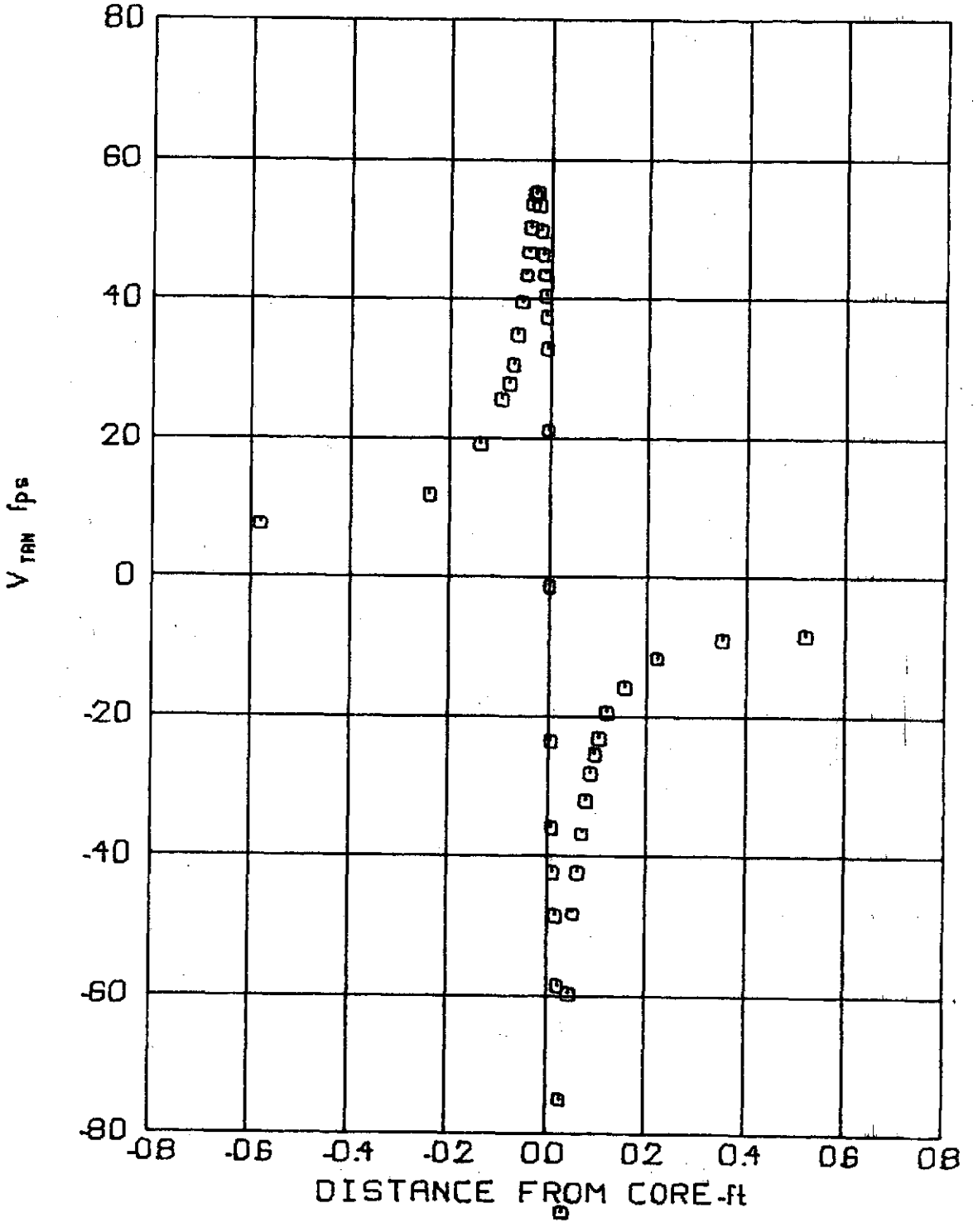

FIG 58 TANGENTIAL VELOCITY PROFILE

V_∞ = 105.8 f/s Z/C = 2
α = 8° t = .01259 sec

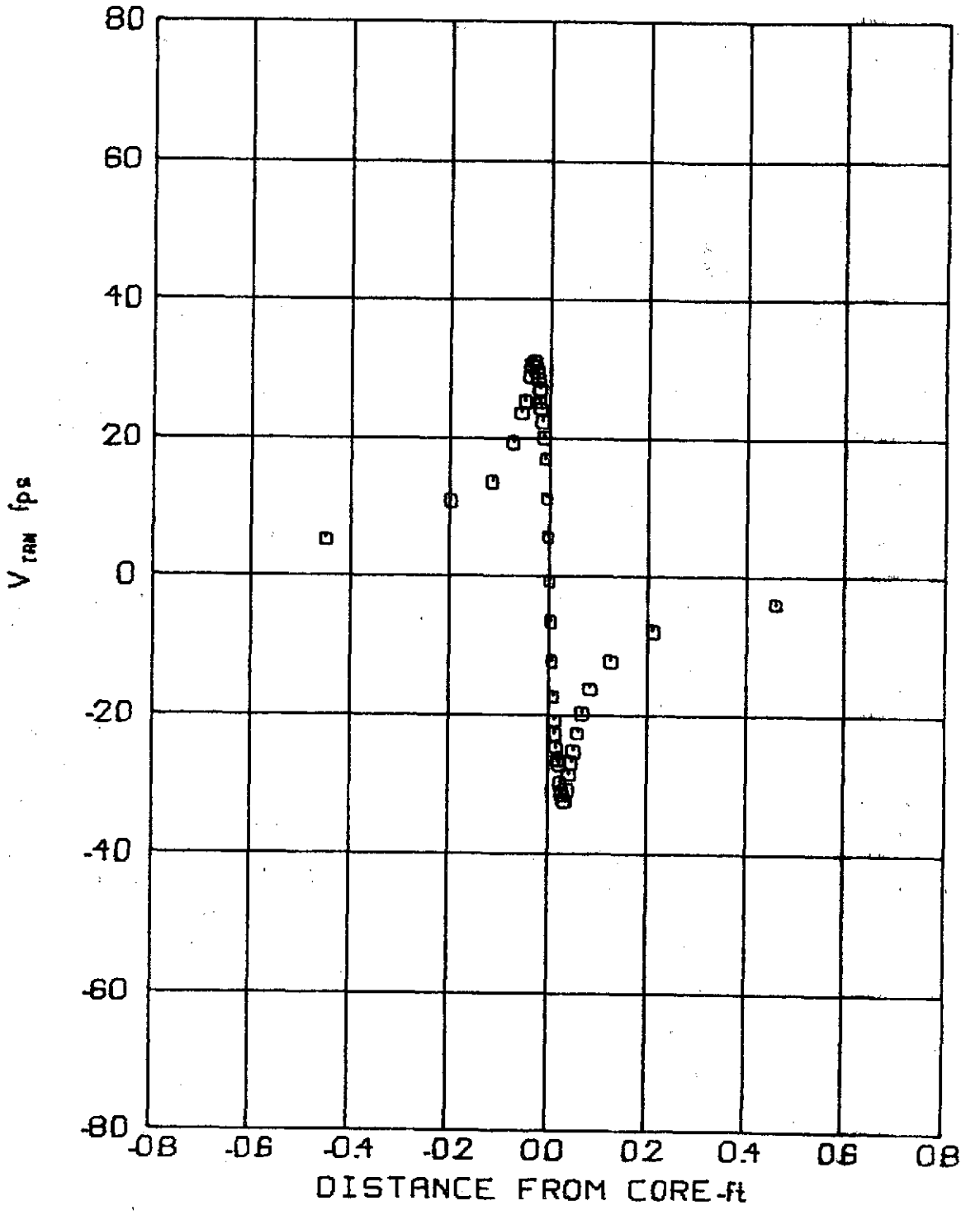

FIG 59 TANGENTIAL VELOCITY PROFILE

V_∞ = 69.7 f/s Z/C = 5
α = 8° t = .04780 sec

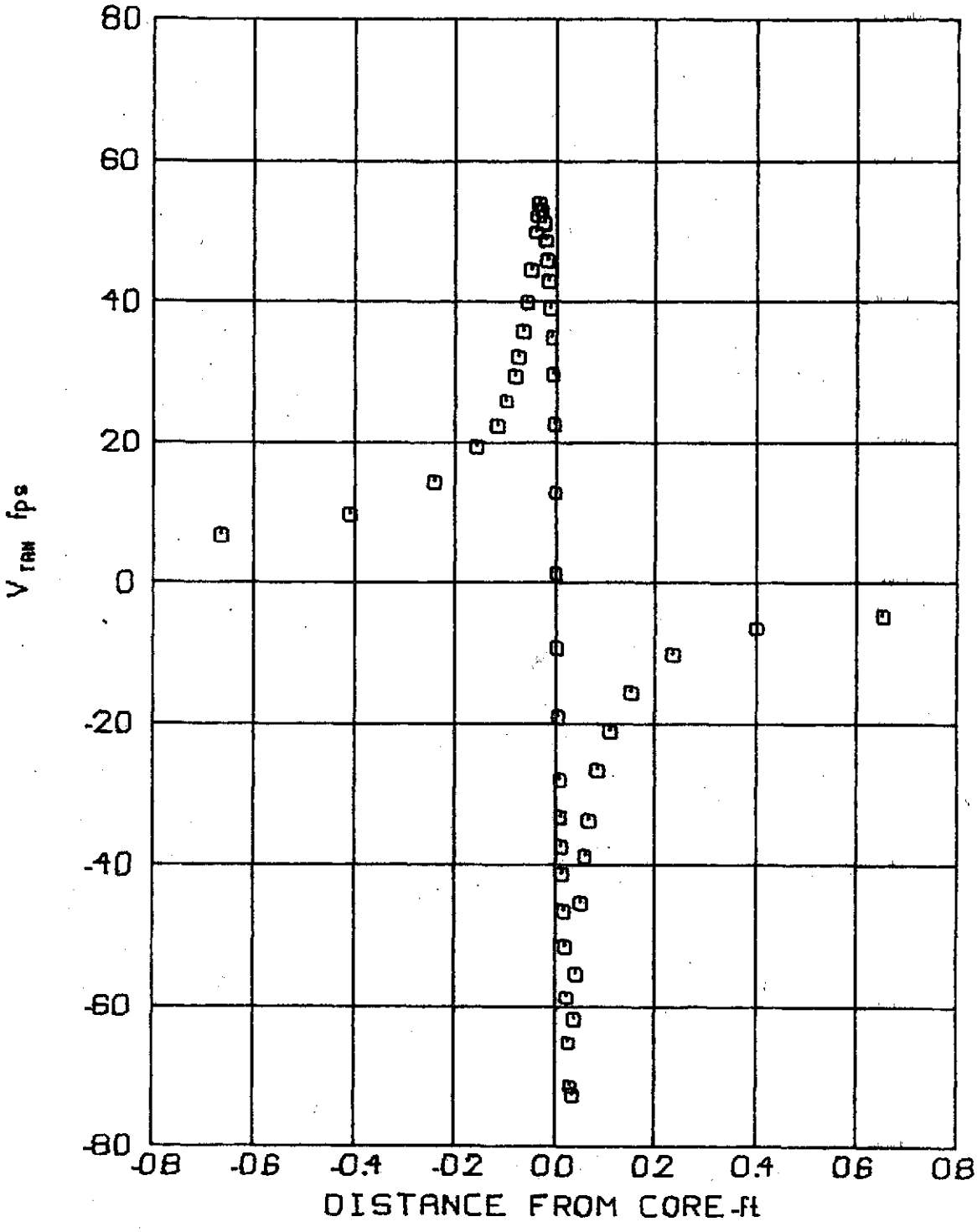

FIG 60 TANGENTIAL VELOCITY PROFILE

V_∞ = 103.9 f/s Z/C = 5
α = 8° t = .03207 sec

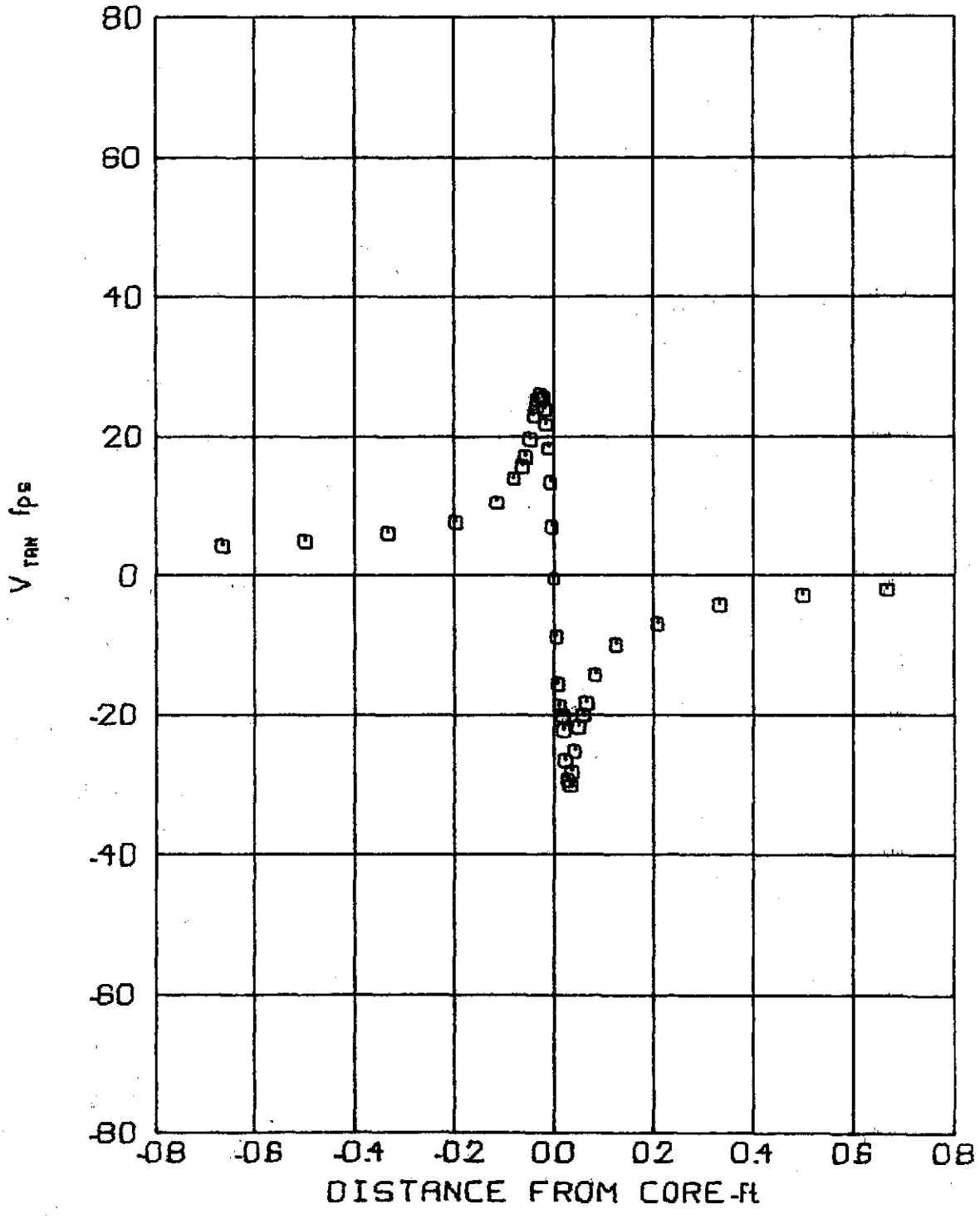

FIG 61 TANGENTIAL VELOCITY PROFILE

V_∞ = 66.1 f/s Z/C = 10
α = 8° t = .10076 sec

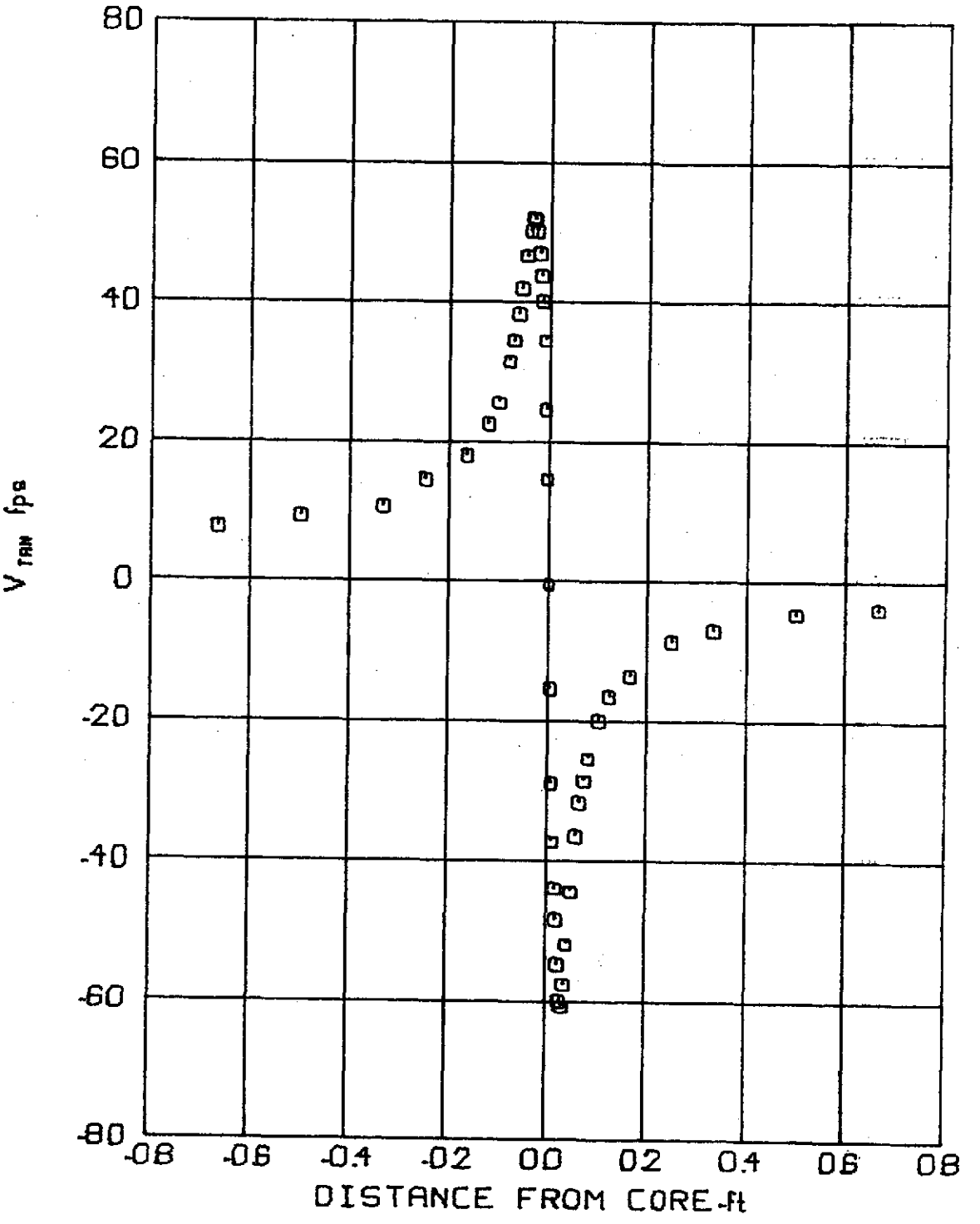

FIG 62 TANGENTIAL VELOCITY PROFILE

V_∞ = 98.8 f/s Z/C = 10
α = 8° t = .06742 sec

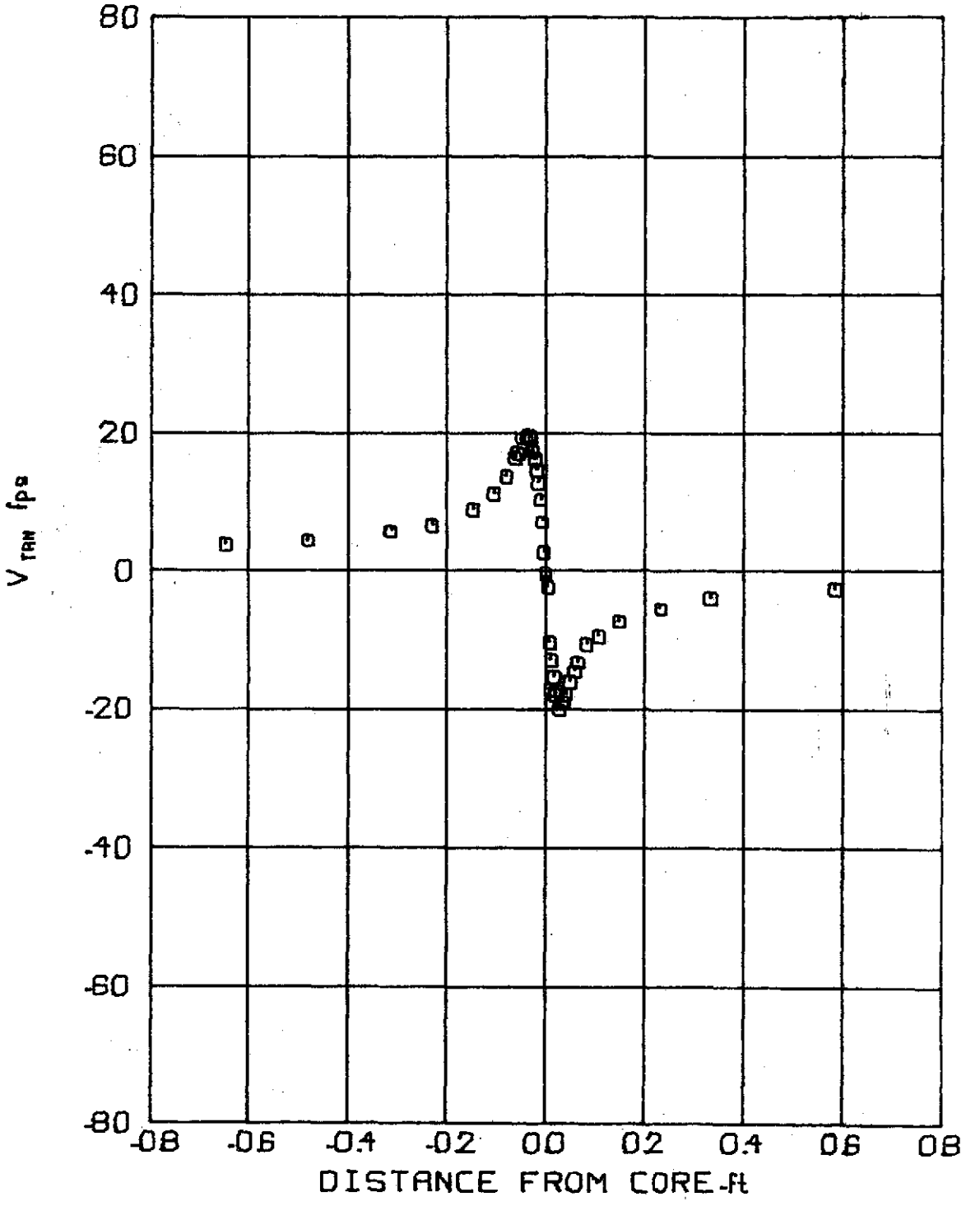

FIG 63 TANGENTIAL VELOCITY PROFILE

V_∞ = 48.7 f/s Z/C = 15
α = 8° t = .20529 sec

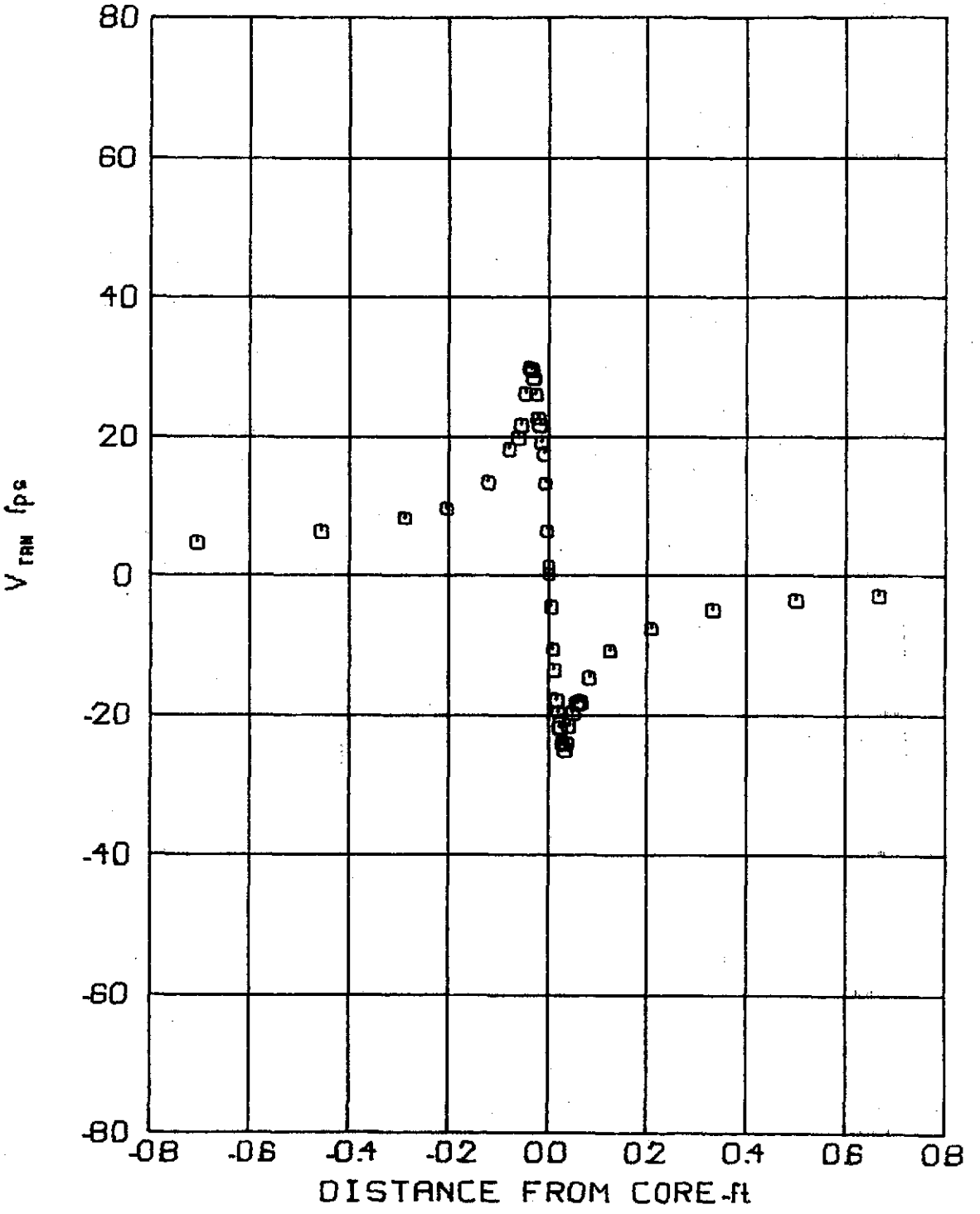

FIG 64 TANGENTIAL VELOCITY PROFILE

V_∞ = 65.8 f/s Z/C = 15
α = 8° t = .15195 sec

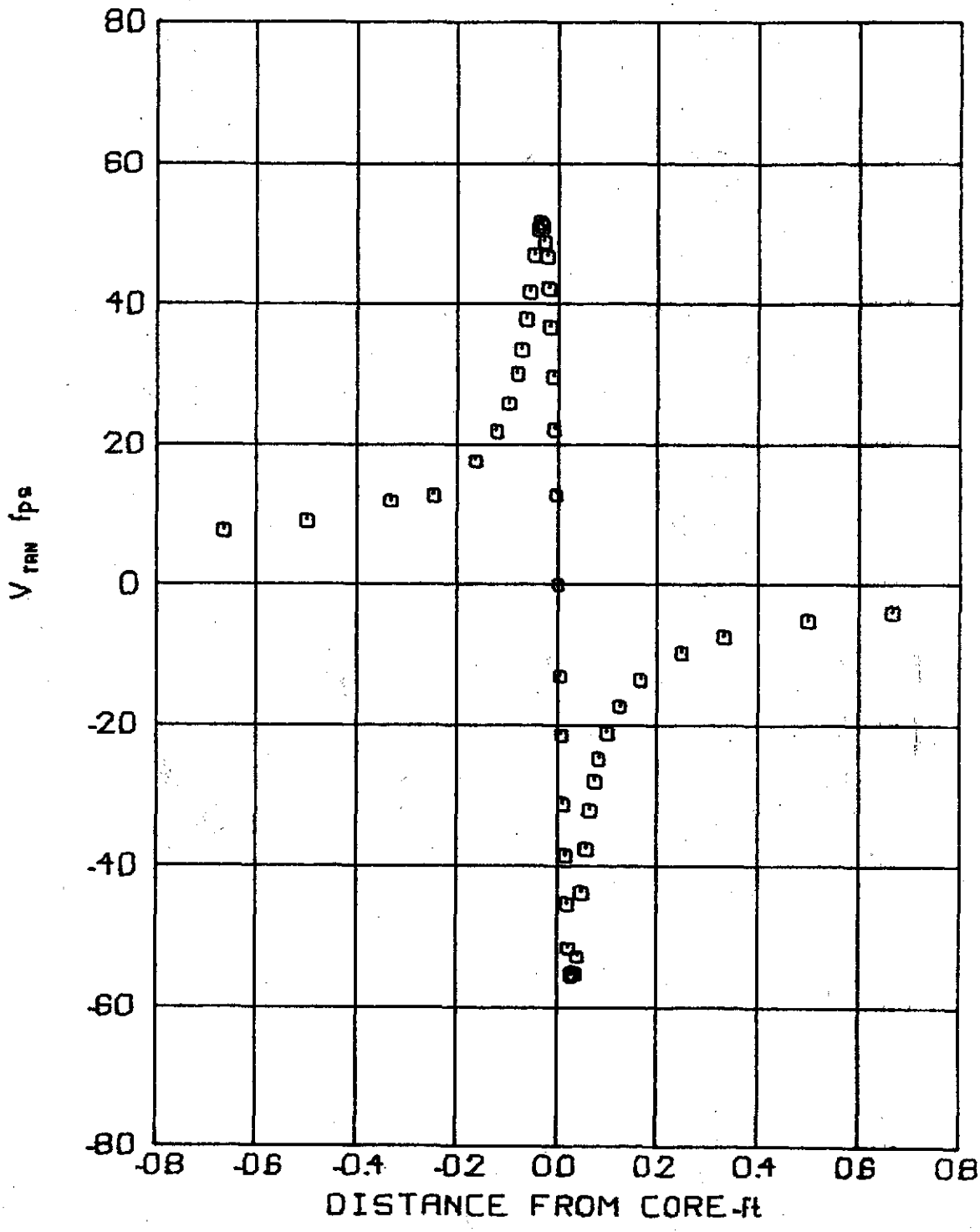

FIG 65 TANGENTIAL VELOCITY PROFILE

V_∞ = 100.4 f/s Z/C = 15
α = 8° t = .09957 sec

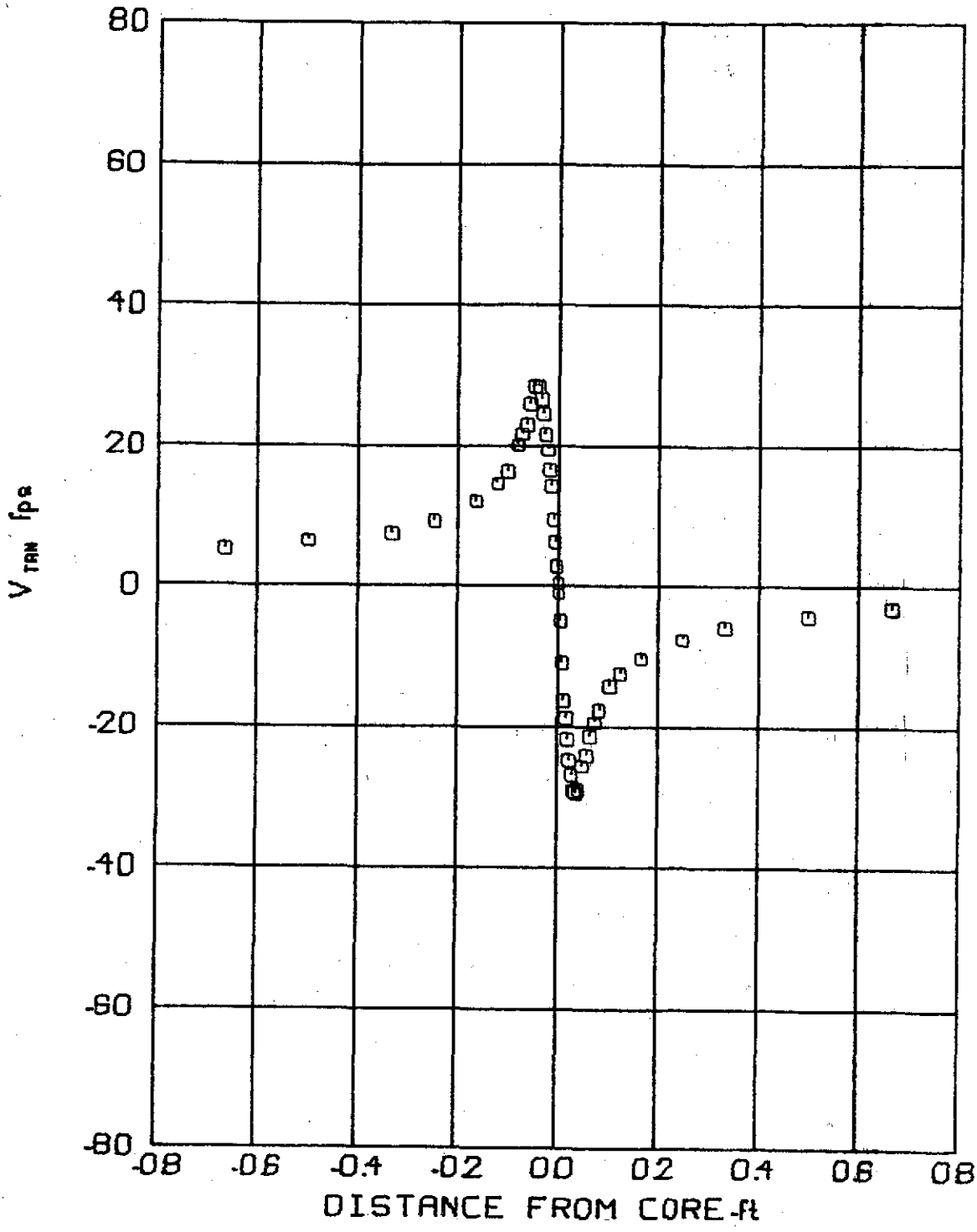

FIG 66 TANGENTIAL VELOCITY PROFILE

V_∞ = 69.0 f/s Z/C = 20
α = 8° t = .19303 sec

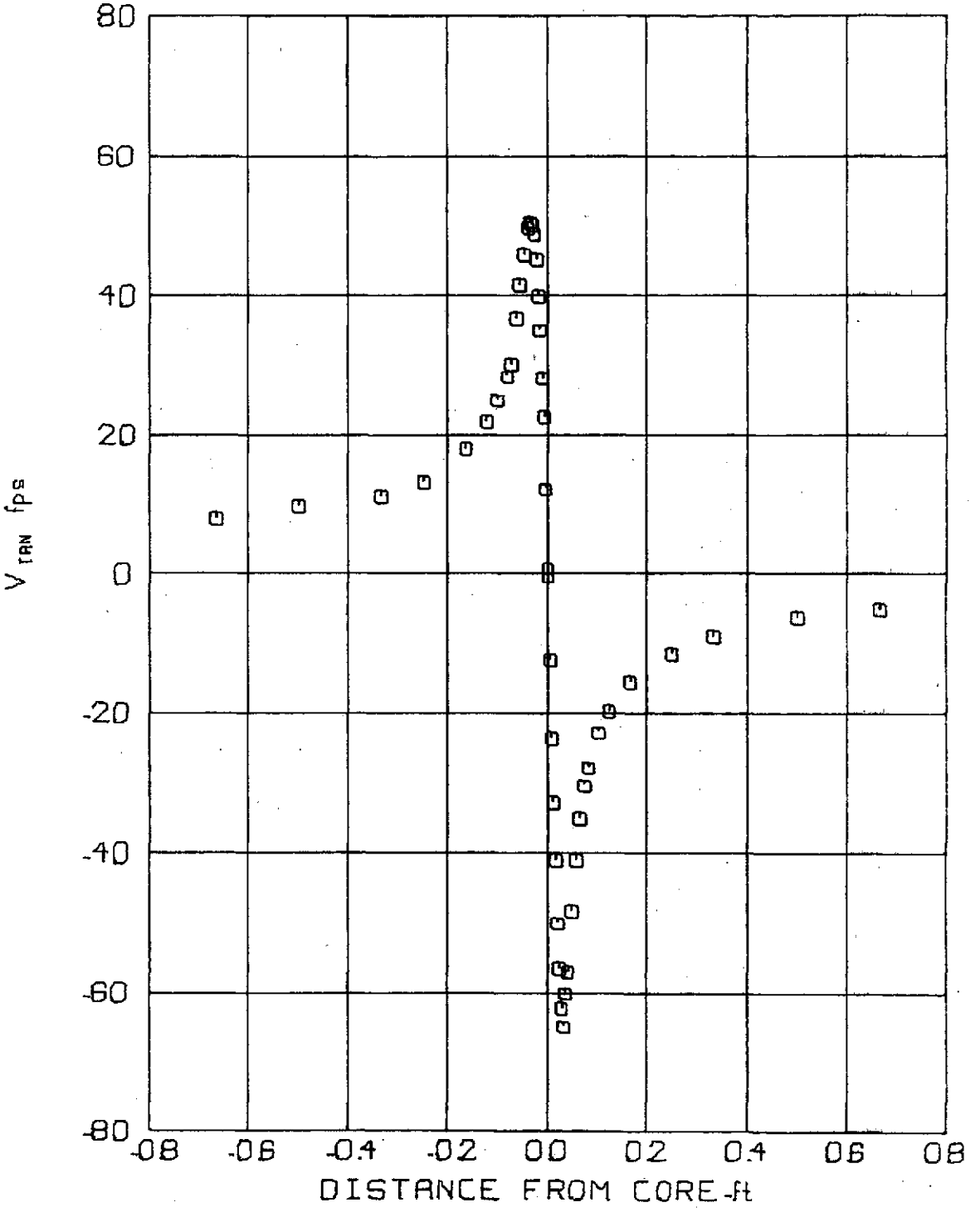

FIG 67 TANGENTIAL VELOCITY PROFILE

V_∞ = 104.7 f/s Z/C = 20
α = 8° t = .12729 sec

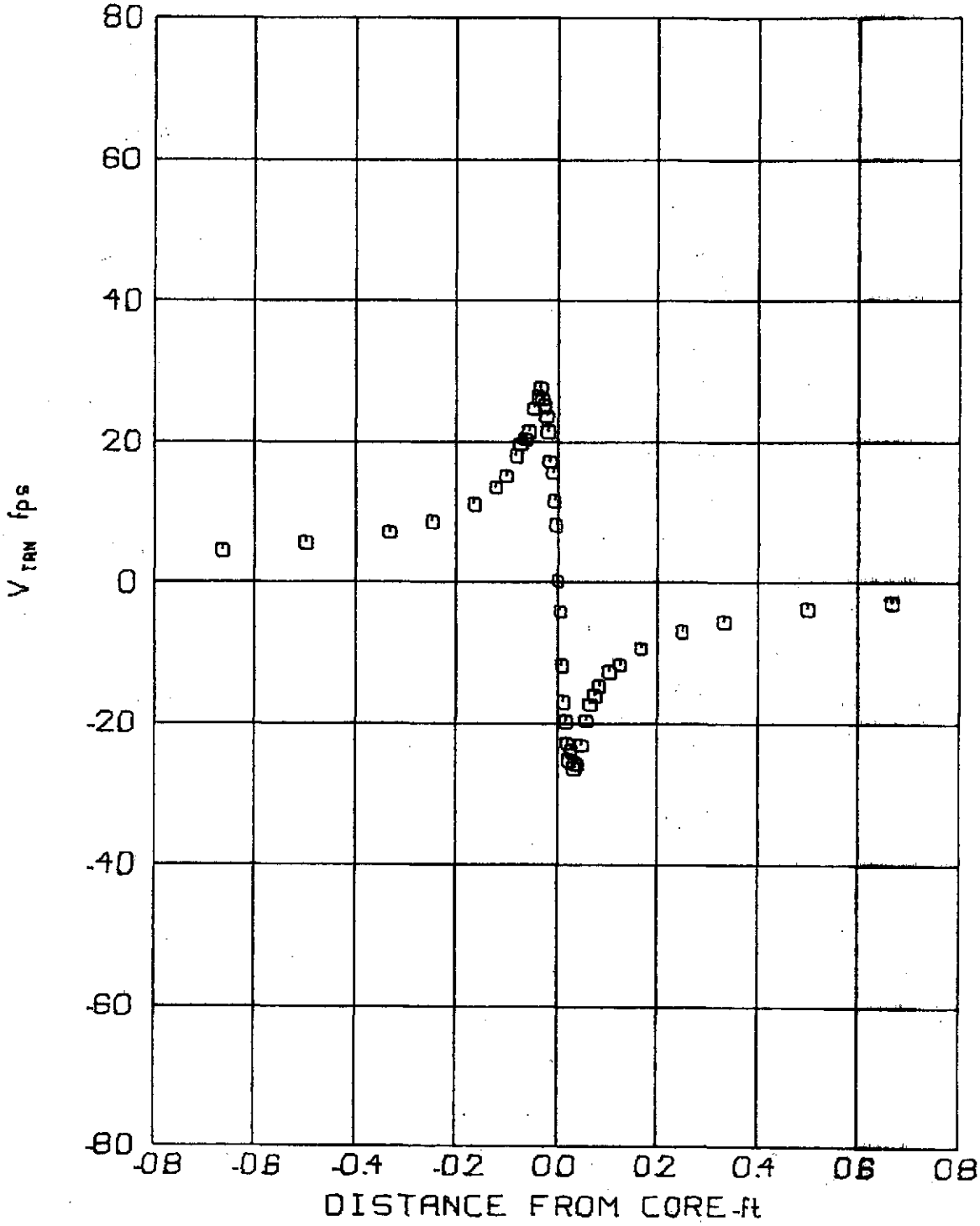

FIG 68 TANGENTIAL VELOCITY PROFILE

V_∞ = 68.2 f/s Z/C = .25
α = 8° t = .24413 sec

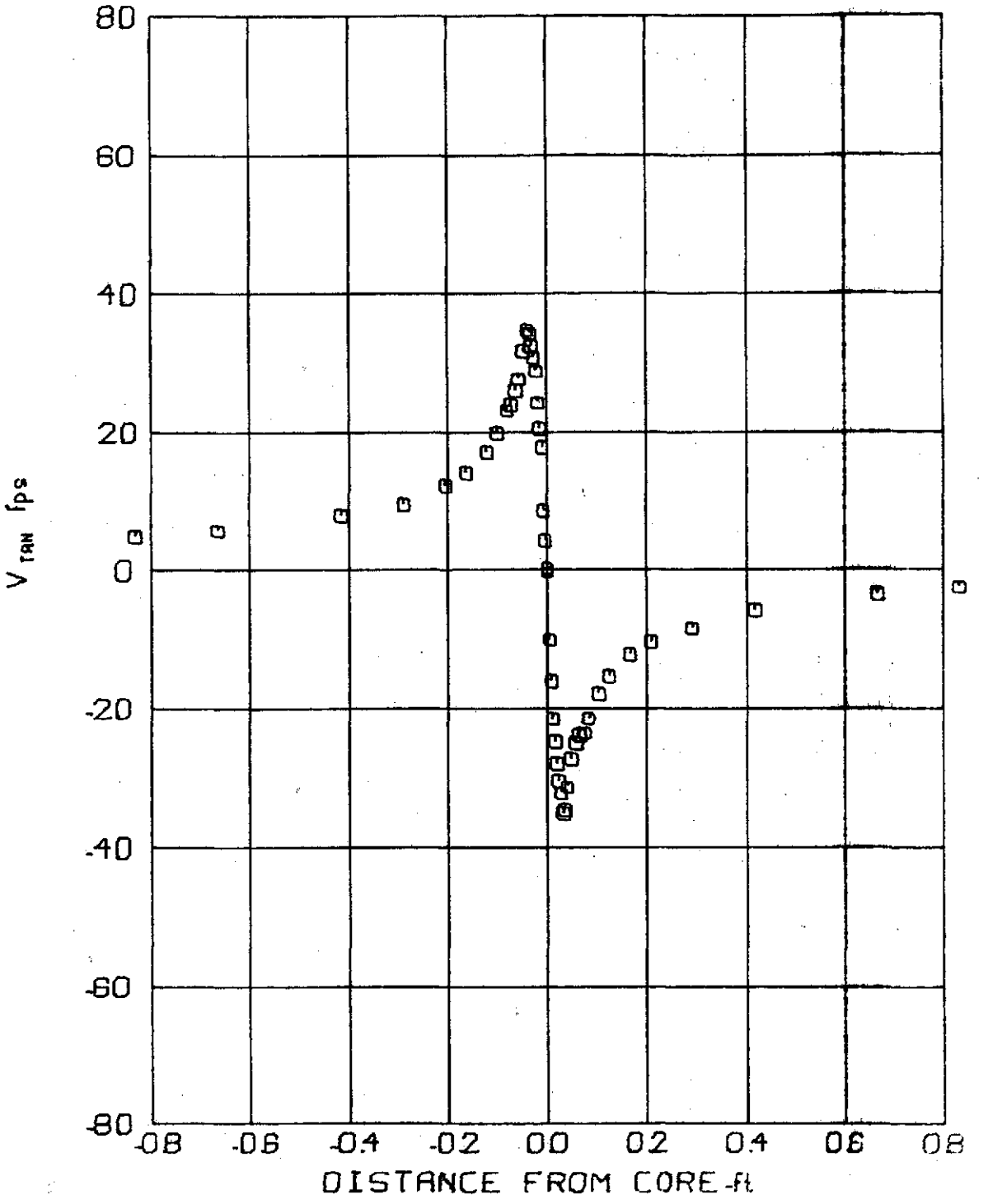

FIG 69 TANGENTIAL VELOCITY PROFILE

V_∞ = 86.5 f/s Z/C = 25
α = 8° t = .19256 sec

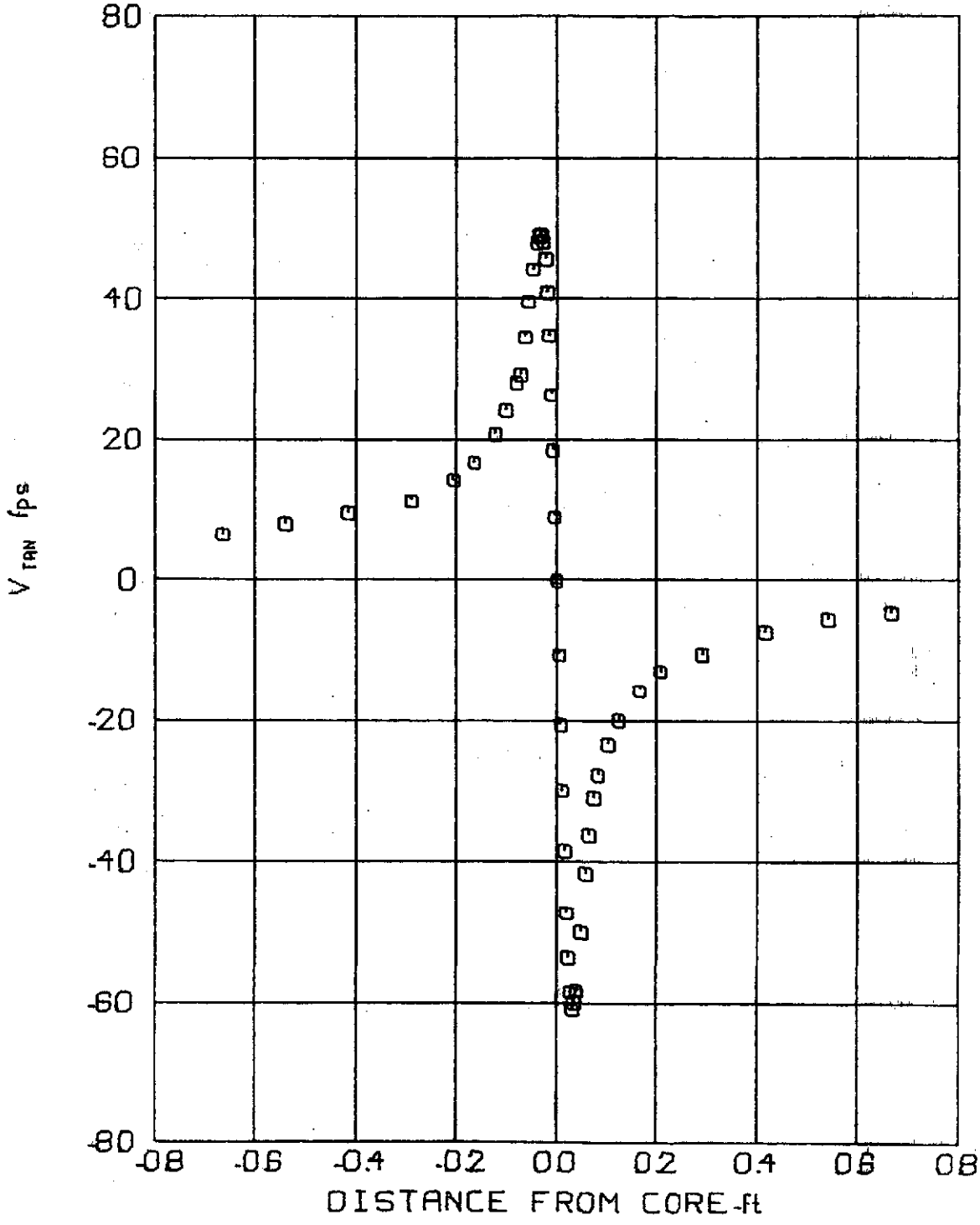

FIG 70 TANGENTIAL VELOCITY PROFILE

V_∞ = 105.3 f/s Z/C = 25
α = 8° t = .15818 sec

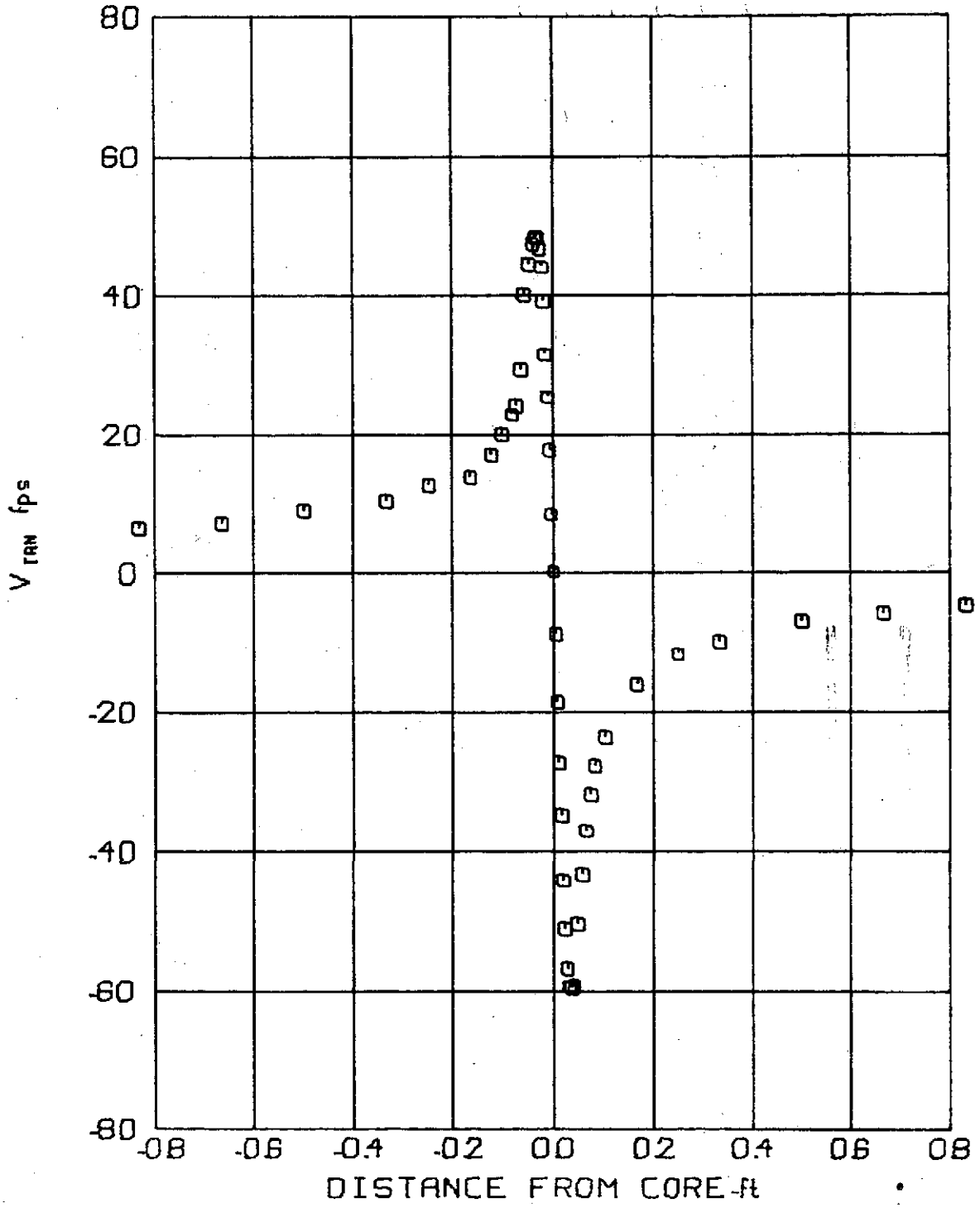

FIG 71 TANGENTIAL VELOCITY PROFILE

V_∞ = 104.0 f/s Z/C = 30
α = 8° t = .19221 sec

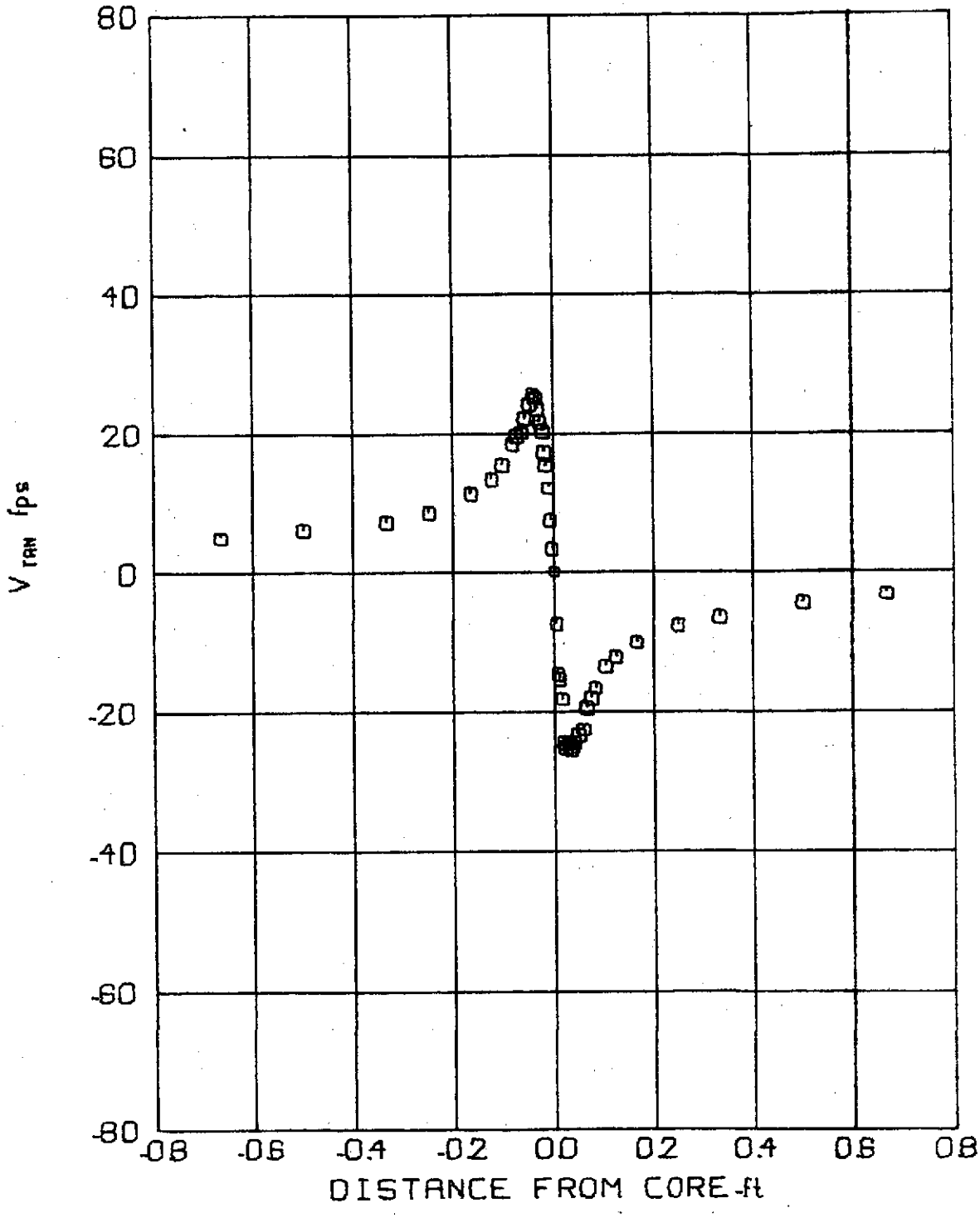

FIG 72 TANGENTIAL VELOCITY PROFILE

V_∞ = 68.0 f/s Z/C = 30
α = 8° t = .29398 sec

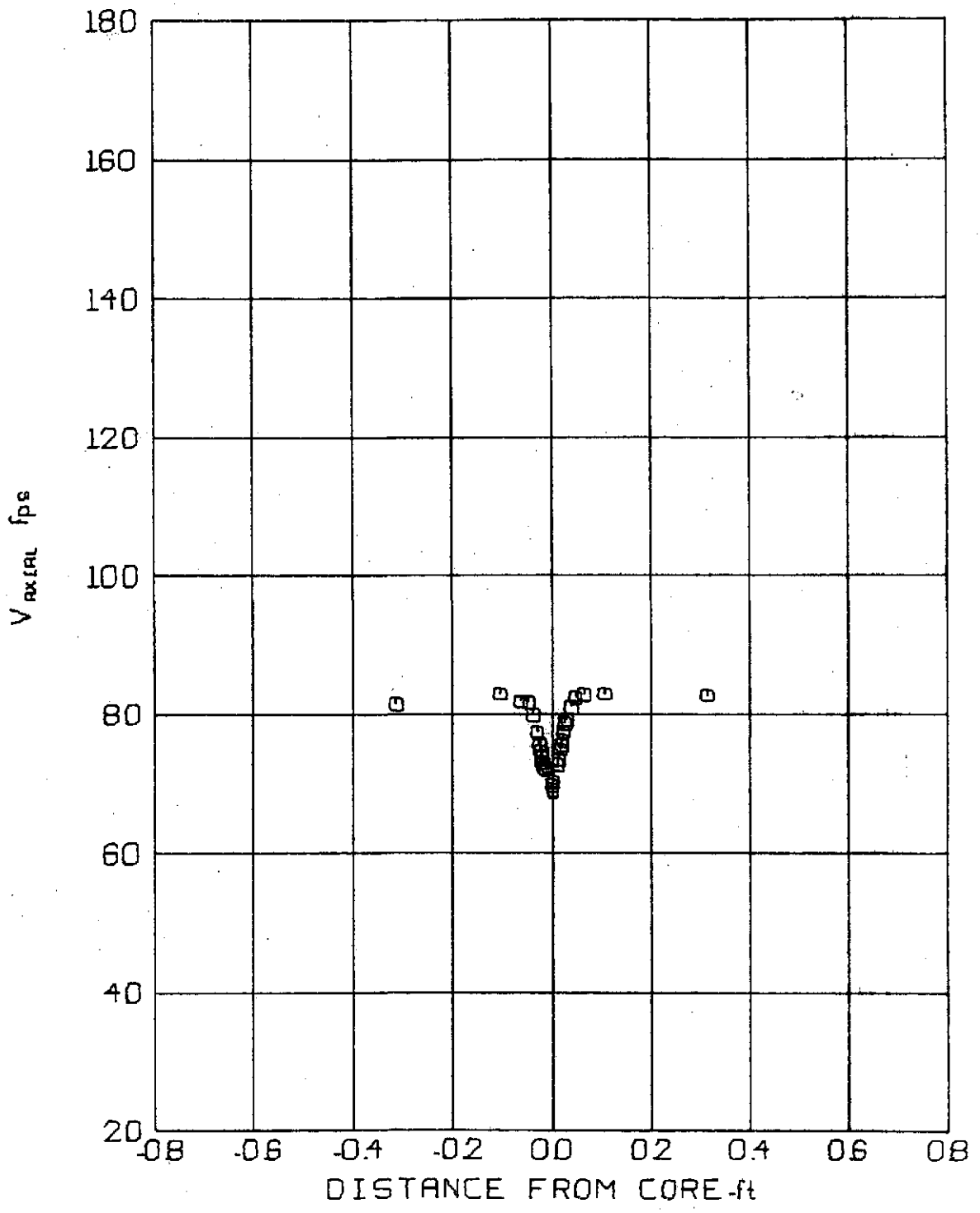

FIG 73 AXIAL VELOCITY PROFILE

V_∞ = 86.8 f/s Z/C = 2
α = 4° t = .01535 sec

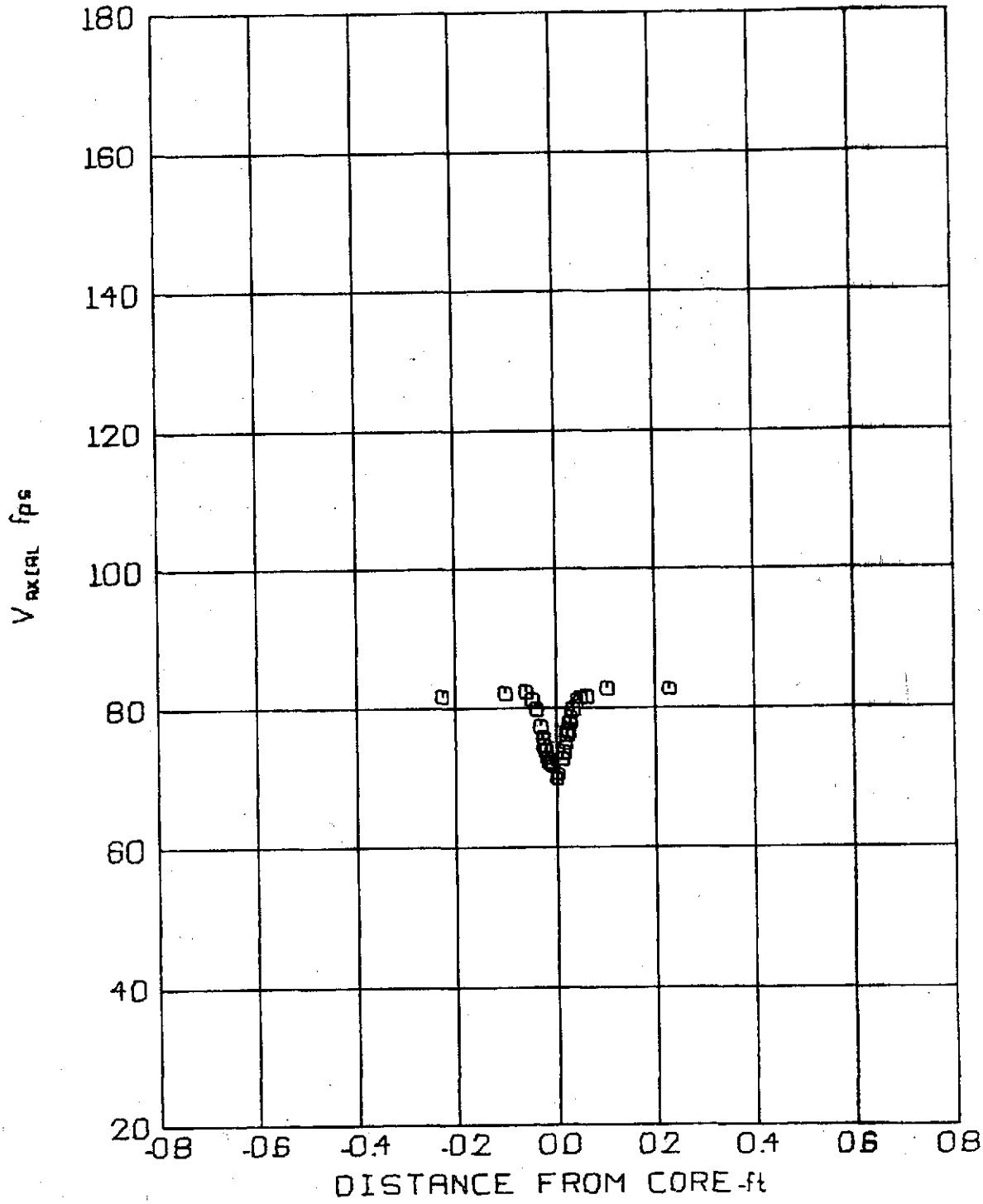

FIG 74 AXIAL VELOCITY PROFILE

V_∞ = 86.7 f/s Z/C = 5
α = 4° t = .03840 sec

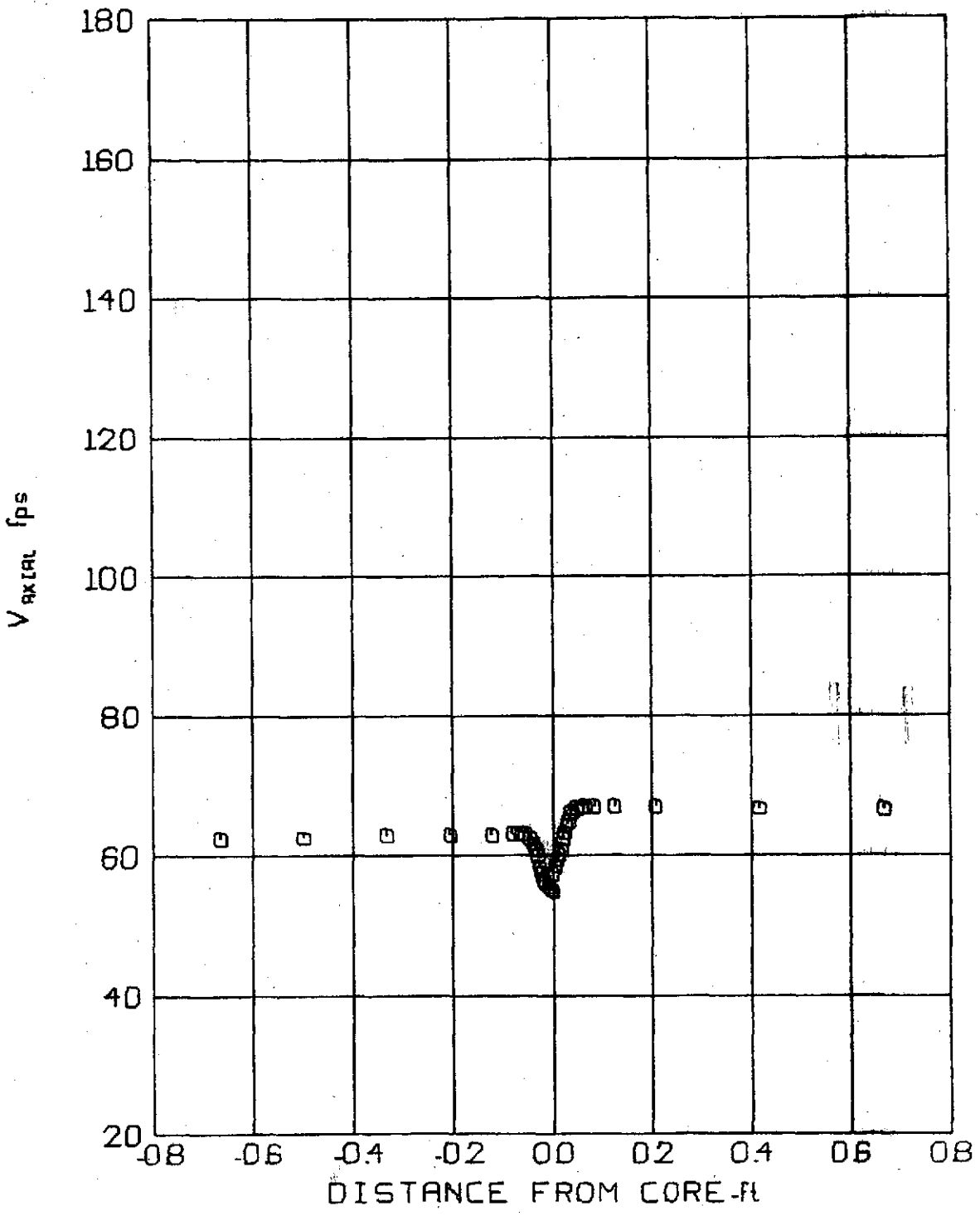

FIG 75 AXIAL VELOCITY PROFILE

V_∞ = 68.6 f/s Z/C = 10
α = 4° t = .09713 sec

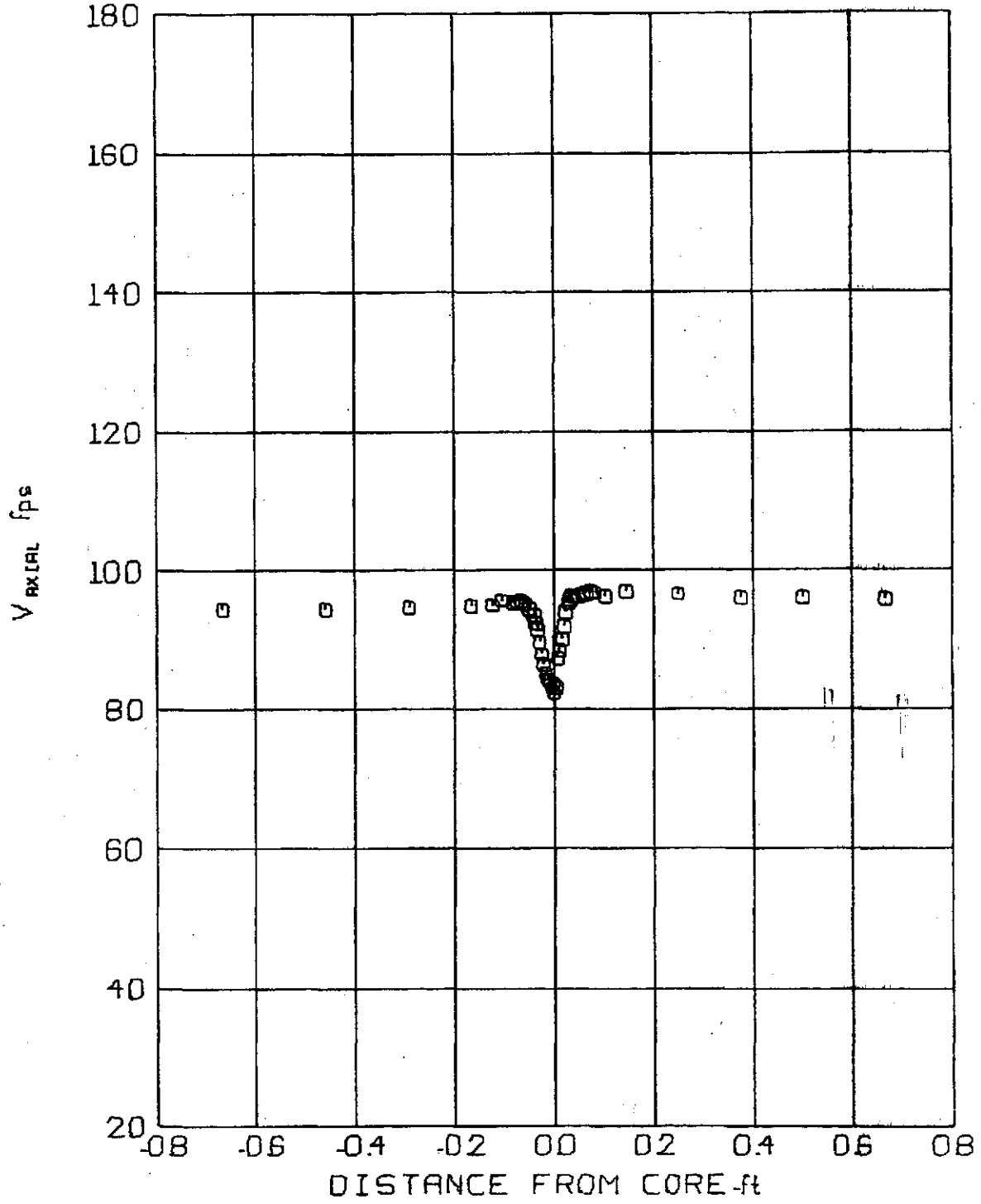

FIG 76 AXIAL VELOCITY PROFILE

V_∞ = 98.3 f/s Z/C = 10
α = 4° t = .06780 sec

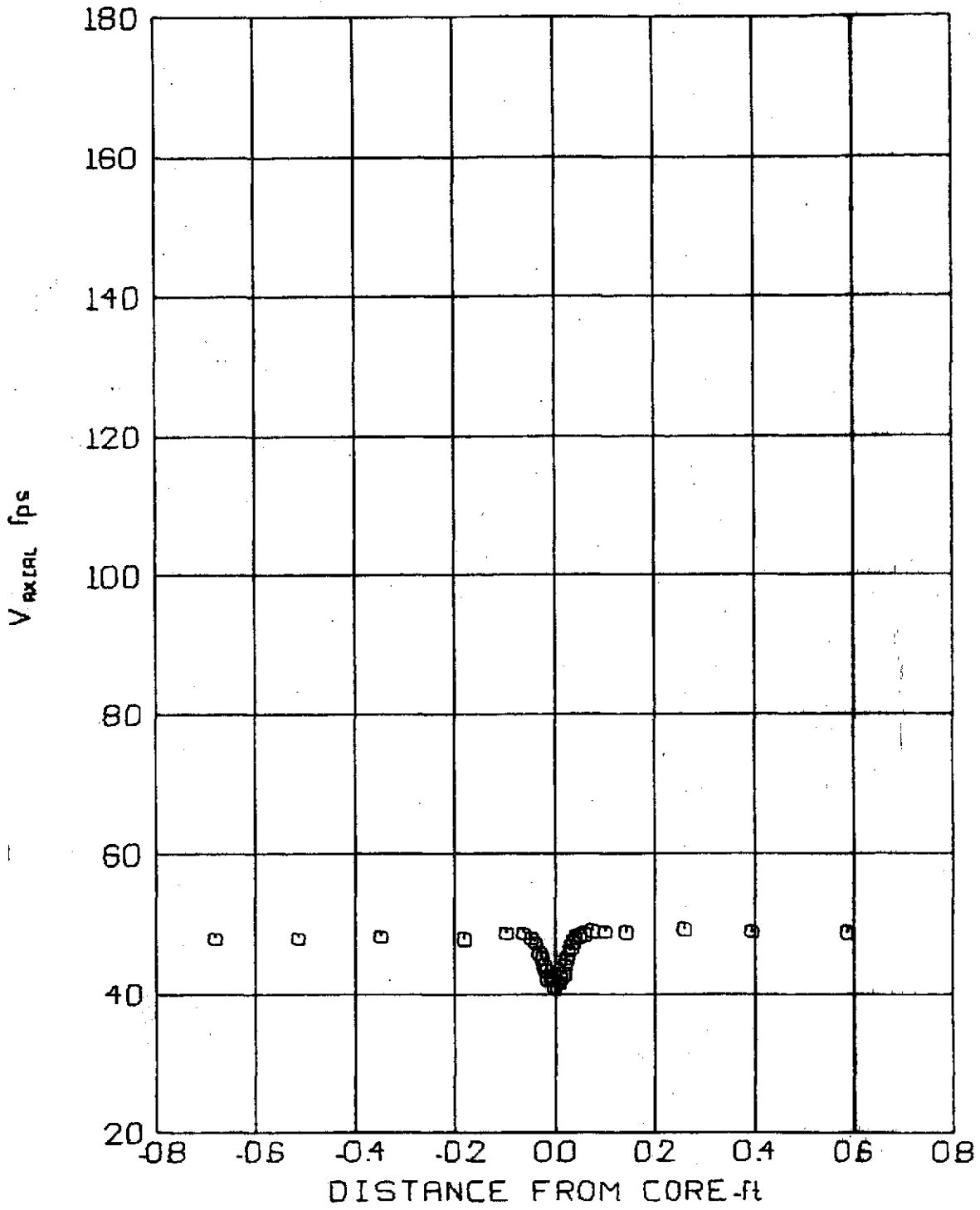

FIG 77 AXIAL VELOCITY PROFILE

V_∞ = 49.3 f/s Z/C = 15
α = 4° t = .20246 sec

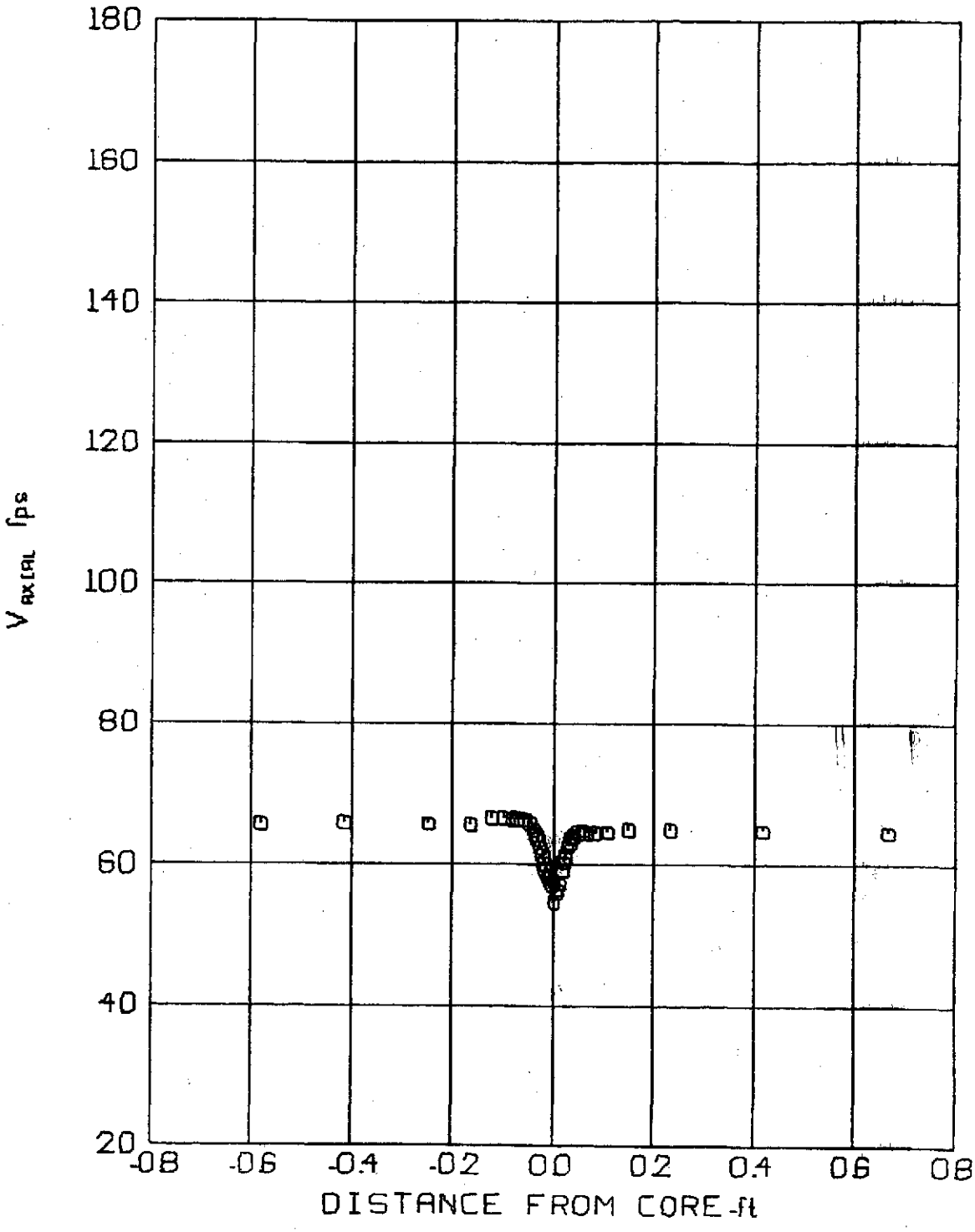

FIG 78 AXIAL VELOCITY PROFILE

V_∞ = 67.2 f/s Z/C = 15
α = 4° t = .14879 sec

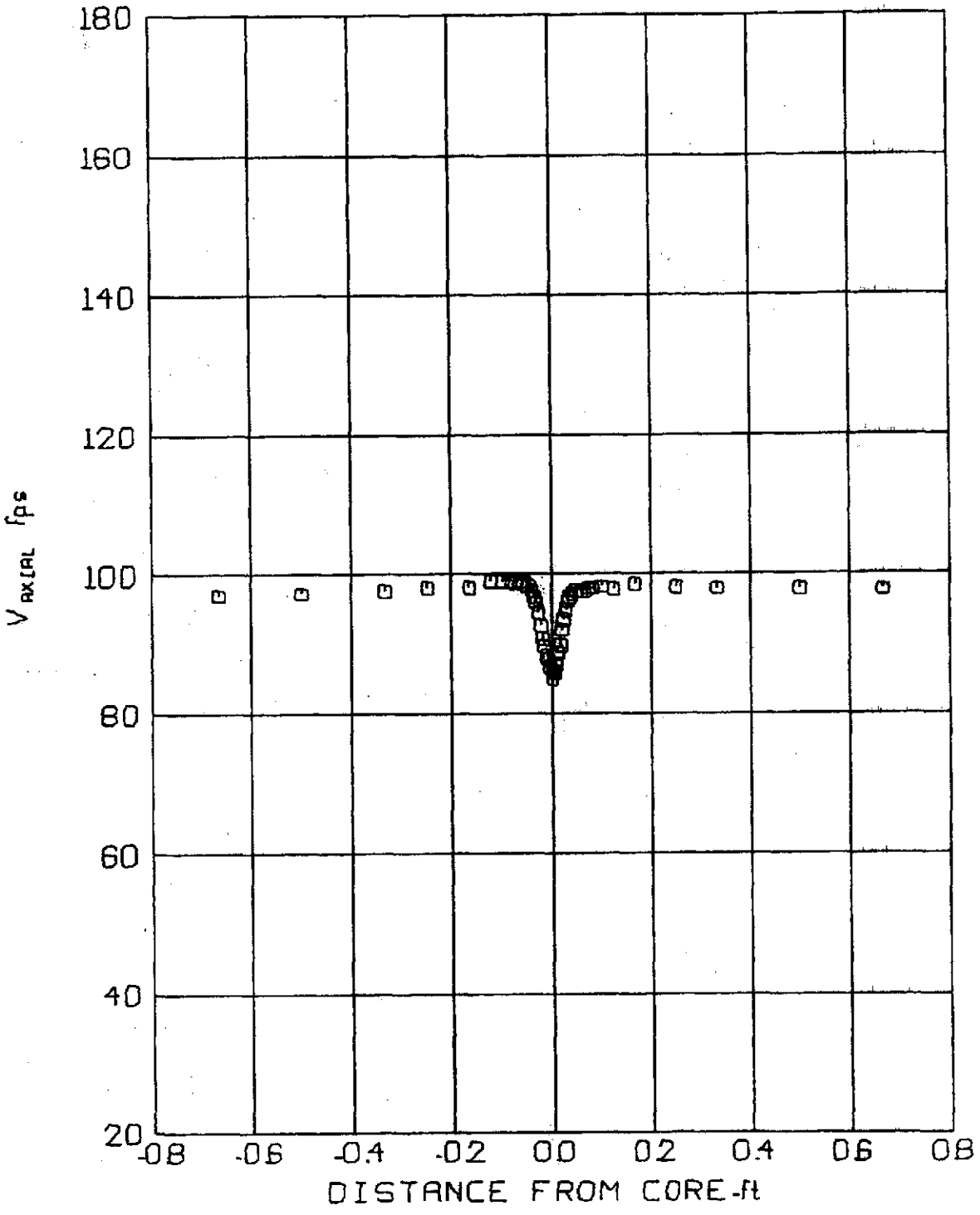

FIG 79 AXIAL VELOCITY PROFILE

V_∞ = 100.8 f/s Z/C = 15
α = 4° t = .09920 sec

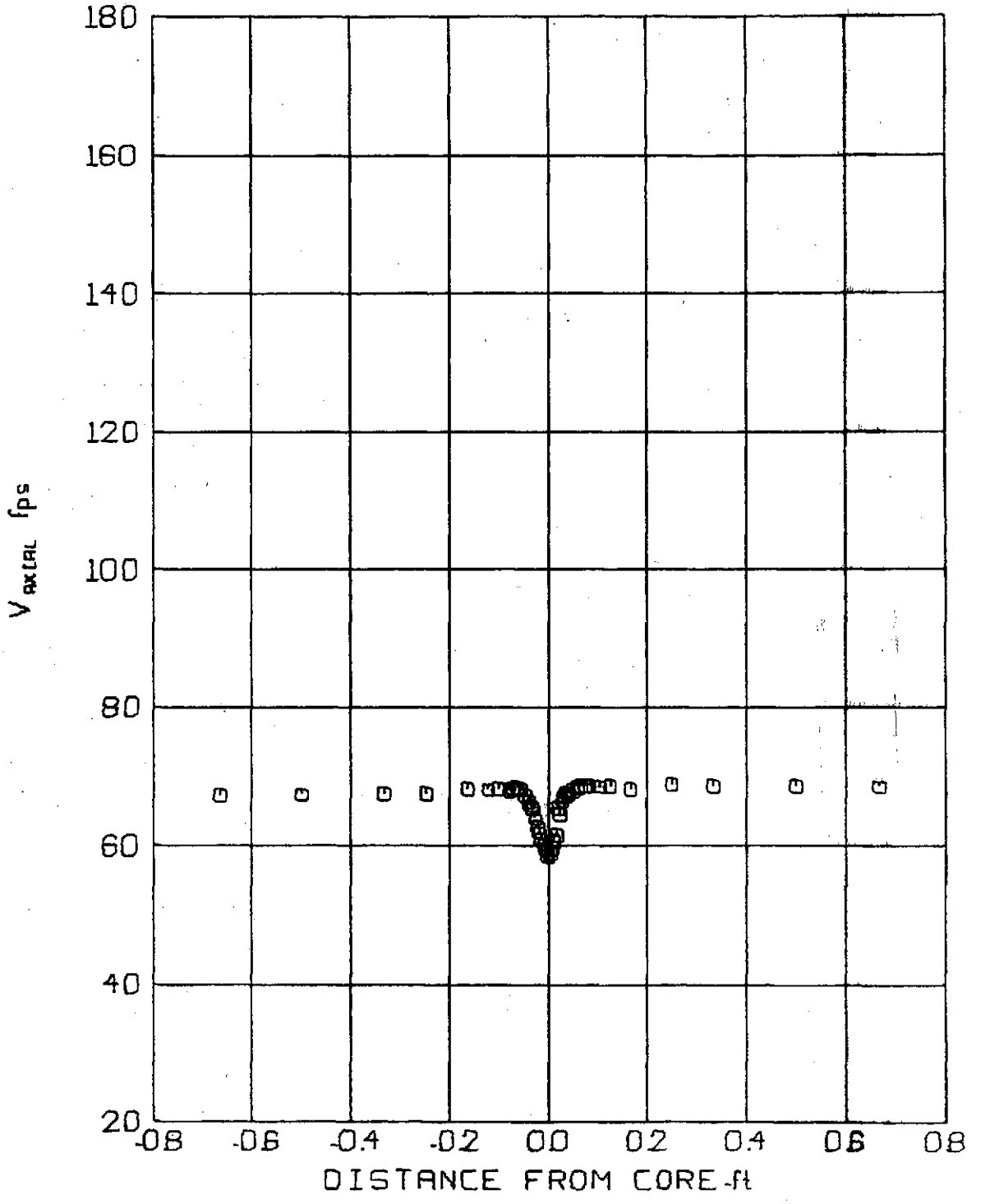

FIG 80 AXIAL VELOCITY PROFILE

V_∞ = 68.4 f/s Z/C = 20
α = 4° t = .19469 sec

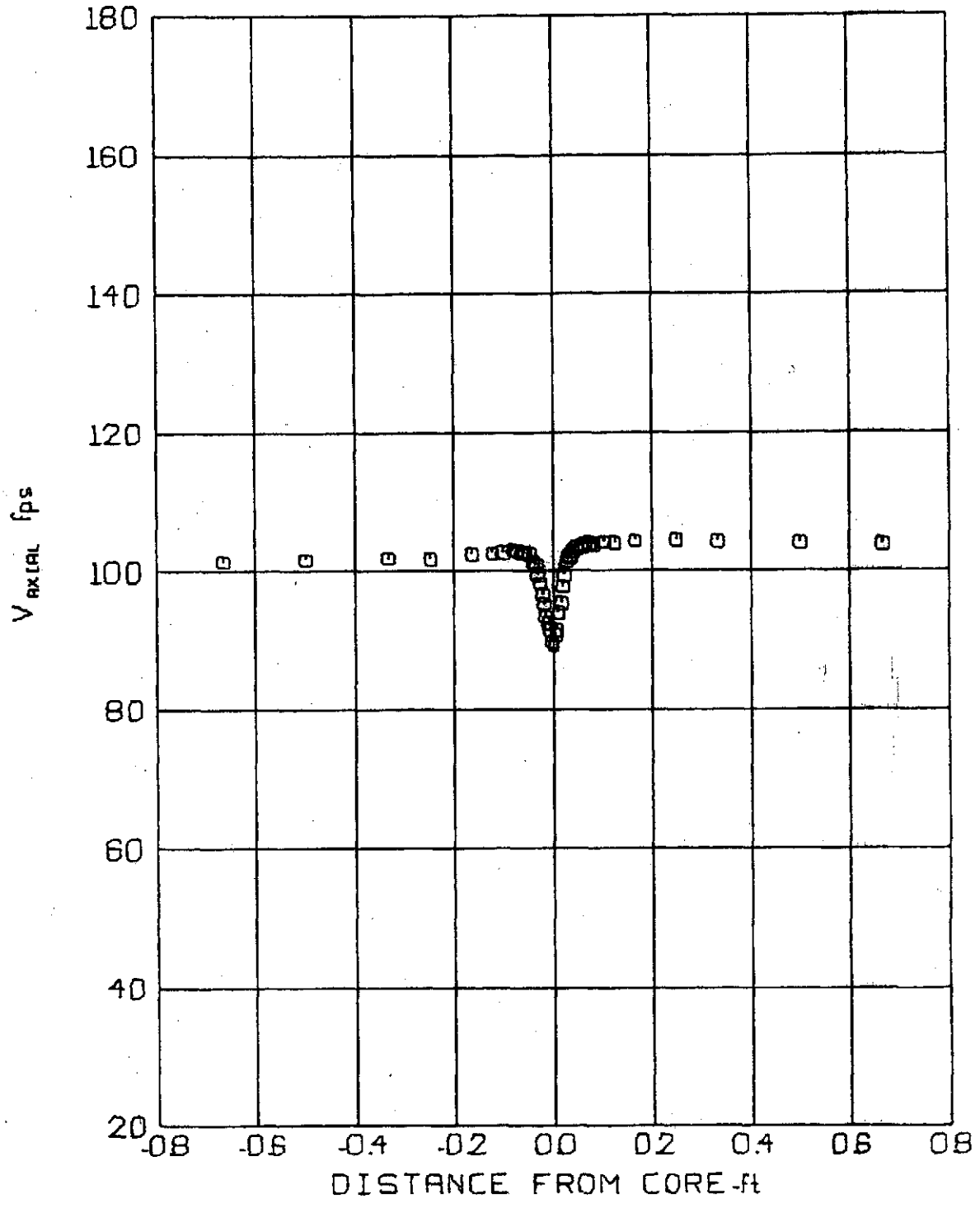

FIG 81 AXIAL VELOCITY PROFILE

V_∞ = 103.3 f/s Z/C = 20
α = 4° t = .12897 sec

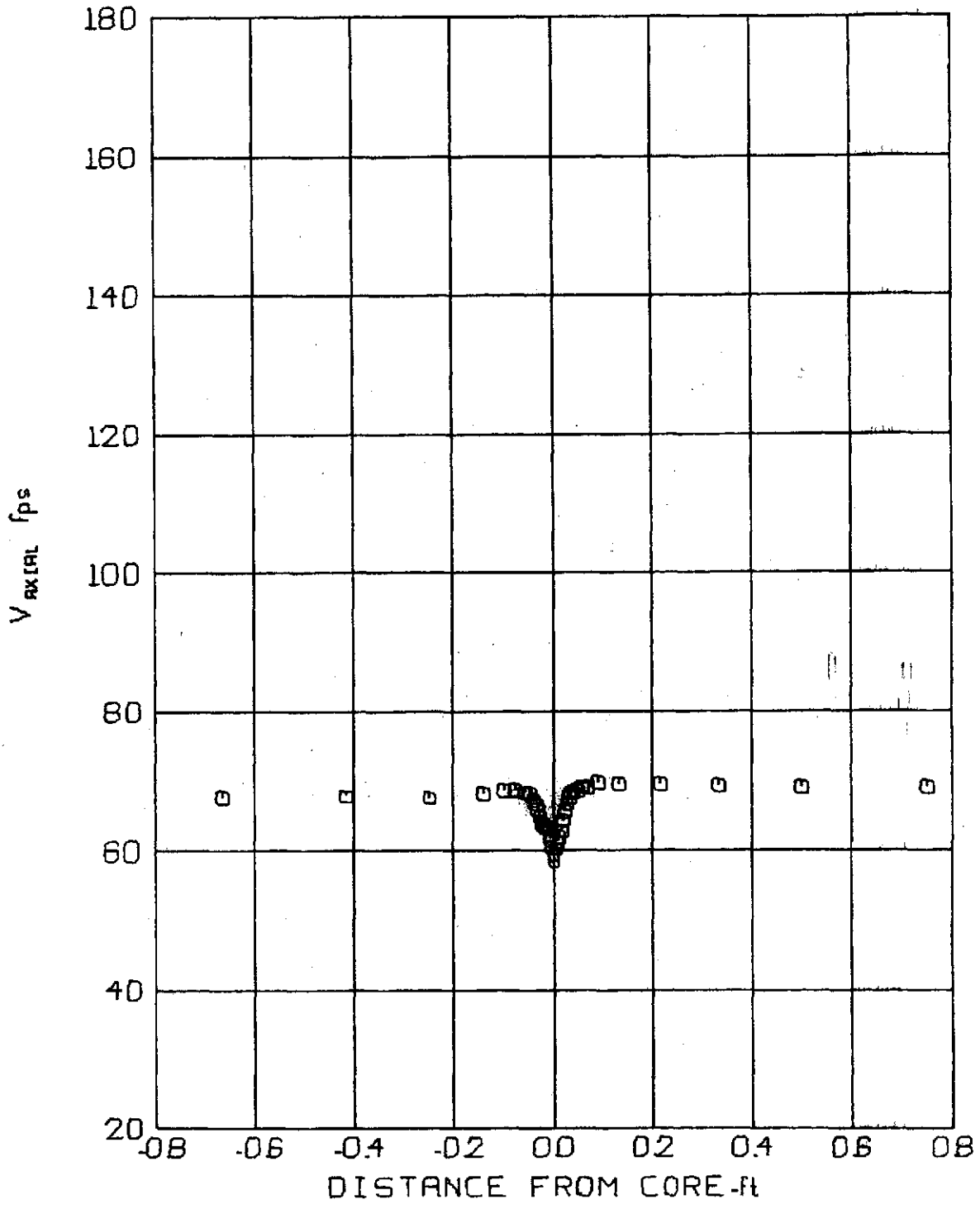

FIG 82 AXIAL VELOCITY PROFILE

V_∞ = 68.4 f/s Z/C = .25
α = 4° t = .24337 sec

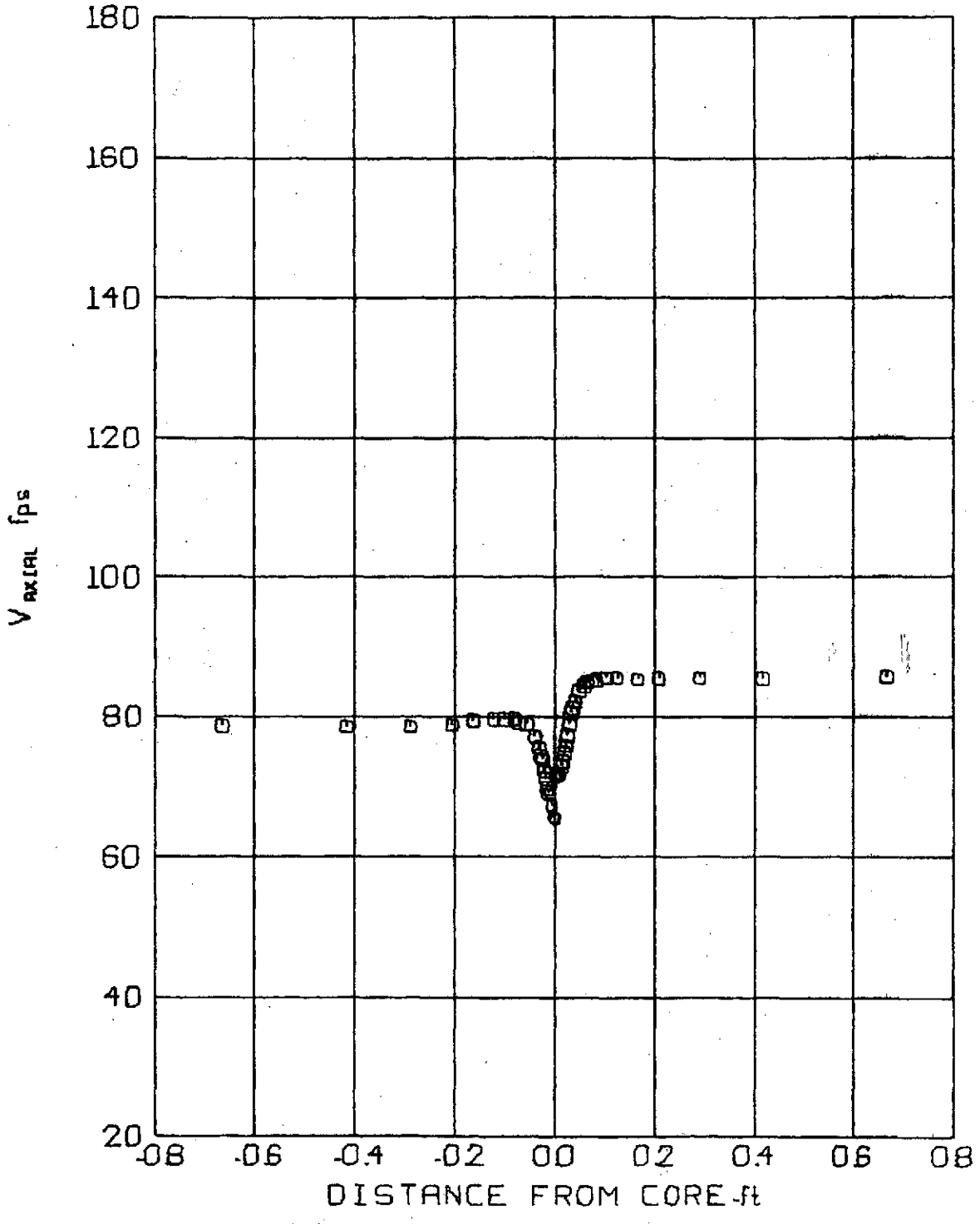

FIG 83 AXIAL VELOCITY PROFILE

V_∞ = 86.5 f/s Z/C = 25
α = 4° t = .19256 sec

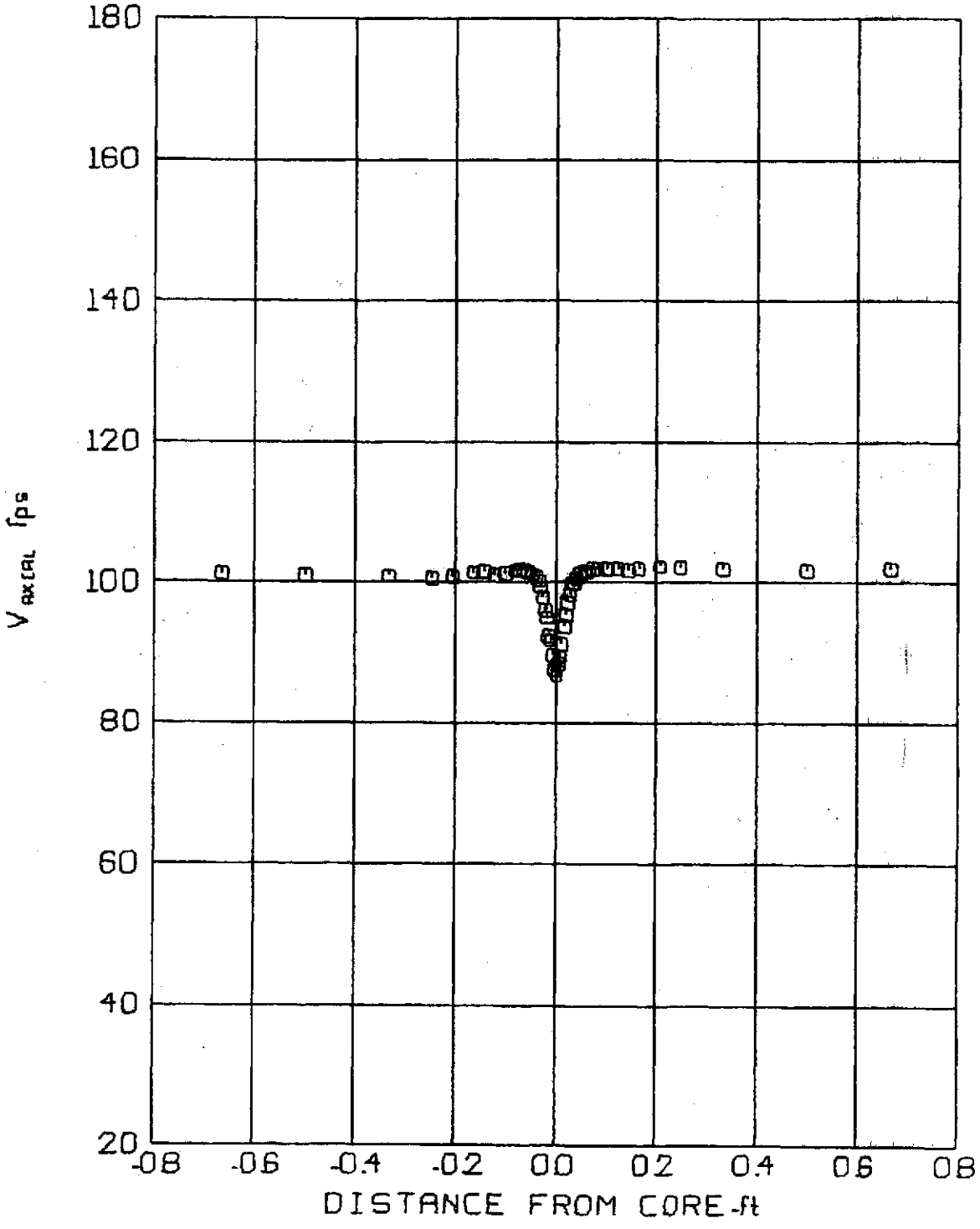

FIG 84 AXIAL VELOCITY PROFILE

V_∞ = 102.8 f/s Z/C = .25
α = 4° t = .16199 sec

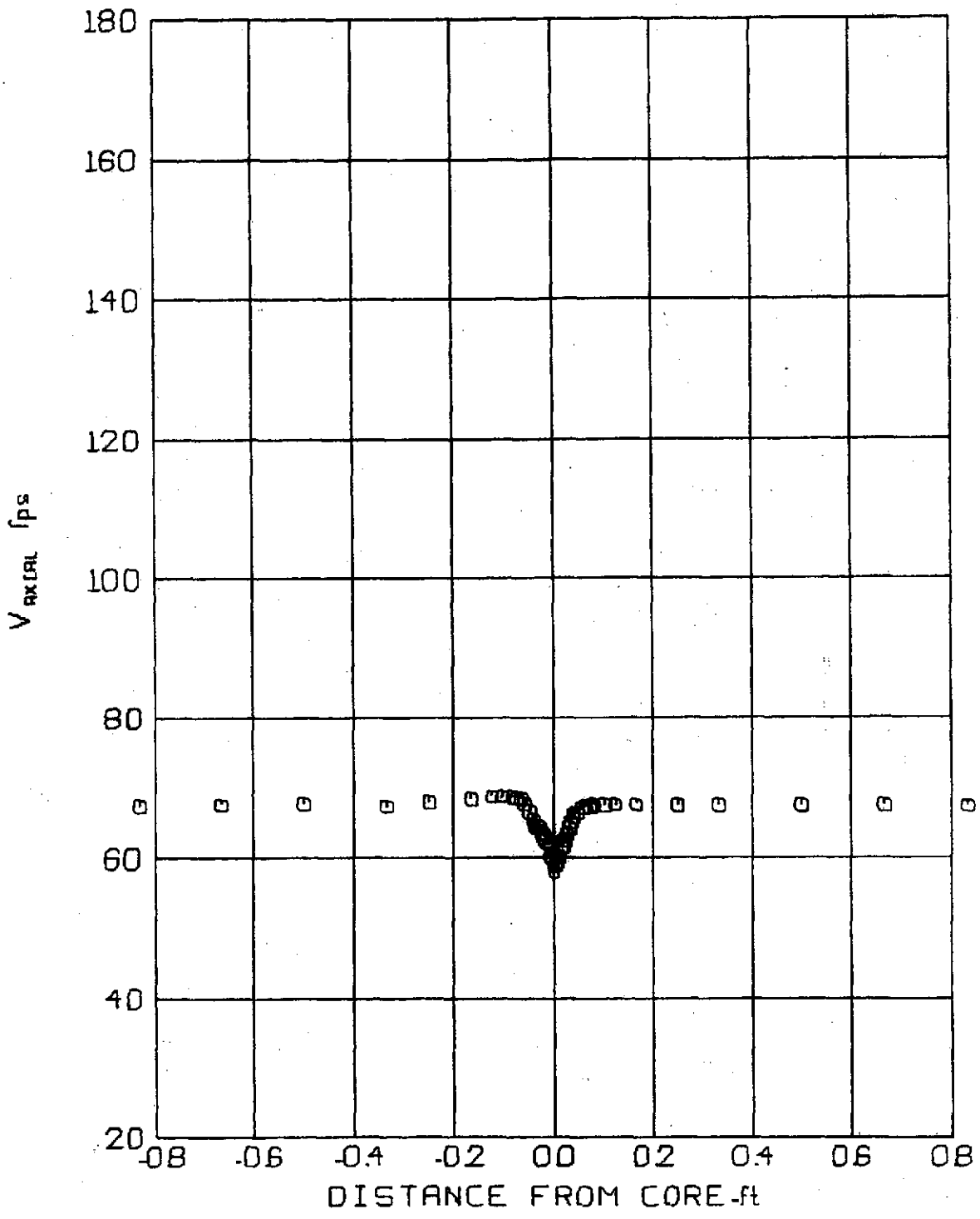

FIG 85 AXIAL VELOCITY PROFILE

V_∞ = 69.4 f/s Z/C = 30
α = 4° t = .28790 sec

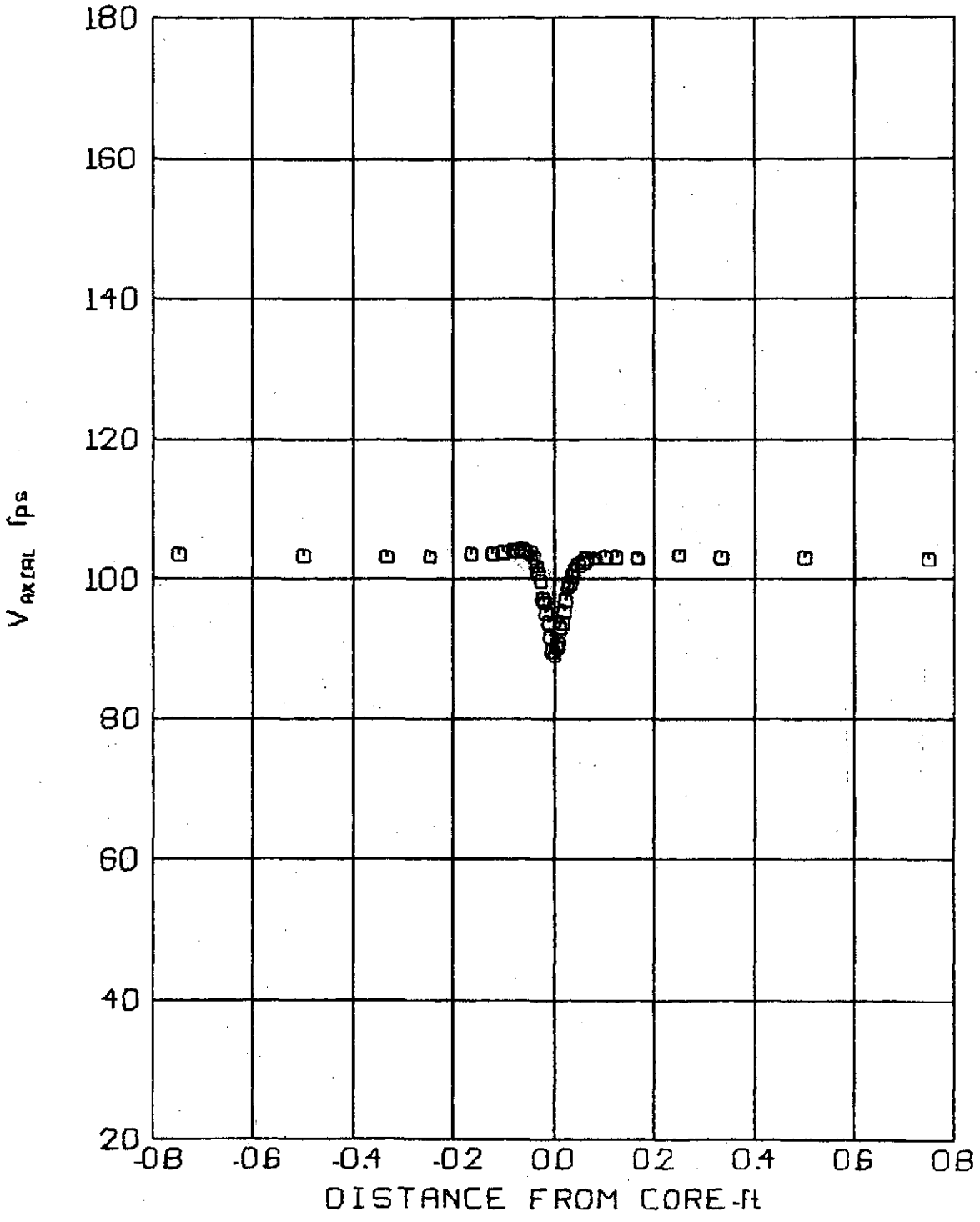

FIG 86 AXIAL VELOCITY PROFILE

V_∞ = 105.6 f/s Z/C = 30
α = 4° t = .18928 sec

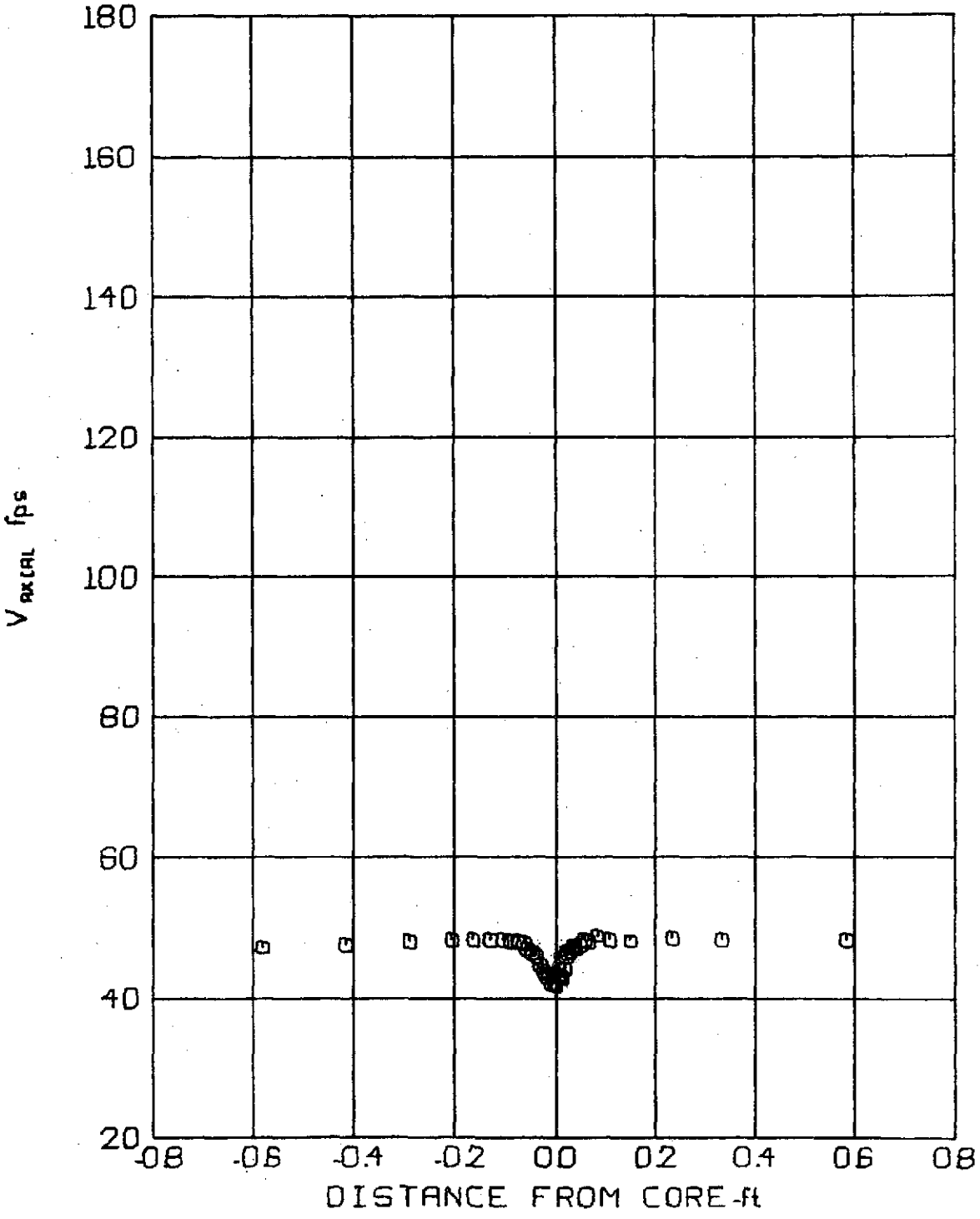

FIG 87 AXIAL VELOCITY PROFILE

V_∞ = 49.1 f/s Z/C = 15
α = 6° t = .20348 sec

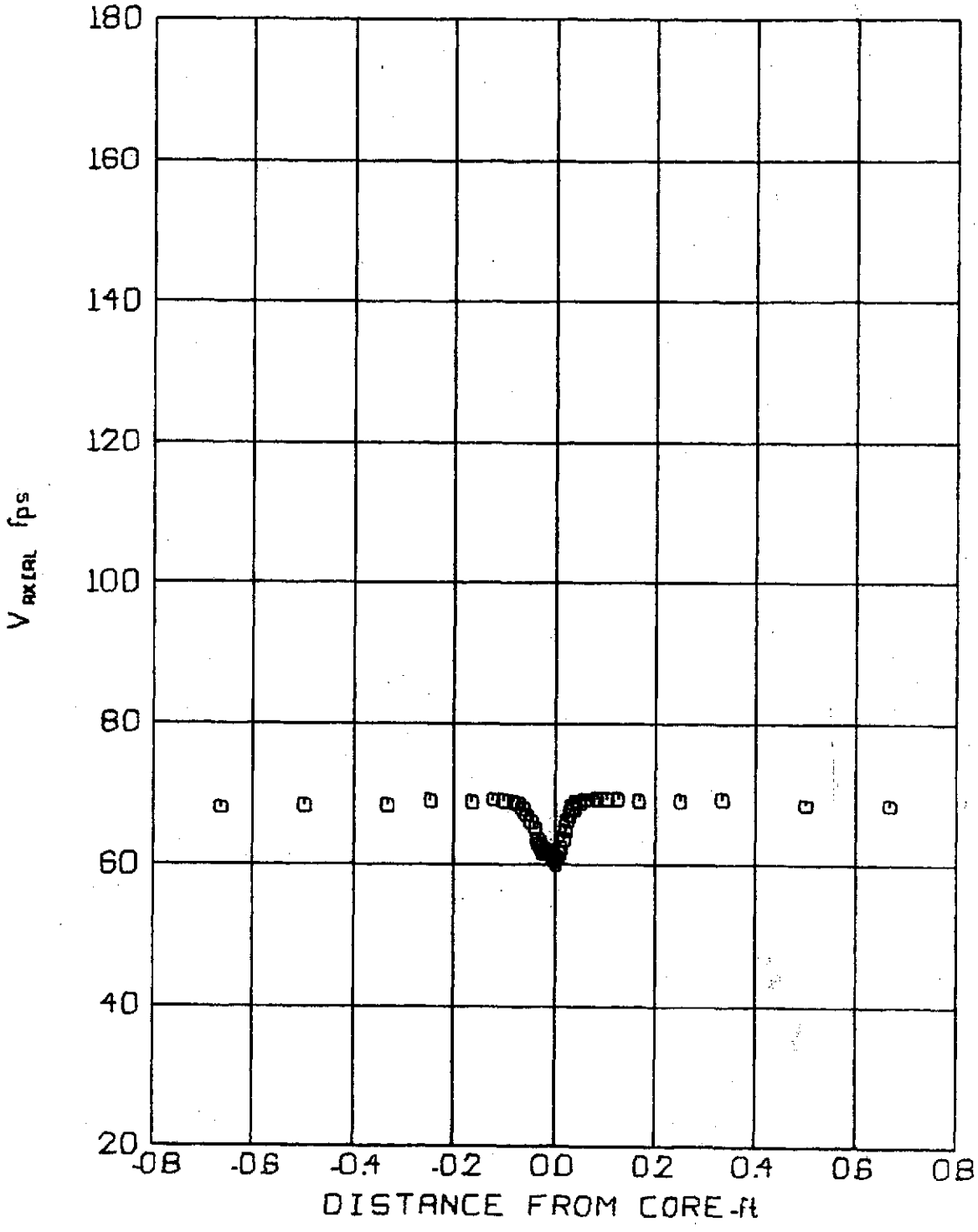

FIG 88 AXIAL VELOCITY PROFILE

V_∞ = 69.5 f/s Z/C = 20
α = 6° t = .19162 sec

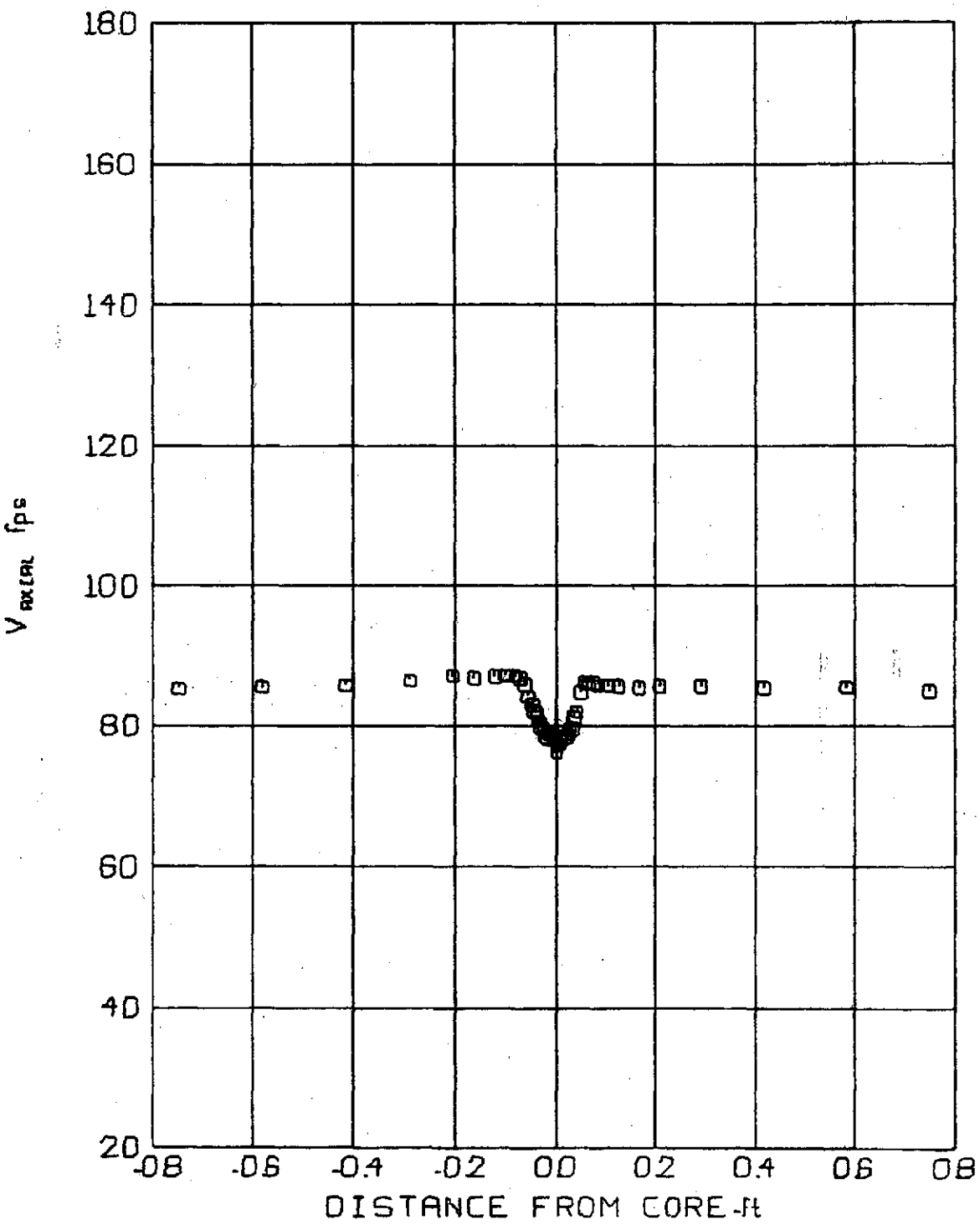

FIG 89 AXIAL VELOCITY PROFILE

V_∞ = 86.9 f/s Z/C = .25
α = 6° t = .19174 sec

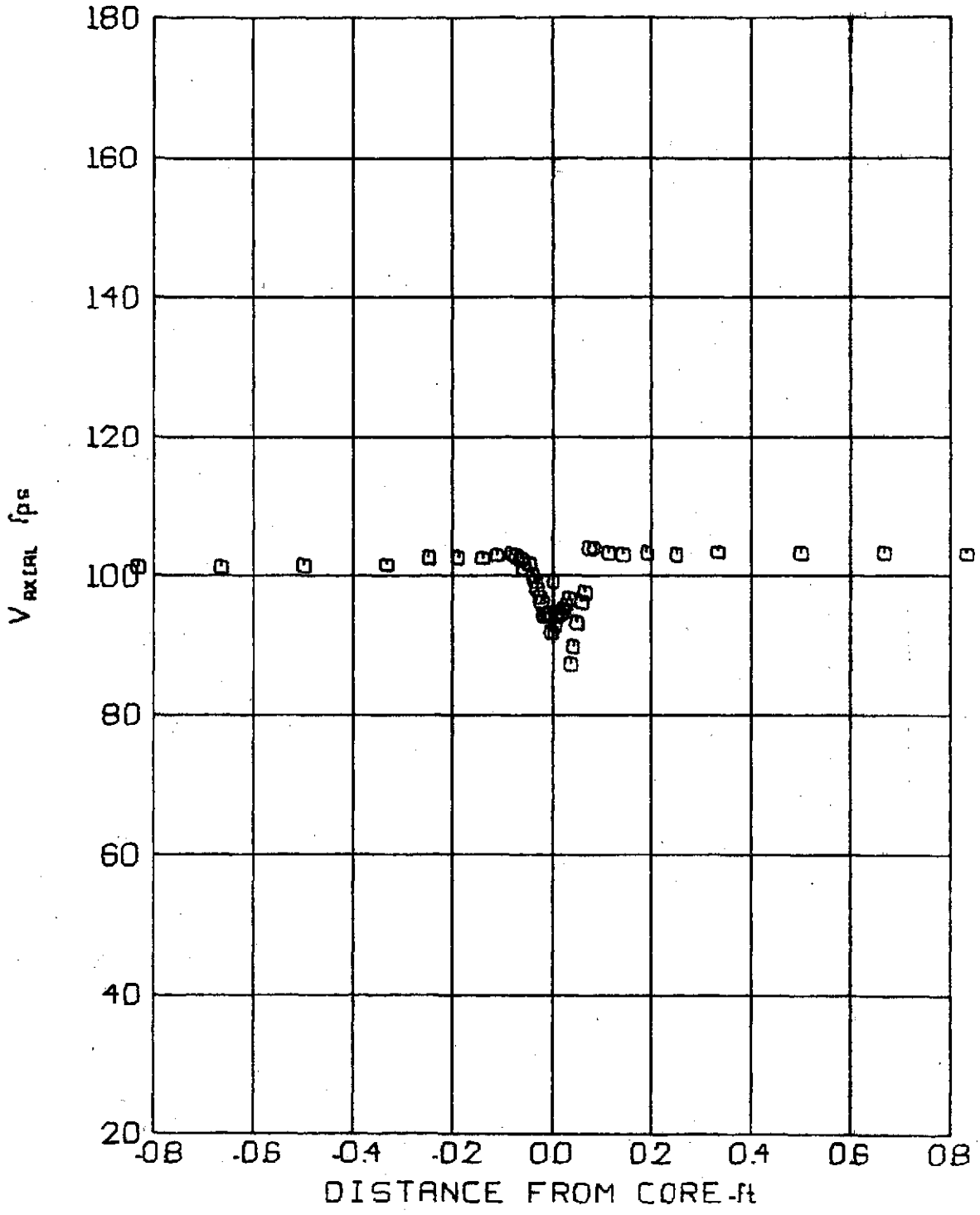

FIG 90 AXIAL VELOCITY PROFILE

V_∞ = 103.6 f/s Z/C = 30
α = 6° t = .19288 sec

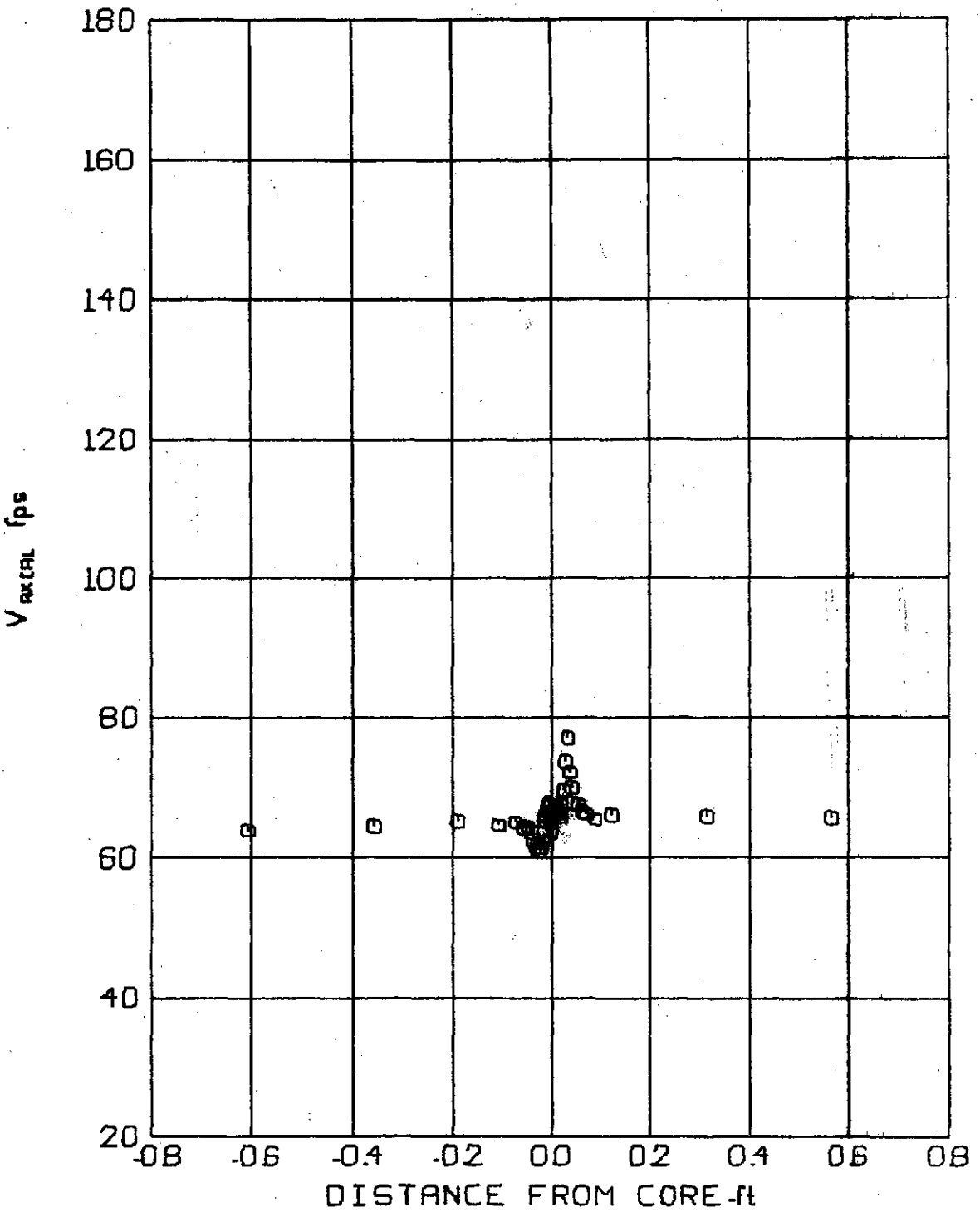

FIG 91 AXIAL VELOCITY PROFILE

V_∞ = 68.7 f/s Z/C = 2
α = 8° t = .01939 sec

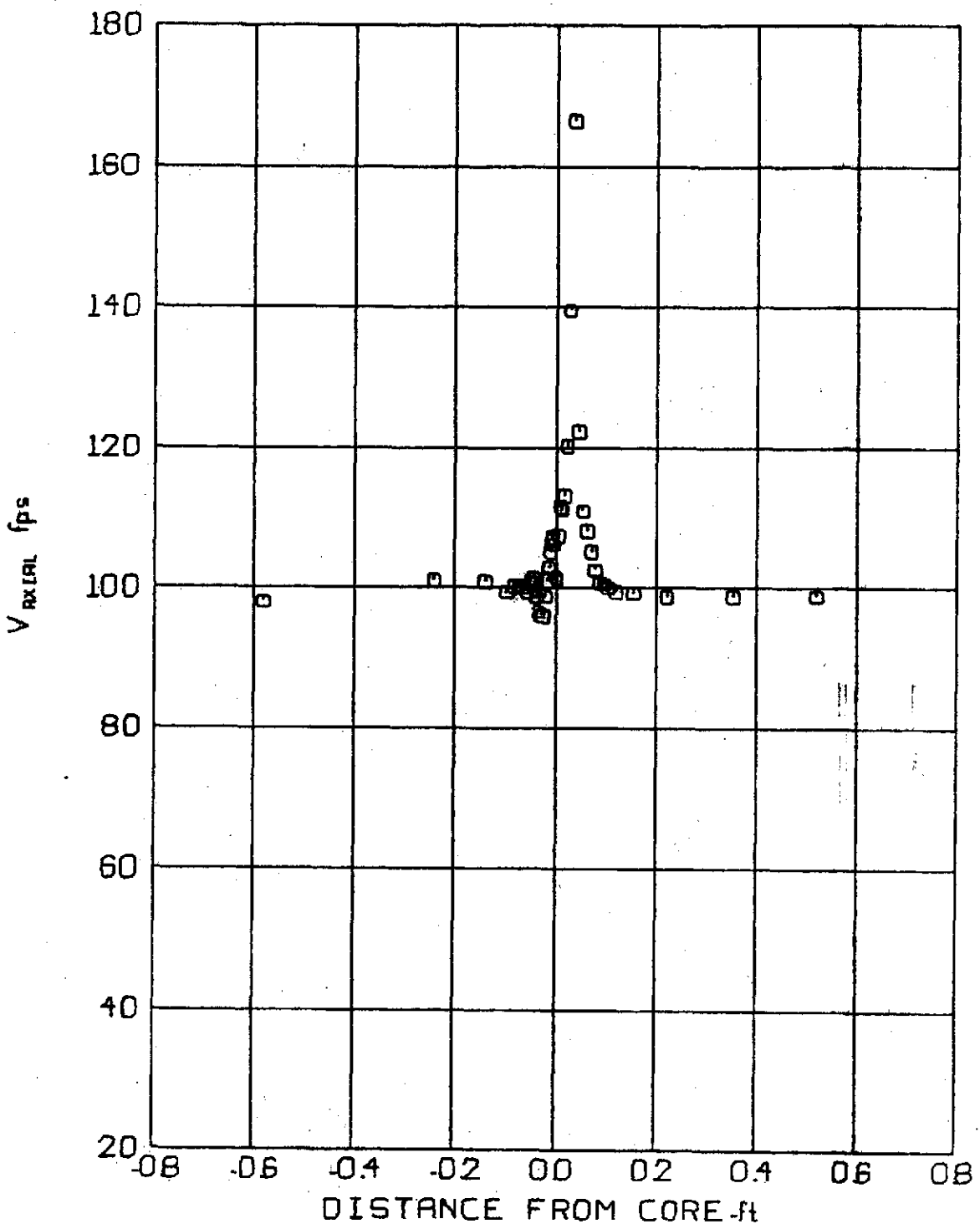

FIG 92 AXIAL VELOCITY PROFILE

V_∞ = 105.8 f/s Z/C = 2
α = 8° t = .01259 sec

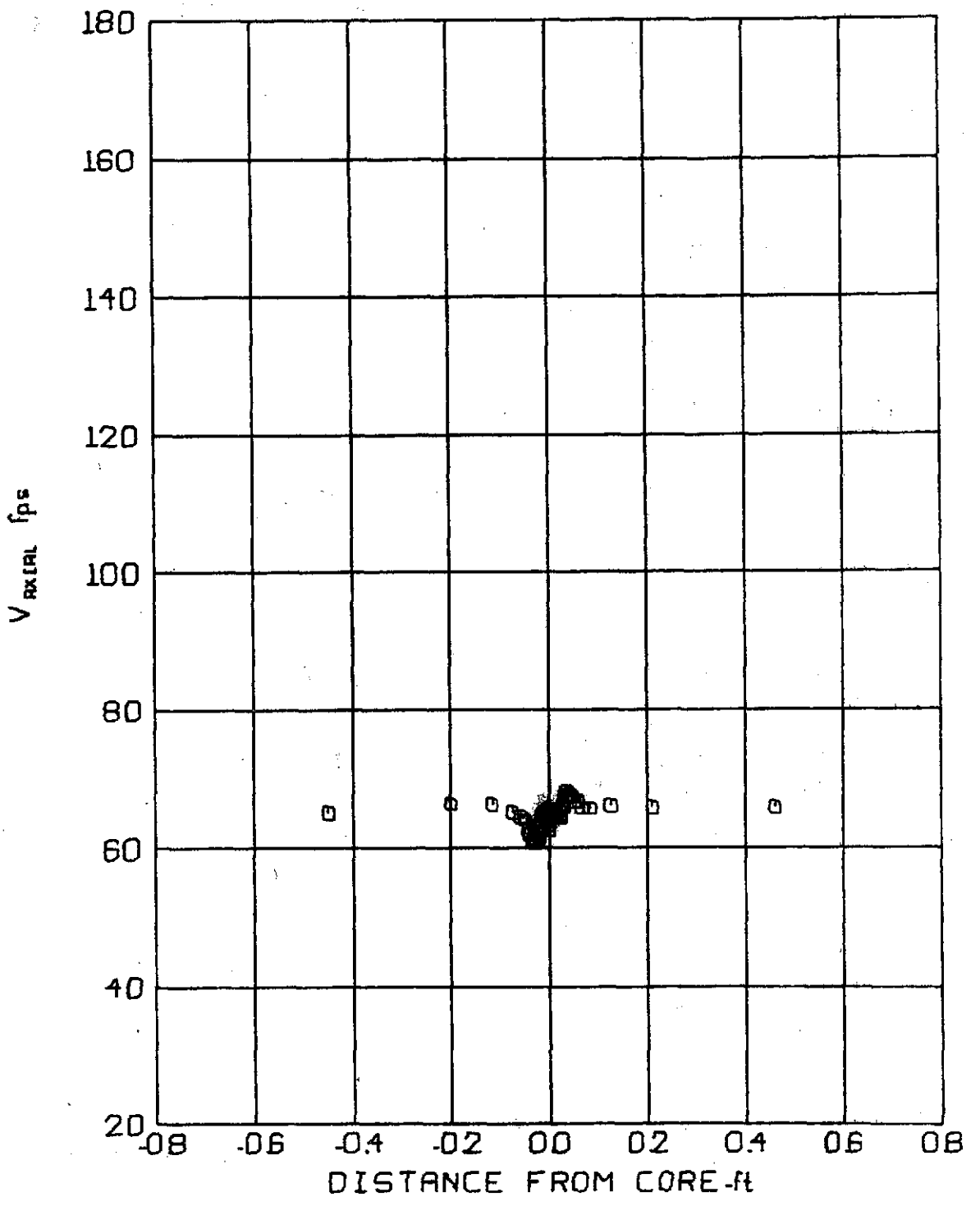

FIG 93 AXIAL VELOCITY PROFILE

V_∞ = 69.7 f/s Z/C = 5
α = 8° t = .04780 sec

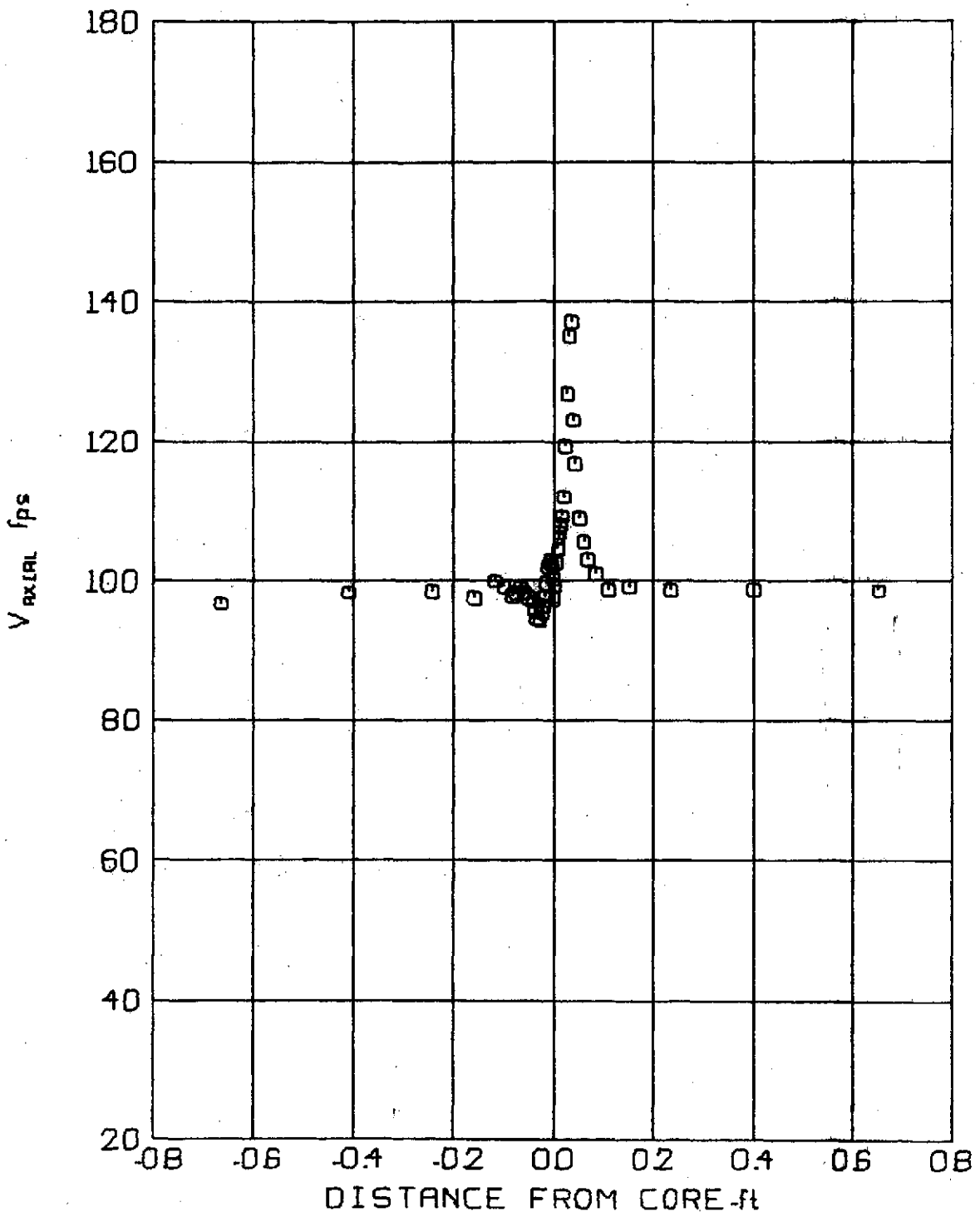

FIG 94 AXIAL VELOCITY PROFILE

V_∞ = 103.9 f/s Z/C = 5
α = 8° t = .03207 sec

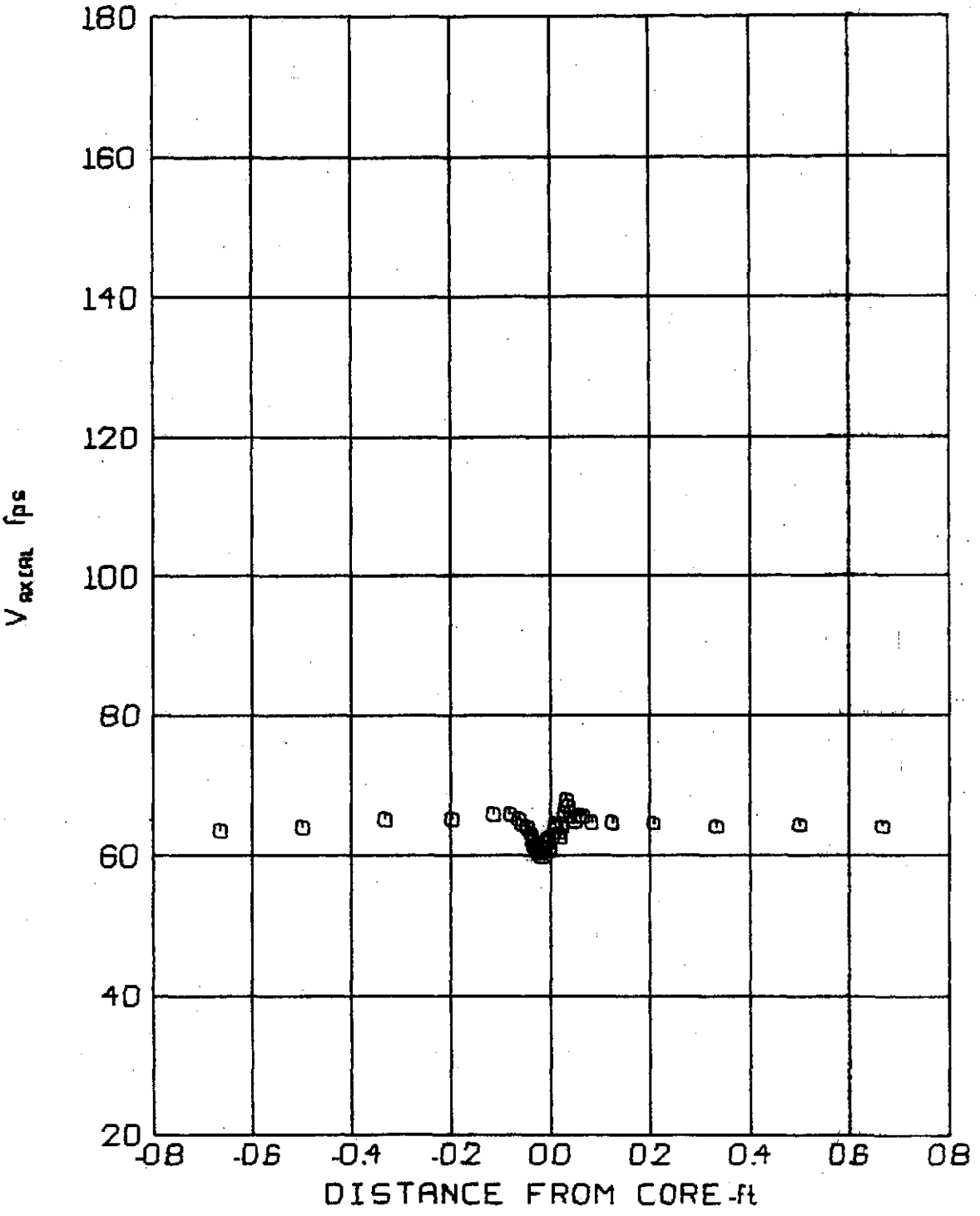

FIG 95 AXIAL VELOCITY PROFILE

V_∞ = 66.1 f/s Z/C = 10
α = 8° t = .10076 sec

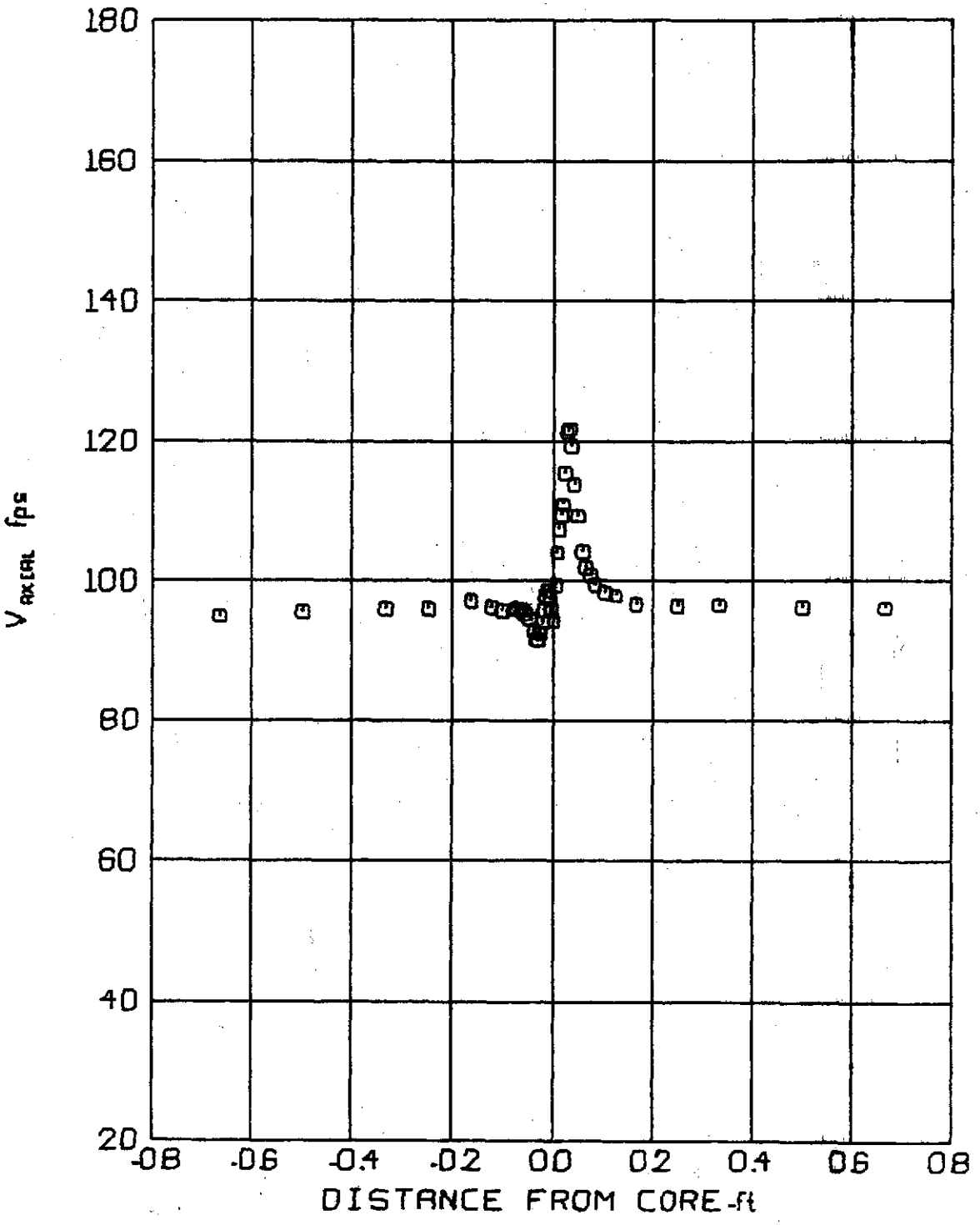

FIG 96 AXIAL VELOCITY PROFILE

V_∞ = 98.8 f/s Z/C = 10
α = 8° t = .06742 sec

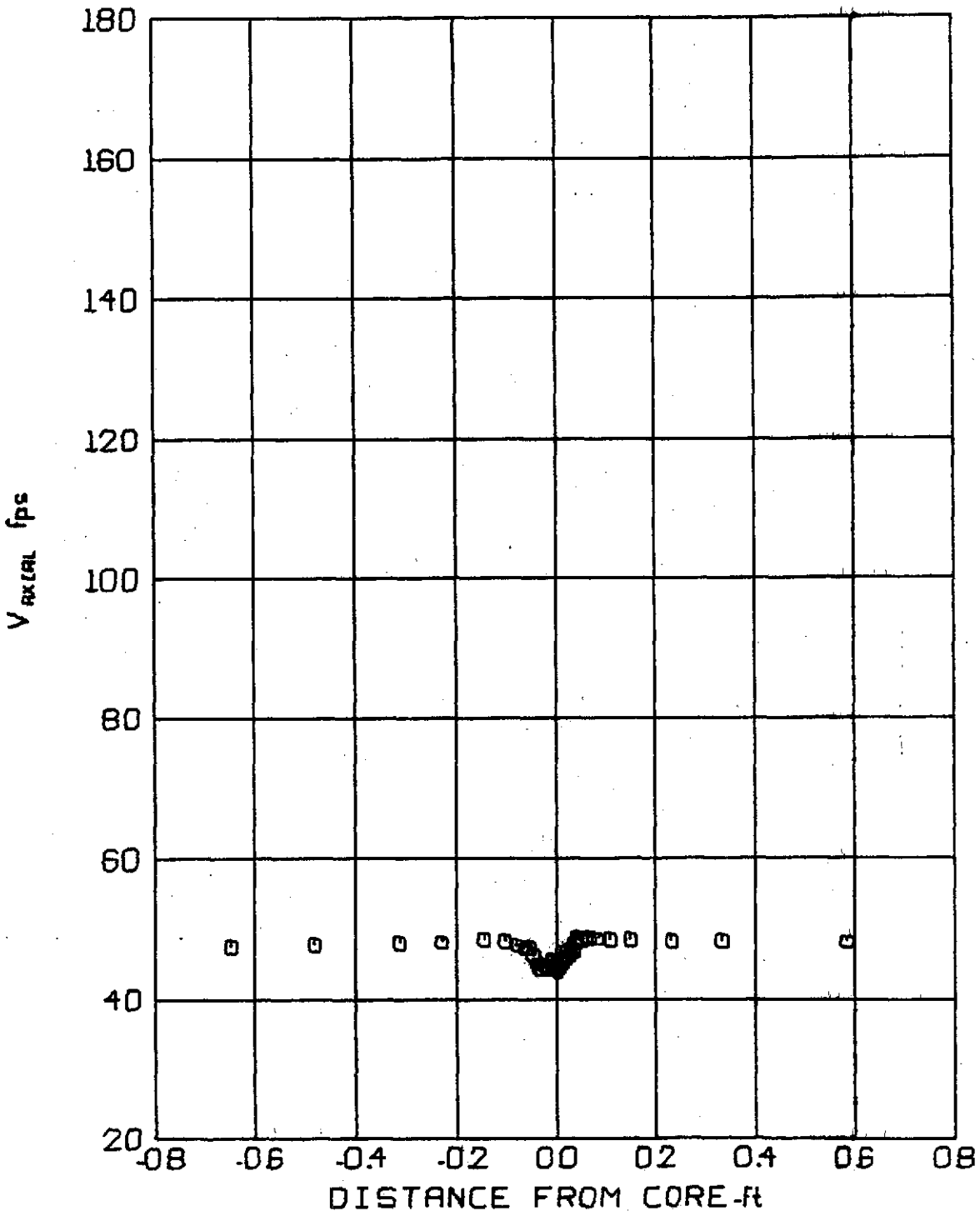

FIG 97 AXIAL VELOCITY PROFILE

V_∞ = 48.7 f/s Z/C = 15
α = 8° t = .20529 sec

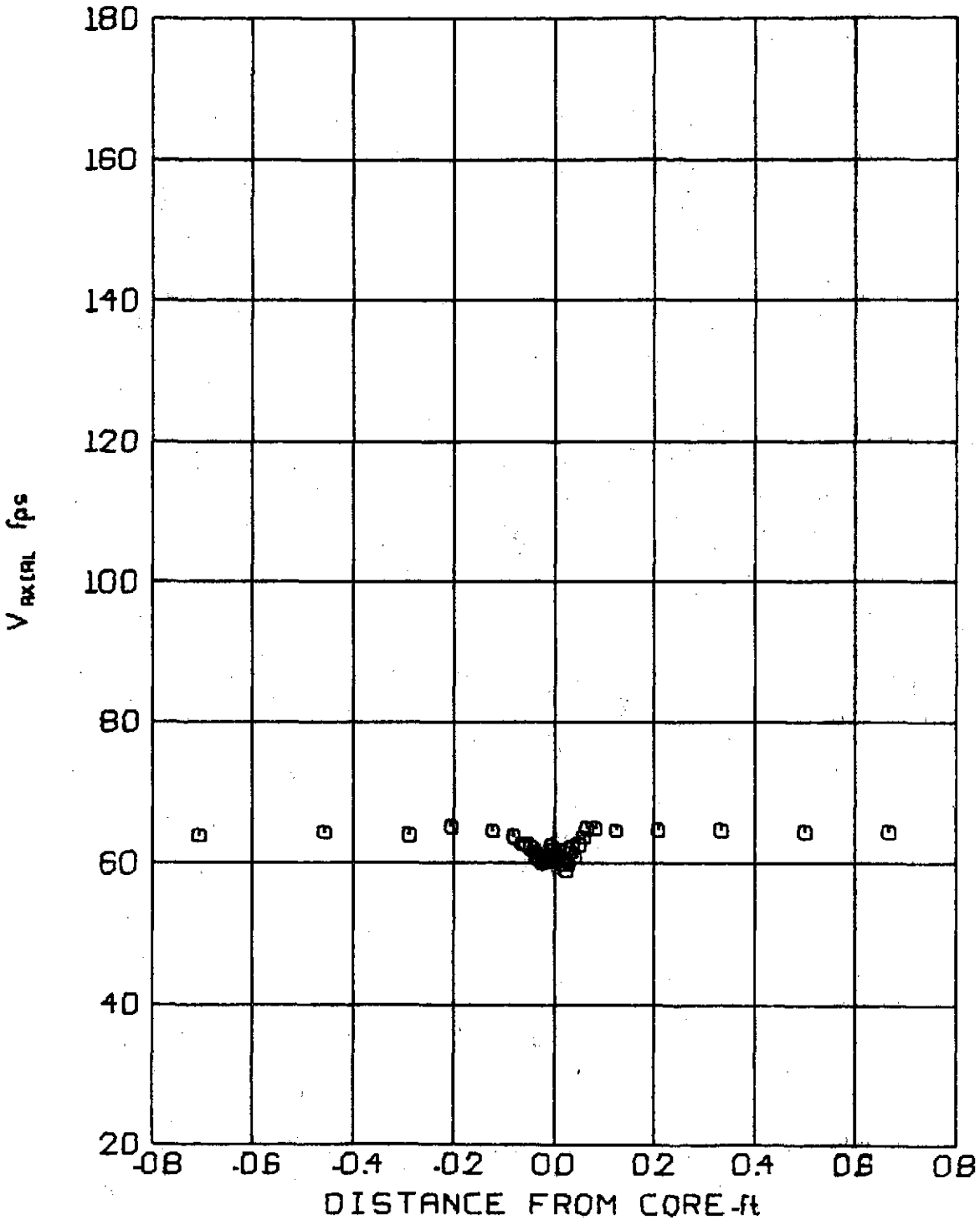

FIG 98 AXIAL VELOCITY PROFILE

V_∞ = 65.8 ft/s Z/C = 15
α = 8° t = .15195 sec

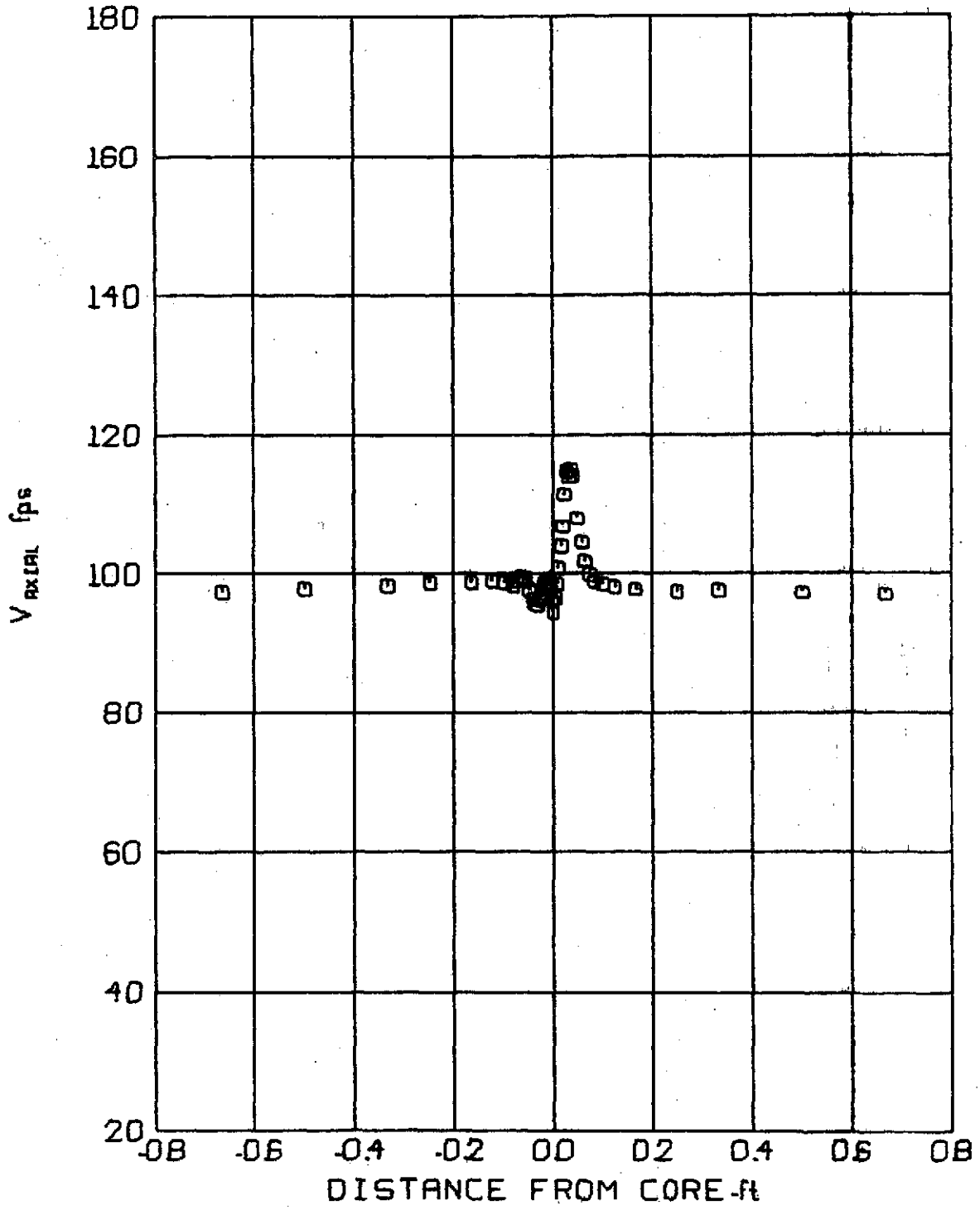

FIG 99 AXIAL VELOCITY PROFILE

V_∞ = 100.4 f/s Z/C = 15
α = 8° t = .09957 sec

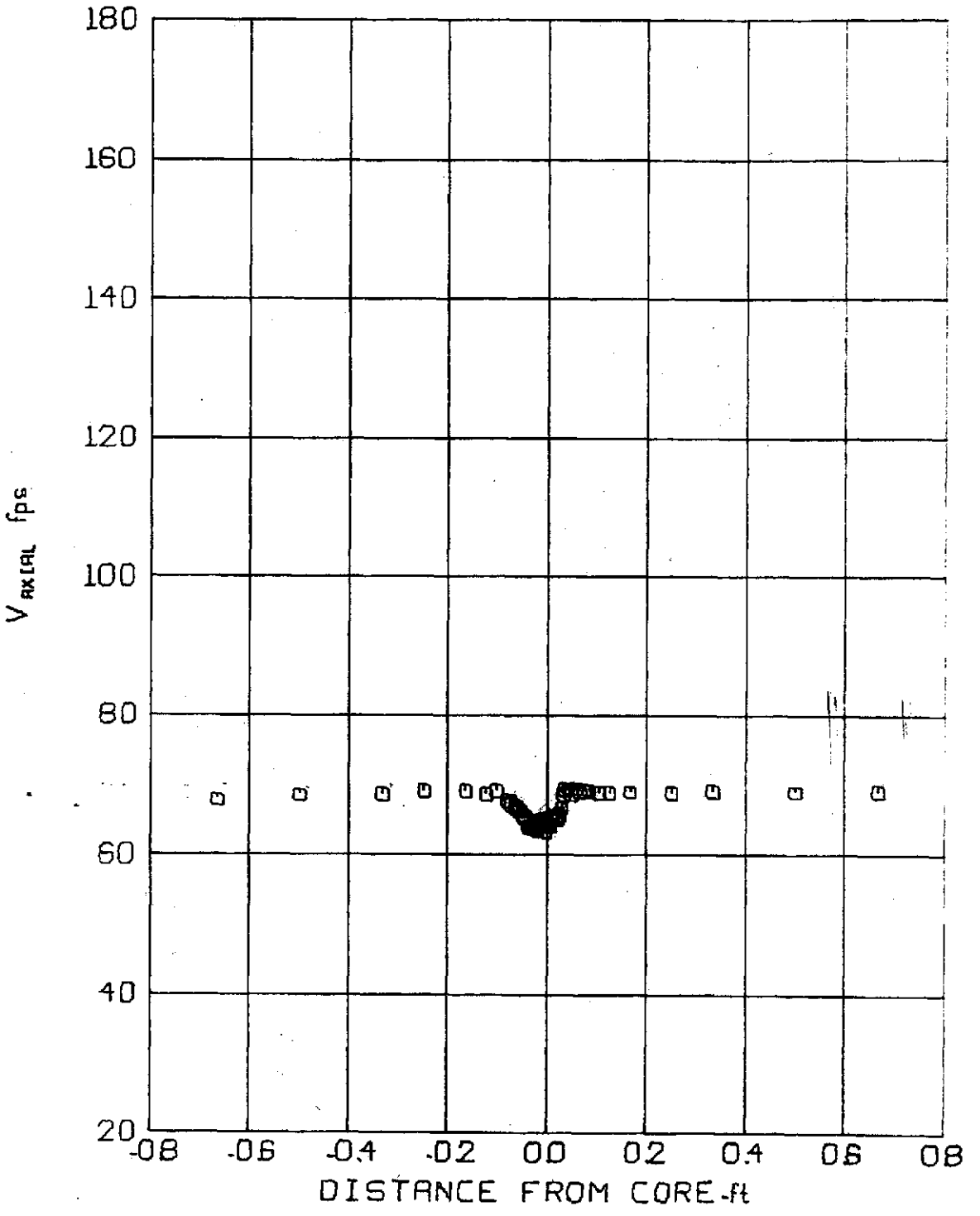

FIG 100 AXIAL VELOCITY PROFILE

V_∞ = 69.0 f/s Z/C = 20
α = 8° t = .19303 sec

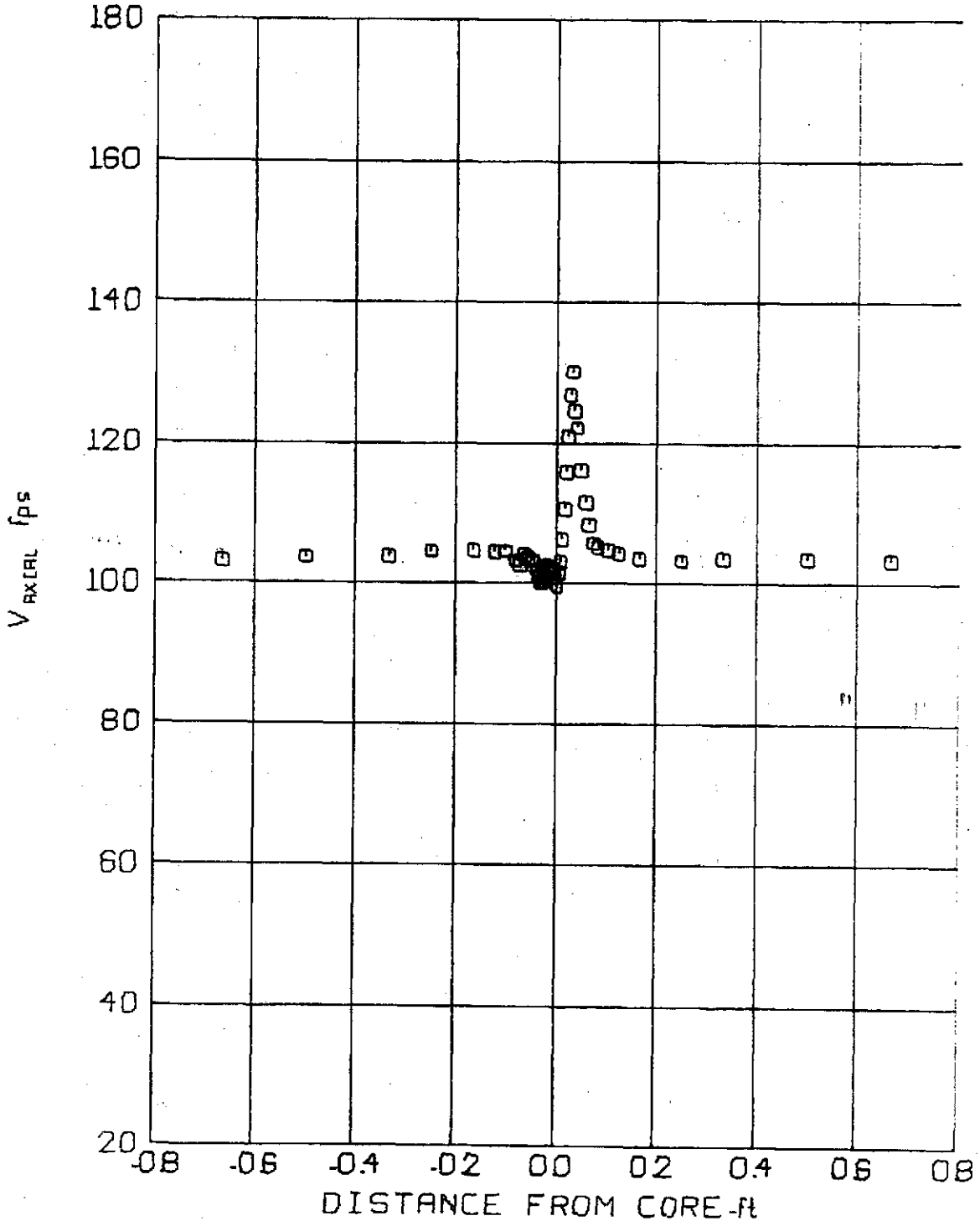

FIG 101 AXIAL VELOCITY PROFILE

V_∞ = 104.7 f/s Z/C = 20
α = 8° t = .12729 sec

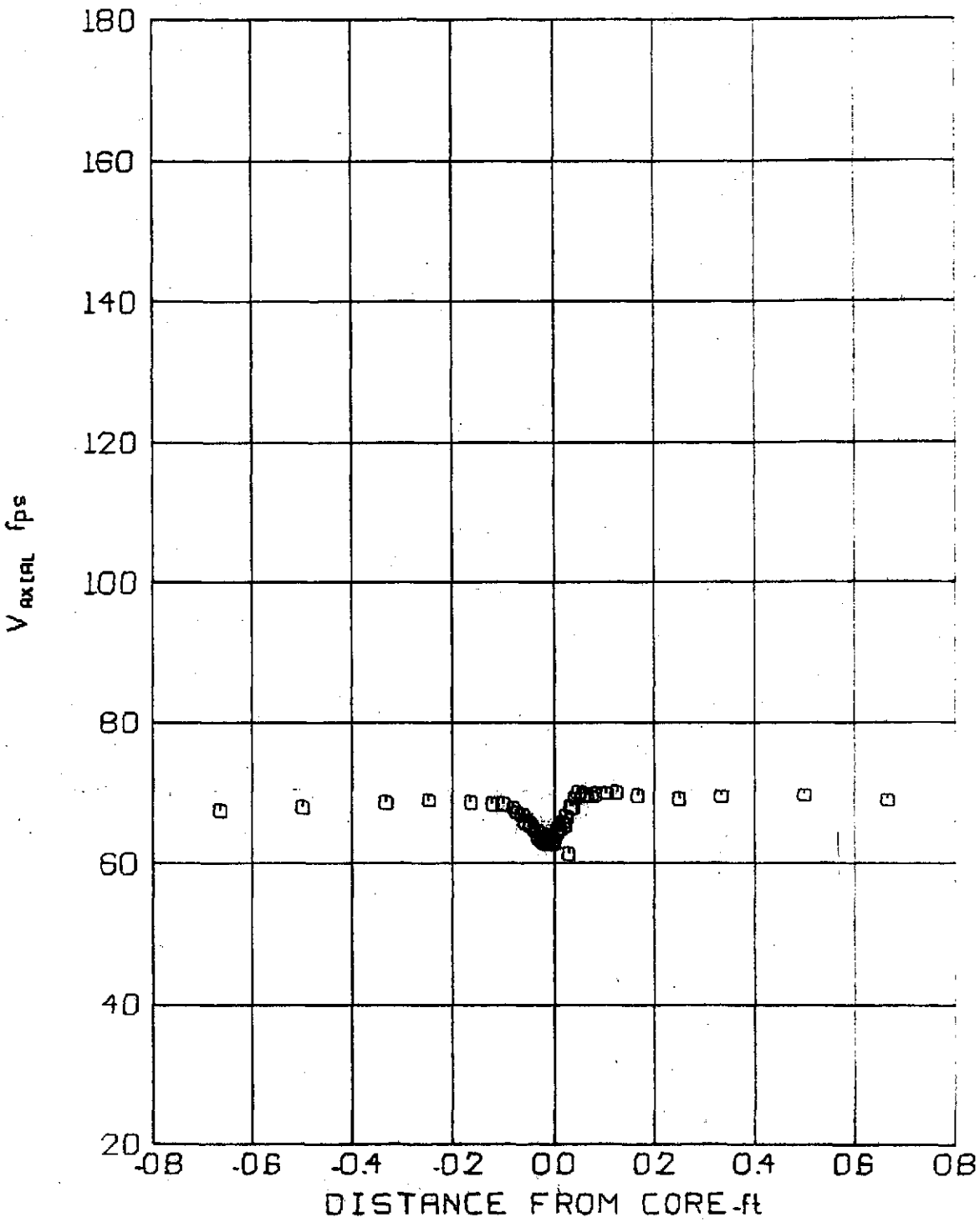

FIG 102 AXIAL VELOCITY PROFILE

V_∞ = 68.2 f/s Z/C = 25
α = 8° t = .24413 sec

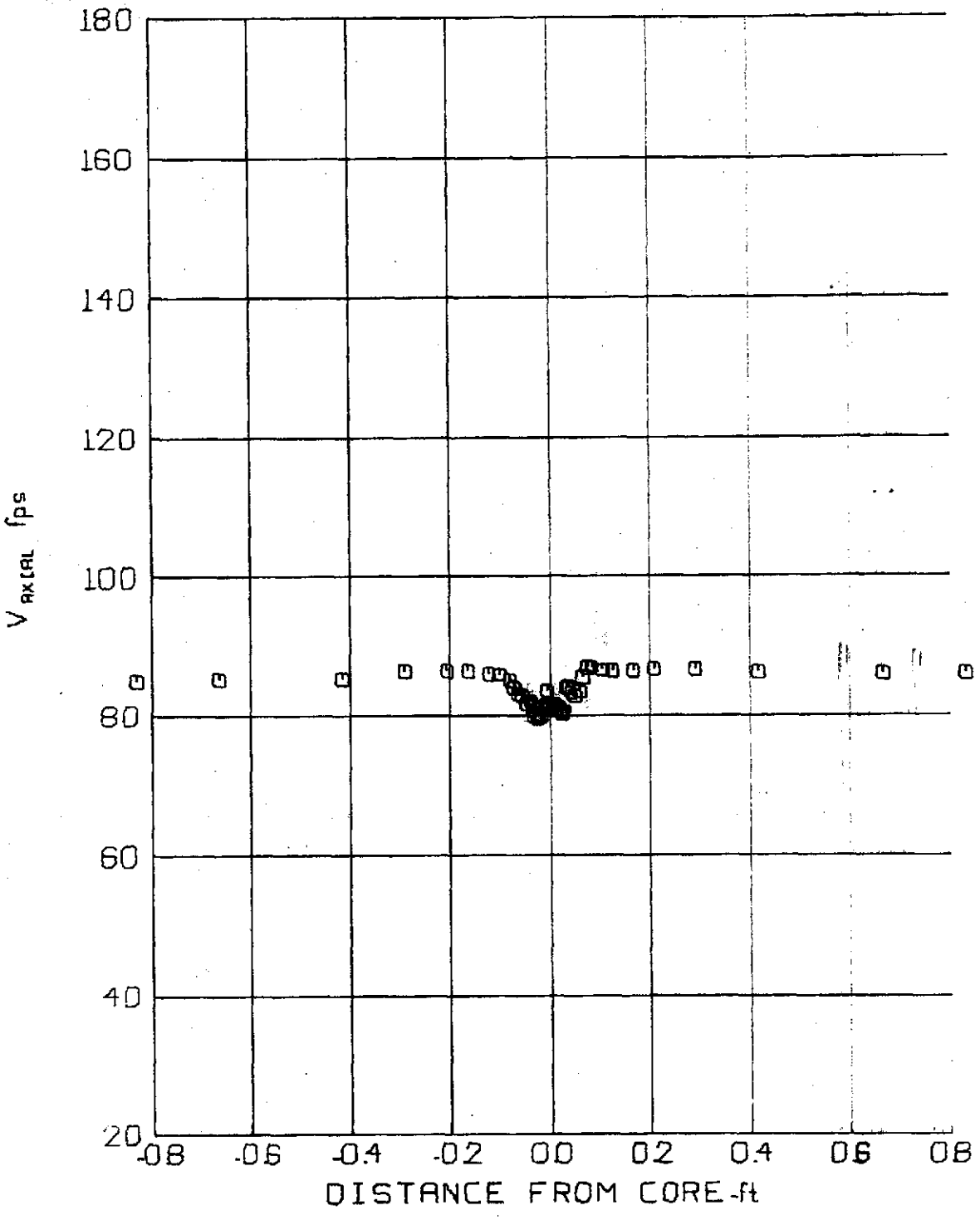

FIG 103 AXIAL VELOCITY PROFILE

V_∞ = 86.5 f/s Z/C = .25
α = 8° t = .19256 sec

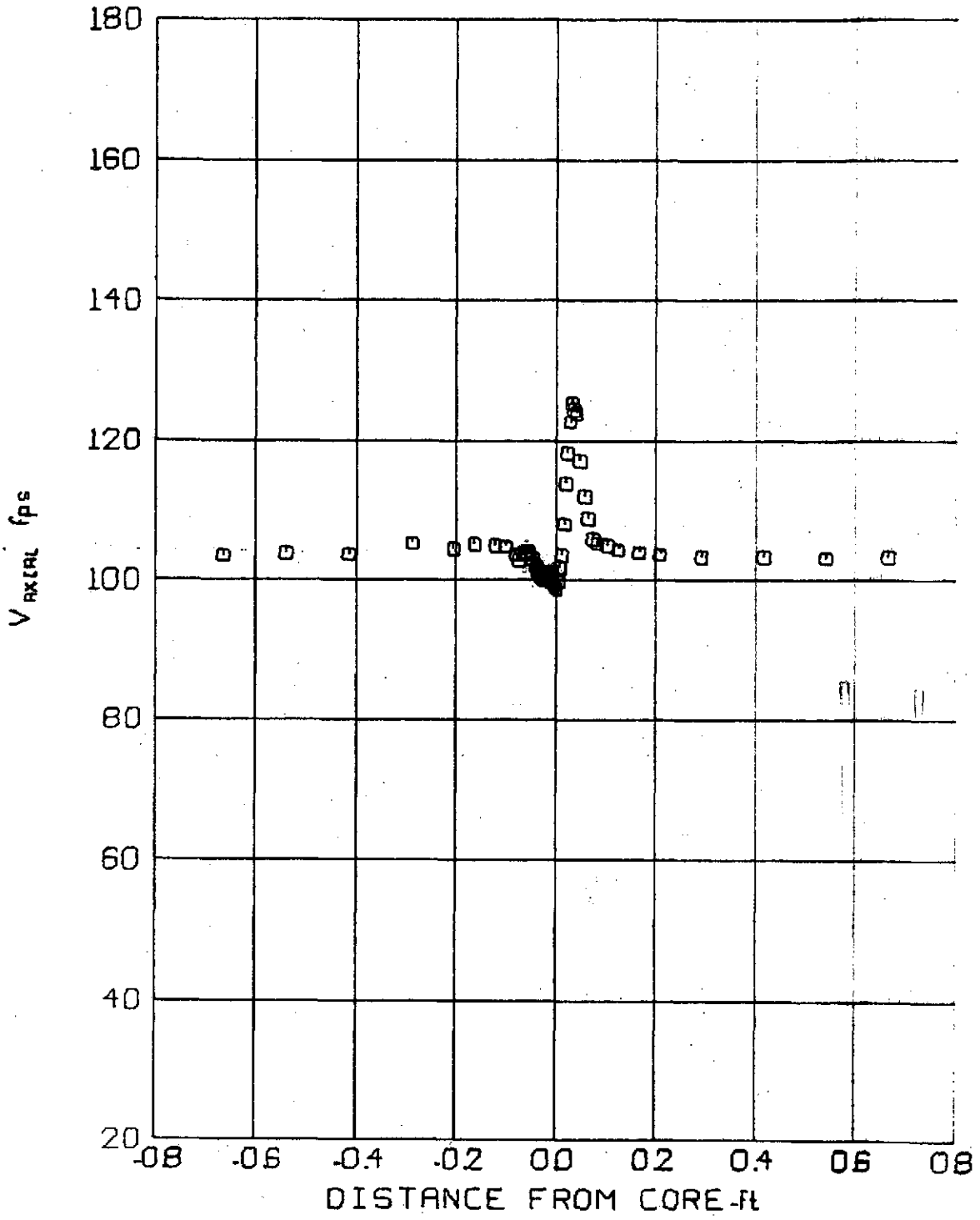

FIG 104 AXIAL VELOCITY PROFILE

V_∞ = 105.3 f/s Z/C = 25
α = 8° t = .15818 sec

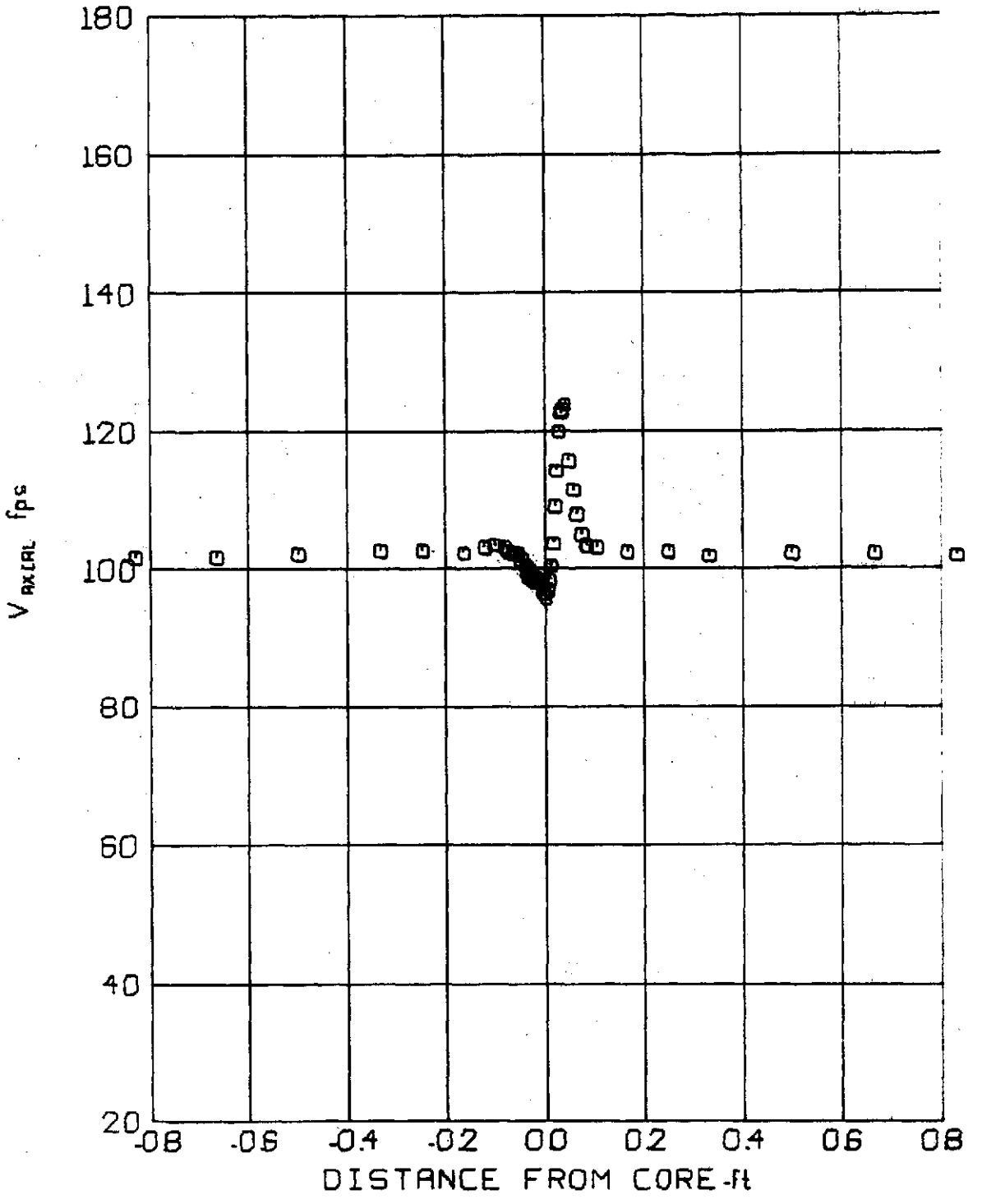

FIG 105 AXIAL VELOCITY PROFILE

V_∞ = 104.0 f/s Z/C = 30
α = 8° t = .19221 sec

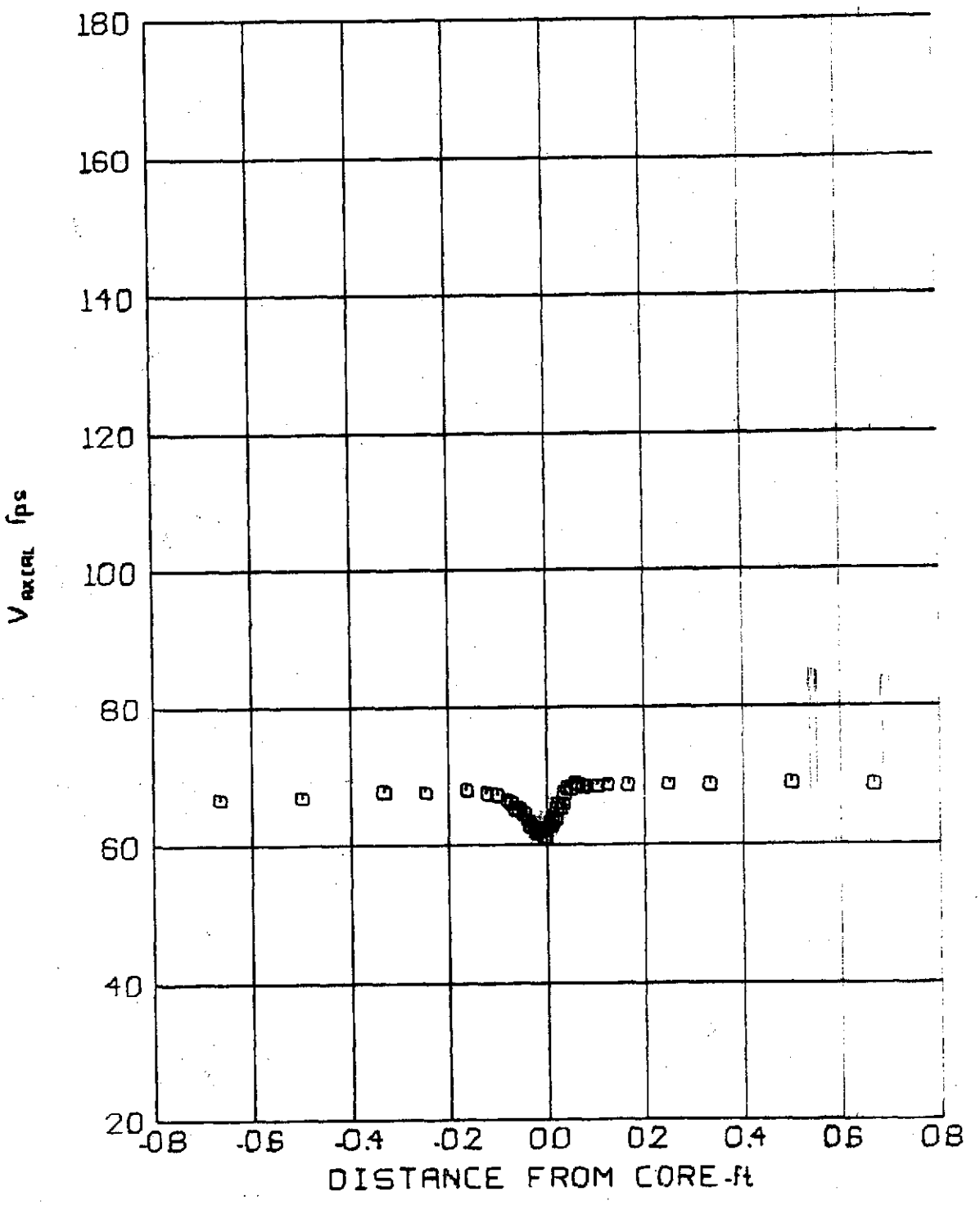

FIG 106 AXIAL VELOCITY PROFILE

V_∞ = 68.0 f/s Z/C = 30
α = 8° t = .29398 sec

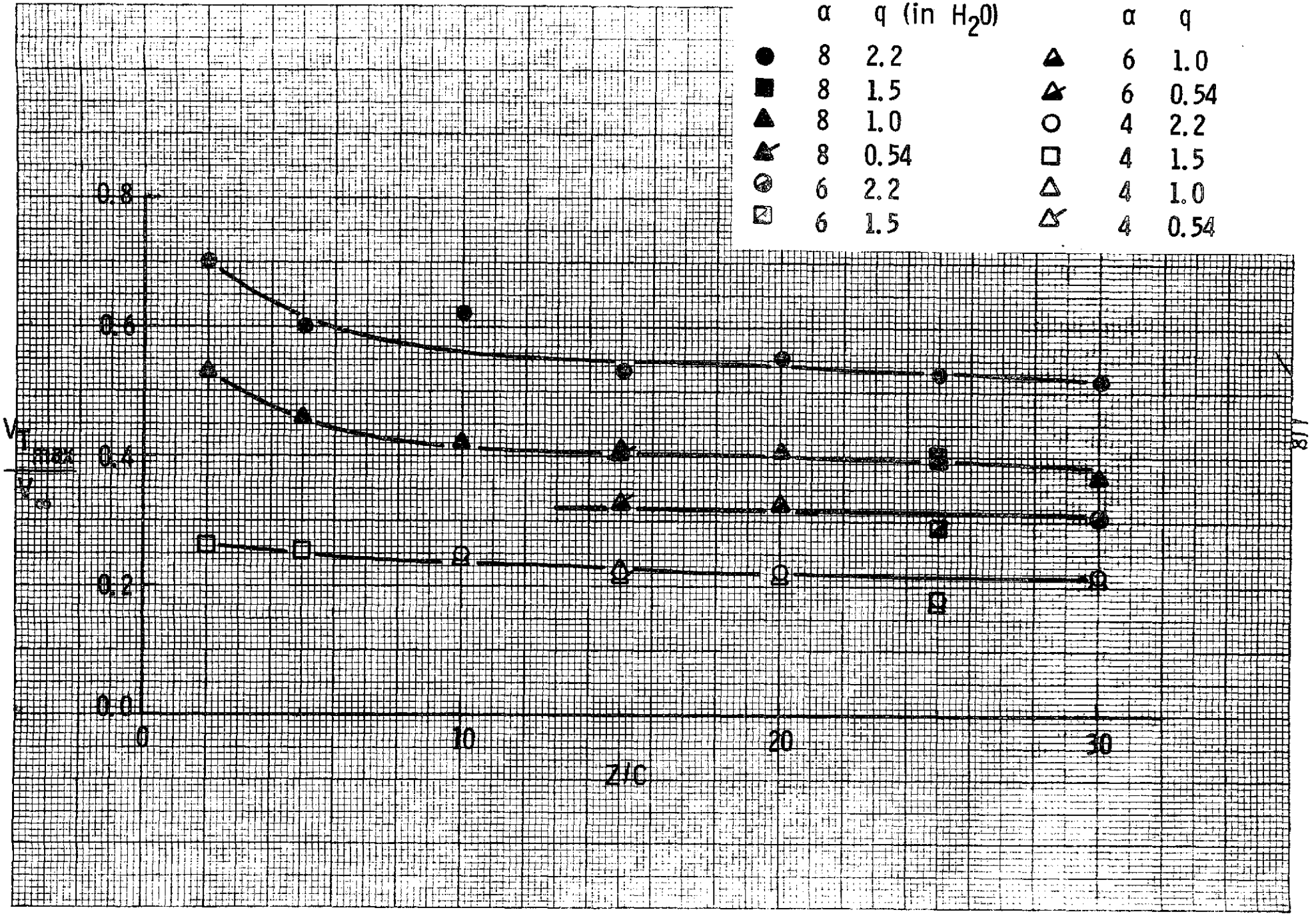

Fig. 107. Maximum Swirl Velocity vs. Downstream Distance

Fig. 108. Maximum Swirl Velocity vs. Age

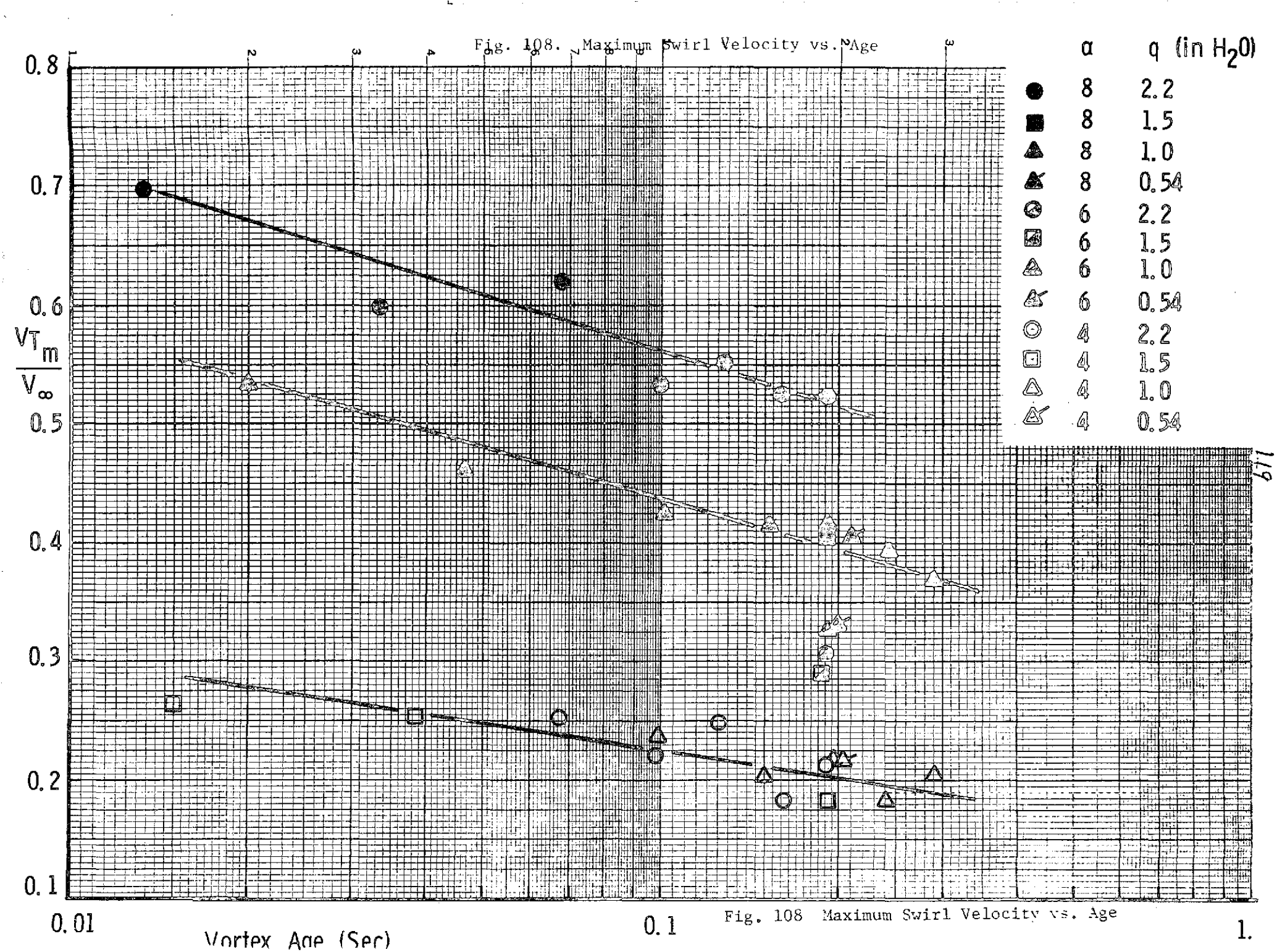

Fig. 108 Maximum Swirl Velocity vs. Age

Fig. 109. Core Size vs. Downstream Distance

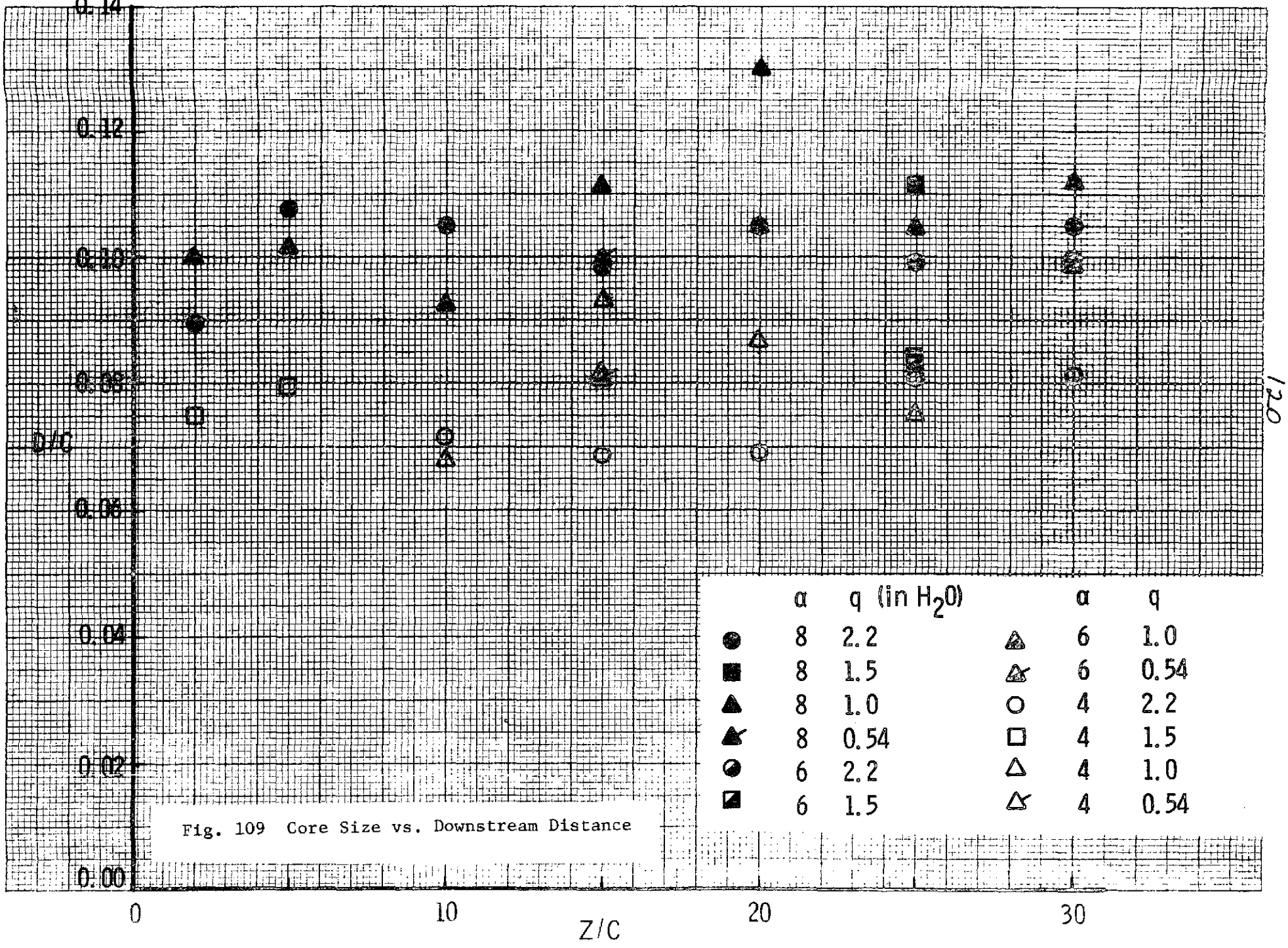

Fig. 109 Core Size vs. Downstream Distance

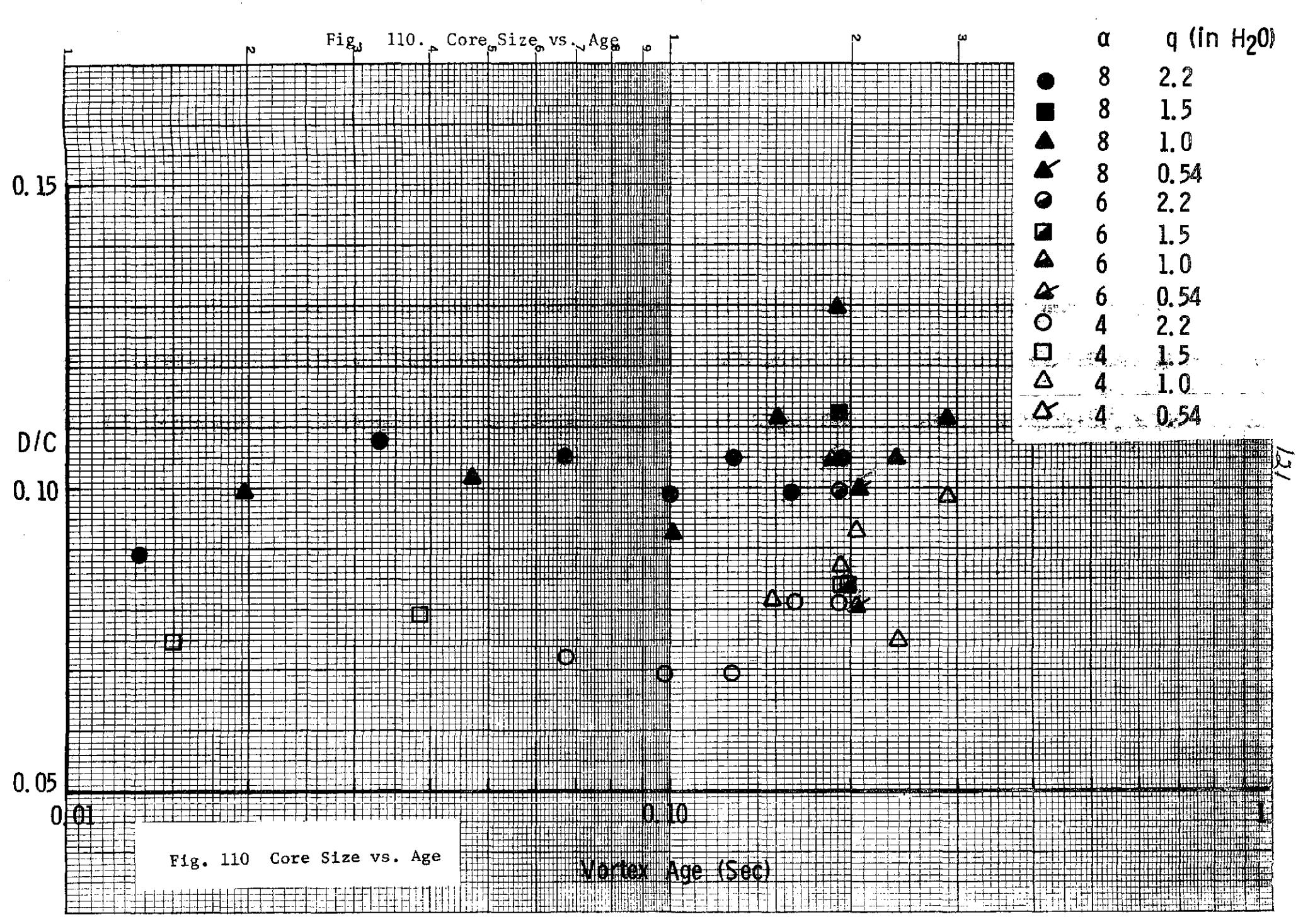

Fig. 110 Core Size vs. Age

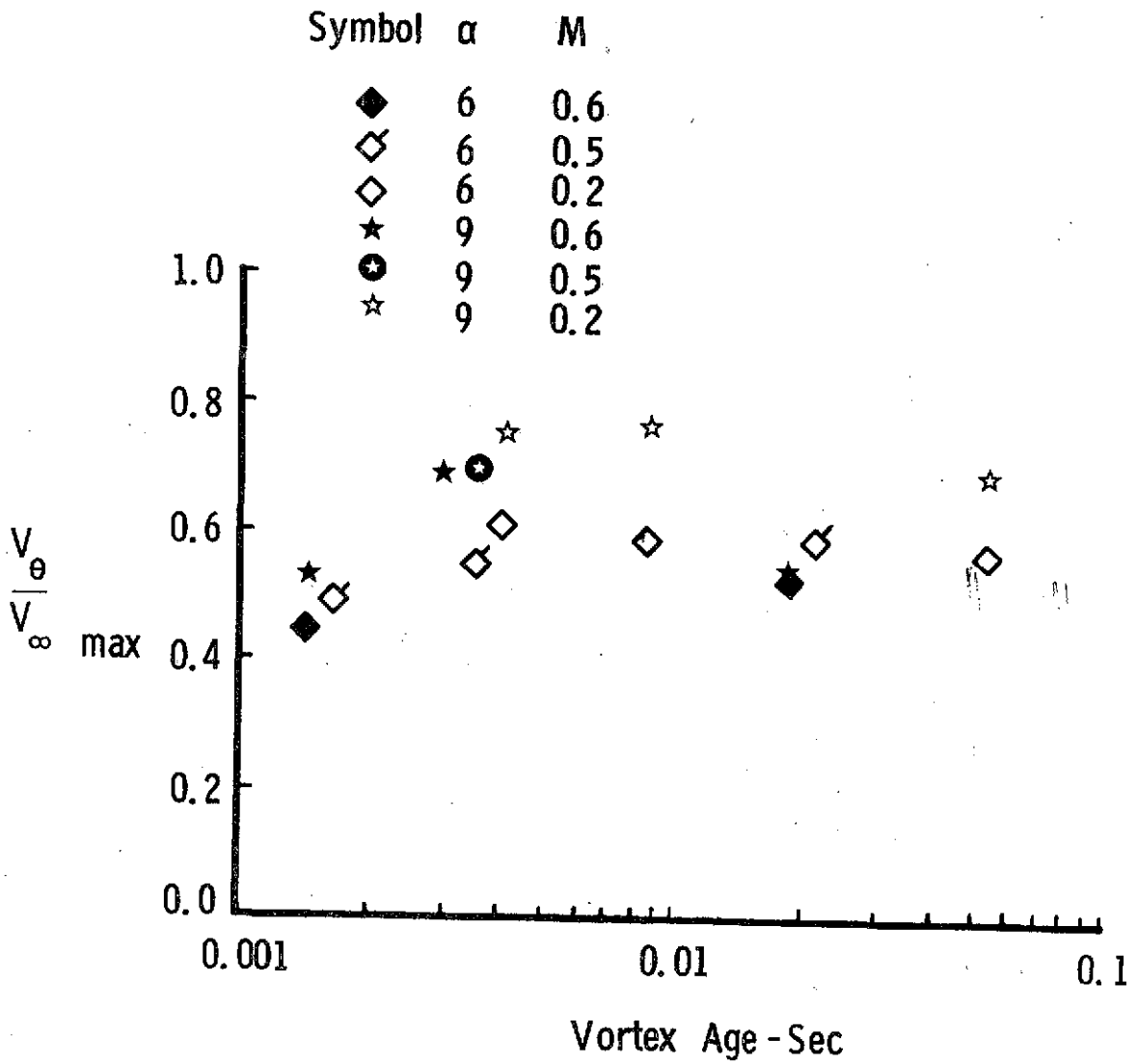

Fig. 111. Data of Rorke and Moffitt

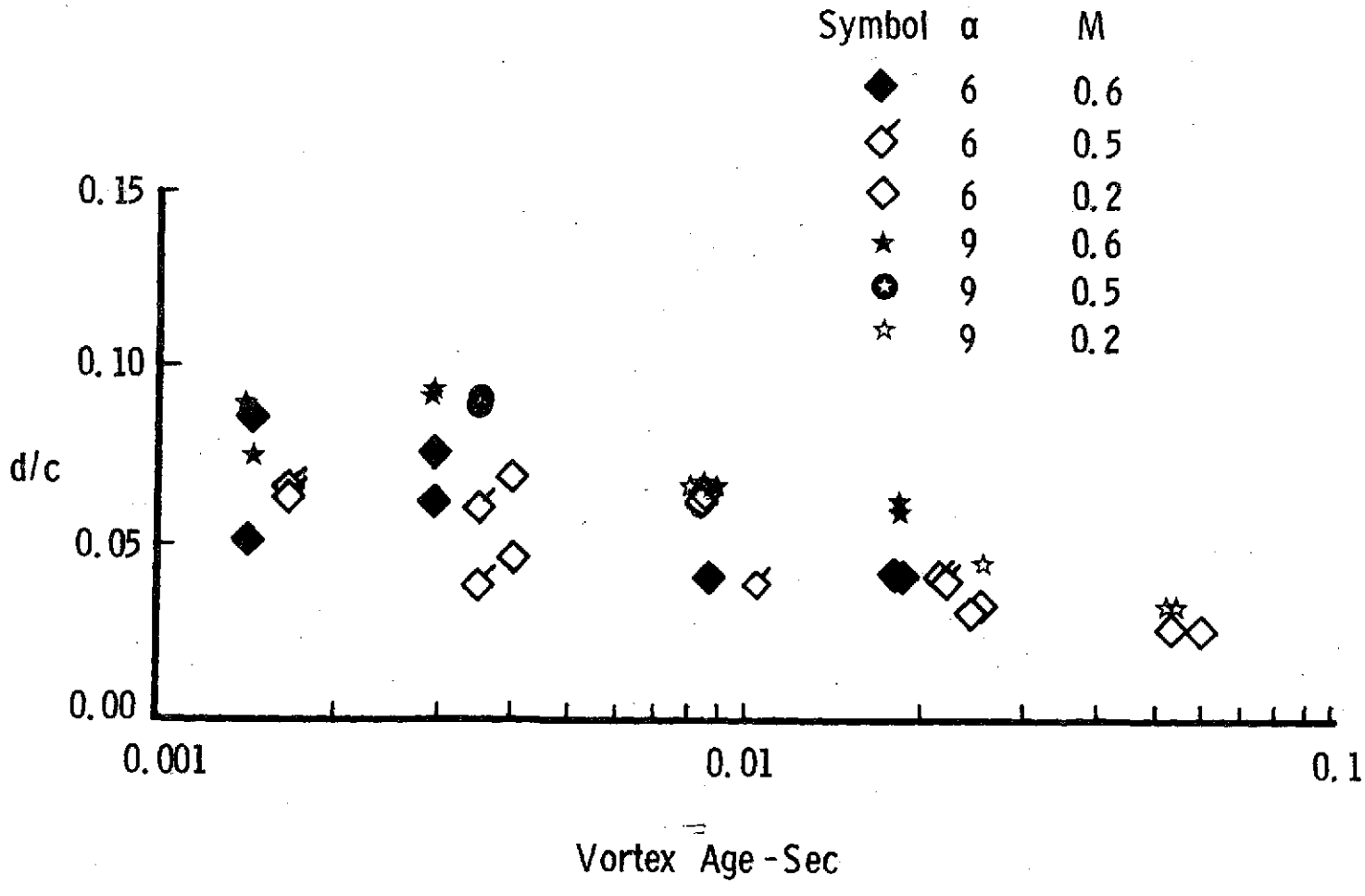

Fig. 112. Data of Rorke and Moffitt

Fig. 113. Combined Test Data

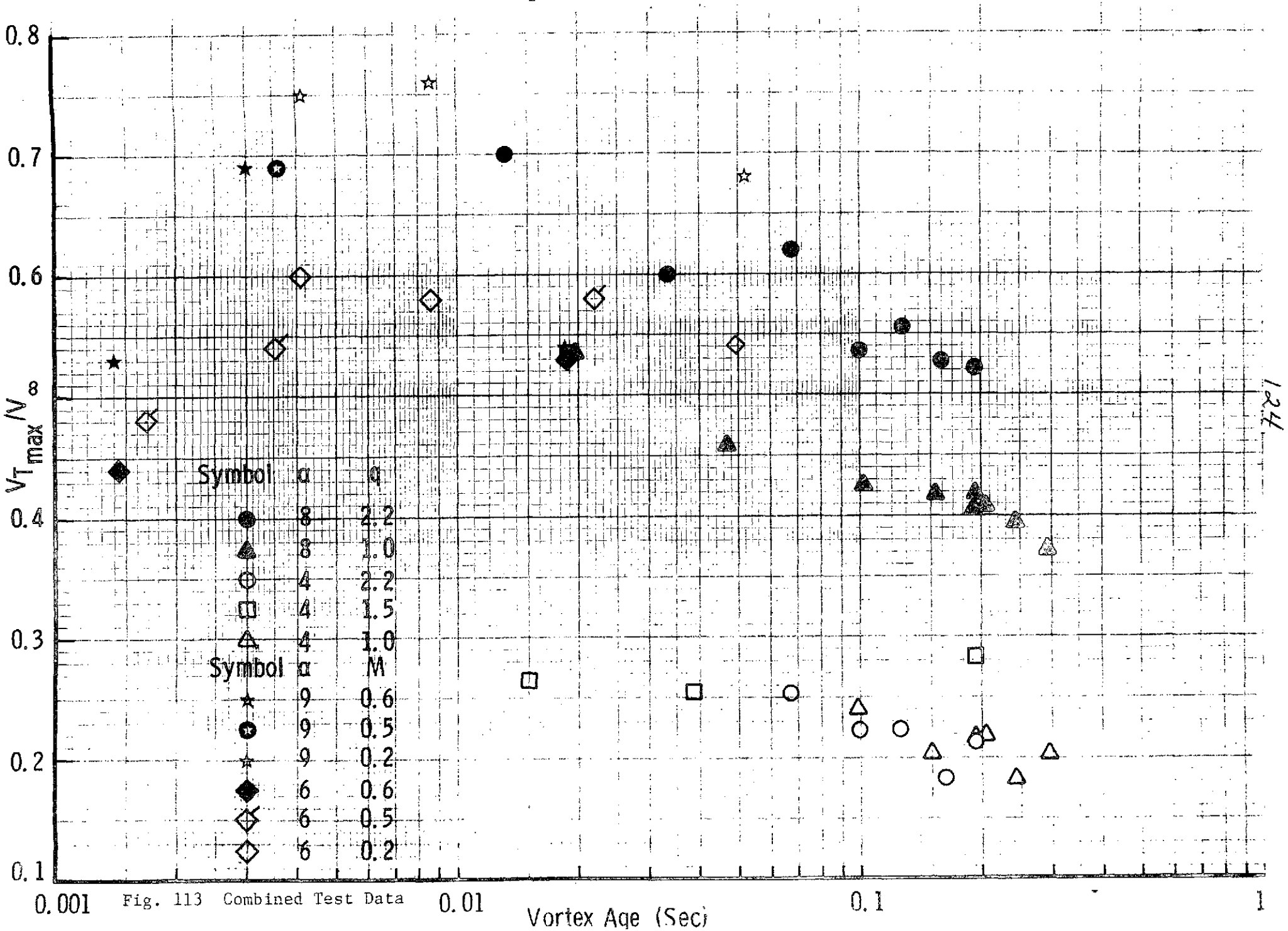

Fig. 113 Combined Test Data

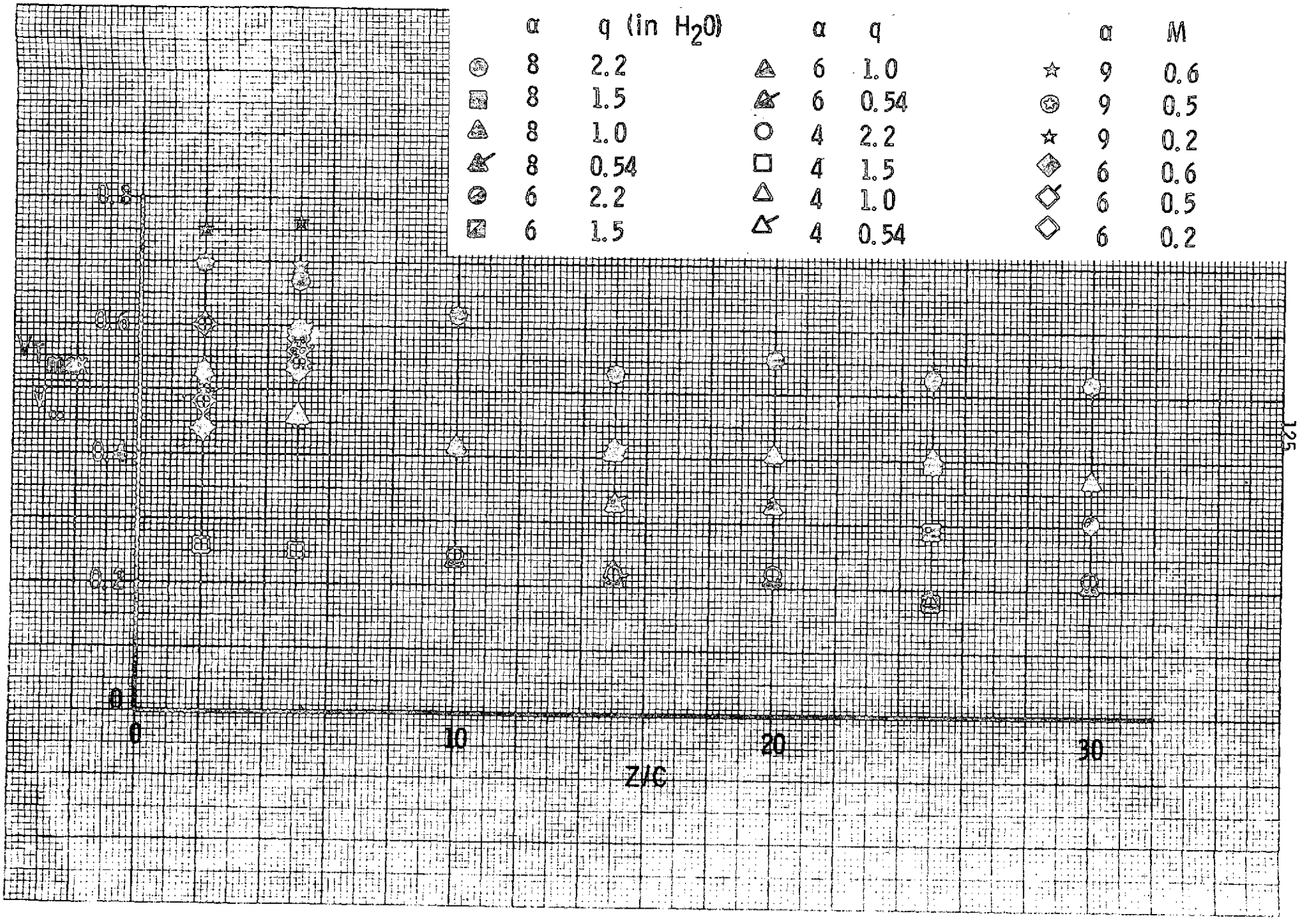

Fig. 114. Combined Test Data

Fig. 115. Axial Velocity vs. Downstream Distance

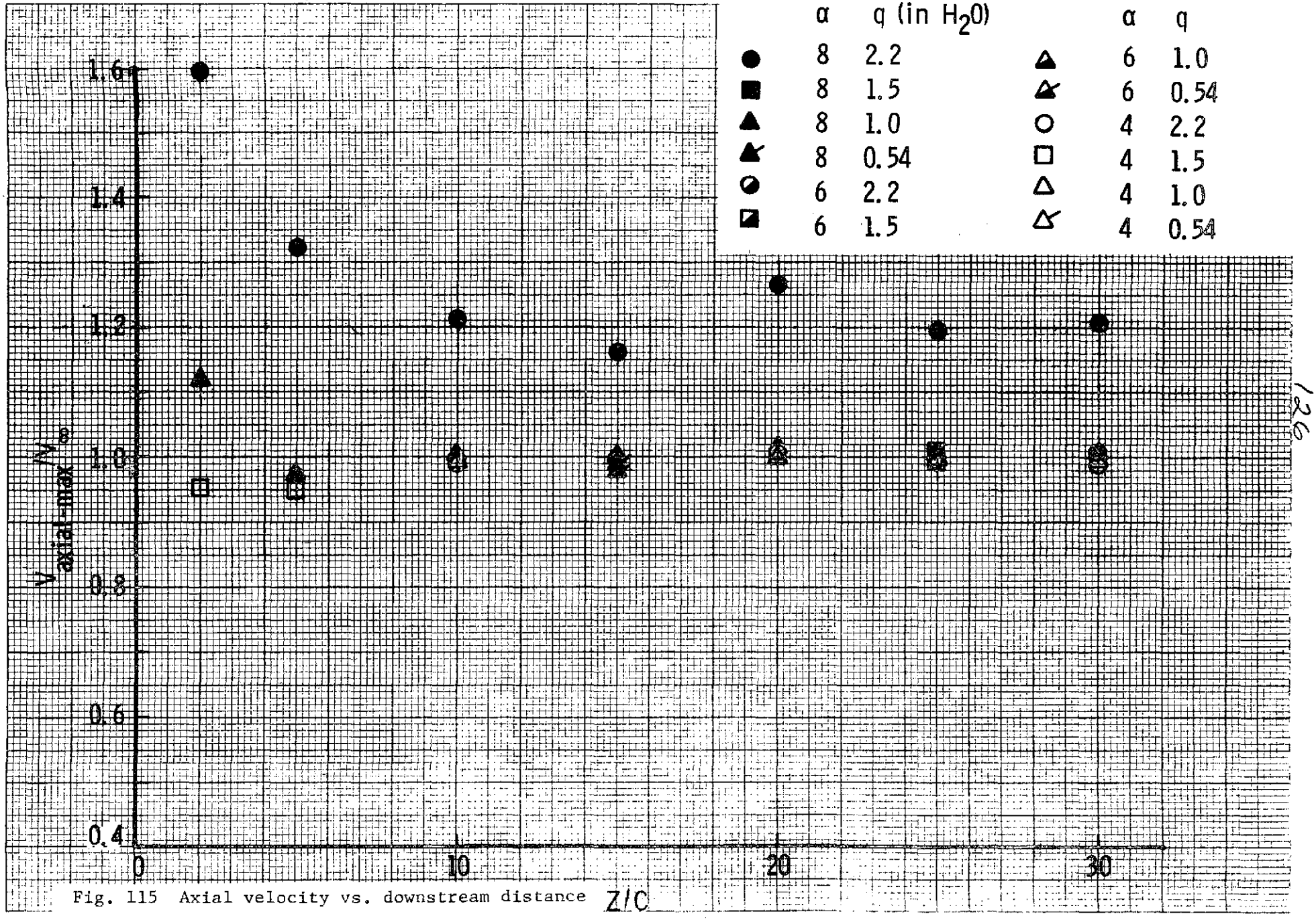

Fig. 115 Axial velocity vs. downstream distance

Fig. 116 Axial velocity vs. vortex age

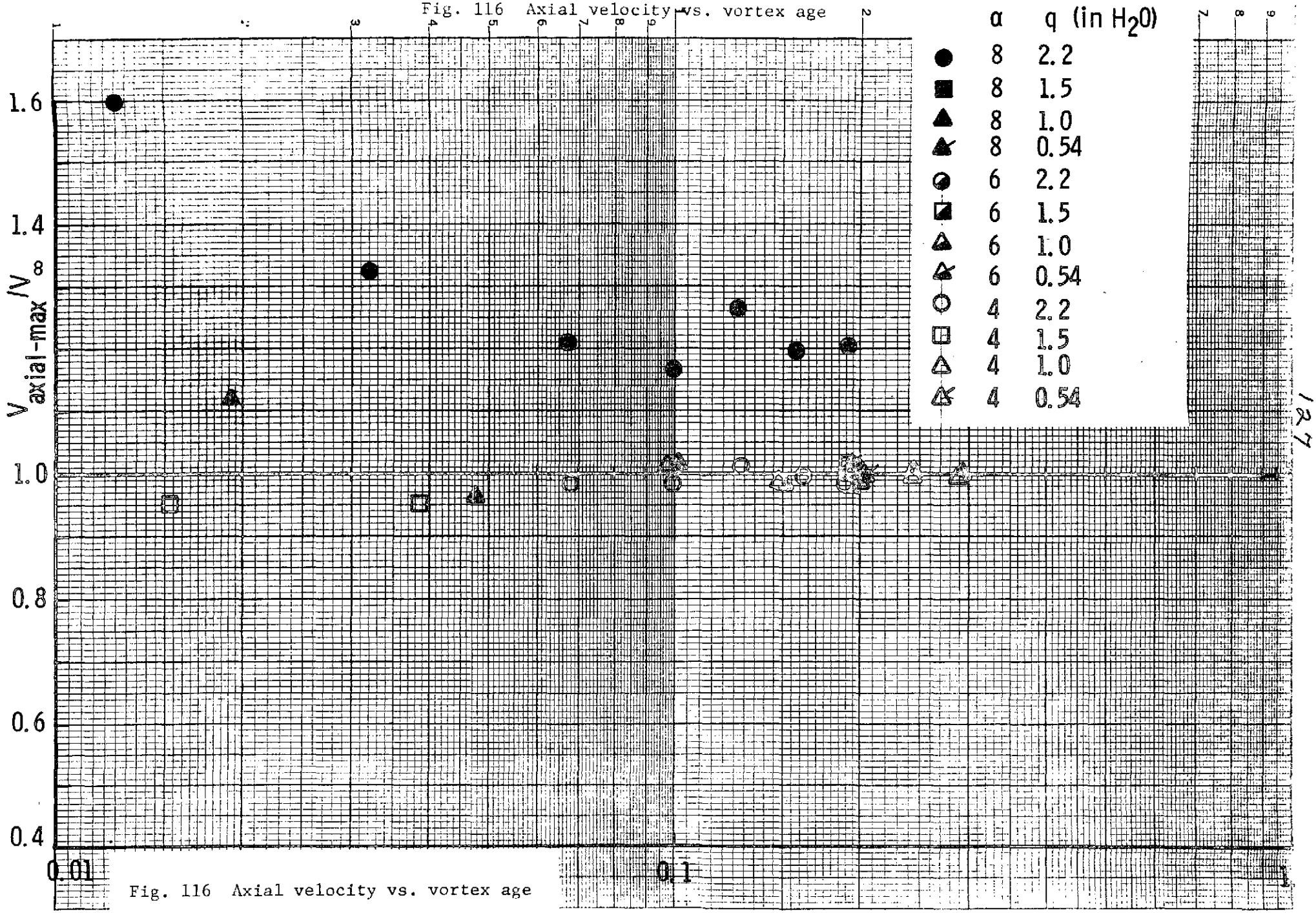

Fig. 116 Axial velocity vs. vortex age